Channel Propagation Model for Train to Vehicle Alert System at 5.9 GHz using Dedicated Short Range Communication

Christopher D. Rowe

Thesis submitted to the faculty of the Virginia Polytechnic Institute and State University in partial fulfillment of the requirements for the degree of

Master of Science
In
Computer Engineering

Carl B. Dietrich, Co-Chair
Joseph G. Tront Co-Chair
Harpreet S. Dhillon

September 7, 2016
Blacksburg, VA

Keywords: DSRC, Path Loss, Channel Model, System Feasibility

Channel Propagation Model for Train to Vehicle Alert System at 5.9 GHz using Dedicated Short Range Communication

Christopher D. Rowe

ABSTRACT

The most common railroad accidents today involve collisions between trains and passenger vehicles at railroad grade crossings [1][2]. Due to the size and speed of a train, these collisions generally result in significant damage and serious injury. Despite recent efforts by projects such as Operation Lifesaver to install safety features at grade crossings, up to 80% of the United States railroad grade crossings are classified as "unprotected" with no lights, warnings, or crossing gates [2]. Further, from January to September 2012, nearly 10% of all reported vehicle accidents were a result of train-to-vehicle collisions. These collisions also accounted for nearly 95% of all reported fatalities from vehicular accidents [2].

To help provide a more rapidly deployable safety system, advanced dedicated short range communication (DSRC) systems are being developed. DSRC is an emerging technology that is currently being explored by the automotive safety industry for vehicle-to-vehicle (V2V) and vehicle-to-infrastructure (V2I) communications to provide intelligent transportation services (ITS). DSRC uses WAVE protocols and the IEEE 1609 standards. Among the many features of DSRC systems is the ability to sense and then provide an early warning of a potential collision [6]. One potential adaption for this technology is for use as a train-to-vehicle collision warning system for unprotected grade crossings. These new protocols pose an interesting opportunity for enhancing cybersecurity since terrorists will undoubtedly eventually identify these types of mass disasters as targets of opportunity.

To provide a thorough channel model of the train to vehicle communication environment that is proposed above, large-scale path loss and small scale fading will both be analyzed to characterize the propagation environment. Measurements were collected at TTCI in Pueblo Colorado to measure the received signal strength in a train to vehicle communication environment. From the received signal strength, different channel models can be developed to characterize the communication environment.

Documented metrics include large scale path loss, Rician small scale fading, Delay spread, and Doppler spread. An analysis of the DSRC performance based on Packet Error Rate is also included.

Channel Propagation Model for Train to Vehicle Alert System at 5.9 GHz using Dedicated Short Range Communication

Christopher D. Rowe

GENERAL AUDIENCE ABSTRACT

Railroad collisions are a large safety concern in the transportation industry. The most common railroad accidents today involve collisions between trains and passenger vehicles at railroad grade crossings [1][2]. Due to the size and speed of a train, these collisions generally result in significant damage and serious injury. Despite recent efforts by projects such as Operation Lifesaver to install safety features at grade crossings, up to 80% of the United States railroad grade crossings are classified as "unprotected" with no lights, warnings, or crossing gates [2]. Further, from January to September 2012, nearly 10% of all reported vehicle accidents were a result of train-to-vehicle collisions. These collisions also accounted for nearly 95% of all reported fatalities from vehicular accidents [2].

To help improve the safety of railroad crossings, a new radio system is being developed to help improve safety. These radios are already being explored in the automotive industry to help provide more safety features in passenger vehicles like cars. The most appealing feature of these new radio systems is the ability to predict collisions and provide feedback to a vehicle operator to prevent the collision. Railroads would like to investigate the feasibility of using these new radios to prevent vehicle and train collisions.

This thesis analyzes the various characteristics of the performance the radio system in a real operating environment to determine the feasibility of using these new radio systems to provide early collision warning.

Acknowledgements

First and foremost I thank God for blessing me with the opportunity to pursue my Master's Degree while working on such a rewarding project. I also thank my family for providing extra support and motivation through the ups and downs that have made up the past two years.

On the academic front, I would like to thank my advisor, Carl Dietrich, for guiding me through my Master's program. I also thank the other committee members, Joseph Tront and Harpreet Dhillon, for providing feedback on my manuscripts. I also would like to thank Dr. Anderson and CDR Tedesso at the United States Naval Academy for allowing me to come in and work on the data processing with them. Their extra mentoring helped me to push this project over the goal line.

Special thanks to the FRA team who helped provide insights and take measurements for this large project. A large thank you goes to the Cybercorps program at Virginia Tech, without their funding I would not have been able to work on such a rewarding project.

Finally, I would like to thank all the professors and students that I have met along the way that have helped shaped my experience at Virginia Tech. Each Professor I have had has challenged me to become a better engineer. To my personal group of friends, thanks for making me unwind and forget the pressures of school. Without you, I would not have survived this process.

Table of Contents

Table of figures

Table of equations

List of Tables

List of Abbreviations

AES-CCM	Advance Encryption Standard in Counter with CBC-MIC
AP	Access Point
AWGN	Additive White Gaussian Noise
BER	Bit Error Rate
BSM	Basic Safety Message
BSS	Basic Service Set
CCH	Control Channel
CDF	Cumulative Distribution Function
CSMA/CA	Carrier Sense Multiple Access/ Collision Avoidance
DER	Distinguished Encoding Rules
DFT	Discrete Fourier Transform
DSRC	Dedicated Short Range Communication
DSSS	Direct-Sequence Spread Spectrum
ECDSA	Elliptic Curve Digital Signature
ECICS	Elliptic Curve Integrated Encryption Scheme
FHA	Federal Highway Administration
I	In-Phase
IP	Internet Protocol
ISI	Inter-Symbol Interference
ITS	Intelligent Transportation Services
LAN	Local Area Network
LLC	Logical Link Control
LOS	Line of Sight
LSB	Least Significant Bit
MAC	Media Access Control
MAN	Metropolitan Area Network
MED	Maximum Excess Delay
MMSE	Minimum Mean Square Error Estimator
MSB	Most Significant Bit
MUTD	Manual on Uniform Traffic Control Devices
OBU	On Board Unit
OCB	Outside the Context of a BSS
OFDM	Orthogonal Frequency Division Multiplexing
PCAP	Packet Capture
PDP	Power Delay Profile
PDU	Protocol Data Unit
PER	Packet Error Rate
PHY	Physical Layer
PLCP	Physical Layer Convergence Procedure
PMD	Physical Medium Dependent

PSD	Power Spectral Density
PPDU	PHY Protocol Data Unit
PSID	Provider Service ID
PTT	Precision Test Track
Q	Quadrature
QAM	Quadrature Amplitude Modulation
QoS	Quality of Service
RMS	Root Mean Square
RSS	Received Signal Stength
RSSI	Received Signal Strength Indication
RSU	Road Side Unit
RTT	Railroad Test Track
SCH	Service Channel
SNAP	Subnetwork Access Protocol
SNR	Signal to Noise Ratio
SV/DGVRR	Shenandoah Valley and Durbin & Greenbrier Valley Railroads
TDL	Tapped Delay Line
TTCI	Transportation Technologies Inc
USDOT	United States Department of Transportation
USRP	Universal Software Radio Peripheral
V2I	Vehicle to Interface
V2V	Vehicle to Vehicle
WAVE	Wireless Access in Vehicular Environments
WSA	WAVE Service Advertisement
WSM	WAVE Short Messages
WSMP	WAVE Short Message Protocol

1 Introduction

1.1 Problem statement

The most common railroad accidents today involve collisions between trains and passenger vehicles at railroad grade crossings [1][2]. Due to the size and speed of a train, these collisions generally result in significant damage and serious injury or even death. Despite recent efforts by projects such as Operation Lifesaver to install safety features at grade crossings, up to 80% of the United States railroad grade crossings are classified as "unprotected" with no lights, warnings, or crossing gates [2]. Additionally, from January to September 2012, collisions between train and vehicles accounted for nearly 10% of all reported vehicle accidents and accounted for nearly 95% of all reported fatalities from all vehicular accidents [2].

To help provide a more rapidly deployable safety system, advanced dedicated short range communication (DSRC) systems are being developed. DSRC is an emerging technology that is currently being explored by the automotive safety industry for vehicle-to-vehicle (V2V) and vehicle-to-infrastructure (V2I) communications to provide intelligent transportation services (ITS). Among the many attractive features DSRC systems have to offer, the ability to sense and provide an early warning of a potential collision is the most advantageous [6]. One potential adaption for this technology is for use as a train-to-vehicle collision warning system for unprotected grade crossings. Systems installed onboard train engines would transmit warning messages to approaching vehicles and roadside warning units. Additionally, systems could provide feedback to train engineers alerting them to potential oncoming traffic. The overall system concept is given in Figure 1.1 below.

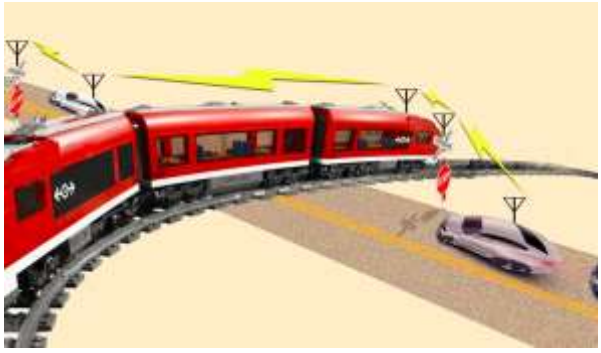

Figure 1.1 DSRC Railroad Safety System Concept

Current conventional grade crossing protection systems can be extremely expensive. For example, the Shenandoah Valley and Durbin & Greenbrier Valley Railroads (SV/DGVRR) recently installed a set of lights, cantilevers, and gates, along with minor road/track work at a cost of approximately $30,000, and indicated a typical cost of $25,000-$50,000 to protect a two-lane grade crossing. A system that could provide protection at even $12,500 per crossing would allow railroads to add protection to identified high-risk unprotected crossings at two to four times the current density. Developing a low-cost system

requires a firm understanding of the operational environment and its effects on the radio channel characteristics.

This thesis addresses the comprehensive documentation and statistical analysis of radio wave propagation parameters in the 5.9 GHz band that DSRC will operate in, to characterize the propagation channel under which DRSC messages will be sent. Using measurements from the outdoor measurement campaign, received signal strength values and statistical parameters such as delay spread, Doppler spread, and Doppler shift are computed to help define and characterize the wireless channel. From these measurements a Rician channel model will be derived to find a channel that best models the propagation environment.

1.2 Brief summary of approach and results

To provide a thorough channel model of the train to vehicle communication environment that is proposed above, large-scale path loss and small scale fading will both be analyzed to characterize the propagation environment. Measurements were collected at TTCI in Pueblo Colorado to measure the received signal strength in a train to vehicle communication environment. From the received signal strength, different channel models can be developed to characterize the communication environment. The large-scale path loss will be modeled using a log-normal shadowing model, discussed in section 2.3.2.1.2. For the small scale fading, Rician K-factors will be derived using the method outlined in section 2.3.2.3.1. The overall performance of alert system will also be analyzed based on the packet error rate.

For the DSRC alert system test, the linear array, the optimized antenna, in most cases did not outperform either of the other two antennas tested, likely because; the beam was not angled such that a receiver, not directly in front of the beam, would be in the antenna's beam. However the antenna could be optimized to provide potentially more receiver coverage. The Omni and Omni diversity antennas performed about the same, with the Omni Diversity providing slightly more robust packet reception. The performance was also consistent between the locations for the OBU.

The small scale fading parameters were compared to similar vehicle to vehicle measurement campaigns explained in references [29],[30], and [31]. Since there are no existing measurement campaigns performed between trains and vehicles in motion, the comparison to existing vehicle to vehicle measurements was used instead. The results found at TTCI, fall in the range of values seen in existing vehicle to vehicle measurement campaigns. However, the range of values in the existing measurement campaigns is large, which suggest the existing campaigns were not performed under comparable environmental conditions.

The large scale path loss models found fit a log-normal model best because the data showed a general increase in path loss as the distance between the transmitter and receiver increased. Rician models were chosen because the propagation environment did not show the severe fading effects where different K values were needed for different distances away from the receiver as suggested in literature. Instead the K values were generally consistent and were taken as an average for each speed the tests were conducted on.

1.3 Organization of thesis

This thesis is organized as follows

Chapter 2 provides background on railroad crossing protection, DSRC systems and the simulator, an explanation of propagation models, and proposed models found in literature that could work in the 5.9 GHz band.

Chapter 3 documents the measurement systems used for the propagation campaign, the measurement campaign test scenarios, and the proposed channel model and implementations.

Chapter 4 analyzes the channel models and parameters and compares the results with the measured results from literature.

Chapter 5 provides a summary and proposes future work for channel characterization at 5.9 GHz for train to vehicle communication systems.

2 Background

2.1 Railroad crossing protection

Railroads have been a major form of transportation in the United States since the 1830s. Today, the United States railroad system is comprised of 750 different railroads that cover 140,000 miles of track. Unfortunately, railroads were not initially designed to avoid railroad crossing collisions because other forms of transportation were relatively slow and could easily stop for an oncoming train. However, as the automobile gained popularity, the highway infrastructure expanded and with the expansion, the number of intersections between railroads and highways increased [2]. These intersections are referred to as highway-rail grade crossings. A grade crossing is more formally defined as a location where a public highway, road, street, or private road crosses railroad tracks at the same level, or grade [2]. An example of a highway rail grade crossing is given in Figure 2.1. Consequently, highway-rail grade crossing safety is a relatively new area of research with great potential to be improved on.

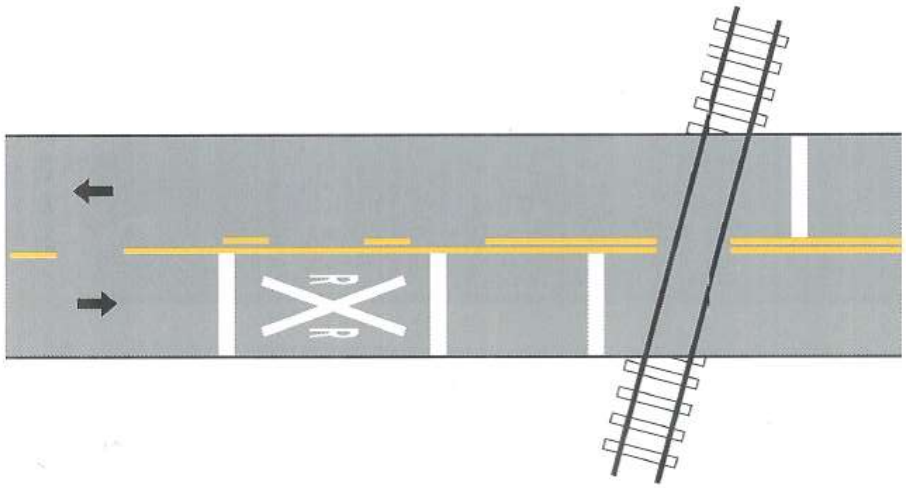

Figure 2.1 Highway Rail Grade Crossing [5]

Conventional grade crossing protection systems can be extremely expensive. The federal government provides funds to eliminate hazards and to maintain highway-rail grade crossings, but only about 50% of the funds are appropriated to install new protective devices [2]. These funds are typically insufficient to protect all the highway-rail grade crossings in a state, causing grade crossings to be prioritized in order of highest safety risk. Consequently, approximately 80% of highway-rail grade crossings are unprotected [11]. The Interstate Commerce Commission classifies a grade crossing as “unprotected” or “not specially protected” if the crossing is not equipped with crossing gates, watchman, and audible or visible signals. Installing gates cost around $150,000 and putting up flashing lights cost about $50,000 per crossing [3]. Additionally, the estimated cost for railroad union workers to maintain and man railroad crossings is $206 million for all workers. As a result, fully protecting a highway-rail grade crossing becomes very costly. Additionally, today’s safety standards for highway-rail grade crossings are developed on a case by case basis since each crossing depends on a large number of variables. Consequently, no single standard system of traffic control device is universally applicable to all highway-rail grade crossings [4]. The

Federal Highway Administration has to determine the appropriate traffic control system based on engineering studies conducted by both the highway agency and the railroad company. As a result, the time and cost it takes to protect a grade crossing varies. The Shenandoah Valley and Durbin & Greenbrier Valley Railroads (SV/DGVRR) indicated a typical cost of $ 25,000-$50,000 for them to protect a two-lane grade crossing, while the cost for crossings at larger roads can be much more expensive. Even after the safety studies are conducted and the appropriate signage, lighting, and barriers are installed, the grade crossing may not be protected completely from vehicle and train collisions. Statistics show that a train-vehicle collision occurs about once every 90 minutes in the U.S. [12]. These accidents occur because the vehicle's operator is unaware of approaching trains.

A new area of research to consider for providing drivers with advanced warning of an approaching train is to use wireless communications. Advanced wireless technologies have emerged rapidly in recent years. However, there have been very limited efforts to improve railroad crossing safety through the use of these communication techniques. Using the cost estimate for SV/DGVRR, a system that could provide protection at even $12,500 per two-lane crossing would allow railroads to add protection to identified high-risk unprotected crossing at two to four times the current density. Development of such a low-cost system requires a thorough approach to gain a firm understanding of the operational environment, including the radio channel characteristics in the case of a wireless system, as well as application of safety principles and best practices, and a focus on railroad industry-specific requirements.

In order to develop a wireless solution to further enhance the safety of highway-rail grade crossings, the system would need to comply with the federal safety standards. However, the standard for wireless safety messages is still evolving; the United States Department of Transportation (USDOT) and Federal Highway Administration (FHA) have created a Manual on Uniform Traffic Control Devices (MUTD) that defines the standard that all traffic control devices must operate under, including railroad crossing safety devices. According to the MUTD, a railroad traffic control device must command attention of a driver and provide adequate time for proper response. The FHA defines adequate time for a railroad crossing as 20 seconds before the arrival of any rail traffic that is travelling at 20mph or faster. To design a system that meets these requirements, the range of the wireless system must be able to reliably reach the vehicle 20 seconds before the train arrives at the crossing and be able to trigger some sort of alert, most likely in the form of a combination of audio, visual, and haptic feedbacks.

2.2 DSRC

Wireless technologies, such as Dedicated Short Range Communication (DSRC), are currently being explored by the automotive safety industry for Vehicle-to-Vehicle (V2V) and Vehicle-to-Infrastructure (V2I) communications to provide Intelligent Transportation Services (ITS) [6]. Among the many appealing features of DSRC systems, the ability to sense and to provide an early warning of a potential collision is attractive for general vehicle safety [13][14]. The DSRC technology can also be adapted for use as a train-to-vehicle collision warning system for unprotected grade crossings [15]. Systems installed onboard train engines would transmit warning messages to approaching vehicles and roadside warning units. Additionally, systems could provide feedback to the train's engineers alerting them about potential oncoming traffic.

In the following sections, are oriented towards the DSRC standard and measuring DSRC performance. Particularly, section 2.2.1 explains how the DSRC standard is designed and implemented as a network. Then, section 2.2.2 is a description of the DSRC simulator developed at Virginia Tech used to measure theoretical performance of DSRC networks.

2.2.1 Description of standard and its applications

DSRC was initially developed to enable a standard for collision prevention using frequent data exchanges between vehicles and roadside infrastructure. The USDOT estimates that using DSRC for vehicle-to-vehicle (V2V) communications can address 82% of all crashes involving unimpaired drivers [Kenney]. DSRC provides a 75 MHz spectrum for communication at the 5.9 GHz frequency band. Existing communication protocols, such as Wi-Fi, LTE, and Bluetooth, would not provide a reliable communication environment because the protocol's overhead is large. These existing communication protocols are designed for sending packets over longer, usually static, distances, greater than 100 meters. The headers include extra information that will not be used in a DSRC network because a DSRC network aims to send many smaller packets to multiple users quickly. Additionally, the DSRC network's structure is constantly changing and will resemble more of an ad-hoc network than a fixed infrastructure network. Consequently, delivering data requires a different routing protocol than existing protocols. Thus the wireless access in vehicular environments (WAVE) was developed on top of IEEE 802.11.

WAVE is the suite of IEEE 1609 standards that are used to build a WAVE network. These standards specify the network architecture, resource manager, security services, networking services, multi-channel operation, and the over air data exchange for Intelligent Transportation Systems. The DSRC/WAVE standard will be used to implement a messaging system between other DSRC radios. Each radio will communicate its current GPS location, speed, and acceleration. The vehicle trajectories can then be calculated to determine whether nearby vehicles are collision threats. If a collision threat is detected the operator of the vehicle will be alerted. The following sections describe how the DSRC/WAVE standards are used.

2.2.1.1 DSRC Components

A simple DSRC network is comprised of two units, the roadside unit (RSU) and the onboard unit (OBU). The RSU is a stationary DSRC radio that connects roaming vehicles to the access network [10]. The OBU is a DSRC radio that is physically connected to a roaming vehicle and accesses both the DSRC network and the vehicle network. The RSU is typically used to alert OBUs about traffic alerts and other infrastructure conditions. As the OBU moves between communication zones, OBUs exchange information with the RSUs.

The DSRC 5.9 GHz frequency band is divided into seven, 10 MHz channels with 5 MHz reserved that serves as a guard band. The channels are allocated such that the center channel, designated as channel 178, is the control channel (CCH) and the remaining channels, channels 172, 174, 176, 180, 182, and 184, are the service channels (SCH). A Diagram of the spectrum allocation is given in Figure 2.2 below. The CCH transmits WAVE Short Messages (WSM) and announces WAVE services available on the SCHs. WSMs will be elaborated in the following section. The SCH is used for IP-based services typically developed for commercial applications such as paying for services and downloading content.

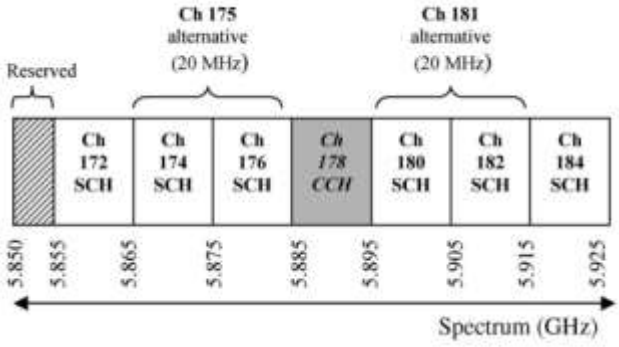

Figure 2.2 DSRC Spectrum Allocation [6]

2.2.1.2 DSRC and WAVE Architecture

The DSRC network follows the OSI network model in that the DSRC network has a PHY, MAC, data link, network, transport, and application layer. Figure 2.3 shows the DSRC network stack. The DSRC PHY layer uses IEEE 802.11 and IEEE 802.11p standards to transmit bits at DSRC's high frequency. The DSRC MAC layer is also built on top of IEEE 802.11 and uses the IEEE WAVE protocol to connect to the Logical Link Control (LLC). The LLC leverages the IEEE 802.2 protocol which is implemented for local area networks (LANs) and metropolitan area networks (MANs) to create links to send data packets. The network layer uses a combination of IPv6 and the WAVE short message protocol (WSMP) to determine the best physical route messages should travel on. The transport layer uses a combination of UDP, TCP, and WSMP to send messages reliably.

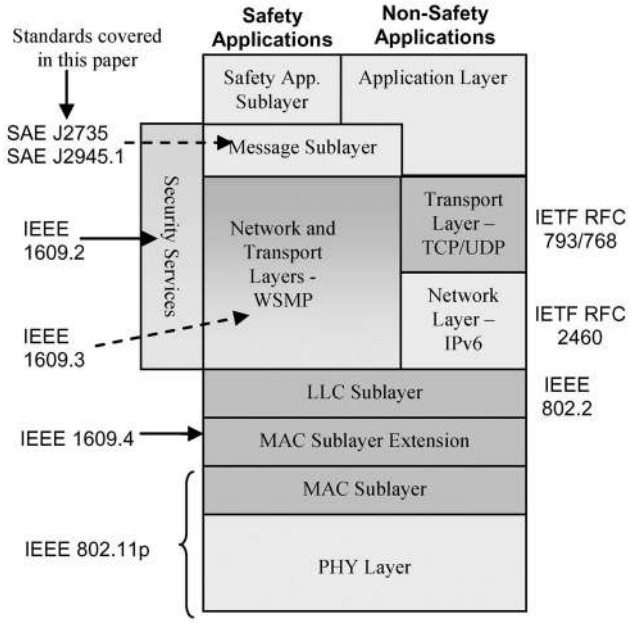

Figure 2.3 DSRC Network Stack [6]

The DSRC PHY layer protocol, as defined in IEEE 802.11 clause 17, is divided into two sublayers, the physical medium dependent (PMD) and the physical layer convergence procedure (PLCP) [7]. The PMD controls the wireless medium using orthogonal frequency division multiplexing (OFDM). The PLCP maps the MAC frame to an OFDM symbol. To transmit a symbol, PLCP receives the MAC frame and adds the PHY layer header to create the PHY protocol data unit (PPDU). The MAC sublayer also gives the PLCP the MAC frame length, the transmit data rate, and the transmit power. The PLCP then gives the PMD transmitter the coded bits of the PPDU for the OFDM signal, the data rate, and the transmit power [6]. The PMD will then pulse shape and modulate the bits to be sent. The PMD receiver on the target DSRC device will then demodulate the data and give the bits to the PLCP. The PMD receiver also determines the received signal strength indication (RSSI), which is used to check the quality of service (QoS). Then the PLCP extracts the MAC frame from the PPDU.

Similar to the PHY layer, the DSRC data link layer is also divided into two sublayers, the MAC sublayer and the LLC sublayer. The MAC sublayer controls when STAs may access the wireless medium to provide efficient use of the wireless channel. To control access, the MAC sublayer establishes the session based rules. The session based rules define the steps that an STA must take before it can communicate. IEEE 802.11 defines the concept of the Basic Service Set (BSS) as the set of STAs that wish to exchange information. There are two types of BSSs, infrastructure and independent, the first one being the more common. In an independent BSS, an access point (AP) STA announces the BSS and the parameters and constraints to join the BSS [6]. In order to communicate in an infrastructure BSS, the STA must first go through the setup process of receiving a beacon frame announcing the BSS, and then the STA must join, authenticate, and associate with the BSS. In an independent BSS, the STAs interact with each other, and the first one to declare a BSS must send out the beacon frame announcing a BSS. For DSRC, however, the setup time delay is not desirable for all communications. Instead, the IEEE 802.11p WAVE amendment defined “outside the context of a BSS” (OCB) to allow for STAs outside of a BSS to transmit. The STA can transmit to a MAC address that is related to either an individual or group of STAs. Communication using OCB eliminates the setup latency associated with BSSs [7]. In either setup, the medium access is controlled with carrier sense multiple access/ collision avoidance (CSMA/CA). The LLC uses the IEEE 802.2 protocol supplemented with subnetwork access protocol (SNAP). The protocol data unit (PDU) is the packet created by the LLC to transmit service to upper layers. PDUs can be exchanged in three ways, one for each type of LLC operation. In the first type of operation, PDUs are exchanged between LLCs without the need of an established data link connection. In the second type of operation, a data link connection is established between two LLCs prior to any exchange of PDUs containing information. In the third type of operation, PDUs are exchanged between LLCs without the need for an established data link connection, but stations are permitted to both send data and request data simultaneously [8].

As seen in the above Figure 2.3, IEEE 1609 is used at the network and transport layers of the DSRC protocol stack. IEEE 1609 has 3 main functions, multichannel operation, network services, and security. Additionally, the DSRC protocol stack splits into two branches above the LLC sublayer. The first uses the WAVE Short Message Protocol (WSMP), which is optimized for the non-routed data exchanges that are

common to vehicular networks. The second uses traditional Internet protocols, principally IPv6, UDP, and TCP.

Multichannel operation is established using the IEEE 1609.4 standard that defines a synchronization method for devices that are switching channels to locate each other. IEEE 1609.4 uses a control channel and time division to allow devices to find each other. Channel 178 is designated as the control channel (CCH) that devices will tune to on a regular basis as shown in Figure 2.2. The remaining channels are designated as service channels (SCH). In order to guarantee that devices will be on the control channel at the same time, time division is used to sync devices. Each time division is 100ms and is divided into two 50ms intervals, one for the CCH and one for the SCH. The intervals are also given a 4ms guard interval to account for any delays in the devices based on GPS clock and to allow for devices to change MACs. When a device wants to find another device, the device tunes to the CCH during the CCH interval. The CCH also broadcasts WAVE service advertisement (WSA) that identifies the available services on each SCH. The device will begin receiving frames as soon as it tunes to the CCH, however, it will not start transmitting frames until the guard interval is complete. If a device does not require a service, the device will remain on the CCH for the duration of the SCH interval, which is the following 50ms. Once a device determines a service to use from the WSA, the device will tune to the corresponding SCH at the end of the CCH interval and use the service(s) available on the SCH. The device will normally tune back to the CCH at the beginning of the next CCH interval. However, IEEE 1609.4 has an immediate departure option, where a device will tune to the CCH immediately following the completion of service. If the service takes longer than one sync interval, an extended access departure is implemented and the device will remain on the SCH until the service is completed and can tune back to the CCH during a CCH interval.

Network services in a DSRC network can be provided using either IP with TCP or UDP or the WAVE short message protocol (WSMP) network protocol. Some services require the implementation of a combination of multiple network protocols. In many traditional internets, the internet protocol (IP) is the network layer standard. IP provides a reliable routing capability given only the address of a device. In vehicular networks, many packets are sent directly from the source to the destination, without the use of routing. As a result, the need for the overhead of IP and UDP can be reduced. The WSMP was developed to accommodate the single hop transmissions associated with vehicular networks. A message sent using the WSMP is a Wave short message (WSM). The WSM format consists of the version, provider service ID (PSID), extension fields, the WSM WAVE element ID, and length followed by the payload. The version is a mandatory one byte field with 4 bits used to represent the version number and 4 reserved bits. Any packet with a version number higher than what a receiver is designed for will be dropped. The PSID indicates the service that the payload is associated with. PSIDs can range from 1-4 bytes in order to use bandwidth more efficiently. The extension fields are used to provide the flexibility of including or omitting an optional field. There are three parts to the extension field, the identifier, the length, and the contents. The identifiers are uniquely defined in the 1609.3 protocol. The length indicates how many bytes the contents field is since the contents can be of variable length. Currently the three extension fields are channel number, data rate in 500Kbps, and transmit power used in dB. The WSM WAVE

element ID is a mandatory one byte field that marks the end of the extension and the format of the payload. Finally, the length is the number of bytes contained in the payload.

The security services provided in a DSRC network are defined in the Security Services for Applications for Management Messages, IEEE 1609.2. The wave security services consist of security processing services that comprise secure data and WSAs and security management services that handle the validity of certificates and private keys [16]. These services ensure that the data is confidential and authentic. WAVE security require the implementation of the following capabilities: generate and verify signed data, encrypt and decrypt data, generate and verify signed WSAs, generate and verify certificate requests, and verify certificate revocation lists. Generating and verifying signed data and encrypting and decrypting data are required in order to provide secure data exchanges. IEEE 1609.2 generates and verifies signed data using Elliptic Curve Digital Signature (ECDSA). To encrypt and decrypt data, IEEE 1609.2 uses the Advance Encryption Standard in Counter with CBC-MIC (AES-CCM) for symmetric cryptography and Elliptic Curve Integrated Encryption Scheme (ECICS) for asymmetric cryptography.

The DSRC application layer consists of a message set defined in the SAE J2375 DSRC message set. The main message of concern from this set is the Basic Safety Message (BSM). SAE J2375 defines each of the messages, but all messages consist of a combination of data structures called data elements and data frames. A data element is the most basic data structure in J2375 and is used to build data frames. The BSM broadcasts a vehicle's position, speed, acceleration, direction, system status, and vehicle size. There are also optional fields available to convey additional information. Most of the messages in J2375 use Distinguished Encoding Rules (DER); but, since the BSM will consume the majority of bandwidth, DER is not used. DER encoding encodes each data element with an identifier, length, and contents. In a standard 39 byte BSM message, DER encoding would add an equal amount of overhead. Consequently, only a few elements in a BSM use DER encoding, the DSRC_MessageID and the BSM_Blob. They are each encoded separately since the BSM_Blob has fixed a length. The DSRC_MessageID is used to determine how to parse the data in a given message. The BSM_Blob is a complex data element that consists of 13 data elements: MsgCount, TemporaryID, DSecond, Latitude, Longitude, Elevation, PositionalAccuracy, TransmissionAndSpeed, Heading, SteeringWheelAngle, AccelerationSet4Way, BrakeSystemStatus, and VehicleSize. The MsgCount is 1 byte counter that increments by one for each transmission and used to calculate packet error rate (PER). TemporaryID is a 4 byte random number used to correlate streams of data to a sender. The value of the TemporaryID changes every few minutes. DSecond is a 2 byte data element with the current time modulo a minute. The Latitude and Longitude are 4 bytes that make up a GPS coordinate with the 2 byte elevation field. PositionalAccuracy is a 4 byte frame the standard deviation of the positional data. TransmissionAndSpeed is a 2 byte frame with the 3 most significant bits (MSB) devoted to the gear the vehicle is in and the 13 least significant bits (LSB) contain the speed in cm/second. The Heading is a 2 byte element that gives the compass heading of the vehicle in 1/80 degree increments. SteeringWheelAngle is a 1 byte field that gives the angle at which the steering wheel is turned in 1.5 degrees, where a negative number indicates a counter clockwise orientation. AccelerationSet4Way is 7 byte frame that gives the acceleration in the longitudinal, lateral, and vertical direction as well as the yaw rate. BrakeSystemStatus is a 2 byte frame that gives the status of the transmission control, anti-lock brakes, stability control, break boost, and auxiliary brakes. Finally,

VehicleSize is a 3 byte frame indicating the width and length of vehicle in cm. A diagram of the DSRC basic safety message described above, is given in Figure 2.4.

Figure 2.4 DSRC Basic Safety Message

Byte1	Byte2	Byte3	Byte4	Byte5	Byte6	Byte7	Byte8
DSRC_MessageID	MsgCount	TemporaryID				DSecond	
Latitude				Longitude			
Elevation		PositionalAccuracy				TransmissionAndSpeed	
Heading		SteeringWheelAngle		AccelerationSet4Ways			
AccelerationSet4Ways (cont.)		BrakeSystemStatus		VehicleSize			

The DSRC_MessageID in combination with the BSM_Blob make up the required data fields in a BSM. However, there are four optional fields that may be included, the EventFlags, PathHistory, PathPrediction, and RTCMPackage. The EventFlags are used to indicate that a specific event occurred. The PathHistory and PathPrediction convey where the vehicle has been and where the vehicle expects to go. Finally, the RTCMPackage conveys the GPS correction data in the RTCM format.

2.2.2 Description of VT DSRC simulator

In order to effectively characterize the channel under which data is being sent while a train is moving through various terrains, an understanding of the PHY layer that DSRC operates in is necessary. At Virginia Tech, a DSRC PHY layer simulator was developed to compare the performance of IEEE 802.11a and IEEE 802.11p, otherwise referred to as WAVE, and the performance of IEEE 802.11p in Rayleigh and Rician fading. Rayleigh fading is the result of multipath fading where the same signal arrives at the receiver but from different paths, resulting in interference. Rician is similar to Rayleigh fading in that they are both a result of multipath propagation, but in the Rician model there is a prominent Line of Sight (LOS) component because there is a clear path from the transmitter to the receiver. The simulator leverages the fact that IEEE 802.11a and IEEE 802.11p are functionally the same except for the operating frequency.

The simulator was built in Matlab using Simulink, a graphical programming environment for modeling and simulating systems. The simulator is made up of four main components, the transmitter block, noise environment block, receiver block, and performance analysis block. The transmitter block generates a random sequence of bits. These bits are then modulated according to one of the available modulation schemes either BPSK ½, BPSK ¾, QPSK ½, QPSK ¾, 16-QAM ½, 16-QAM ¾, 64-QAM ⅔, or 64-QAM ¾. The OFDM symbol size is dependent on the modulation scheme, which, in turn, will also affect the frame size. The OFDM symbol size for each modulation scheme is 1, 1,2,2,4, 4, 6, and 6 respectively resulting in a frame size of 480, 720, 960, 1440, 1920, 2880, 3840, and 4320 respectively. After the bits are modulated, the bits are then OFDM modulated. As in IEEE 802.11a, a pilot addition and a training sequence are attached and then the bits are transmitted. Noise is then added to the bits based on the noise environment set by the user. Both Rayleigh and Rician fading are supported. However, Additive White Gaussian Noise (AWGN) is added in the noise environment for all simulations regardless of the fading model chosen. The receiver will then demodulate the data and remove the training sequence and the pilot.

To analyze the performance, the original bits are compared with the received bits to calculate bit error rate (BER). The analyzer also calculates Signal-to-Noise Ratio (SNR) and E_b/N_0, which is a normalization of SNR per bit. The results show that at the same SNR, IEEE 802.11a and IEEE 802.11p behave the same with IEEE 802.11p having slight, almost negligible, SNR advantages in some modulation schemes as shown in Figure 2.5. The performance of IEE 802.11p in Rayleigh and Rician fading models shows that for large K-factors, the performance is similar to AWGN. For small K-factors there is approximately 1-dB improvement in SNR when the K-factor is reduced by 1 as shown in Figure 2.6 on the following page.

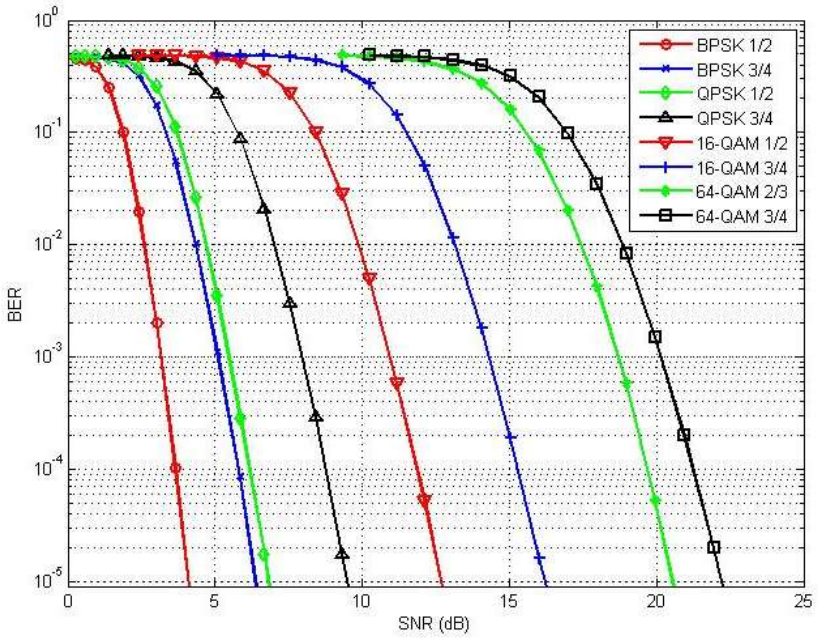

Figure 2.5 Comparison between IEEE 802.11a and 802.11p

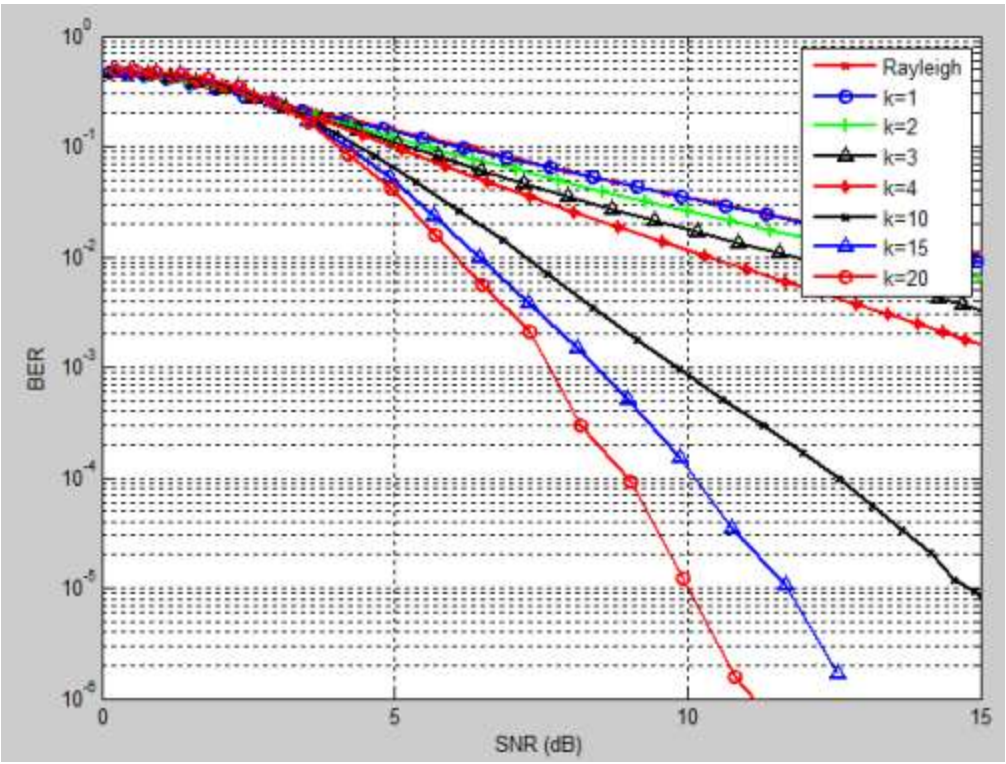

Figure 2.6 Performance of IEEE 802.11p in Rician and Rayleigh fading environments

In current literature, there are very limited papers on the performance of IEEE 802.11p. Often times these papers have inaccurate results that do not provide consistent results or do not follow the DSRC standard accurately. The VT DSRC Simulink based simulator follows the IEEE 802.11p standard to better aid future research on DSRC by providing a realistic physical layer simulator. Although the simulator currently includes only AWGN, Rayleigh fading and Rician fading, its modular design allows for the addition of other fading models. Modifications to the performance analyzer will allow performance to be measured using addition metrics to BER. The Simulink-based simulator's purpose is to provide a reference for use in future research on DSRC radios.

2.3 Terrestrial propagation models applicable to 5.9 GHz in line-of-sight and obstructed channels

2.3.1 Wireless Propagation

In a wireless system, electromagnetic waves are exchanged between the transmitting and receiving antennas. When an electromagnetic wave collides with an object, the direction of propagation will be altered due to reflection, diffraction, or scattering. Figure 2.7 illustrates the phenomenon on the following page.

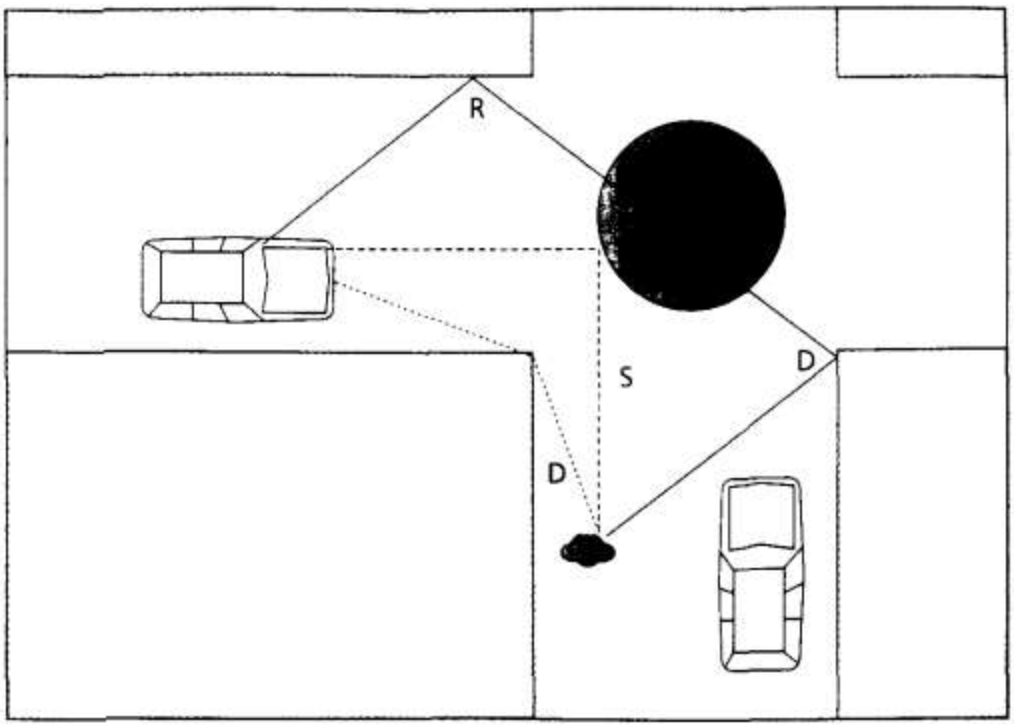

Figure 2.7 Diagram of Reflection (R), Scattering (S), and Diffraction (D) [17]

Reflection occurs when a propagating signal collides with an object that is significantly larger than the signal's wavelength. Reflected instances of the signal may cause either constructive or destructive interference at the receiver. A signal is diffracted if the receiver and transmitter are blocked by an impenetrable object. Scattering occurs when the wireless channel contains objects that are of similar or smaller dimensions than the wavelength of the transmitted signal. The signal is then unpredictably redirected in many directions. Depending on the environment, one of the propagation mechanisms will be dominant. Reflection is more dominant in a LOS propagation environment, while scattering is more likely to occur in a non-LOS environment [17]. The combination of scattering and reflecting results in multipath propagation. Multipath occurs when multiple instances of the signal arrive at the receiver with various delays and attenuation. The LOS signal will arrive at the receiver first with no delay and the subsequent received signals will have non-zero excess delay. The different phases can result in destructive interference which will degrade the signal quality.

2.3.2 Channel Modelling

Understanding how the channel behaves in different environments is important for designing a wireless communication system, like the proposed railroad alert system, that provides optimized service to the system's users. DSRC systems have a nominal range of 1.0 km [6]. However, the range is highly sensitive to the surrounding environment and can be significantly reduced in cluttered or non-line-of-sight conditions that occur at many railroad grade crossings [13]. The DSRC waveform does contain mechanisms that allow for the development of highly reliable and robust communications; thus,

development of communication protocols that can effectively operate in cluttered railroad grade crossing environments is the key to providing an extremely reliable early warning and collision avoidance system.

Channel modeling, or channel characterization, is used to understand how the propagation channel impairs and distorts the transmitted signal in a specific environment [18]. These distortions are the result of multipath fading where the signal arrives at the receiver from different paths due to reflection and scattering. A terrestrial propagation model will consider the physical propagation environment and its effects on multipath fading to characterize a channel [20]. Channel modeling is a simplification of the terrestrial propagation channel based on the most influential aspects of the channel's performance. Most channel models characterize the path loss and the fading statistics of the channel to provide an accurate representation of the propagation environment. Path loss describes how the average received power varies with distance between the transmitter and the receiver, while the fading statistics describe how the instantaneous receiver power varies over time [18]. The goal is to derive parameters for a model to accurately describe how the signal strength will vary over distance and time.

2.3.2.1 Large-Scale Path Loss

Large-scale path loss predicts the average received signal strength at a given distance away from the transmitter. Large-scale propagation models estimate the local average received power over many wavelengths of the carrier frequency [22]. A signal will have less variation over longer distance because the number of multipath signals converging at the receiver tends to be smaller. The actual path loss a signal experiences measures the difference between the transmit power and the received power [22].

Theoretical approaches tend to require knowledge of the environment that is under testing. Empirical approaches, on the other hand, fit curves to the measured data. The empirical approach accounts for all propagation factors without needing to know the specific behavior. There are three empirical path loss models that are typically adopted, the log-distance, log-normal, and dual-slope path loss models.

2.3.2.1.1 Log-Distance Path Loss Model

Received signal power has been shown, both in theoretical and in measured data, to decrease logarithmically with distance. The path loss is then given by (2.1) taken from [22].

$$PL_{dB}(d) = \mathrm{PL}_{dB}(d_0) + 10nlog\left(\frac{d}{d_0}\right) \quad (2.1)$$

Where the d_0 is the close-in reference distance, determined from measurements near the transmitter, and n is the path loss exponent that indicates the rate at which the path loss increases with distance, d [22]. The path loss exponent n will change with the environment. Table 2.1 gives some common n values. Choosing a referencing distance is also important to establish an accurate model. Depending on the range of the cellular system, d_0 needs to be adjusted. For large cellular systems often 1km is used and for smaller systems, a smaller d_0 is chosen. The path loss at d_0 can be found using the following equation

$$PL_{dB}(d_0) = 20\log_{10}\left(\frac{4\pi}{\lambda}\right) \quad (2.2)$$

Where

$$\lambda = \frac{c}{f} \quad (2.3)$$

c is the speed of light, *f* is the carrier frequency of the signal, and λ is the resulting wavelength.

Table 2.1 Path Loss exponents for Different Environments

Environment	Path Loss Exponent, *n*
Free space	2
Urban area cellular radio	2.7 to 3.5
Shadowed urban cellular radio	3 to 5
In building line-of-sight	1.6 to 1.8
Obstructed in building	4 to 6
Obstructed in factories	2 to 3

2.3.2.1.2 Log-Normal Shadowing

The above model assumes that the surrounding environment will have uniform obstructions, which is not always a safe assumption. Measurements have shown that at any distance *d*, the path loss at that location is random and follows a log-normal distribution. That is

$$PL_{dB}(d) = \mathrm{PL}_{dB}(d_0) + 10nlog\left(\frac{d}{d_0}\right) + X_\sigma \quad (2.4)$$

Where *X* is a zero mean Gaussian random variable with standard deviation σ in dB [22].

The log-normal distribution describes the random shadowing effects that occur over a large number of measurement locations which have the same transmitter to receiver separation distance, but have different levels of clutter on the propagation path. When this phenomenon occurs, it is referred to log-normal shadowing. Log-normal shadowing suggests that measured signal levels at a specific transmitter to receiver separation distance have a Gaussian distribution about the distance-dependent mean of d_0, where the measured signal levels have values in dB units. The standard deviation of the Gaussian distribution that describes the shadowing also has units in dB. Thus, the random effects of shadowing are accounted for using the Gaussian distribution. More accurate models will consider using other distributions, like the small-scale fading distributions that will be discussed in section 2.3.2.3 because these distributions better model the variation of the signal in a given environment more reliably.

Log-normal path loss models are computed using linear regression techniques. From the regression, the path loss exponent, *n*, is derived. The standard deviation can also be calculated for Gaussian distributed data. The random variable X can be substituted with a more accurate small scale fading model that will be described in section 2.3.2.3 and the corresponding parameters will also have to be derived based on the empirical data.

2.3.2.1.3 Dual-Slope Path Loss Model

In vehicular channel modelling, it has been shown in both [23] and [24] that a dual-slope path loss model can better model the path loss in a vehicle to vehicle communication setting because of the

constantly fluctuating LOS and non-LOS conditions encountered on the highway and in urban environments.

The dual-slope path loss model is a piecewise extension of the log-normal path loss model and can be expressed as the following piecewise function [21]

$$PL(d) = \begin{cases} \mathrm{PL}_{dB}(d_0) + 10n_1 log\left(\frac{d}{d_0}\right) + X_{\sigma_1} & if\ d \le d_0 \\ \mathrm{PL}_{dB}(d_0) + 10n_1 log\left(\frac{d_b}{d_0}\right) + 10n_2 \log\left(\frac{d}{d_b}\right) + X_{\sigma_2} & if\ d > d_b \end{cases} \quad (2.5)$$

Where d_b is considered the breakpoint at which the first Fresnel zone touches the ground, and n_1 and n_2 are the path loss exponents for the dual-slopes.

Fresnel zones represent consecutive regions where multipath waves have a path length from the transmitter to receiver which are nλ/2 greater than the total path length of a line-of-sight path [22]. Waves that hit the ground at these points will result in constructive interference. The first Fresnel zone is considered the point at which a wave has traveled d_b+λ/4 to reach the receiver [23]. The breakpoint distance can then be calculated as

$$d_b = \frac{4h_{TX}h_{rx} - \frac{\lambda^2}{4}}{\lambda} \quad (2.6)$$

Where λ is the wavelength and h_{TX} and h_{RX} are the heights of the transmitter and receiver respectively. It has also been shown in [24] that the using a breakpoint distance less than the theoretical breakpoint distance can provide a better fit. The more commonly used breakpoint distances are in the 100m-200m range.

The dual-slope path loss modeling provides more flexibility to model the data since the data can be broken into groups where different propagation behavior maybe observed.

2.3.2.2 Small Scale Fading Channel Parameters

Multipath channel parameters describe how specific aspects of the channel behave given specific conditions. These parameters help to develop a channel model. The parameters can be used to compare with existing channel models that can be modified to fit the new channel's parameters. The key parameters to channel modeling are the power delay profile (PDP), the root mean square (RMS) delay spread, the Doppler shift, and the Doppler spread.

2.3.2.2.1 Power Delay Profile

The PDP is a graph of the received signal strength versus excess delay and gives an indication of the impact that multipath has on the channel. Each point in the environment the channel is considered a linear filter with an impulse response h(t). Taking the spatial average of $|h(t)|^2$ in a local area for several locations will derive the PDP for that given area [21]. Typically, this is done using a channel sounder. The PDP gives the received signal intensity as a function of the time delay due to multipath propagation, represented as P(τ), where τ is the delay [22]. When a channel is affected by multipath propagation,

dispersion affects the transmitted signal. The power delay profile provides a measure of the dispersion of the transmitted power over different paths in a multipath propagation model. An example of a PDP is given in Figure 2.8 below.

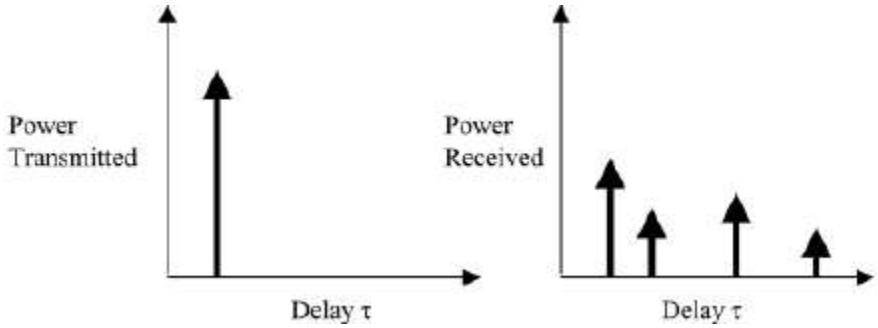

Figure 2.8 Example PDP [25]

2.3.2.2.2 Root Mean Square Delay Spread

To understand the RMS delay spread, the maximum excess delay (MED) needs to be defined. The MED is the maximum delay such that the received power drops X dB below the maximum received power, where X is a defined real number [22]. The MED represents the average delay of the area. In Figure 2.9 below, the maximum excess delay is shown as the point where the signal falls 10 dBm below the peak received signal level.

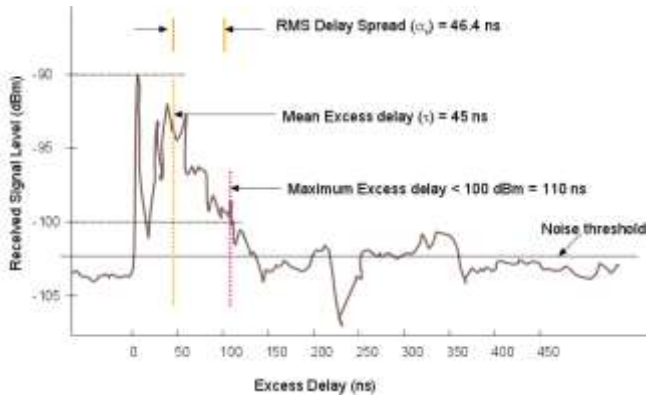

Figure 2.9 Example Mean Excess Delay [22]

Mean excess delay can be defined as [22]

$$\bar{\tau} = \frac{\sum_{i=0}^{N-1} \tau_i P(\tau_i)}{\sum_{i=0}^{N-1} P(\tau_i)} \quad (2.7)$$

The RMS delay spread represents the variation of the delay of the multipath signals. Delay spread is a measure of multipath presence in a wireless communication channel and is defined as the difference between the first received multipath component, typically the LOS component, and the most recent multipath component [22].

The RMS delay spread is then defined as

$$\sigma_\tau = \sqrt{\overline{\tau^2} - (\overline{\tau})^2} \quad (2.8)$$

Where

$$\overline{\tau^2} = \frac{\sum_{i=0}^{N-1} \tau_i{}^2 P(\tau_i)}{\sum_{i=0}^{N-1} P(\tau_i)} \quad (2.9)$$

The RMS delay spread gives an indication of the amount of Inter-Symbol Interference (ISI). Consequently, the effects of dispersion can be directly related to the RMS delay spread.

2.3.2.2.3 Doppler Shift

A Doppler shift occurs from a transmitter or receiver moving during a transmission. As the mobile unit moves at a constant velocity, v, from point X to point Y, the distance the signal has to travel changes. As a result, a phase shift occurs from the change in distance between the transmitter and receiver [22]. The phase shift is calculated as follows based on the following figure

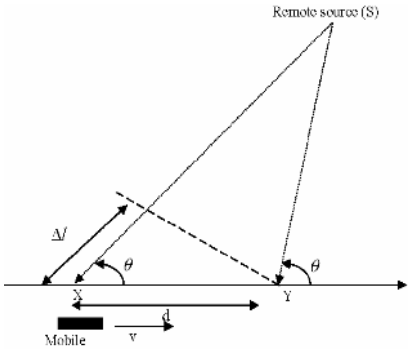

Figure 2.10 Diagram of a Doppler Shift [22]

$$\Delta\varphi = \frac{2\pi v \Delta t}{\lambda} \cos\theta \quad (2.10)$$

2.3.2.2.4 Doppler Spread

Signals traveling along different paths can have different Doppler shifts, corresponding to different rates of change in phase. The difference in Doppler shifts between different signal components contributing to a single fading channel tap is known as the Doppler spread. RMS Doppler spread is the measure of the spectral broadening caused by the velocity of the mobile radios and is the range of frequencies that the Doppler spectrum is non-zero [22].

The Doppler spread can be calculated similarly to the delay spread using the following equations [22]:

$$\sigma_\omega = \sqrt{E[\omega^2] - (E[\omega])^2} \quad (2.11)$$

where

$$E[\omega^n] = \frac{\sum_{i=0}^{N-1} \omega_i{}^n S(\omega_i)}{\sum_{i=0}^{N-1} S(\omega_i)} \quad (2.12)$$

Where S(ω) is the power spectrum of the signal.

2.3.2.3 Fading

Based on the dispersion characteristics of the channel, the channel will undergo various fading. Fading describes the rapid fluctuations of the amplitude, phase, or multipath delay of a signal over a short period of time or distance. The fading model will model the variation of the signal in time, as opposed to the large scale path loss model that predicts the signal strength over a given distance. Multipath propagation causes fading because different instances of the signal arrive at the receiver at the same time. Fading occurs from both multipath delay spread and the Doppler spread. However, fading due to Doppler spread does not affect the propagation path loss model [22]. Two types of fading are associated with multipath delay spread, flat fading and frequency selectivity. Flat fading occurs when the bandwidth of signal is less than the bandwidth of the channel and the delay spread is less than the symbol period. Frequency selectivity occurs when the bandwidth of the signal is greater than the bandwidth of the channel and the delay spread is greater than the symbol period. Similarly, there are two types of fading associated with the Doppler spread, fast and slow fading. Fast fading occurs when there is a high Doppler spread. Consequently, the channel varies faster than the baseband signal varies. Slow fading occurs when there is low Doppler spread and the baseband signal will vary faster than the channel will vary [22].

2.3.2.3.1 Rayleigh and Rician Fading Models

Fading due to multipath delay spread can be represented by statistical models. Typically, a Rayleigh fading model is used to describe the statistical time varying behavior of the received envelope of a flat fading signal. The Rayleigh distribution has the following probability density function [22]:

$$p(r) = \begin{cases} \frac{r}{\sigma^2} \exp\left(-\frac{r^2}{2\sigma^2}\right) & (0 \le r \le \infty) \\ 0 & (r < 0) \end{cases} \quad (2.13)$$

Where σ is the RMS value of received signal before envelope detection and σ^2 is the time average power of the received signal before envelope detection. Typically, σ^2 is found from taking the expected power of the received.

$$E[r^2] = 2\sigma^2 \quad (2.14)$$

When there is a line of sight component, the Rayleigh distribution can be modified to a Rician distribution. As a result the received signal will be a multipath components superimposed on a stationary dominant signal. The Rician distribution is given by [22]

$$p(r) = \begin{cases} \frac{r}{\sigma^2} \exp\left(-\frac{r^2 + A^2}{2\sigma^2}\right) I_0\left(\frac{Ar}{\sigma^2}\right) & (A \geq 0, r \geq 0) \\ 0 & (r < 0) \end{cases} \quad (2.15)$$

The parameter A denotes the maximum amplitude of the LOS component. $I_0(\bullet)$ is the modified Bessel function. The Rician distribution is usually given in terms of the parameter K which is the ratio between the maximum amplitude of the LOS component and the variance of the multipath signal. The parameter K completely specifies the Rician distribution. K is given by the following:

$$K = \frac{A^2}{2\sigma^2} \text{ or } K(dB) = 10\log\left(\frac{A^2}{2\sigma^2}\right) \quad (2.16)$$

Where A and σ^2 have the following relationship

$$E[r^2] = 2\sigma^2 + A^2 \quad (2.17)$$

Often times, discerning A from the variation σ is not easily computed. K can then be estimated using the moment method estimation [26]. Where the received signal [26]

$$g(t) = V + v(t) \quad (2.18)$$

is composed of a complex constant value V and v(t) is a complex zero mean time variant process. Taking the time average of the power gain, $G = |g(t)|^2$, the average power gain can be written as

$$G_a = |V|^2 + \sigma^2 \quad (2.19)$$

Then the variance of the power gain can be calculated as

$$G_v{}^2 = E[(G - G_a)^2] = [\sigma^4 + 2|V|^2\sigma^2] \quad (2.20)$$

Then rewriting in terms of V and σ [26]

$$|V|^2 = \sqrt{\left[G_a{}^2 - G_v{}^2\right]} \quad (2.21)$$

$$\sigma^2 = G_a - \sqrt{\left[G_a{}^2 - G_v{}^2\right]} \quad (2.22)$$

Finally K is then written as

$$K = \frac{|V|^2}{\sigma^2} \quad (2.23)$$

2.3.2.3.2 Nakagami and Weibull Fading Models

The Nakagami and Weibull fading models provide a more generalized version of the Rayleigh fading model. The Nakagami model is parameterized by the fading severity, while the Weibull model provides more flexibility to model Nakagami shapes.

The Nakagami model has the probability distribution function [21]:

$$\mathrm{p}(\mathrm{r};\mathrm{m},\Omega) = \frac{2\mathrm{m}^{\mathrm{m}}}{\Gamma(\mathrm{m})\Omega^{\mathrm{m}}}\mathrm{r}^{2\mathrm{m}-1}\exp(-\frac{\mathrm{m}}{\Omega}\mathrm{r}^{2}) \quad (2.24)$$

Where

$$\mathrm{m} = \frac{\mathrm{E}^{2}[\mathrm{r}^{2}]}{\mathrm{VAR}[\mathrm{r}^{2}]} \quad (2.25)$$

and

$$\Omega = \mathrm{E}[\mathrm{r}^{2}] \quad (2.26)$$

In the probability distribution function given by (2.24), *r* is the amplitude of the received signal, Ω is the average received power of the signal, and *m* is the inverse of the normalized variance of r^2. $\Gamma(\bullet)$ is the gamma function. The Rayleigh distribution is achieved when m = 1. Nakagami distributions tend to fit well in urban environments. The Nakagami distribution is usually the preferred model in mobile environments because of its ability to model fading scenarios worse than Rayleigh fading. [21].

Deriving an appropriate m value from measured data requires estimation using moments. The k^{th} moment,μ_k, for a Nakagami random variable, R, is defined as [27]

$$\mu_k = E[R^k] = \frac{1}{N}\sum_{i=1}^{N} {r_i}^k = \frac{\Gamma\left(m+\frac{k}{2}\right)}{\Gamma(m)}(\frac{\Omega}{m})^{\frac{k}{2}} \quad (2.27)$$

Then rewriting in terms of moments

$$\frac{\Gamma\left(m+\frac{k}{2}\right)}{\Gamma(m)m^{\frac{k}{2}}} = \frac{\mu_k}{{\mu_2}^{\frac{k}{2}}} \quad (2.28)$$

Unfortunately for odd k, transcendental equations must be solved toe find m. Additionally, when k=2, (2.28) reduces to identity, 1=1, but; for k = 4, m can be found as

$$m = \frac{{\mu_2}^2}{\mu_4 - {\mu_2}^2} \quad (2.29)$$

According to [27], this closed form expression is referred to as the inverse normalized variance estimator. However, [28] found that a better moment based estimator could be derived if non-integer moments were included. The new random variable X is then defined as

$$X_i = {R_i}^{1/p} \quad (2.30)$$

Then (2.27) is rewritten as

$$E[X^k] = E\left[R^{k/p}\right] = \frac{1}{N}\sum_{i=1}^{N} {r_i}^{k/p} = \frac{\Gamma\left(m+\frac{k}{2p}\right)}{\Gamma(m)}(\frac{\Omega}{m})^{\frac{k}{2p}} \quad (2.31)$$

For a given p, the ratio of any two moments of X can be solved to find m. Unfortunately, this also usually results in solving transcendental equations again. However, taking the ratio of the $(2p+1)^{th}$ moment and the first moment of X, the following ratio is derived.

$$\frac{E[X^{2p+1}]}{E[X]} = (1 + \frac{1}{2mp})\Omega \quad (2.32)$$

Rewriting in terms of m

$$m = \frac{E[X]\Omega}{2p(E[X^{2p+1}] - E[X]\Omega} \quad (2.33)$$

This results in a new family of estimators to find the fading parameter m, which is denoted as $m_{1/p}$

$$m_{\frac{1}{p}} = \frac{\mu_{\frac{1}{p}}\mu_2}{2p(\mu_{2+\frac{1}{p}} - \mu_{\frac{1}{p}}\mu_2)} \quad (2.34)$$

For p = ½, the estimator in (2.29) is derived, and when p = 1, a new estimator is found.

$$m = \frac{\mu_1\mu_2}{2(\mu_3 - \mu_1\mu_2)} \quad (2.35)$$

The resulting estimator (2.35) has less variance than the estimator in (2.29) because the higher order moments will deviate more from the true moment than lower order moments. These results are confirmed in [28].

The Weibull distribution uses parameters that shift the distribution between an exponential and Rayleigh distribution. The Weibull model has the following probability distribution function [21]

$$\mathrm{p}(\mathrm{r};\alpha,\mathrm{b}) = \frac{\alpha \mathrm{b}}{\mathrm{r}_0}\left(\frac{\mathrm{br}}{\mathrm{r}_0}\right)^{\alpha-1} \exp\left(-\left(\frac{\mathrm{br}}{\mathrm{r}_0}\right)^{\alpha}\right) \quad (2.36)$$

Where

$$\mathrm{b} = \sqrt{\frac{2}{\alpha}\Gamma\left(\frac{2}{\alpha}\right)} \quad (2.37)$$

Here, α is a shape parameter to better fit the distribution and b is a normalization factor. When α = 1/2, the distribution becomes a Rayleigh distribution. The Weibull distribution models both indoor and outdoor environments.

2.3.2.4 Existing Channel Models

There are many existing channel models for established wireless communications. However, the majority of existing wireless communication system models do not account for the high mobility of DSRC systems. In DSRC systems, transmitters and receivers will have high mobility and low antenna elevations [18]. These characteristics increase the probability that the link will be obstructed. Consequently, the existing cellular models cannot be directly used to determine a DSRC system's performance. The high mobility of a DSRC system also subjects the channel to both time-dispersion and frequency-dispersion. The main parameters of interest for DSRC networks are then the environment (urban, suburban, and

rural), vehicle speeds, and direction of transmission. New channel models are being derived to model V2V channels which can be used as a building block for Train to Vehicle channel modelling.

2.3.2.4.1 Large-Scale Path Loss

In most recent literature pertaining to large-scale path loss in vehicle to vehicle communications, the dual-slope path loss model has been adopted because of the flexibility to model LOS and non-LOS aspects of the channel.

In [31] a measurement campaign was conducted using DSRC prototypes at 5.9 GHz. Their measurement system consisted of a transmitter and receiver. The transmitter was made up of 2 signal generator to achieve the 5.9 GHz carrier frequency, a low pass and a bandpass filter to filter out harmonics, and amplifiers to account for the attenuation of the signal from the two signal generators. The receiver was comprised of a low noise amplifier to increase sensitivity, a high pass filter to filter isolate the signal, a down converter and signal analyzer to digitize the data. GPS data was also recorded to help accurately synchronize the data. Measurements were conducted in suburban environments only. To compute the large-scale path loss model, the received signal strength and distance between the transmitter and receiver were calculated. A dual-slope model was chosen to fit the data since the measured data showed a distinct change in slope after a certain distance. Originally, the breakpoint distance, d_b, was calculated using the method described in (2.6 above, but an engineering decision was made to use a d_b = 100m to decrease the standard deviation of fitted model. The following results were found for the large-scale path loss

Table 2.2 Large Scale Path Loss Model Parameters

Parameter	Data Set 1	Data Set 2
Path Loss Exponent n_1	2.1	2
Standard Deviation σ_1 (dB)	2.6	5.6
Path Loss Exponent n_2	3.8	4
Standard Deviation σ_2 (dB)	4.4	8.4
Breakpoint Distance d_b (m)	100	100

[23] also conducted a measurement campaign at 5.6 GHz. Measurements were conducted using the RUSKLUND channel sounder, which performs multiple-input multiple-output (MIMO) measurements based on the switched array principle. Two standard 1.47 m high station wagons, Volvo V70 cars, were used during the measurement campaign. An omnidirectional antenna was placed on the roof of the transmitting and receiving vehicles. Videos were taken through the windscreen of each car and GPS data was also logged during each measurement. Both highway and urban environment measurements were conducted. To derive the large scale fading model, the effects of small scale fading were filtered out by taking the average of the received signal strength over a distance of 15λ. The data was then divided into LOS, non-LOS, and obstructed LOS based on the video data recorded. Then the data was fit to dual-slope path loss model. The non-LOS, however, did not have enough data points to fit a model to. The results are given in Table 2.3 on the following page.

Table 2.3 Large-Scale Path Loss Model Parameters

Parameter		LOS	Obstructed LOS
Path Loss Exponent n_1	Urban	-1.81	-1.93
	Highway	-1.66	none
Standard Deviation σ_1 (dB)	Urban	4.15	6.67
	Highway	3.95	6.12
Path Loss Exponent n_2	Urban	-2.85	-2.74
	Highway	-2.88	-3.18
Standard Deviation σ_2 (dB)	Urban	4.15	6.67
	Highway	3.95	6.12
Breakpoint Distance d_b (m)	Urban	104	104
	Highway	104	104

2.3.2.4.2 Small-Scale Fading

The most common method to develop a channel model is to use the stochastic method. Deterministic methods can also be used to derive a channel model. However, these methods tend to be computationally intensive because deterministic methods solve Maxwell's equations or use analytical descriptions of basic propagation mechanisms to characterize the physical channel parameters [18]. Deterministic methods require a geographical description of the physical environment and of the electromagnetic properties of the objects in the environment [18]. Consequently, deterministic methods provide a very specific channel model for a given environment. Stochastic methods use measured channel data and does not require an understanding of the environmental geometry [18]. Stochastic methods will also produce an environment specific channel model; but, because of the large amount of data used to derive the channel, the model is able to be applied to similar environments.

Stochastic models describe the random distribution that the channel parameters behave. A commonly adopted stochastic model used a Tapped Delay Line (TDL) channel model with a Weibull distribution. A TDL channel model is used frequently to describe the impulse response of a multipath channel with a discrete number of impulses [25]. The impulse response is given as follows[25]:

$$h(t,\tau) = \sum_{i=1}^{N} c_i(t)\delta(\tau - \tau_i) \qquad (2.38)$$

The impulse response will vary with time. There will be N coefficients, $c_i(t)$, that also vary with time. Choosing N and τ_i will depend on what above a specified noise threshold. The following figure shows a 4-tap model.

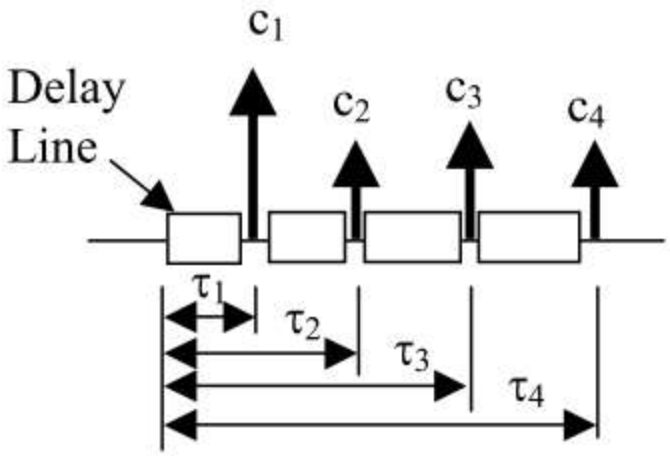

Figure 2.11 Tapped Delay Line Impulses [25]

In [29], a Tapped delay line was created using a Weibull distribution to model the taps. They conducted measurements to develop a V2V channel model. Data was collected data using two vans traveling through urban, rural, and highway environments using a channel sounder centered at 5.12GHz. The channel sounder collects PDPs to measure and statistically characterize the CIR and propagation path loss. They developed a tapped delay line CIR, however a persistence process was incorporated that accounts for a propagation path disappearing. Since the environment was constantly changing the persistence process turns off certain multipath propagation components that fall below a certain power threshold, in this case 25 dB from the main tap. A Weibull distribution was fit to determine whether a tap was on or off based on the PDP data. The RMS delay spread was also calculated for each environment. The RMS delay spread results are given in the following table

Table 2.4 RMS delay spread (nano seconds)

Region	Min	Mean	Max
Urban (antenna in car)	2.7	236	1210
Urban (antenna outside car)	3	125.8	1328.6
Highway, low traffic	0.3	53.2	1113.4
Highway, high traffic	0.5	126.8	1773.4
Small city	0.7	160	1276

Other studies have modelled the channel using existing fading models to predict the received signal strength. In [30], a Rician fading model was developed to show the probability of a received signal was lower than a certain level. [30] conducted a similar measurement campaign to [29]. A transmitter and receiver with operating frequency 5.2GH on broadband radio local area networks were used to characterize the noise seen in the channel. The system was used in urban, suburban, and highway vehicle scenarios. However, the results for urban and suburban were found to closely mirror each other. To characterize the fading statistics, the cumulative distribution function (CDF) is calculated to show the probability the received signal level is below a certain value, which can be used to identify probability of

signal loss. The campaign found that among the Nakagami, Rayleigh, and Rician distributions, the Rician distribution fit the CDF best because of the large number of LOS situations they tested in.

Finally, from the same measurements conducted in [31], the fading characteristics were then modeled using a Nakagami distribution. The results showed that as the Nakagami distribution showed Rician fading behavior the closer the vehicles were together and tended towards Rayleigh fading as the vehicles got further apart.

3 Approach / Methodology

3.1 DSRC measurements and analysis

3.1.1 Measurement Configuration

The performance of the DSRC system was evaluated while operating on two different stretches of railroad track, to provide different testing environment scenarios, the railroad test track (RTT) and precision test track (PTT). A DSRC on-board unit (OBU) was installed on the locomotive engine and a DSRC road-side unit (RSU) and an OBU were installed at three different locations off to the side of the railroad and precision test tracks. Both the RSU and OBU installed on the side of the track were stationary. The RSU is stationary because in a real DSRC network, the RSUs will be mounted on the side of roads as a permanent structure. The OBU on the side of the track was stationary for safety reasons. The PTT location had physical obstructions installed to evaluate the performance of DSRC in an obstructed environment. Two different antennas were installed on the locomotive at locations that TTCI specified. DSRC performance data were recorded for two laps around the track for each antenna and for several different speeds. GPS coordinates of the locomotive were recorded at a rate of 10 Hz.

3.1.2 TTCI

Test site 1 (RTT) is located in an open environment and has a longer distance to test over, compared to test site 2 (PTT). A diagram of the test tracks is given on the following page in Figure 3.1. The results collected from test site 1 can represent a somewhat unobstructed environment because of the open space and longer track. The RTT test site data is used to represent a rural highway-rail grade crossing.

Test site 2 (PTT) is near one of the locomotive maintenance buildings, and is used to mimic an urban/suburban grade crossing. All the radio devices are placed near buildings. Also a set of 8 railroad cars was positioned along the mag-lev track adjacent to the PTT with separation distance of 30 feet, to mimic two-lane roads; the concept is illustrated in Figure 3.2, although in the measurements hopper cars were used in place of the locomotives shown in Figure 3.3 (b).

Figure 3.1 Diagram of test sites at TTCI

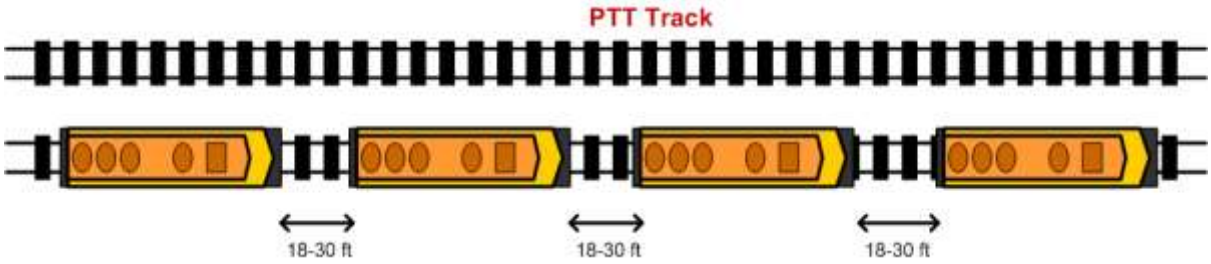

Figure 3.2 Diagram of PTT track setup

For DSRC measurements at TTCI, one DSRC OBU was installed on the locomotive engine and operated on channel 174 or 178. The DSRC RSU and remaining DSRC OBU were located at wayside locations. The RSU was mounted on a bucket truck while the OBU was mounted on a car. For each of the test sites, the locomotive engine made a “pass” through the measurement region. For each pass, the locomotive engine accelerated to the desired test speed and maintained a constant speed through the test area, and then decelerated to a stop after it passed beyond the test area. Figure 3.3 shows the location of the RSU and OBU for test site 1.

The wayside units have the following physical configurations:

RSU #1 was installed about 15~17 feet high by using a bucket truck at a distance of 40 feet from the track centerline.

OBU #2 was installed about 6 feet high on a simulated vehicle located at a perpendicular distance of 50 or 200 meters from the grade crossing; the distances are chosen based on reasonable minimum and maximum stopping distances for wet pavement as discussed in the requirement section.

The antennas of OBU #1 are installed about 5 inches higher than the top of the locomotive.

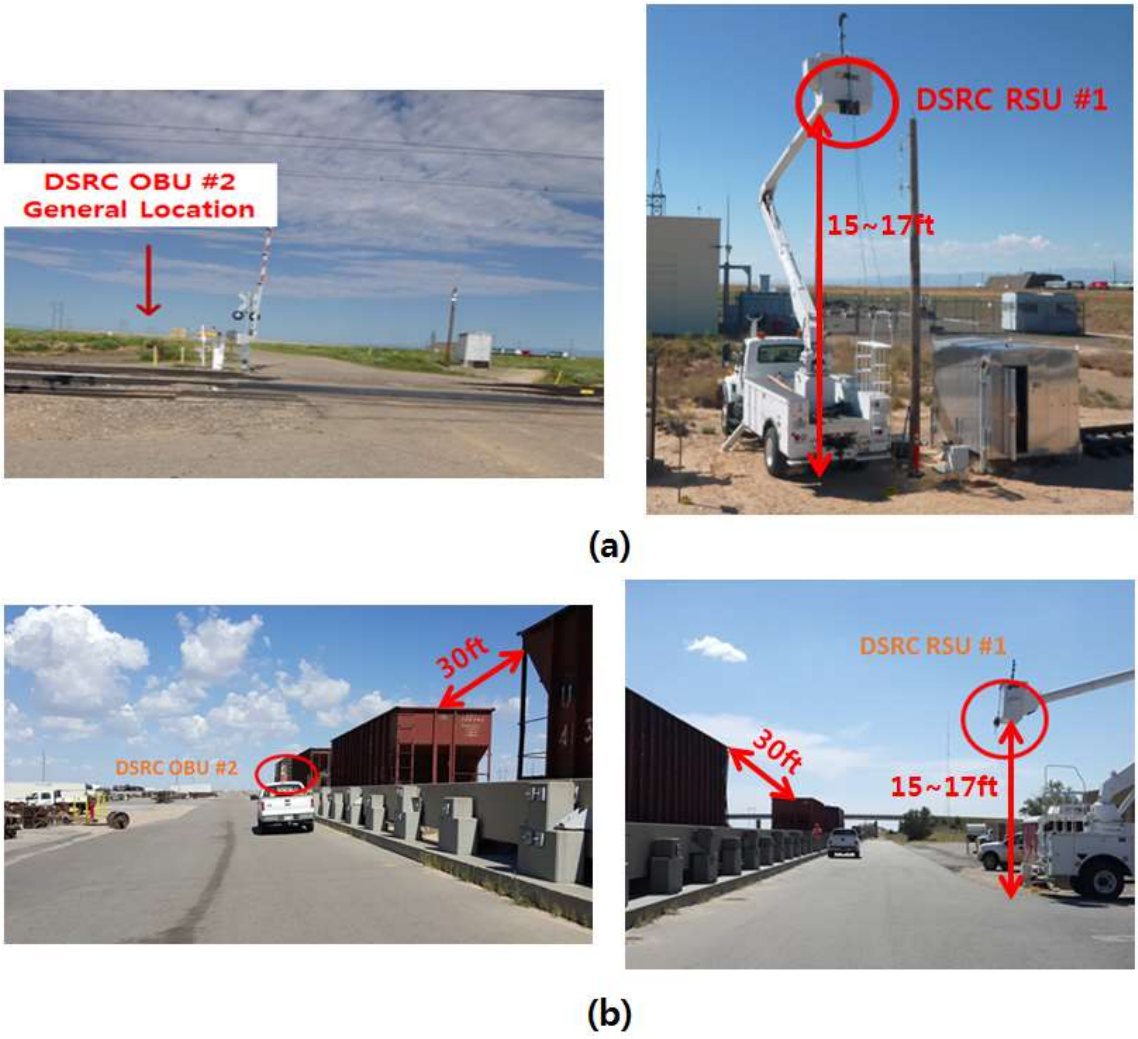

Figure 3.3 (a) Desired DSRC RSU and OBU Locations at RTT Grade Crossing. (b) Desired DSRC RSU and OBU Locations at PTT Grade Crossing.

For test site 2 (PTT), the wayside units have the following physical configurations:

OBU #2 was installed on top of a simulated vehicle which placed near the PTT Track a few feet away from railroad cars, such that the railroad cars were between OBU #2 and the locomotive. OBU #2 was placed beside the third railroad car as seen by the approaching locomotive.

RSU #1 was positioned at a height of approximately 15~17 feet using a bucket truck at a distance of 40 feet from the simulated grade crossing.

Figure 3.3 (b) shows OBU #2 and RSU #1 position for test site 2.

For both test sites 1 and 2, some common variables are used for both Propagation Characterization tests and DSRC Performance Characterization. The locomotive engine speeds, antenna configuration, transmitter power, and distance between track and OBU on the vehicle are the controlled variables for the test.

The maximum speed at which the locomotive engine can run is 79 mph. However, a more typical speed of operation for urban environments is around 20 mph. Therefore, the tests were run using locomotive speeds of 20 and 79 mph, as well as 50 mph in order to test the system's reliability at an intermediate speed.

The antennas used for the transmitter and for the receivers are different. For the transmitter, three types of antennas are used: omnidirectional, omni-diversity (2-antenna diversity using omnidirectional antennas), and an eight-element linear array as shown in Figure 3.4, below. All three type of antennas used MobileMark ECO12-5500-WHT Omni antenna which has 12 dBi Gain at 5.5 GHz. VT and TTCI constructed a linear array antenna using 8 MobileMark 12 dBi antennas. All receivers used two MobileMark ECO6-5500-WHT omnidirectional antennas which have 6 dBi Gain at 5.5 GHz.

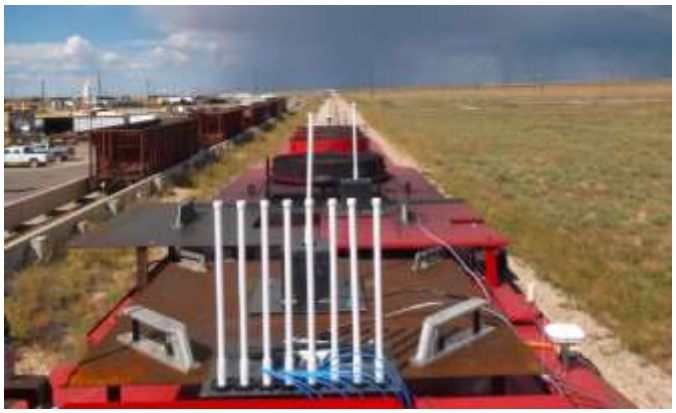

Figure 3.4 Antennas on the Locomotive

For transmission power, two different power levels were used: private and public safety. Private power level is 11 dBm and public safety power level is 23 dBm; the DSRC unit generated 20 dBm and 32 dBm, but approximately 10 dBm loss occurred through cables. All the tests were run with the same setup at each of the two different power levels.

The distance between track and OBU on the vehicle was varied. The distance variable only applied for test site #1, at the RTT. Two different distances were used for the test, 50 meters and 200 meters. These two distances are the minimum stopping distance of a vehicle traveling at 25 and 65 mph respectively.

The following tables give the specific scenarios that measurements were conducted for at TTCI. All the same measurements were conducted at both the RTT and PTT test sites, however for the RTT test site the receiving units placed at two different distances away from the track, 50 m and 200 m away from the track. This resulted in a total of 54 test cases.

Table 3.1 TTCI Test Cases

Test #	Antenna	Locomotive Speed	Power Level
1	Omni	20 MPH	Private (Low)
2			Public (High)
3		50 MPH	Private (Low)
4			Public (High)
5		79 MPH	Private (Low)
6			Public (High)
7	Omni/Diversity	20 MPH	Private (Low)
8			Public (High)
9		50 MPH	Private (Low)
10			Public (High)
11		79 MPH	Private (Low)
12			Public (High)
13	Linear Array	20 MPH	Private (Low)
14			Public (High)
15		50 MPH	Private (Low)
16			Public (High)
17		79 MPH	Private (Low)
18			Public (High)

The collected PCAP files will be analyzed in Matlab and parsed for GPS data to determine the reliability that a packet will be received before the train and vehicle will collide. Given the structure of the DSRC Basic Safety message in Figure 2.4, a parser was created in Matlab to read the bytes of a PCAP file containing DSRC Basic Safety messages, see Appendix A and Appendix B. Approximately 4 packets were sent per second. Since most of the fields in the message were held constant for simplicity, the GPS and MsgCount fields were used to determine a unique packet. Then packets were grouped every 15 meters to determine the PER. PER for each 15 meter window was calculated as follows

$$PER = 1 - \frac{\#\ Unique\ Packets\ Received}{\#\ Packets\ Transmitted} \quad (3.1)$$

The PER is then plotted as a function of distance away from the receiver. The PER analysis software is given in Appendix D.

The reliability of system is also shown in Google Earth plots, generated using Matlab code seen in Appendix C. The plots show whether a packet was successfully received by either one of or both of the receiver units. These plots show realistically how far away a packet can be expected to be received from and the maximum warning distance that is likely to be able to be achieved for a specific environment.

3.2 Channel measurements and analysis

3.2.1 Measurement configuration

A broadband vector sliding correlator channel sounder, based on the design in [32] was used to record wideband PDPs at all measurement locations. A basic block diagram of the channel sounder is shown in Figure 3.5. Both transmitter and receiver were software-defined radio implementations in GNU Radio running on a USRP B200. For our implementation, the receiver down converted, filtered, and recorded the full RF waveform; Matlab post processing was performed to correlate with the PN sequence and extract channel parameters.

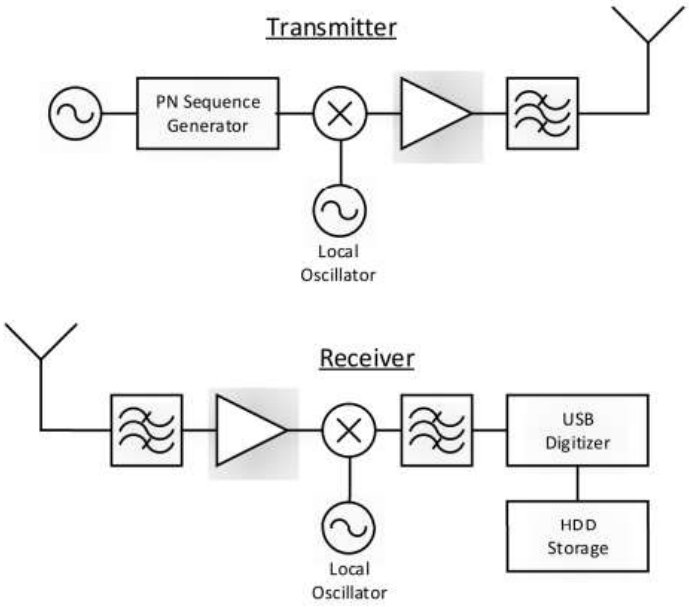

Figure 3.5 Block Diagram of the Propagation Measurement System [32]

The channel sounder used an 11-bit (2047 chip) pseudorandom noise code clocked at 15.36 MHz with GPS disciplined oscillators providing a highly stable frequency reference at transmitter and receiver.

In order to accurately characterize broadband propagation over long distances, the transmitter utilized a high-power amplifier and omnidirectional antenna. The transmitter output power (as measured at the input to the antenna) was 35.1 dBm, the antenna gain was 0 dBi, for a net EIRP of 35.1 dBm. For the on board receivers, one used 0 dBi omnidirectional antenna identical to the transmitter, and the other used a 20 dBi pyramidal horn antenna. To calibrate the measurement system, the transmitter and receiver were cable connected through an attenuator and measurements were recorded at varying levels of attenuation.

The transmitter was installed at a fixed roadside location and two separate receivers were installed on board the locomotive engine.

3.2.2 TTCI

For this measurement campaign, two locations were selected to emulate typical rural and suburban/light-urban grade crossing scenarios. Each environment was configured to have line-of-sight, non line-of-sight, and heavily cluttered links in order to fully characterize the types of conditions that would be encountered by typical DSRC systems. At each site, the transmitter was located approximately 15 meters from the railroad track; each site had a test zone through which the train traveled at a constant velocity. The test zone started 2km before the transmitter and extended a distance of 1 km past the transmitter. The received signal was continuously recorded for the entire transit of the test zone and GPS coordinates of the train were recorded at a rate of once per second.

Propagation measurements were performed on the Transportation Technologies Inc. (TTCI) Railroad Test Track (RTT) and PTT test track, as illustrated in Figure 3.6. The RTT site was configured to emulate a large open rural environment with minimal clutter or obstacles near either the transmitter or path of the train. The PTT site was configured to emulate a suburban or light urban environment that contained buildings, vehicles, and general clutter within 100 meters of the track.

Figure 3.6 Example Measurement Scenario on the RTT Test Site

The transmit antenna was mounted at a fixed location and height, receive antennas were mounted on the roof of the front of the train. The transmitter antenna was attached to the top of bucket truck boom arm with heights adjustable between 2m and 12m, as shown in Figure 3.6. The receiver antennas were mounted on the roof of front of the train with a small plastic radome to protect them from debris. All antennas were vertically polarized for the duration of the measurement campaign.

Additionally, a set of 7 railroad cars were parked on a track between the PTT and the transmitter shown in both Figure 3.2 and Figure 3.3(b). These cars were separated by gaps of 15m, to emulate a downtown environment where roadways would be interspersed between buildings. The transmitter was configured

to operate at a center frequency of 5800 MHz in order to avoid interference with a DSRC system that was operating concurrently with the channel sounder.

At each test track, the transmitter was placed at a fixed location 15m from the track, and configured to be in one of three height categories:

• Low: 2m above ground level at both the RTT and PTT. This height is chosen to emulate the link between the train and a roadside vehicle.

• Medium: 25ft (RTT) and 30ft (PTT) above ground level. This height emulated communication to a wayside unit mounted at or below the height of the local clutter field.

• High 10m (RTT) or 12m (PTT) above ground level. This height emulated long-range communication to a wayside unit mounted above the local clutter environment.

For each antenna height and track combination the locomotive made 2-4 runs through the 3km test zone, at one of three speeds: 20 MPH (32km/h), 50 MPH (80 km/h), and 79 MPH (127 km/h). The low speed is representative of a train traveling through a densely populated area or around a station, the middle speed is the typical cruising speed of a freight train in the U.S., and the high speed is the maximum allowed speed for freight and passenger rail across most of the U.S.

3.2.3 General analysis approach

The data gathered from the channel sounding measurement campaign were analyzed in Matlab. The received signal is cross correlated with the PN-sequence to determine the delay spread and Doppler characteristics of the channel. The I and Q data for each test scenario is cross correlated with the PN-sequence to calculate the PDP. From the PDP, the Power Spectral Density (PSD) is calculated using the Welch method.

Welch's method is used to estimate the PSD of a signal [33]. The data is first partitioned into K batches with M points in each batch. Each consecutive batch will be shifted down S points. For each batch, the Discrete Fourier Transform (DFT), $X_k(v)$, is computed at some frequency v.

$$v = \frac{i}{M} where - (\frac{M}{2} - 1) \leq i \leq M/2 \quad (3.2)$$

$$X_k(v) = \sum_{m=(k-1)S}^{M+(k-1)S-1} x[m]w[m]\exp(-2j\pi vm) \quad (3.3)$$

Where w[m] is the window function.

Then for each batch, the modified periodogram value, $P_k(v)$ if formed from the DFT.

$$P_k(v) = \frac{1}{W}|X(v)|^2 \quad (3.4)$$

Where

$$W = \sum_{m=0}^{M} w^2(m) \quad (3.5)$$

Finally the PSD is estimated as follows

$$S_x(v) = \frac{1}{K}\sum_{k=1}^{K} P_k(v) \quad (3.6)$$

The Doppler frequency is then taken as frequency at which the maximum value of the PSD occurs at.

To calculate the average delay spread, the normalized PDP magnitude is searched for any magnitude that exceeds three standard deviations from the expected value. The indices of the occurrences of these values is then normalized to the first index of occurrence and multiplied by the sampling period. The peak magnitudes are then multiplied by the derived scalar, and then averaged to produce average delay spread as denoted by equation (2.7). Then the RMS delay spread is calculated using the method described in section 2.3.2.2.2 using equations (2.8) and (2.9).

The RMS Doppler Spread is calculated in a similar manner to the average delay spread. The RMS Doppler spread is derived from the power spectrum. The power spectrum of the signal,$S_h(\omega)$, is the Fourier transform of the autocorrelation function. Similarly, then spectrum is searched for any magnitudes that exceed the threshold of the distribution. Then, the indices of the occurrences of these values is then normalized to the first index of occurrence and multiplied by the sampling frequency. The peak magnitudes are then multiplied by the derived scalar, and then averaged to produce average Doppler spread as denoted by equation (2.7) where n = 1. Then the RMS Doppler spread is calculated using the method described in section2.3.2.2.4 using equations (2.11) and (2.12) .

3.3 Channel modeling and simulation

In order to accurately predict the behavior of the channel in a train to vehicle environment, both the large-scale path loss and small scale fading need to be considered. The following sections explain the methods to derive the models and the simulations conducted to correctly fit the data.

To model the channel both a large-scale path loss and small scale fading models will be derived. The models will then be fit to the measured and compared to show the models that are best suited for describing the railroad environment tested.

3.3.1 Large-Scale Path Loss

The most effective large-scale path loss models shown in literature thus far have used the dual-slope path loss model. The measured data from TTCI will use both the log-normal path loss model and the dual-slope path loss model to provide multiple models for the given environments.

In order to accurately measure RSS, the data needs to be calibrated. The USRP used to create the channel sounder, does not return calibrated, but rather uncalibrated data. Consequently, there is a different calibration curve for each receiver gain setting that needs to be derived to calibrate the data. These calibration curves will convert the raw received signal strength that is calculated from the I and Q data into actual received signal strength power levels.

The calibration curve is found by measuring the USRP's received power at different attenuation levels of the carrier frequency using a signal generator. The USRP was connected to a signal generator that was generating a signal with carrier frequency 5.8GHz, to match the carrier frequency used in the measurements at TTCI. The signal was then attenuated following the attenuation levels in Table 3.2. The attenuation was held constant for about 2 seconds then the attenuation was decreased. The I and Q data are then cross correlated with PN-Sequence and filtered for noise. The average power is taken over 1 second intervals then converted to dB. Plotting the received signal strength on a time plot shows a step function of the received signal strength as the attenuation was decreased in time, where each step represents a different attenuation level as shown in Figure 3.7 Example RSS Plot in Time, below. Figure 3.7 shows the transmitter turning on and then gradually stepping the attenuation down based on the values in Table 3.2.

Measurements were conducted for the following receiver gain settings

Table 3.2 Test Scenarios for Calibration Curve Fitting

Receiver Gain Setting	Attenuation Levels Tested
-40	-40,-45,-50,-55,-60,-65,-70,-75,-80,-85,-90
-68	-40,-45,-50,-55,-60,-65,-70,-75,-80,-85,-90

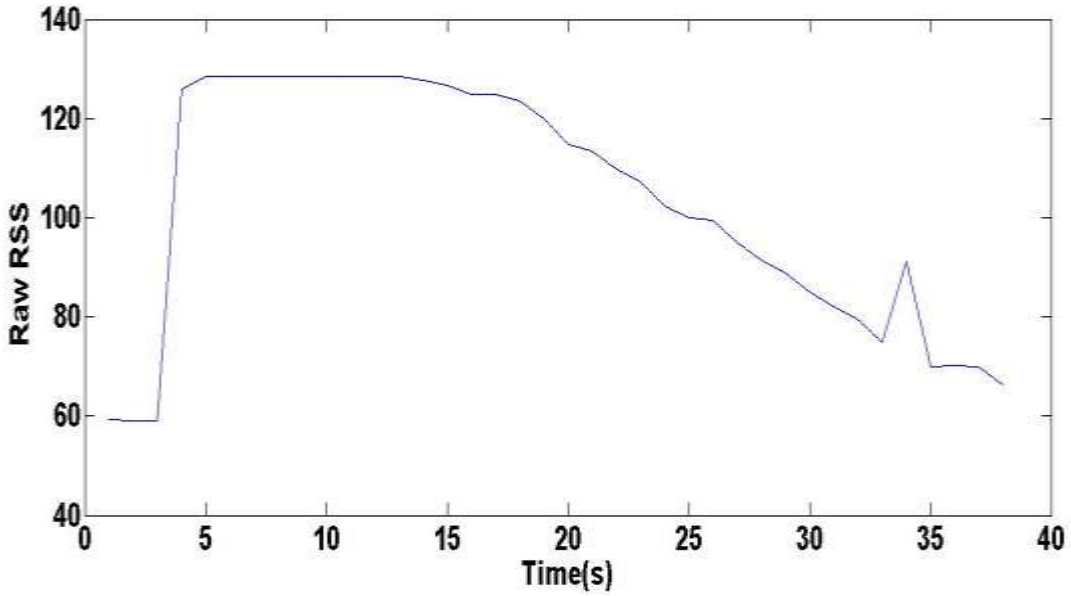

Figure 3.7 Example RSS Plot in Time

The raw RSS is then mapped to a recorded attenuation setting. Then, the recorded attenuation is plotted as a function of the raw received power. A linear regression (y=mx+b) is then fit to the sample points. A linear regression is chosen because the USRP is known to only apply linear transformations to the data. However, a polynomial fit could have been used as well because the USRP hardware does not behave perfectly linear in all environments. To calibrate the measured data from TTCI, the PDPs will

then be substituted into the derived calibration curve to determine the actual power of the received signal.

The following curves were produced and their parameters are given in Table 3.3.

Figure 3.8 Fitted Calibration Curves

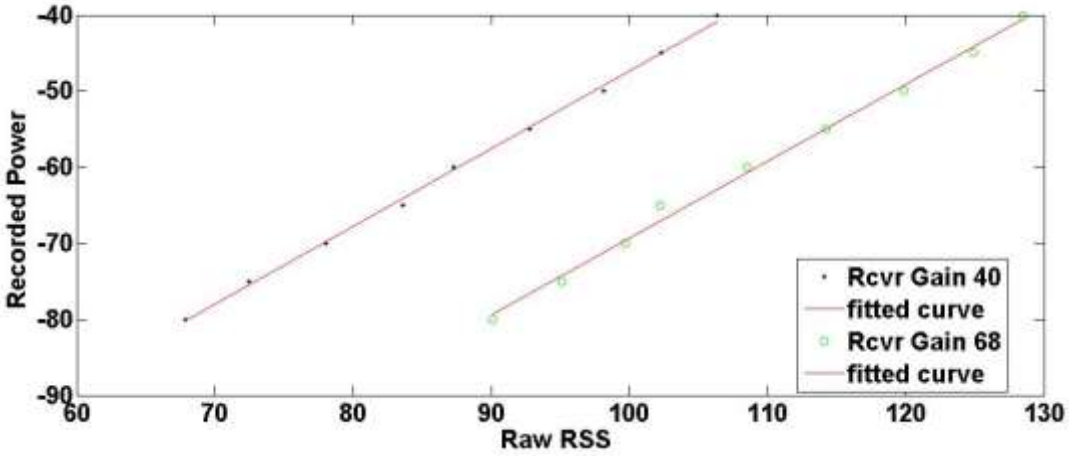

Table 3.3 Calibration Curve Regression Parameters

Receiver Gain Setting	m	b	r^2
40	1.026	-113.2	0.9985
68	1.011	-170.4	0.9949

When determining if the regression is a good fit, the r^2 coefficient is used. r^2 is a statistical measure of how close the data are to the fitted regression. r^2 is calculated as follows

$$r^2 = 1 - \frac{\sum {e_i}^2}{\sigma^2} \quad (3.7)$$

Where

$$e_i = y_i - f_i \quad (3.8)$$

Where y_i are the measured values, f_i are the expected values from the regression, and σ^2 is the variance of the measured values.

From the definition above, r^2 can be interpreted as the percent of explained variation of the measured data. Based on the r^2 values that resulted from the regression, the fitted regressions describe close to 100% of the variation in the data. In theory, these regressions can be declared a good fit for the calibration curves. However, to ensure the calibration curves were correct, the raw calibration data was run through the calibration curves and converted to RSS. The plots showed that at a receiver gain of 40, the plotted RSS curve fell on the expected attenuation levels tested, but at a receiver gain of 68, the plotted RSS curve fell below the expected attenuation levels. This result suggests that the gain offset value for a receiver gain setting of 68 was too high. To determine the amount the offset needed to be adjusted, the average difference between the expected and calibrated results was taken. The results are

given in Table 3.4 on the following page. A new offset was not for the receiver gain setting of 40 because the calibrated results fell within ±3 dB of the expected value.

Table 3.4 Adjusted Offset Values

RCVR Gain Value	Calculated Offset	Adjustment Factor	New Offset
40	-113.2	0	-113.2
68	-170.4	36.4	-134.0

The results of the derived calibration curves from the measured data and the adjusted calibration curve based on the recorded power for a receiver gain setting of 68 is given in Figure 3.9.

Figure 3.9 Comparison of Derived and Adjusted Calibration Curves at Receiver Gain setting of 68

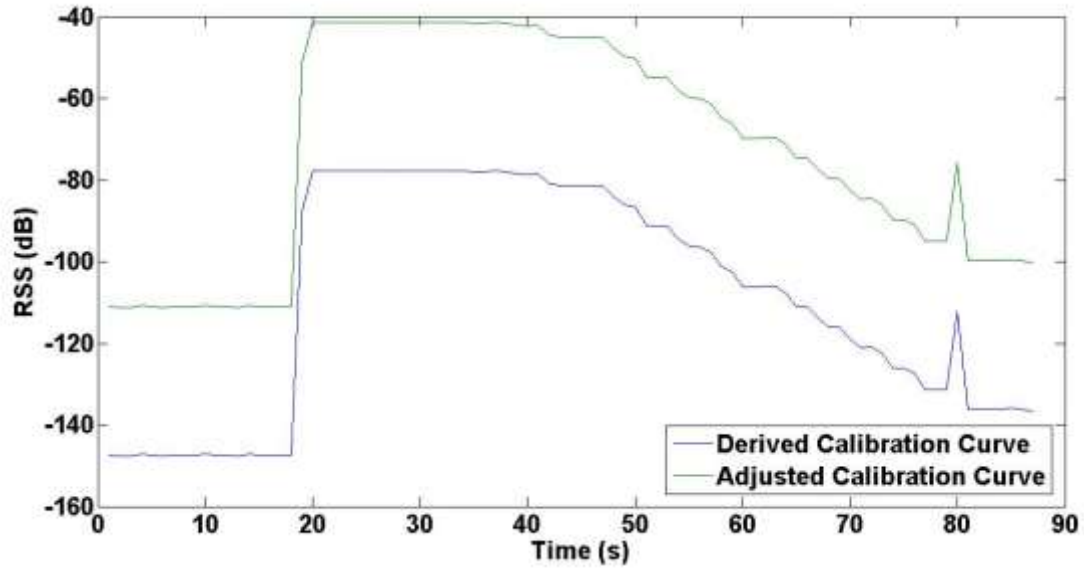

The remaining offset values can then be found by fitting a line to the new offset values. The line parameters are given in Table 3.5. The offset for any receiver gain setting is then found using (3.9).

Table 3.5 Offset Line Parameters

m	-0.7429
b	-83.49

$$Offset = m * (RCVRGain) + b \quad (3.9)$$

From the derived calibration curves, the remaining calibration curves can be estimated. It is assumed that the slope will be the same for all the regression curves, and only the intercept will change. The slope used will be 1 since the expected calibration should only rely on an offset value for each receiver gain setting. The offset will be calculated from (3.9) above. The Table 3.6, on the following page, shows the estimated parameters all of the receiver gain settings.

Table 3.6 Estimated Calibration Curves

Receiver Gain Setting	m	b
40	1.0	-113.2
46	1.0	-117.7
48	1.0	-119.1
50	1.0	-120.6
52	1.0	-122.1
53	1.0	-122.9
55	1.0	-124.3
60	1.0	-128.0
63	1.0	-130.3
65	1.0	-131.8
66	1.0	-132.5
68	1.0	-134.0

These new regression are linear shifts of the derived regressions. The shifts of the plots are shown in Figure 3.10.

Figure 3.10 Plot of All the Calibration Curves

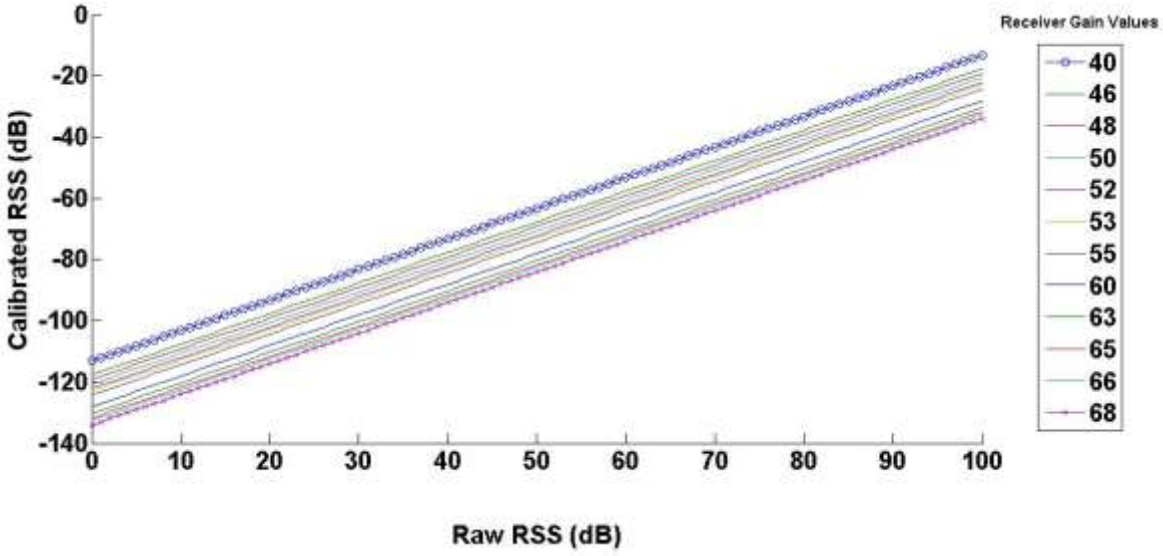

RSS will be derived using the following method. Using the raw I and Q data returned from the USRP, The PDP can be derived by cross correlating the PN-sequence from the channel sounder with the I and Q data. Then, the PDP will be filtered for noise using a noise threshold. The samples will then be calibrated using the derived calibration curves. The average RSS for each half second will be calculated as the vector sum of the calibrated data divided by the number of PDPs in a half second. The Matlab code for this process is given in Appendix E.

The RSS values will then be converted into a measure of path loss in dB. RSS represents the received power of the signal. The received power P_R is equal to the sum of the transmit power P_T, transmitter

antenna gain G_T, and the receiver antenna gain G_R, minus the path loss experienced, where all the values are in dB. The relationship between received power and path loss is given in (3.10) below [22].

$$P_R = P_T + G_T + G_R - P_L \quad (3.10)$$

The transmit power, transmitter antenna gain, and receiver antenna gain are all values that are known before measurements are taken. The antenna gains are based on the model of antenna used and their gain values can be found on their specifications sheet. Table 3.7, below, gives a summary of the power and gain values used for the measurements taken at TTCI.

Table 3.7 Power/Gain Parameters

Parameter	Power (W)	Power (dB)
Transmit Power	3.1	34.9 dBm
Horn Antenna	N/A	20 dB
Discone Antenna	N/A	3.6 dB

The transmit antenna gain will be chosen based on the type of antenna used during the measurement, while the receive antenna gain will be the gain of the discone antenna because a second discone antenna was setup up as the receiver. The transmit power was held constant across all measurements. The path loss will then be calculated for as defined in (3.11) for the horn antenna and as defined in (3.12) for the discone antenna.

$$P_L = 34.9 + 20 + 3.6 - RSS \quad (3.11)$$
$$P_L = 34.9 + 3.6 + 3.6 - RSS \quad (3.12)$$

From these path loss values, the breakpoint distance can be determined, if necessary, based on the shape of the plot for the dual-slope path loss model. Then the data will be fit into log-normal regressions. The Matlab code to generate the plots are given in Appendix G.

The path loss exponent, *n*, will be found using the minimum mean square error estimator (MMSE). The error, *e*, of a measured value is found by taking the measured value, p_i, and subtracting expected value, $\widehat{p_i}$, as shown in (3.13), below [22].

$$e = (p_i - \widehat{p_i}) \quad (3.13)$$

The sum of the squared errors between the measured and expected values is then given as [22]

$$J = \sum_{i}^{k} (p_i - \widehat{p_i})^2 \quad (3.14)$$

For path loss, the measure path loss either (3.11) or (3.12) will be substituted for p_i, and the expected values will be calculated as

$$\widehat{p_i} = PL(d_0) - 10n \log_{10}(\frac{d_i}{d_0}) \quad (3.15)$$

Substituting into (3.14),

$$J(n) = \sum_{i}^{k} \left(p_i - (PL(d_0) - 10n \log_{10} \frac{d_i}{d_0}) \right)^2 \quad (3.16)$$

(3.16) will be minimized by solving for *n* when the derivative of J(n), given in , is equal to zero.

$$\frac{dJ(n)}{dn} = \sum_{i}^{k} 2(p_i - PL(d_0))10 \log_{10} \frac{d_i}{d_0} + 2n \left(10 \log_{10} \frac{d_i}{d_0} \right)^2 \quad (3.17)$$

Then solving for *n*

$$n = \frac{PL(d_0) \sum_i^k 10 \log_{10} \frac{d_i}{d_0} - \sum_i^k p_i 10 \log_{10} \frac{d_i}{d_0}}{\sum_i^k \left(10 \log_{10} \frac{d_i}{d_0} \right)^2} \quad (3.18)$$

The path loss exponent can then be estimated using the MMSE given in (3.18).

The standard deviation can also be calculated from the received signal strength for these path loss models using equation (3.19).

$$\sigma = \sqrt{\frac{\sum_{i=1}^{k} (\hat{p}_i - p_i)^2}{k}} \quad (3.19)$$

The Matlab code to calculate these values is given in Appendix M.

3.3.2 Small-Scale Fading

For the test scenarios that were conducted at TTCI, a Rician channel model can be applied for this application. The vehicle to vehicle channel model proposed in literature accounts for many realistic scenarios that many cars and trucks may encounter on an everyday basis. However, the test scenarios conducted in literature model a different application for DSRC. The alert system for the measurements conducted at TTCI implements one DSRC transmitter on the train as a mobile transmitter and the receiver as a fixed roadside unit. A second receiver was placed inside a truck to emulate the environment an on-board unit would be subject to. However, the vehicle was stationary, due to safety concerns. Consequently the measurements conducted at TTCI will not represent the mobile to mobile channel models conducted in literature. The proposed models from literature, however, do provide a base point from which a channel model can be developed.

As demonstrated in [31], when the distance between the transmitter and receiver is small, a Rician distribution can be used and when the distance between transmitter and receiver is large, a Rayleigh distribution can be used to model received signal strength. However, a Nakagami model was used to derive the above behavior.

In order to find the small scale fading model, a Continuous Wave (CW) sinusoidal signal was transmitted on the RTT test site with the train moving at 20mph, 50mph, and 79 mph. The signal envelope is then calculated so that the method in 2.3.2.3.1 can be applied to derive the K-factors.

4 Results

4.1 DSRC measurement results

Using the methods described at the end of section 3.1.2, the PER was derived to provide an approximation of how well the DSRC alert system will work when deployed in a real world environment. Three different antenna types were used, an Omni directional antenna, an Omni Directional Antenna setup for diversity operation, and a Linear Array. The Linear Array is designed such that the beam of the antenna, all of the energy, is directed in front of the train, so that the warning times could be maximized.

The PER was expected to follow a 'U' shape in linear units because as the train and transmitter approached the receiver, the PER would decrease. The PER was then expected to stay low while the transmitter and the receiver were in close proximity. As the train and transmitter continued moving along the track, the PER would then increase again until packets were no longer able to be received. The 'U' shape expectation fits the expected behavior of the DSRC system because the DSRC system is designed for short range communications. Consequently, there will be a window of the track where the packets would be expected to be received reliably.

When the DSRC advance warning system was operated in the open track with minimal obstacles, pessimistically, warning times were usually above 5 seconds at the maximum speed, but were larger at slower speeds. The linear array in most cases did not outperform either of the other two antennas tested, likely because; the beam was not angled such that a receiver, not directly in front of the beam, would be in the antenna's beam. However the antenna could be optimized to provide potentially more receiver coverage. The Omni and Omni diversity antennas performed about the same, with the Omni Diversity providing slightly more robust packet reception. The performance was also consistent between the locations for the OBU.

It should also be noted that these test scenarios are a pessimistic, worst case scenario, because the modulation scheme chosen, was a 64 QAM that results in a higher signal to noise ratio than a lower order modulation scheme such as BPSK or QPSK.

4.1.1 RTT Results

The RTT results are split into two sets of scenarios. The first scenario is where the On Board Unit was placed at a distance of 50 meters to represent a vehicle approaching the Highway Rail-Grade Crossing from a relatively short stopping distance. The second scenario is where the On Board unit was placed at a distance of 200 meters to represent a vehicle approaching the Highway Rail-Grade Crossing from a further stopping distance.

Overall the measurements suggest that the DSRC warning system could work in open spaces. The lowest warning times seen were around 5 seconds. The performance of the system could also be greatly improved to optimize the number of receivers in each antenna beam and to make the modulation scheme more robust. Using commercially available antennas and radios, the pessimistic warning times of around 10 seconds were recorded, which is more than the average driver needs to react to the

brakes. Additionally, if this system becomes integrated with smart driving cars, the driver's reaction time may no longer be a factor, because vehicles will be able to stop themselves. More measurements and test scenarios should be conducted before a final conclusion is made.

4.1.1.1 On Board Unit at 50 Meters

Table 4.1 summarizes the advanced warning distance and time the DSRC system was able to produce at the RTT test site with the OBU placed 50m away from the track.

Table 4.1 Summary of performance metrics for the RTT test site OBU at 50m

Antenna	Train Speed	Power Level	PER < .2				PER < .5				PER < .8			
			Distance (m)		Time (s)		Distance (m)		Time (s)		Distance (m)		Time (s)	
			RSU	OBU	RSU	OBU	RSU	OBU	RSU	OBU	RSU	OBU	RSU	OBU
Omni	20 MPH	Low	325	>1100	22	>100	350	>1100	30	>100	525	>1100	90	>100
		High	325	>1100	22	>100	625	>1100	70	>100	900	>1100	95	>100
	50 MPH	Low	325	>1100	10	>60	350	>1100	15	>60	525	>1100	17	>60
		High	315	>1100	10	>60	425	>1100	20	>60	675	>1100	25	>60
	79 MPH	Low	200	>1100	5	43	225	>1100	7	45	300	>1100	10	55
		High	360	>1100	12	43	600	>1100	18	50	725	>1100	20	60
Omni/ Diversity	20 MPH	Low	N/A	875	N/A	97	N/A	900	N/A	100	N/A	900	N/A	101
		High	300	N/A	33	N/A	325	N/A	36	N/A	350	N/A	39	N/A
	50 MPH	Low	475	>1100	20	>45	775	>1100	34	>45	1050	>1100	47	>45
		High	675	>1100	30	>45	800	>1100	35	>45	1050	>1100	46	>45
	79 MPH	Low	350	>1100	10	37	575	>1100	16	42	850	>1100	24	55
		High	675	>1100	10	41	800	>1100	22	>50	1050	>1100	29	58
Linear Array	20 MPH	Low	100	150	11	16	125	450	13	50	150	725	16	81
		High	250	325	27	36	275	750	30	83	825	>1100	92	>100
	50 MPH	Low	275	350	12	15	280	725	12	32	300	750	13	33
		High	275	325	12	14	280	725	12	32	825	>1100	36	>60
	79 MPH	Low	100	150	3	4	125	325	3	9	150	725	4	20
		High	100	325	3	9	150	700	4	19	200	>1100	5	40

Data was unable to be collected at the OBU for the Omni/Diversity antenna at 20mph, high power test case. The data for the RSU for the Omni/Diversity antenna at 20mph, low power test does not show any advanced warning time, likely because this test was run first and changes were made to the location of the receiver that were not noted. The OBU was able to receive packets at a greater distance than the RSU, resulting in greater warning times. The OBU was placed before the RSU and may have been obstructing the line of sight of the RSU at further distances. The RSU was also placed near more reflective materials that may have resulted in more multipaths. Generally there appears to be minimal correlation between the PER and the distance packets can be received, as seen between the 20mph cases and the 50mph cases. However, at the maximum speed, the distance packets can be received at decreases, likely due to fewer packets being sent prior to arrival. The advanced warning time is affected by the speed of the train because the relationship between speed, time, and distance. At moderate to low speeds, the DSRC system produced warning times >10s. At high speed, the advanced warning time

could drop as low as 3 seconds. Additionally, while operating at high power, the system's advanced warning times increased.

Plots of the PER and Google Earth Visualization of the received packets are given in Appendix P and Appendix Q.

4.1.1.2 On Board Unit at 200 Meters

Table 4.2 summarizes the advanced warning distance and time the DSRC system was able to produce at the RTT test site with the OBU placed 200m away from the track.

Table 4.2 Summary of performance metrics for the RTT test site OBU at 200m

Antenna	Train Speed	Power Level	PER < .2				PER < .5				PER < .8			
			Distance (m)		Time (s)		Distance (m)		Time (s)		Distance (m)		Time (s)	
			RSU	OBU	RSU	OBU	RSU	OBU	RSU	OBU	RSU	OBU	RSU	OBU
Omni	20 MPH	Low	325	>1100	36	>100	400	>1100	44	>100	450	>1100	50	>100
		High	400	>900	44	>100	800	>900	89	>100	900	>900	100	>100
	50 MPH	Low	200	1100	8	49	275	>1100	12	>60	300	>1100	13	>60
		High	325	>1100	14	50	350	>1100	15	>60	450	>1100	20	>60
	79 MPH	Low	300	>1100	8	30	325	>1100	9	35	350	>1100	10	40
		High	350	>1100	19	30	525	>1100	14	50	925	>1100	26	>60
Omni/ Diversity	20 MPH	Low	200	>900	22	>100	275	>900	30	>100	325	>900	36	>100
		High	450	>1100	50	>100	875	>1100	97	>100	>1100	>1100	>100	>100
	50 MPH	Low	375	>1100	16	>50	825	>1100	36	>50	850	>1100	38	>50
		High	450	>1100	20	>50	800	>1100	35	>50	1050	>1100	46	>50
	79 MPH	Low	300	1000	8	25	312	>1100	8	40	325	>1100	9	45
		High	275	>1100	7	30	300	>1100	8	35	475	>1100	13	40
Linear Array	20 MPH	Low	125	175	13	19	175	300	19	33	200	450	22	50
		High	225	250	25	27	825	925	92	103	900	950	100	106
	50 MPH	Low	125	250	5	11	175	300	7	13	200	450	8	20
		High	200	250	8	11	225	875	10	39	325	925	14	41
	79 MPH	Low	200	175	5	4	225	300	6	8	250	450	7	12
		High	175	250	4	7	225	875	6	24	250	900	7	25

The OBU was able to receive packets at greater distances than the RSU, resulting in greater warning times. It is unlikely that the OBU was obstructing the line of sight in these tests because the OBU was placed 200m away from the track and is well clear of the RSU's line of sight. The RSU was still placed near more reflective materials that may have resulted in more multipath interference. Generally there appears to be minimal correlation between the PER and the distance packets can be received, as seen between the 20mph cases and the 50mph cases. However, at the maximum speed, the distance packets can be received at decreases, likely due to fewer packets being sent prior to arrival. The advanced warning time is affected by the speed of the train because the relationship between speed, time, and distance. At moderate to low speeds, the DSRC system produced warning times averaging >10s. At high

speed, the advanced warning time could drop as low as 2 seconds. Additionally, while operating at high power, the system's advanced warning times increased.

Plots of the PER and Google Earth Visualization of the received packets are given in Appendix P and Appendix Q.

4.1.2 PTT Results

For the PTT scenarios, as shown in Figure 3.2, extra Box Cars were placed between the train track and the receiving OBU and RSU to emulate an urban or obstructed transmission environment. Unfortunately, data was unable to be collected at the 20 mph runs at low power. Consequently, these results will also provide a very pessimistic performance metric for the DSRC advanced warning system in an urban environment. The results are consistent across the different configurations. Packets were able to be reliably received typically between 125 and 150m, which results in advanced warning times between 3 and 5 seconds. A summary of the results are given in Table 4.3.

Table 4.3 Summary of performance metrics for the PTT test site

Antenna	Train Speed	Power Level	PER < .2				PER < .5				PER < .8			
			Distance (m)		Time (s)		Distance (m)		Time (s)		Distance (m)		Time (s)	
			RSU	OBU	RSU	OBU	RSU	OBU	RSU	OBU	RSU	OBU	RSU	OBU
Omni	20 MPH	Low	N/A	N/A	N/A	N/A	N/A	N/A	N/A	N/A	N/A	N/A	N/A	N/A
		High	N/A	150	N/A	16	25	175	3	19	37	200	4	22
	50 MPH	Low	100	100	4	4	150	125	6	5	175	200	7	8
		High	150	150	6	6	162	175	7	7	175	200	7	8
	79 MPH	Low	100	100	2	2	150	125	4	3	175	175	5	5
		High	125	150	3	4	162	175	4	5	175	200	5	5
Omni/ Diversity	20 MPH	Low	N/A	N/A	N/A	N/A	N/A	N/A	N/A	N/A	N/A	N/A	N/A	N/A
		High	N/A	N/A	N/A	N/A	N/A	N/A	N/A	N/A	N/A	N/A	N/A	N/A
	50 MPH	Low	N/A	75	N/A	3	N/A	112	N/A	5	50	150	2	6
		High	N/A	100	N/A	4	N/A	112	N/A	5	75	150	3	6
	79 MPH	Low	N/A	75	N/A	2	25	112	1	3	75	150	2	4
		High	N/A	100	N/A	2	N/A	112	N/A	3	50	150	1	4
Linear Array	20 MPH	Low	N/A	N/A	N/A	N/A	N/A	N/A	N/A	N/A	N/A	N/A	N/A	N/A
		High	N/A	100	N/A	11	N/A	112	N/A	12	50	150	5	16
	50 MPH	Low	25	75	1	3	62	100	2	4	100	112	4	5
		High	75	100	3	4	100	112	4	5	125	150	5	6
	79 MPH	Low	N/A	N/A	N/A	N/A	N/A	N/A	N/A	N/A	N/A	N/A	N/A	N/A
		High	50	100	2	2	87	112	2	3	125	150	3	4

In the PTT test scenarios, the OBU and RSU received packets at similar distances, resulting in similar warning times. Generally there appears to be minimal correlation between the PER and the distance packets can be received, as seen between all the speeds tested. The advanced warning time is affected

by the speed of the train because the relationship between speed, time, and distance. In the cluttered environment, the advanced warning times were generally less than five seconds. However, Since this is emulating an urban environment, it is likely that drivers will be not be driving as fast as in the rural setting and the 5 second advanced warning time could be enough time for a driver to react to the incoming warning.

Plots of the PER and Google Earth Visualization of the received packets are given in Appendix P and Appendix Q.

4.2 Channel measurement results

The Delay spread and Doppler spread were calculated using the method described in sections 2.3.2.2.2 and 2.3.2.2.4. Plots of the Delay spread and Doppler spread will also be given in google earth to determine if multipath propagation factors were affecting the values at different locations on the track. The calculated data will be compared to similar vehicle to vehicle measurement campaigns. However, there are no existing measurement campaigns performed between trains and vehicles in motion, the comparison to existing vehicle to vehicle measurements will be used instead. The results found at TTCI, fall in the range of values seen in existing vehicle to vehicle measurement campaigns. However, the range of values in the existing measurement campaigns is large, which suggest the existing campaigns were not performed under comparable environmental conditions.

The Geographic Visualization plots show the spread values on a color gradient scale. The green values represent values closer to zero while the red and values represent larger values, 50ns for the delay spread and 2000 Hz for the Doppler spread. Black represents an extreme value or no value available for that location. Plots are condensed into one image and staggered, however all the test were run on the track.

4.2.1 RTT Results

The following table gives a summary of the results seen at the RTT test site for the Horn antenna and the following figures give a geographic representation of the measurements in google earth.

Table 4.4 Summary of Horn RTT Delay and Doppler Spread Measurements

	Delay Spread (ns)			Doppler Spread (Hz)		
Antenna Height	20 mph	50 mph	79 mph	20 mph	50 mph	79 mph
6 ft	64.76	257.873	199.095	790.861	1075.024	1032.217
25 ft	18.739	14.601	21.206	630.845	602.447	610.237
32 ft	91.738	145.678	22.934	706.524	900.282	839.518

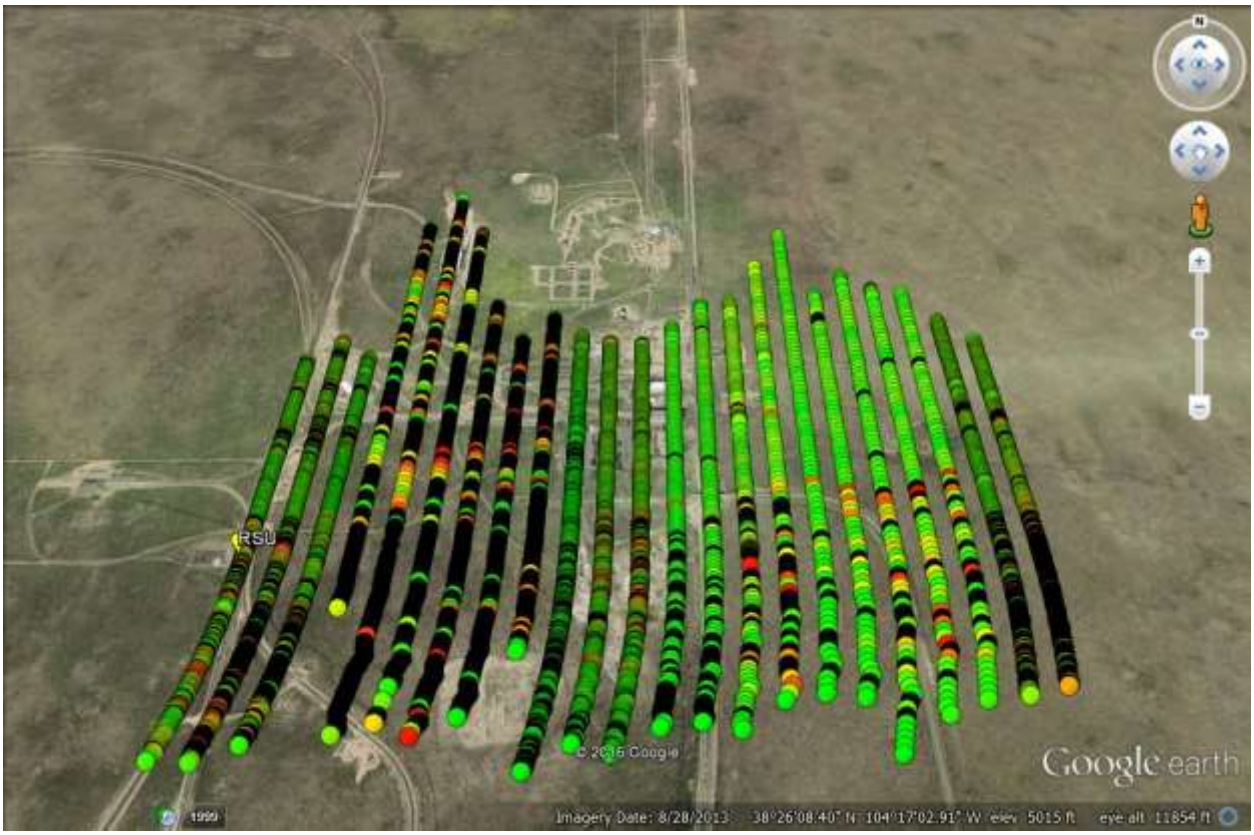

Figure 4.1 Horn RTT Delay Spread Visualization in Google Earth

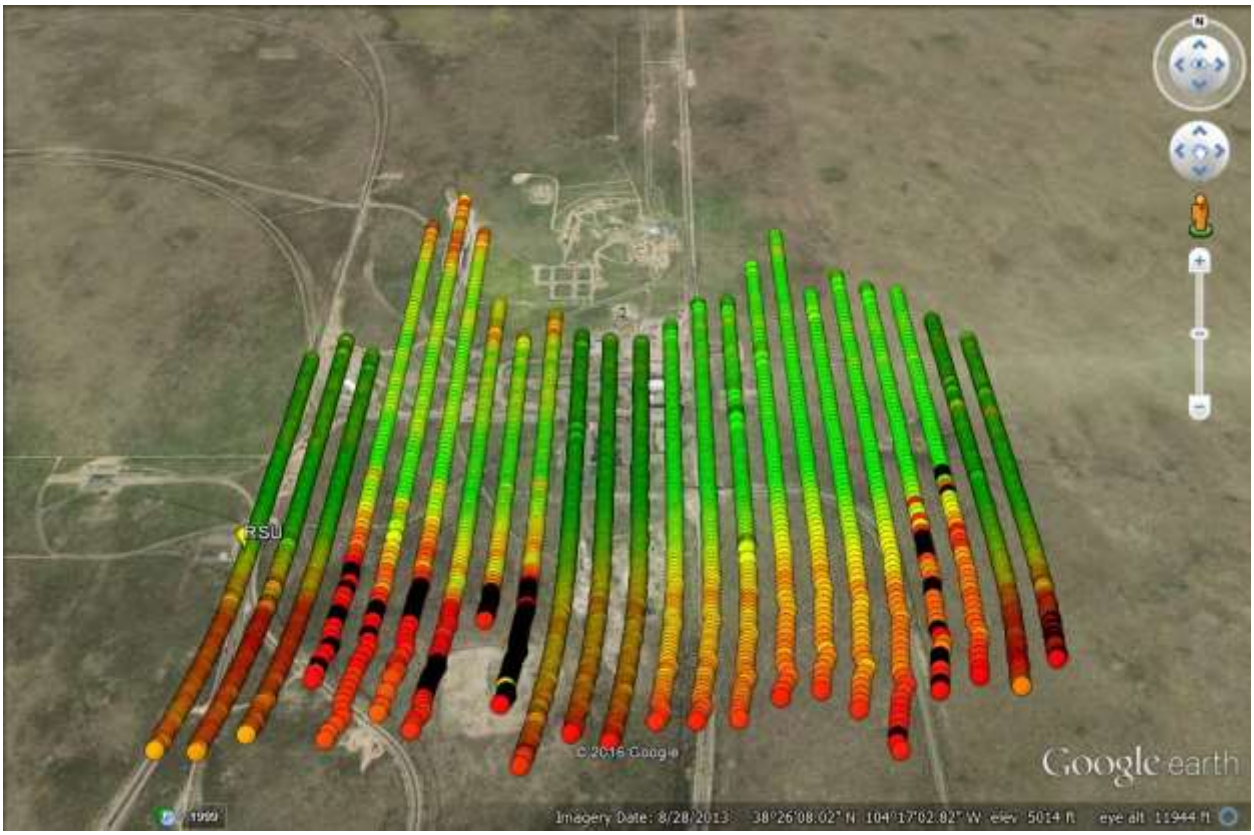

Figure 4.2 Horn RTT Doppler Spread Visualization in Google Earth

The Horn results show that both the delay spread and Doppler spread decrease as the distance between the transmitter and receiver decreases, which is expected because number of obstacles between the transmitter and receiver decreases, the stronger the line of sight component is, which decreases the effects of other multipath signals.

Table 4.5 gives a summary of the results seen at the RTT test site for the Discone antenna and Figure 4.3 and Figure 4.4 give geographic representations of the measurements in google earth.

Table 4.5 Summary of Discone RTT Delay and Doppler Spread Measurements

	Delay Spread (ns)			Doppler Spread (Hz)		
Antenna Height	20 mph	50 mph	79 mph	20 mph	50 mph	79 mph
6 ft	0.525	3.684	7.747	597.143	1084.990	788.858
25 ft	13.550	7.798	10.011	1011.176	1005.478	830.55
32 ft	0.119	4.598	13.710	866.912	625.537	1129.443

Figure 4.3 Discone RTT Delay Spread Visualization in Google Earth

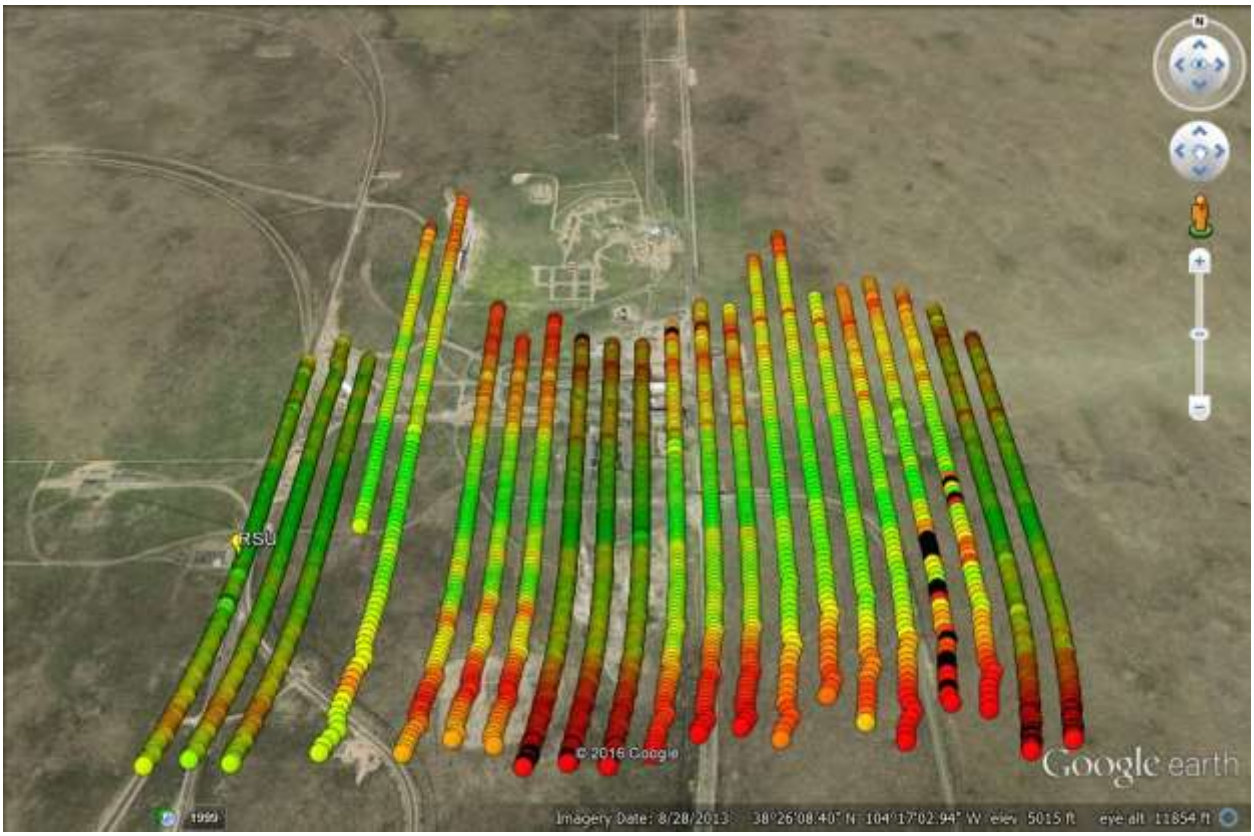

Figure 4.4 Discone RTT Doppler Spread Visualization in Google Earth

The Discone results show that both the delay spread and Doppler spread decrease as the distance between the transmitter and receiver decreases, which is expected because number of obstacles between the transmitter and receiver decreases, the stronger the line of sight component is, which decreases the effects of other multipath signals. The Discone antenna show that smaller spreads were produced for larger portions of the test scenarios.

4.2.2 PTT Results

The following table gives a summary of the results seen at the PTT test site for the Horn antenna and the following figures give a geographic representation of the measurements in google earth.

Table 4.6 Summary of Horn PTT Delay and Doppler Spread Measurements

	Delay Spread (ns)			Doppler Spread (Hz)		
Antenna Height	20 mph	50 mph	79 mph	20 mph	50 mph	79 mph
6 ft	131.973	56.082	73.317	762.950	826.375	752.265
20 ft	20.575	55.007	7.533	684.558	711.836	527.887
40 ft	6.265	18.291	194.714	746.243	808.012	652.728

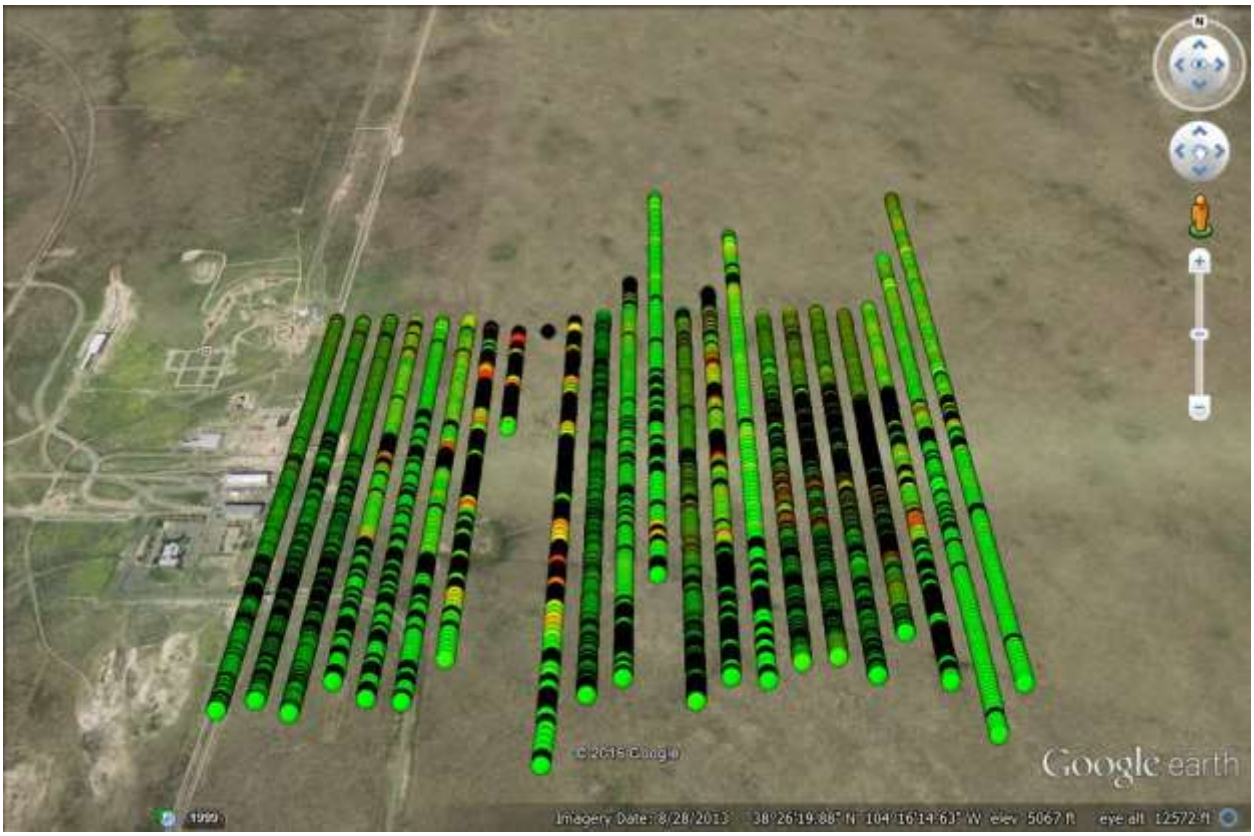

Figure 4.5 Horn PTT Delay Spread Visualization in Google Earth

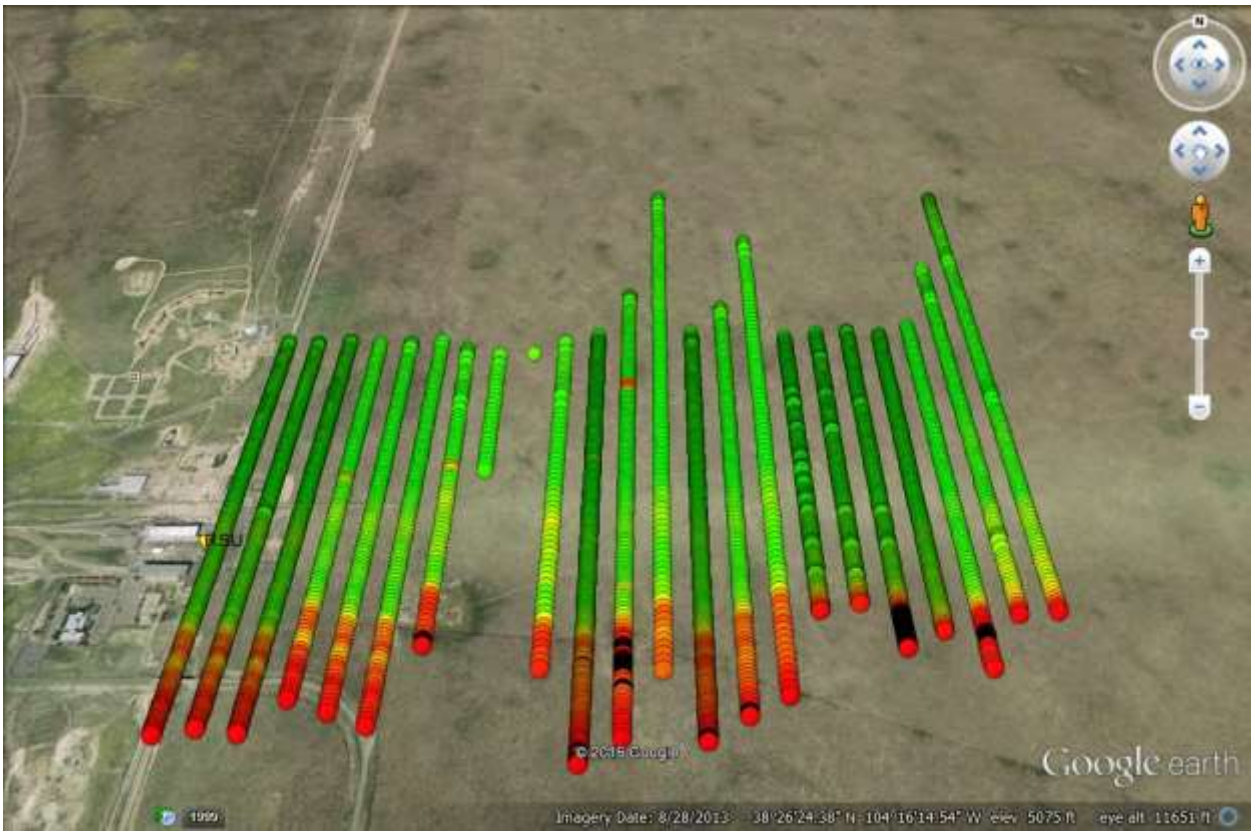

Figure 4.6 Horn PTT Doppler Spread Visualization in Google Earth

The Horn results show that both the delay spread and Doppler spread decrease as the distance between the transmitter and receiver decreases, which is expected because number of obstacles between the transmitter and receiver decreases, the stronger the line of sight component is, which decreases the effects of other multipath signals. However, as the transmitter gets very close to the receiver, the spreads begin to get slightly larger. This is due to the fact that the PTT test site was set up with obstacles near the receiver to emulate an urban environment. After a certain distance passed the receiver, the spreads show very large values because of a bridge that the train passed under blocking the line of sight.

Table 4.7 gives a summary of the results seen at the RTT test site for the Discone antenna and Figure 4.7 and Figure 4.8 give geographic representations of the measurements in google earth.

Table 4.7 Summary of Discone PTT Delay and Doppler Spread Measurements

	Delay Spread (ns)			Doppler Spread (Hz)		
Antenna Height	20 mph	50 mph	79 mph	20 mph	50 mph	79 mph
6 ft	1.359	5.640	14.336	666.965	672.816	643.17
20 ft	0.346	22.068	36.197	312.402	448.064	438.119
40 ft	2.941	9.164	3.825	405.394	437.655	469.813

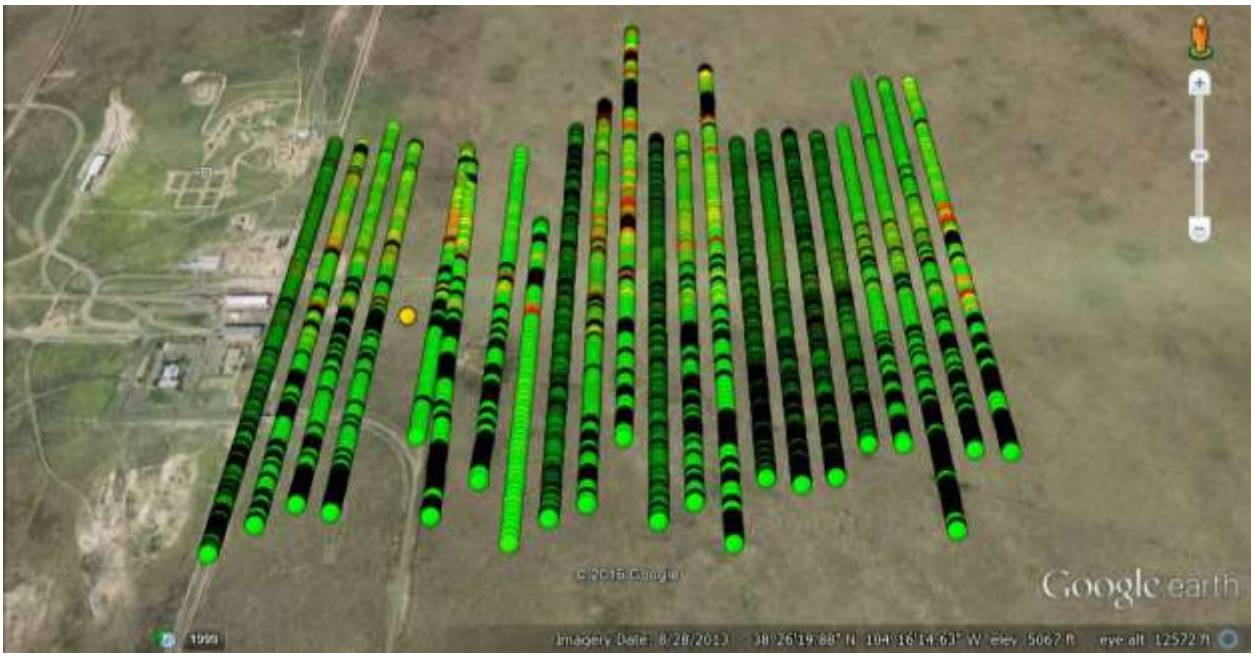

Figure 4.7 Discone PTT Delay Spread Visualization in Google Earth

Figure 4.8 Discone PTT Doppler Spread Visualization in Google Earth

The Discone results show that both the delay spread and Doppler spread decrease as the distance between the transmitter and receiver decreases, which is expected because number of obstacles between the transmitter and receiver decreases, the stronger the line of sight component is, which decreases the effects of other multipath signals. However, as the transmitter gets very close to the receiver, the spreads begin to get slightly larger. This is due to the fact that the PTT test site was set up with obstacles near the receiver to emulate an urban environment. Again, after a certain distance passed the receiver, the spreads show very large values because of a bridge that the train passed under blocking the line of sight.

4.3 Channel modeling

The path loss was calculated using the methods described in 3.3.1 so that a path loss model could be derived to find the path loss exponent for the large-scale path loss. The log-normal path loss model was chosen because the data showed a general increase in path loss as the distance between the transmitter and receiver increased. Although there are points that also show an increase in path loss as the distance between the transmitter and receiver decrease, log-normal model is still chosen because these point are likely due to an estimated receiver location, since the GPS location of the receiver was not recorded. The path loss exponents fell between 2 and 3 which was the expected range. According to Table 2.1, a path loss exponent closer to 2 corresponds with a free space propagation environment and a path loss exponent corresponds with an urban environment.

4.3.1 RTT Results

The path loss exponents are summarized in Table 4.8. Figure 4.9 to Figure 4.14 plot the path loss values that were calculated and the fitted path loss curve for each scenario tested. The calculated path loss exponents fall in the expected range of between 2 and 3. These results are expected because the system was operating under mainly a free space environment. However, for the higher path loss exponents seen by the Discone antenna suggest that the system was operating in a more obstructed environment. The Discone antenna's path loss exponents do decrease as the antenna height is raised because the line of sight component of the signal becomes stronger. These path loss models are also a based on an estimated receiver location, since the GPS location of the receiver was not recorded. Consequently the plots could show up to 50m of error, due to the speed of the train and the estimated GPS location.

Table 4.8 RTT Path Loss Model Summary

Antenna Type	Antenna Height (ft)	Path Loss Exponent (n)	Standard Deviation (σ)
Horn	6	2.1453	10.2696
	25	2.2914	14.0143
	32	2.1587	12.2731
Discone	6	3.0839	11.5290
	25	2.7923	8.5745
	32	2.7788	10.8051

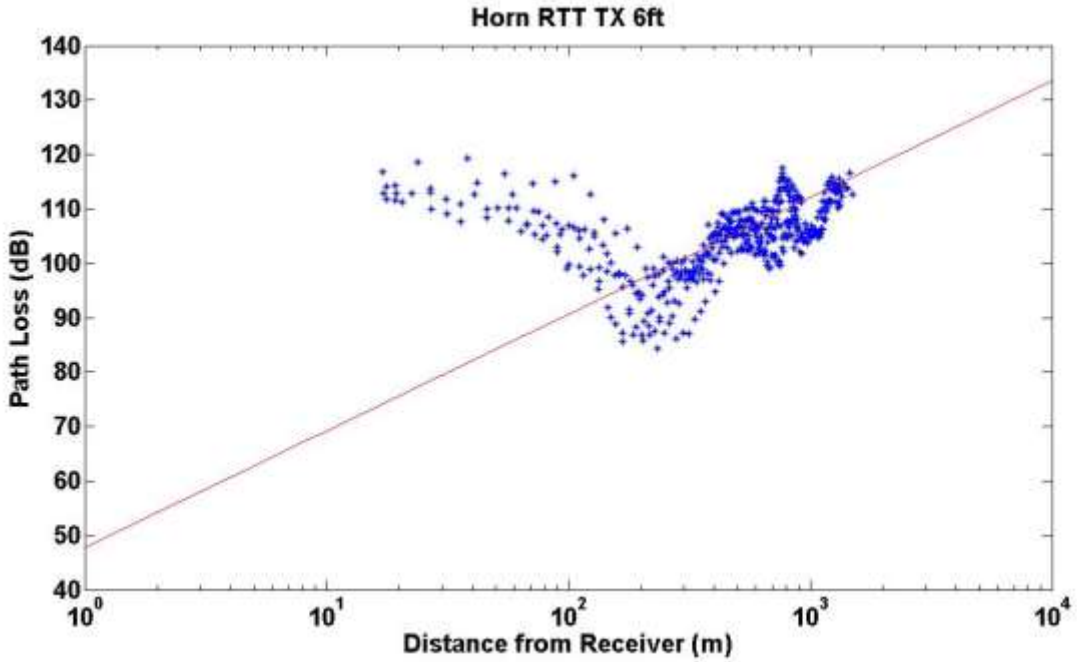

Figure 4.9 Path Loss model for the Horn antenna at a height of 6ft

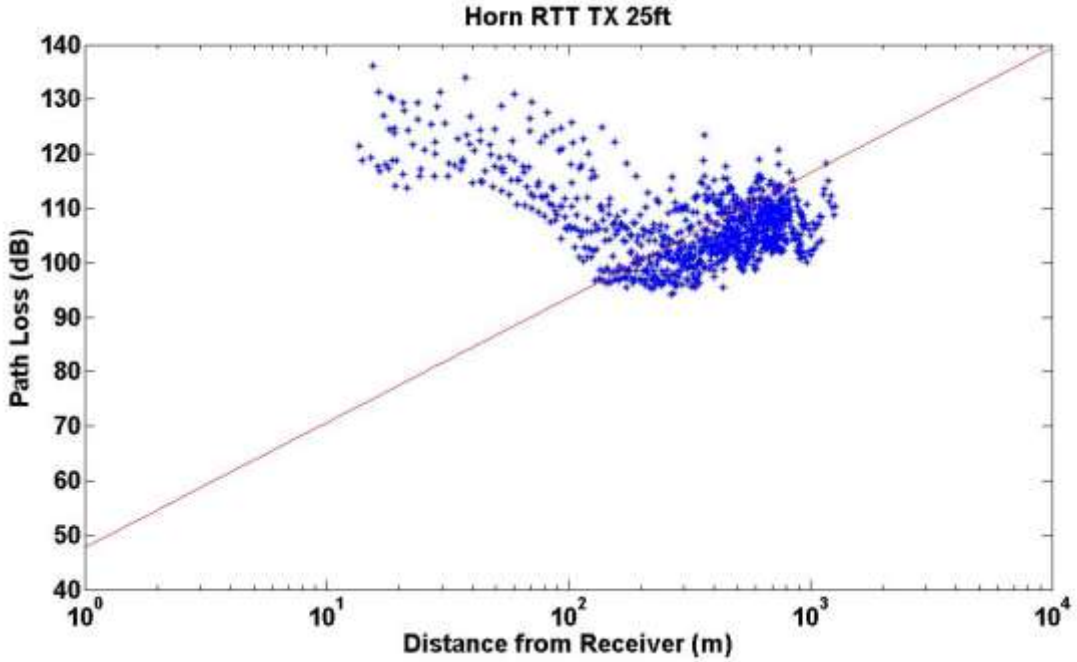

Figure 4.10 Path Loss model for the Horn antenna at a height of 25ft

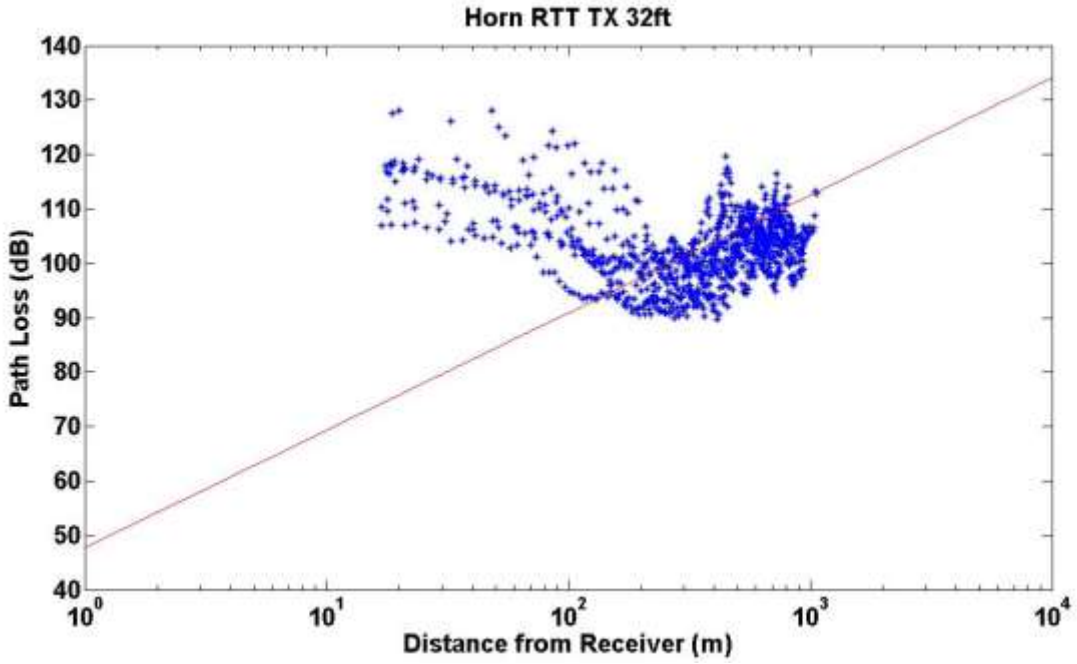

Figure 4.11 Path Loss model for the Horn antenna at a height of 32ft

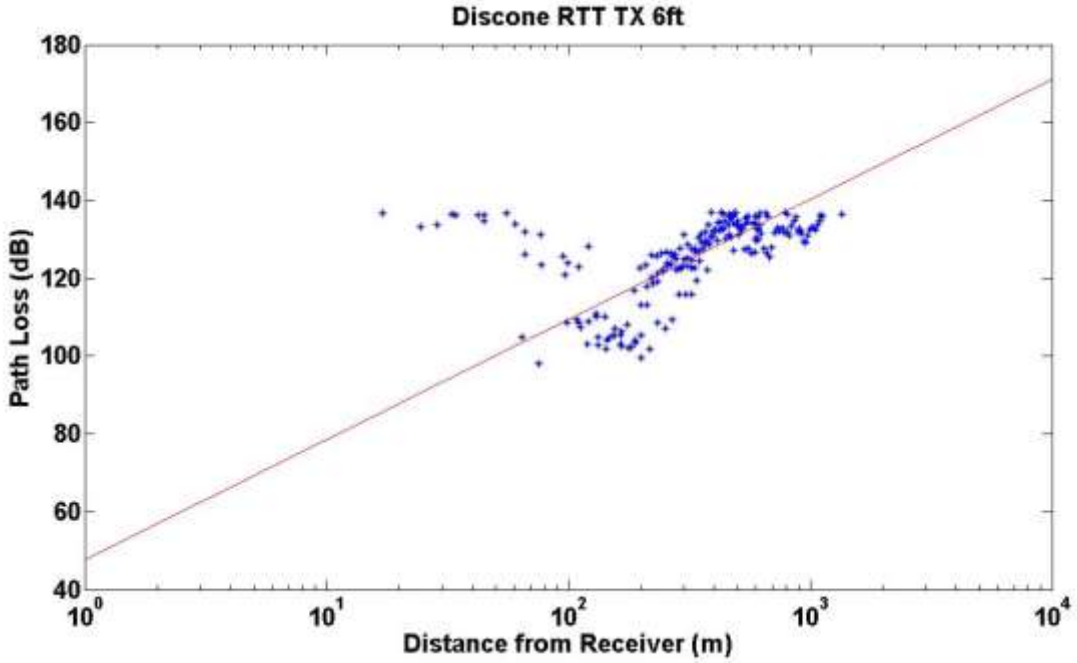

Figure 4.12 Path Loss model for the Discone antenna at a height of 6ft

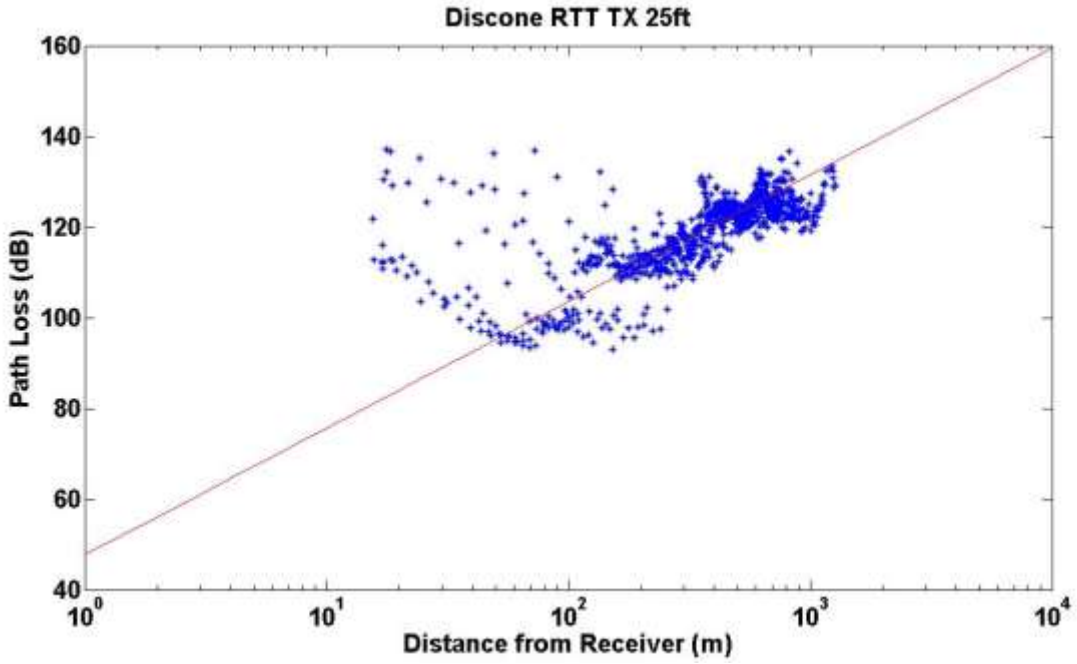

Figure 4.13 Path Loss model for the Discone antenna at a height of 25ft

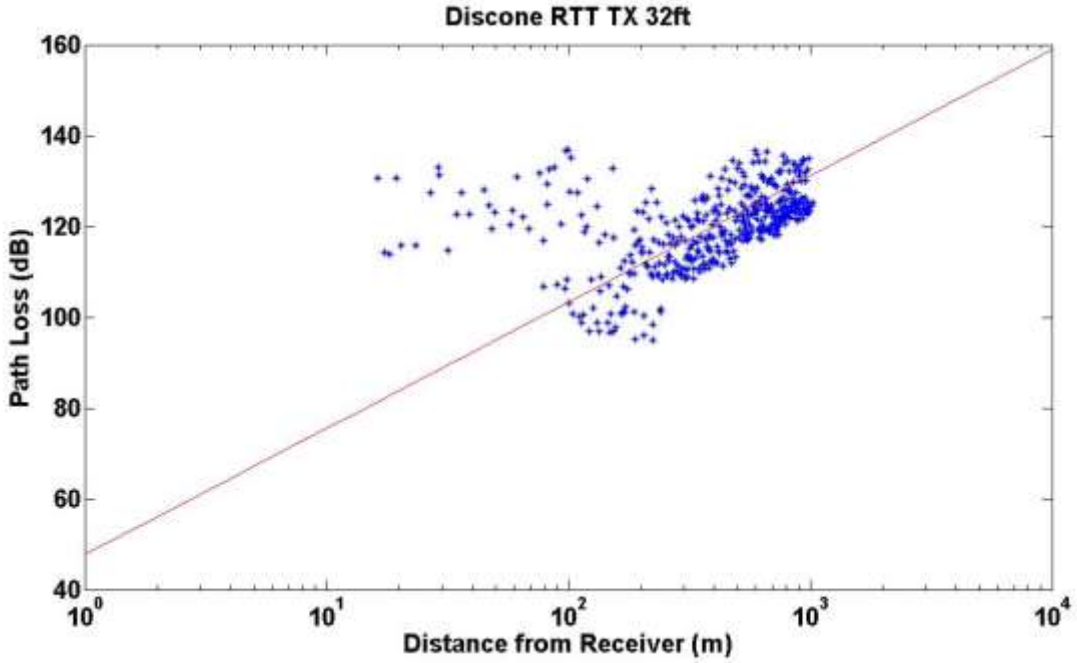

Figure 4.14 Path Loss model for the Discone antenna at a height of 32ft

4.3.2 PTT Results

The path loss exponents are summarized in Table 4.9. Figure 4.9 to Figure 4.14 plot the path loss values that were calculated and the fitted path loss curve for each scenario tested. The calculated path loss exponents fall in the expected range of between 2 and 3, this time falling closer to 3. These results are

expected because the system was operating under a more cluttered urban-like environment. These path loss models are also a based on an estimated receiver location, since the GPS location of the receiver was not recorded. Consequently the plots could show up to 50m of error, due to the speed of the train and the estimated GPS location. The Path Loss models show that as the transmitter and receiver distance gets shorter the path loss increases. The increase occurs because the obstructions were placed only around the receiver, otherwise the transmitter was operating in an environment that was closer to free space but still had more obstructions than the RTT test site.

Table 4.9 PTT Path Loss Model Summary

Antenna Type	Antenna Height (ft)	Path Loss Exponent (n)	Standard Deviation (σ)
Horn	6	2.1321	14.0539
	20	2.3273	12.6482
	40	2.4806	15.1446
Discone	6	2.7613	12.2964
	20	2.5898	10.6355
	40	2.8026	9.1178

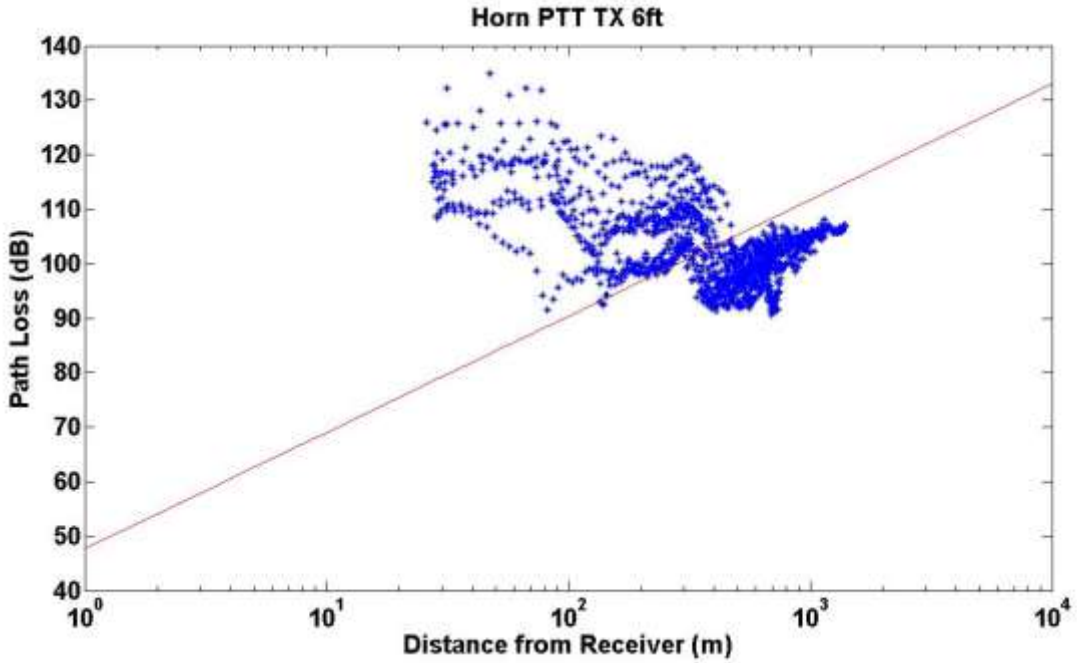

Figure 4.15 Path Loss Model for the Horn antenna at 6ft

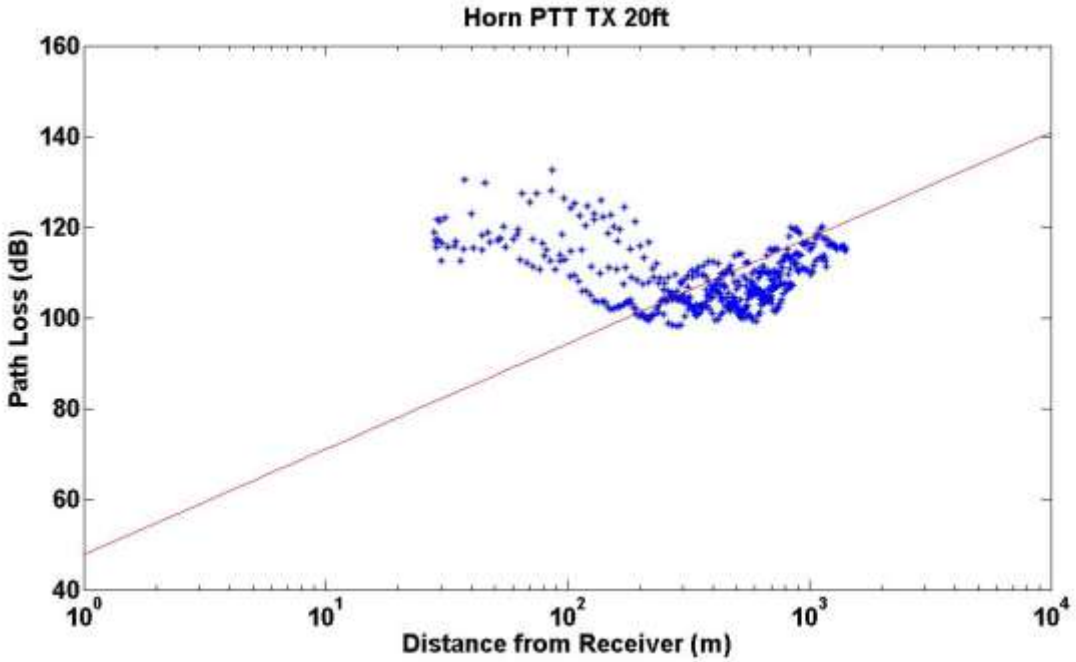

Figure 4.16 Path Loss Model for the Horn antenna at 20ft

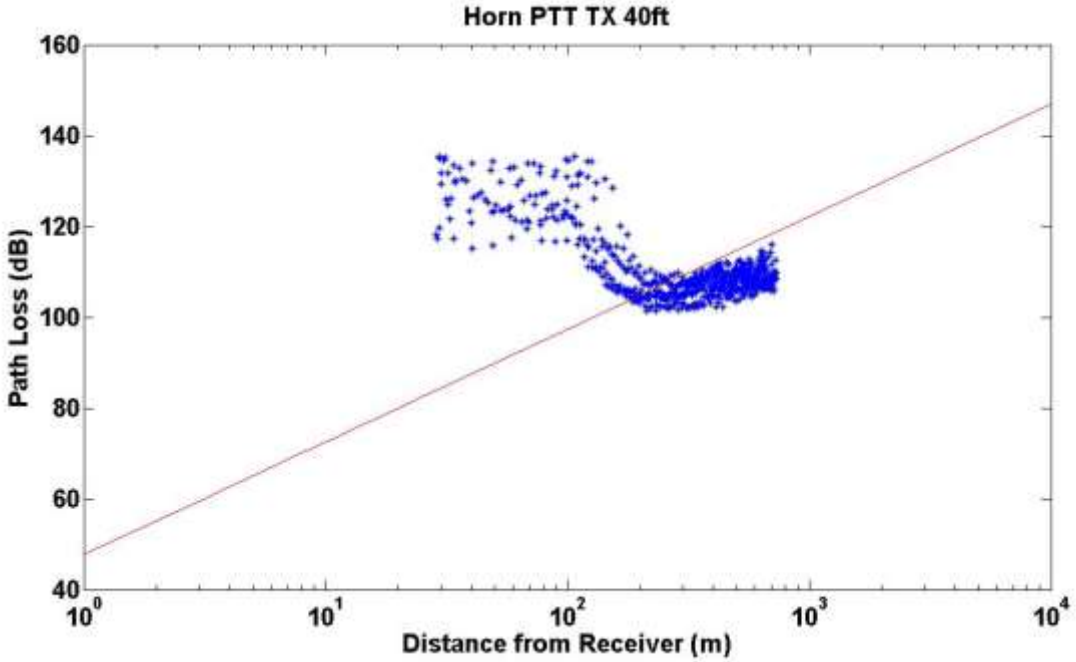

Figure 4.17Path Loss Model for the Horn antenna at 40ft

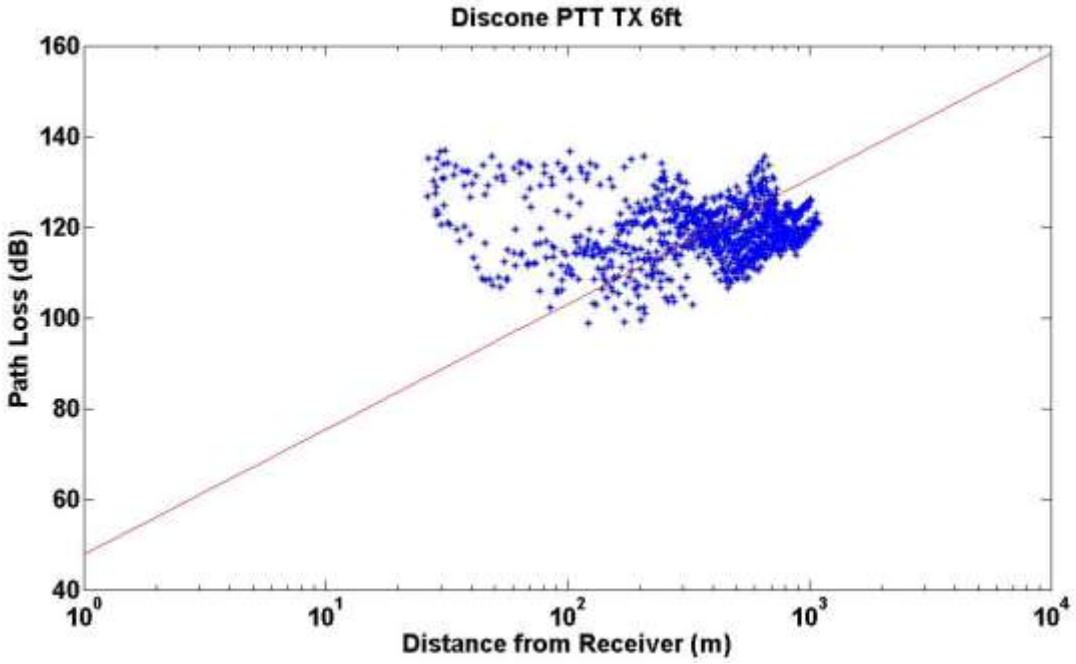

Figure 4.18 Path Loss Model for the Discone Antenna at 6ft

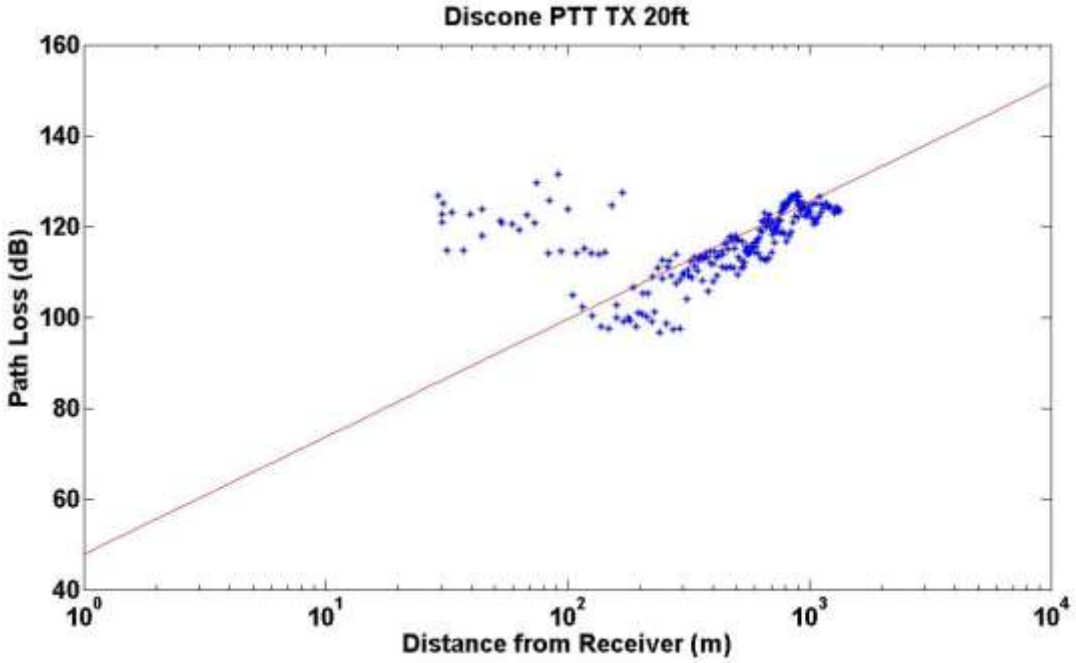

Figure 4.19 Path Loss Model for the Discone Antenna at 20ft

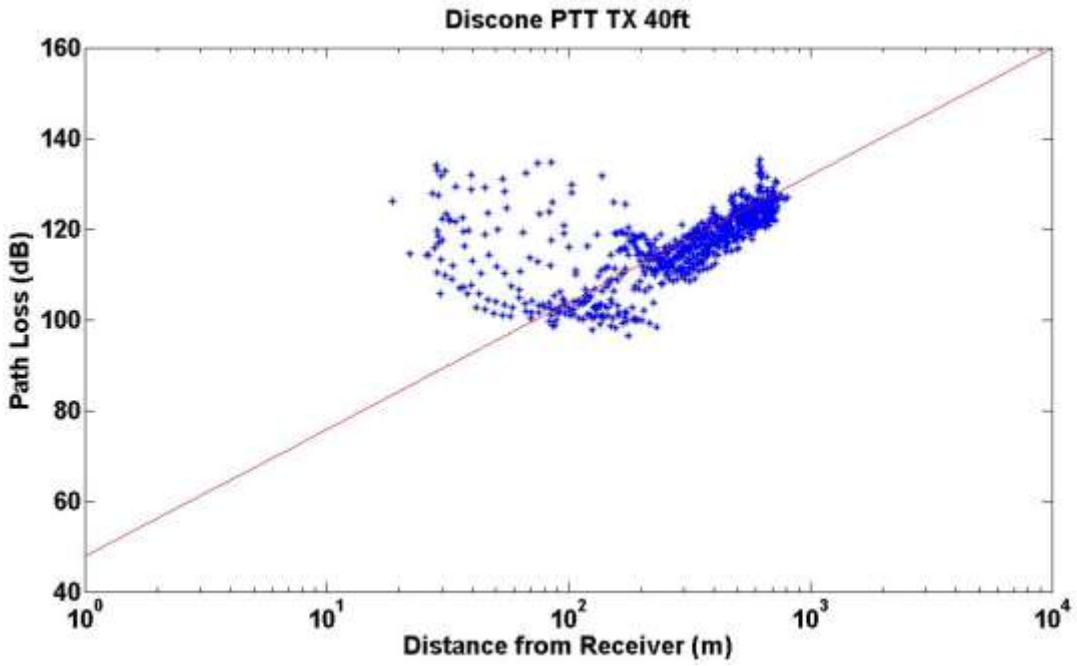

Figure 4.20 Path Loss Model for the Discone Antenna at 40ft

4.3.3 Small Scale Fading Model

The Rician K-factors were also calculated using the method described in 3.3.2. Rician models were chosen because the propagation environment did not show the severe fading effects where different K values were needed for different distances away from the receiver as suggested in literature. Instead the K values were generally consistent and were taken as an average for each speed the tests were conducted on. Table 4.10, below, shows the average Rician K-factor in dB for each speed. As shown in Figure 4.21, on the following page, the K values are generally consistent across the entire track that is made evident by the lack of change in color across the plots. The K-factors suggest that there is a line of sight component that is present which is expected because the RTT test site had minimal obstructions.

Table 4.10 Average Rician K-Factors (dB)

Antenna	20 mph	50 mph	79 mph
Discone	10.89	9.76	11.31
Horn	14.00	11.01	10.70

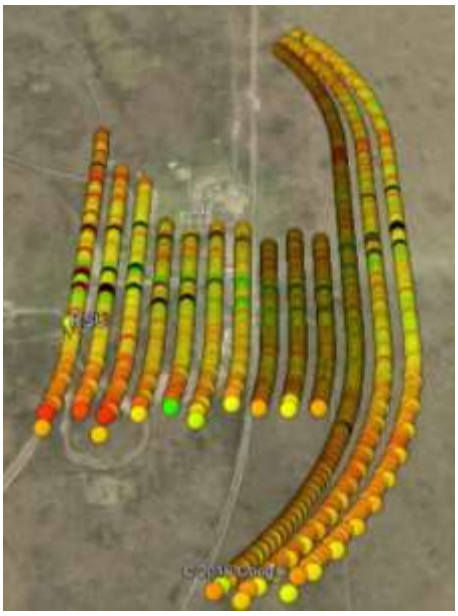

Figure 4.21 Google Earth Plot of K values in dB

5 Conclusions and Future Work

5.1 Summary of Results

This thesis serves as documentation and analysis of propagation data for train to vehicle scenarios at 5.9 GHz to facilitate the deployment of DSRC radios as a low cost advanced warning system. The motivation for this propagation research was prompted by the development of DSRC in the 5.9 GHz band as a dedicated band for vehicle to vehicle communications. Along with research opportunities in DSRC systems, the improved vehicle safety as a result of these systems is very high with the effects of advanced collision warning able to decrease the number of traffic accidents.

To test the DSRC alert system, the PER was derived to provide an approximation of how well the DSRC alert system will work when deployed in a real world environment. Three different antenna types were used, an Omni directional antenna, an Omni Directional Antenna setup for diversity operation, and a Linear Array. The Linear Array is designed such that the beam of the antenna, all of the energy, is directed in front of the train, so that the warning times could be maximized. When the DSRC advance warning system was operated in the open track with minimal obstacles, pessimistically, warning times were usually above 5 seconds at the maximum speed, but were larger at slower speeds. The linear array in most cases did not outperform either of the other two antennas tested, likely because; the beam was not angled such that a receiver, not directly in front of the beam, would be in the antenna's beam. However the antenna could be optimized to provide potentially more receiver coverage. The Omni and Omni diversity antennas performed about the same, with the Omni Diversity providing slightly more robust packet reception. The performance was also consistent between the locations for the OBU.

The Delay spread and Doppler spread were calculated to determine the small scale fading characteristics of the DSRC alert system channel. Plots of the Delay spread and Doppler spread were given in google earth to determine if multipath propagation factors were affecting the values at different locations on the track. The calculated data was compared to similar vehicle to vehicle measurement campaigns. Since there are no existing measurement campaigns performed between trains and vehicles in motion, the comparison to existing vehicle to vehicle measurements was used instead. The results found at TTCI, fall in the range of values seen in existing vehicle to vehicle measurement campaigns. However, the range of values in the existing measurement campaigns is large, which suggest the existing campaigns were not performed under comparable environmental conditions.

The large scale path loss models found fit a log-normal model best because the data showed a general increase in path loss as the distance between the transmitter and receiver increased. Although there are points that also show an increase in path loss as the distance between the transmitter and receiver decrease, log-normal model is still chosen because these point are likely due to an estimated receiver location, since the GPS location of the receiver was not recorded. Consequently the plots could show up to 50m of error, due to the speed of the train and the estimated GPS location. The calculated path loss exponents fall in the expected range of between 2 and 3. These results are expected because the system was operating under mainly a free space environment. However, for the higher path loss exponents seen by the Discone antenna suggest that the system was operating in a more obstructed environment.

The Discone antenna's path loss exponents do decrease as the antenna height is raised because the line of sight component of the signal becomes stronger.

5.2 Contributions

The primary contribution of this thesis was a highly detailed feasibility study for DSRC systems as an advanced warning system for train and vehicle collisions. Extensive software applications were also developed to analyze the performance of DSRC system in terms of packet error rate and post processing software was developed to convert I/Q data into received signal strength values. Multiple visualization techniques were also implemented in Matlab to provide a clear picture of the propagation environment. These software packages were then used to characterize the propagation environment a radio alert system may experience when deployed in a railroad environment. The DSRC implementation in this thesis proves to be a feasible alert system, but should be improved upon to provide a more robust alert system.

5.3 Future Work

There is a significant amount of propagation work to be done at 5.9 GHz as it pertains to train to vehicle communications. Residential environments, real urban environments, and foliage heavy environments must be considered. Delay between the packet reception and driver's reaction to the alert are also critically important, as they determine whether or not advanced warning can be given adequately. These studies would be ideally supplemented with an optimization of data rate and modulation scheme so that the maximum amount of data can be transmitted with the highest likelihood of being received. Additionally finding the optimum antenna beam orientation should be considered so that the distance a packet can be received from is also optimized for advanced warning.

References

[1] “Railroad Accident Questions,” Levin, Papantonio, Thomas, Mitchell, Echsner & Proctor, Attorneys at Law, [Online] 2012, http://train-accident-law.com/faq.html

[2] “FRA Office of Safety Analysis Web Site,” Federal Railroad Administration Office of Safety Analysis, [Online] 2013 http://safetydata.fra.dot.gov/OfficeofSafety/Default.aspx

[3] "Railroad-Highway Grade Crossing Handbook - Safety | Federal Highway Administration." Railroad-Highway Grade Crossing Handbook - Safety | Federal Highway Administration. Federal Railroad Administration, Aug. 2007. Web. 05 Feb. 2016.

[4] "Manual on Uniform Traffic Control Devices for Streets and Highways." (n.d.): n. pag. United States Department of Transportation, May 2012. Web. 05 Feb. 2016.

[5] Railroad-Highway Grade Crossing Handbook. Rep. Federal Highway Administration, Aug. 2007. Web.

[6] J. B. Kenney, "Dedicated Short-Range Communications (DSRC) Standards in the United States," in Proceedings of the IEEE, vol. 99, no. 7, pp. 1162-1182, July 2011.

[7] IEEE Standard 802.11-2012, Part 11 Wireless LAN Medium Access Control (MAC) and Physical Layer (PHY) Specifications

[8] IEEE Computer Society. "IEEE Standard for Information Technology - Telecommunications and Information Exchange between Systems - Local and Metropolitan Area Networks - Specific Requirements. Part 11: Wireless LAN Medium Access Control (MAC) and Physical Layer (PHY) Specifications Amendment 4: Protected Management Frames." (n.d.): n. pag. Internet Engineering Task Force. IEEE, 15 July 2010. Web. 4 Apr. 2016.

[9] "ISO/IEC Standard for Information Technology- Telecommunications and Information Exchange Between Systems- Local and Metropolitan Area Networks- Specific Requirements- Part 2: Logical Link Control (Incorporates IEEE Stds 802.2-1989, 802.2a-1993, 802.2b-1993, 802.2d-1993, 802.2e-1993, and 802.5p-1993)." (n.d.): n. pag. Web.

[10] Y. L. Morgan, "Notes on DSRC & WAVE Standards Suite: Its Architecture, Design, and Characteristics," in IEEE Communications Surveys & Tutorials, vol. 12, no. 4, pp. 504-518, Fourth Quarter 2010.

[11] P. Levin, Thomas, Mitchell, Echsner & Proctor, Attorneys at Law. (2012). Railroad Accident Questions. Available: http://train-accident-law.com/faq.html

[12] P. Subramanian, V. Navda, P. Deshpande, and S. R. Das, "A measurement study of inter-vehicular communication using steerable beam directional antenna," presented at the Proceedings of the fifth ACM international workshop on VehiculAr Inter-NETworking, San Francisco, California, USA, 2008.

[13] Hsu, C. Liang, L. Ke, and F. Huang, "Verification of On-Line Vehicle Collision Avoidance Warning System using DSRC," World Academy of Science, Engineering and Technology, vol. 55, pp. 377-383, 2009.

[14] Y. Xue, L. Jie, N. F. Vaidya, and Z. Feng, "A vehicle-to-vehicle communication protocol for cooperative collision warning," in The First Annual International Conference on Mobile and Ubiquitous Systems: Networking and Services, 2004, pp. 114-123.

[15]J. Singh, A. Desai, F. Acker, S. Ding, S. Prakasamul, A. Rachide, et al., "Cooperative intelligent transport systems to improve safety at level crossing," in The 12th Global Level Crossing and Trespass Symp., London, 2012.
[16]IEEE. "1609.2-2013 - IEEE Standard for Wireless Access in Vehicular Environments - Security Services for Applications and Management Messages." IEEE 1609.2. IEEE, 2013. Web. 04 Apr. 2016.
[17]J. B. Andersen, T. S. Rappaport and S. Yoshida, "Propagation measurements and models for wireless communications channels," in IEEE Communications Magazine, vol. 33, no. 1, pp. 42-49, Jan 1995.
[18]Vehicular-to-Vehicular Channel Characterization and Measurement Results Andrés J. Campuzano, Herman Fernández, David Balaguer, Antonio Vila, Bernardo Bernardo-Clemente, Vicent M. Rodrigo-Peñarrocha, Juan Reig, Alejandro Valero-Nogueira and Lorenzo Rubio
[19]L. Rubio, J. Reig and H. Hernandez. Propagation Aspects in Vehicular Networks. Vehicular Technologies: Increasing Connectivity. Miguel Almeida (Ed.): InTech, 2011.
[20]M. S. Pontes and L. A. R. S. Mello, "Review on terrestrial propagation channel modelling," Antennas and Propagation (EuCAP), 2010 Proceedings of the Fourth European Conference on, Barcelona, Spain, 2010, pp. 1-5.
[21]T. K. Sarkar, Zhong Ji, Kyungjung Kim, A. Medouri and M. Salazar-Palma, "A survey of various propagation models for mobile communication," in IEEE Antennas and Propagation Magazine, vol. 45, no. 3, pp. 51-82, June 2003.
[22]Rappaport, Theodore S. Wireless Communications: Principles and Practice. 2nd ed. Upper Saddle River, N.J;London;: Prentice Hall PTR, 2001. Web.
[23]T. Abbas, F. Tufvesson, and J. Karedal, “Measurement based Shadow Fading Model for Vehicle-to-Vehicle Network Simulations,” Computing Research Repository (CoRR), vol. abs/1203.3370, pp. 1-13, 2012
[24]R. Chen and Z. Zhong, "Analysis on V2V connectivity under dual-slope path loss model in urban scenarios," General Assembly and Scientific Symposium (URSI GASS), 2014 XXXIth URSI, Beijing, 2014, pp. 1-4.
[25]Jain, Raj. "Channel Models A Tutorial." Research Gate. Web. 26 May 2016.
[26]L. J. Greenstein, D. G. Michelson and V. Erceg, "Moment-method estimation of the Ricean K-factor," in IEEE Communications Letters, vol. 3, no. 6, pp. 175-176, June 1999.
[27]A. Abdi and M. Kaveh, "Performance comparison of three different estimators for the Nakagami m parameter using Monte Carlo simulation," in IEEE Communications Letters, vol. 4, no. 4, pp. 119-121, April 2000.
[28]J. Cheng and N. C. Beaulieu, "Generalized moment estimators for the Nakagami fading parameter," in IEEE Communications Letters, vol. 6, no. 4, pp. 144-146, April 2002.
[29]I. Sen and D. W. Matolak, "Vehicle–Vehicle Channel Models for the 5-GHz Band," in IEEE Transactions on Intelligent Transportation Systems, vol. 9, no. 2, pp. 235-245, June 2008.
[30]J. Maurer, T. Fugen and W. Wiesbeck, "Narrow-band measurement and analysis of the inter-vehicle transmission channel at 5.2 GHz," Vehicular Technology Conference, 2002. VTC Spring 2002. IEEE 55th, 2002, pp. 1274-1278 vol.3.

[31]L. Cheng, B. E. Henty, D. D. Stancil, F. Bai and P. Mudalige, "Mobile Vehicle-to-Vehicle Narrow-Band Channel Measurement and Characterization of the 5.9 GHz Dedicated Short Range Communication (DSRC) Frequency Band," in IEEE Journal on Selected Areas in Communications, vol. 25, no. 8, pp. 1501-1516, Oct. 2007.

[32]C. R. Anderson, “Design and implementation of an ultrabroadband millimeter-wavelength vector sliding correlator channel sounder and in-building multipath measurements at 2.5 & 60 GHz,” Master’s thesis, Virginia Tech, May 2002.

[33]Solomon, Otis M., Jr. "PSD Computations Using Welch's Method. [Power Spectral Density (PSD)] (Technical Report) | SciTech Connect." Sandia Labratories (1991): n. pag. PSD Computations Using Welch's Method. [Power Spectral Density (PSD)] (Technical Report) | SciTech Connect. Web. 12 June 2016.

Appendix A

TX PCAP Parser

```
function [DMSLon, DMSLat,numPackets] = PCAP_GPS_Parser_TX(infile)
    fid = fopen(infile);
    data = fread(fid)';
    fclose(fid);
    tempdata = data;

    [~,m] = size(tempdata);
    pcapHeader = 6*4;
%do a byte swap to get the bits into linux hexdump format
    for i=1:2:m
    if(i+1<=m)
        bytes = tempdata(i:i+1);
        data(i) = bytes(2);
        data(i+1) = bytes(1);
    else
        data(i) = 0;
        data(i+1) = tempdata(i);
    end
    end
    m = m-pcapHeader;
    file_header = dec2hex(data(1:pcapHeader));
    packetHeader = 16;
    start = pcapHeader +1;
%need to correct the 32 bit Endians to get correct values, we care about
%some of this data
    for i = start:4:start+packetHeader-1
    swap = data(i:i+3);
    data(i) = swap(3);
    data(i+1) = swap(4);
    data(i+2) = swap(1);
    data(i+3) = swap(2);
    end
    packet_header = data(start:start+packetHeader-1);
    packetLen = bitshift(packet_header(packetHeader-
3),24)+bitshift(packet_header(packetHeader-
2),16)+bitshift(packet_header(packetHeader-
1),8)+bitshift(packet_header(packetHeader),0);
%size of all our packets for this pcap
    start = start+packetHeader;
    numPackets = m/(packetLen+packetHeader);
%loop over the packets
    j = 1;
    DMSLat = zeros([1,numPackets]);
    DMSLon = zeros([1,numPackets]);
    while(j<=numPackets)
    if(mod(start,2) == 0)
        tstart = start -1;
    else
        tstart = start;
    end
    %byteswap individually again
    for i = tstart:2:tstart+packetLen-1
    swap = data(i:i+1);
```

```
    data(i) = swap(2);
    data(i+1) = swap(1);
    end
    packetBody = data(start:start+packetLen-1);
    lat = dec2hex(packetBody(107:110));
    lon = dec2hex(packetBody(111:114));
    lat = strcat(lat(1,:),lat(2,:),lat(3,:),lat(4,:));
    lon = strcat(lon(1,:),lon(2,:),lon(3,:),lon(4,:));
    lat = typecast(uint32(sscanf(lat, '%x')), 'int32');
    lon = typecast(uint32(sscanf(lon, '%x')), 'int32');
    lat =
double(sign(lat))*double(abs(floor(lat/10000000)))+double(rem(lat,10000000))/
10000000.0;
    lon =
double(sign(lon))*double(abs(floor(lon/10000000)))+double(rem(lon,10000000))/
10000000.0;
    DMSLat(j) = lat;
    DMSLon(j) = lon;
%skip the next packet header;
%Assumes that all packets are the same length
    start = start+packetLen+packetHeader;
    j=j+1;
    end

end
```

Appendix B

RX PCAP Parser

```
function [DMSLon, DMSLat, numPackets] = PCAP_GPS_Parser_RX(infile)
fid = fopen(infile);
data = fread(fid)';
fclose(fid);
tempdata = data;

[n,m] = size(tempdata);
pcapHeader = 6*4;
%do a byte swap to get the bits into linux hexdump format
for i=1:2:m
    if(i+1<=m)
        bytes = tempdata(i:i+1);
        data(i) = bytes(2);
        data(i+1) = bytes(1);
    else
        data(i) = 0;
        data(i+1) = tempdata(i);
    end
end
m = m-pcapHeader;
file_header = dec2hex(data(1:pcapHeader));
packetHeader = 16;
start = pcapHeader +1;
%need to correct the 32 bit Endians to get correct values, we care about
%some of this data
for i = start:4:start+packetHeader-1
    swap = data(i:i+3);
    data(i) = swap(3);
    data(i+1) = swap(4);
    data(i+2) = swap(1);
    data(i+3) = swap(2);
end
packet_header = data(start:start+packetHeader-1);
packetLen = bitshift(packet_header(packetHeader-
3),24)+bitshift(packet_header(packetHeader-
2),16)+bitshift(packet_header(packetHeader-
1),8)+bitshift(packet_header(packetHeader),0);
%size of all our packets for this pcap
start = start+packetHeader;
numPackets = m/(packetLen+packetHeader);
%loop over the packets
j = 1;
DMSLat = zeros([1,numPackets]);
DMSLon = zeros([1,numPackets]);
while(j<=numPackets)
    if(mod(start,2) == 0)
        tstart = start -1;
    else
        tstart = start;
    end
    %byteswap individually again
    for i = tstart:2:tstart+packetLen-1
    swap = data(i:i+1);
```

```
    data(i) = swap(2);
    data(i+1) = swap(1);
    end
    packetBody = data(start:start+packetLen-1);
    lat = dec2hex(packetBody(115:118));
    lon = dec2hex(packetBody(119:122));
    lat = strcat(lat(1,:),lat(2,:),lat(3,:),lat(4,:));
    lon = strcat(lon(1,:),lon(2,:),lon(3,:),lon(4,:));
    lat = typecast(uint32(sscanf(lat, '%x')), 'int32');
    lon = typecast(uint32(sscanf(lon, '%x')), 'int32');
    lat =
double(sign(lat))*double(abs(floor(lat/10000000)))+double(rem(lat,10000000))/
10000000.0;
    lon =
double(sign(lon))*double(abs(floor(lon/10000000)))+double(rem(lon,10000000))/
10000000.0;
    DMSLat(j) = lat;
    DMSLon(j) = lon;
%skip the next packet header;
%Assumes that all packets ar the same length
    start = start+packetLen+packetHeader;
    j=j+1;
end
end
```

Appendix C

Matlab Code For Google Earth DSRC Plots

```
clear all; close all;
format long;
TXFile = 'RTT/Tx/rtt_txa27.pcap';
RSUFileA = 'RTT/STA1(RSU)/rtt_rxa27.pcap';
RSUFileB = 'RTT/STA1(RSU)/rtt_rxb27.pcap';
OBUFileA = 'RTT/STA2(OBU)/rtt_rxa27.pcap';
OBUFileB = 'RTT/STA2(OBU)/rtt_rxb27.pcap';
RSUFileAinfo = dir(RSUFileA);
RSUFileBinfo = dir(RSUFileB);
OBUFileAinfo = dir(OBUFileA);
OBUFileBinfo = dir(OBUFileB);

[TXDMSLon,TXDMSLat,numPacketsTx] = PCAP_GPS_Parser_TX(TXFile);
%unique Packets for RSU
if ((RSUFileAinfo.bytes > 24) &&(RSUFileBinfo.bytes>24))
    RX1Overlap = uniqueIndices(TXFile,RSUFileA, RSUFileB);
else
    if(RSUFileAinfo.bytes > 24)
        RSUFile = RSUFileA;
    elseif(RSUFileBinfo.bytes>24)
        RSUFile = RSUFileB;
    end
    [RX1DMSLon, RX1DMSLat, numPacketsRX1] = PCAP_GPS_Parser_RX(RSUFile);
    index = 1;
    start = 1;
    for i = 1:numPacketsRX1
        testLon = RX1DMSLon(i);
        testLat = RX1DMSLat(i);
        for j = start:numPacketsTx
            if((testLon == TXDMSLon(j))&&(testLat == TXDMSLat(j)))
                RX1Overlap(index) = j;
                index = index +1;
                start = j+1;
                break;
            end
        end
    end
end

%unique OBU Packets
if ((OBUFileAinfo.bytes > 24) &&(OBUFileBinfo.bytes>24))
    RX2Overlap = uniqueIndices(TXFile,OBUFileA, OBUFileB);
else
    if(OBUFileAinfo.bytes > 24)
        OBUFile = OBUFileA;
    elseif(RSUFileBinfo.bytes>24)
        OBUFile = OBUFileB;
    end
    [RX2DMSLon, RX2DMSLat, numPacketsRX2] = PCAP_GPS_Parser_RX(OBUFile);
    index = 1;
    start = 1;
    for i = 1:numPacketsRX2
        testLon = RX2DMSLon(i);
```

```
        testLat = RX2DMSLat(i);
        for j = start:numPacketsTx
            if((testLon == TXDMSLon(j))&&(testLat == TXDMSLat(j)))
                RX2Overlap(index) = j;
                index = index +1;
                start = j+1;
                break;
            end
        end
    end
end

index = 1;
[~,m1] = size(RX1Overlap);
[~,m2] = size(RX2Overlap);
for i = 1:m1
    for j = 1:m2
        if(RX1Overlap(i)==RX2Overlap(j))
            bothOverlap(index) = RX1Overlap(i);
            index = index +1;
            break;
        end
    end
end

%determine what group points need to be plotted with
[~,mB] = size(bothOverlap);
for i = 1:mB
    bothLon(i) = TXDMSLon(bothOverlap(i));
    bothLat(i) = TXDMSLat(bothOverlap(i));
end
index = 1;
for i = 1:m1
    if(~ismember(RX1Overlap(i),bothOverlap))
       RX1Lon(index) =  TXDMSLon(RX1Overlap(i));
       RX1Lat(index) =  TXDMSLat(RX1Overlap(i));
       index = index +1;
    end
end
index = 1;
for i = 1:m2
    if(~ismember(RX2Overlap(i),bothOverlap))
       RX2Lon(index) =  TXDMSLon(RX2Overlap(i));
       RX2Lat(index) =  TXDMSLat(RX2Overlap(i));
       index = index +1;
    end
end
index = 1;
for i = 1:numPacketsTx
    if(~(ismember(i,RX1Overlap)||(ismember(i,RX2Overlap))))
        TXLon(index) =TXDMSLon(i);
        TXLat(index) =TXDMSLat(i);
        index = index +1;
    end
end
```

```
blue = 'FFFF0000';
yellow = 'FF00D5FF';
green = 'FF00FF00';
k = kml('Test Case 4');
f = k.createFolder('TX');
f.scatter(TXLon, TXLat, 'name', 'TX Points', 'iconColor', 'FFFFFFFF');
f.scatter(RX1Lon, RX1Lat, 'name', 'RSU', 'iconColor', yellow);
f.scatter(RX2Lon, RX2Lat, 'name', 'OBU', 'iconColor', blue);
f.scatter(bothLon, bothLat,'name', 'overlapping', 'iconColor', green);

k.run;
```

Appendix D

Matlab Code for PER calculations

```
%PTT DATA CSV
%get the subdirectories names
clear all; close all;
format long;

path = 'PTT';
subs = dir(path);
numSubs = size(subs);
units = zeros([numSubs-2, 1]);
for i = 3:numSubs(1)
    units{i-2}= subs(i).name;
end

%get all the files

for i = 1:numSubs(1)-2
    d = strcat(path,'/',units{i});
    files = dir(d);
    numFiles = size(files);
    k = 1;
    for j = 3:numFiles(1)
        if(files(j).bytes>24)
            fileNames{i,k} = files(j).name;
            k=k+1;
        end
    end
    nFiles(i) = k-1;
    D{i} = d;
end

%group files together
for i = 1:nFiles(1)
    [~,m] = size(fileNames{1,i});
    index = str2num(fileNames{1,i}(m-6:m-5));
    k = 1;
    TxFiles{index} = fileNames{1,i};
    for j = 1:nFiles(2)
        [~,n] = size(fileNames{2,j});
        match = str2num(fileNames{2,j}(n-6:n-5));
        if(match == index)
            matchFileA{index,k} = fileNames{2,j};
            k=k+1;
        end
    end
    k = 1;
    for j = 1:nFiles(3)
        [~,n] = size(fileNames{3,j});
        match = str2num(fileNames{3,j}(n-6:n-5));
        if(match == index)
            matchFileB{index,k} = fileNames{3,j};
            k=k+1;
        end
    end
end
```

```
%find the max length of data:
MAXR = 0;
[~,m] = size(TxFiles);
for i = 1:m
    [~,s] = size(TxFiles{i});
    if s > 0
        [TXDMSLon,TXDMSLat,numPacketsTx] =
PCAP_GPS_Parser_TX(strcat(D{1},'/',TxFiles{i}));
        R = 6371000; %average radius of earth in meters
        TXLonRad = TXDMSLon * pi/180.0;
        TXLatRad = TXDMSLat * pi/180.0;
        n = 25;
        distances = DistanceBetweenGPS(TXLonRad,TXLatRad,R,n);
        [~,mR] = size(distances);
        allDistances(i,1:mR) = distances;
        if(mR>MAXR)
            MAXR=mR;
        end
    end;
end

% %Process Data for first set of files
for i = 1:m
    [~,s] = size(TxFiles{i});
    if s > 0
        [~,isB] = size(matchFileA{i,2});
        if( isB == 0)
            [TXDMSLon,TXDMSLat,numPacketsTx] =
PCAP_GPS_Parser_TX(strcat(D{1},'/',TxFiles{i}));
            [RX1DMSLon, RX1DMSLat, numPacketsRX1] =
PCAP_GPS_Parser_RX(strcat(D{2},'/',matchFileA{i,1}));
            index = 1;
            start = 1;
            for k = 1:numPacketsRX1
                testLon = RX1DMSLon(k);
                testLat = RX1DMSLat(k);
                for j = start:numPacketsTx
                    if((testLon == TXDMSLon(j))&&(testLat == TXDMSLat(j)))
                        RX1Overlap(index) = j;
                        index = index +1;
                        start = j+1;
                        break;
                    end
                end
            end

        else
            [TXDMSLon,TXDMSLat,numPacketsTx] =
PCAP_GPS_Parser_TX(strcat(D{1},'/',TxFiles{i}));
            file1 = strcat(D{2},'/',matchFileA{i,1});
            file2 = strcat(D{2},'/',matchFileA{i,2});
            [RX1DMSLon, RX1DMSLat, numPacketsRX1] =
PCAP_GPS_Parser_RX(file1);
            [RX2DMSLon, RX2DMSLat, numPacketsRX2] =
PCAP_GPS_Parser_RX(file2);
            %get the msg counts
            msgCount1 = getMsgCnt(file1);
```

```
            msgCount2 = getMsgCnt(file2);
            txCount = getMsgCntTX(strcat(D{1},'/',TxFiles{i}));

            index = 1;
            start = 1;
            for k = 1:numPacketsRX1
                testLon = RX1DMSLon(k);
                testLat = RX1DMSLat(k);
                msgCount = msgCount1(k);
                for j = start:numPacketsTx
                    if((testLon == TXDMSLon(j))&&(testLat ==
TXDMSLat(j))&&(msgCount == txCount(j)))
                        RX1Overlap(index) = j;
                        index = index +1;
                        start = j+1;
                        break;
                    end
                end
            end
            start = 1;
            for k = 1:numPacketsRX2
                testLon = RX2DMSLon(k);
                testLat = RX2DMSLat(k);
                msgCount = msgCount2(k);
                for j = start:numPacketsTx
                    if((testLon == TXDMSLon(j))&&(testLat ==
TXDMSLat(j))&&(msgCount==txCount(j))&&(~ismember(j,RX1Overlap)))
                        RX1Overlap(index) = j;
                        index = index +1;
                        start = j+1;
                        break;
                    end
                end
            end
            sort(RX1Overlap);
        end
        %calculate the PERs
        R = 6371000; %average radius of earth in meters
        TXLonRad = TXDMSLon * pi/180.0;
        TXLatRad = TXDMSLat * pi/180.0;
        n = 25;
        indices = DistanceBetweenGPS(TXLonRad,TXLatRad,R,n);
        [numRX1,numPacketsTXRange]=findPacketsInRange(RX1Overlap,indices);
        [~,mR] = size(indices);
        PER = zeros([1 mR-1]);
        for k = 1:mR-1
            PER(k) = 1-(numRX1(k)/numPacketsTXRange(k));
        end
        range = [1:MAXR-1]*n;
        dataToOut(1,1:MAXR-1) = range;
        dataToOut(i+1,1:mR-1) = PER;
        dataToOut(i+1,mR:MAXR-1) = ones([1 MAXR-mR]);
    end
end
```

Appendix E

Matlab Code to Convert I/Q data to RSS

```
clear all; close all;
matlabpool(4);
% Load the captured data file
%
d = 'D:\TTCI_Horn\*.dat';
prefix = 'D:\TTCI_Horn\';
set(0, 'DefaultAxesFontSize', 20)
set(0, 'DefaultAxesFontWeight','Bold')
% Set the sampling frequency
fs=30.72/2;                     % Divided by 2 to account for downsampling
fs = fs*1e6;
Ts = 1/fs;

% Obtain the 2047 bit PN Sequence
pnseq = csvread('PN_2047.txt');
%
pnseq = 2*pnseq - 1;  % Make pn seq an antipodal sequence
%
pnlength = length(pnseq);  % Length of the PN Sequence in Chips
%
pntime = 0:Ts:Ts*(pnlength-1);

filename = dir(d);
Q = length(filename);
outdata(Q)=struct('time',[],'RSSI',[],'small',[]);
parfor q = 1:Q;
    file = strcat(prefix,filename(q).name);
    q
    %GET RECIEVER GAIN FROM MATCHING LOG FILE
    timestamp = strsplit(char(filename(q).name),'d');
    timestamp = char(timestamp(1));
    timestamp = timestamp(1:19);
    logFile = strcat(prefix,timestamp,'_log.txt');
    f = fopen(logFile, 'r');  % Open file for reading
    log_data = textscan(f, '%s', 'Delimiter', '\r\n');
    fclose(f);
    RXGVal = strsplit(char(log_data{1,1}(4)),':');
    RXGVal = str2double(char(RXGVal(2)));
    offset = -0.7429*RXGVal-83.49;

    datafile = fopen(file, 'rb');           % 'rb' = default file access,
Big-endian ordering
    % Read and process data file in blocks
    numpnseq = 3752;                        % number of pn-sequence blocks to
process for approx 1/2 sec of data
    segsize = 2*pnlength*numpnseq;            % segment size to process
(factor of 2 to account for 2 samples per chip)

    % Process each data segment.  Check for end of file at each iteration.
    counter = 0;
    %K = 512;   %FFT size
    %PXX_OUT = zeros(K,1000);
    RSSI = zeros(1000,1);
    RSSISmall = zeros(1000,1);
```

```
    while (~feof(datafile))%&&(counter<2)
        counter = counter+1                     % Tracks number of iterations

        z = fread (datafile, [2,segsize], 'float');
        data = z(1,:) + z(2,:)*1i;
        [r, c] = size (data);
        data = reshape (data, c, r);

        ds_data = decimate(data,2,'fir');
        M = length(ds_data);

        if M < 5e5
            break
        end

        m = 0:M-1;

        % Now, we need to handle correlating the Inphase and Quadrature in
order to
        % generate the Magnitude and Phase PDP's

        i_data = real(ds_data);
        q_data = imag(ds_data);

        % Run the cross-correlation, generate the time vector, and plot the
results
        % Note that the time vector starts at an offset of the PN length

        pdp_i = xcorr(i_data,pnseq');
        pdp_q = xcorr(q_data,pnseq');
        L = length(pdp_i);
        %
        % Since the first L/2 -1 correlation results = 0, these values are
        % discarded to preserve memory and minimize calculations
        %
        pdp_i = pdp_i(floor(L/2):L);
        pdp_q = pdp_q(floor(L/2):L);
        pdp_complex = pdp_i+1i*pdp_q;
        pdp_mag = abs(pdp_complex);
        %PDP phase

        thres = 3*std(pdp_complex);
        b = find(pdp_mag>=thres);
        if isempty(b)
            shift = 0;
            RSSI(counter) = NaN;
        else

            RSSwatts = sum((pdp_i(b).^2)+(pdp_q(b).^2))./numpnseq;
            RSSdBu = 10.0*log10(RSSwatts)+30;
            calRSSdBm = RSSdBu +offset;
            RSSI(counter) = calRSSdBm;

            %Small Scale RSSI
            shift = min(b)-1;
            % Circular shift magnitude sequence so that first peak is at
index 1
            pdp_mag = circshift(pdp_mag,-shift);
            pdp_i = circshift(pdp_i,-shift);
            pdp_q = circshift(pdp_q,-shift);
```

```
            %pdp_phase = circshift(pdp_phase,-shift);
            LL = floor(length(pdp_mag)/pnlength);
            % Reshape normalized magnitude vector to a matrix with 2047 rows
            pdp_mag_small = reshape(pdp_mag(1:pnlength*LL),2047,LL);
            %pdp_phase_small = reshape(pdp_phase(1:pnlength*LL),2047,LL);
            pdp_I_small = reshape(pdp_i(1:pnlength*LL),2047,LL);
            pdp_Q_small = reshape(pdp_q(1:pnlength*LL),2047,LL);
            [row, col] = size(pdp_mag_small);

            small_temp = zeros(col-1,1);
            for nn = 1:col-1
                ind = find(pdp_mag_small(:,nn)>thres);
                if isempty(ind)
                    RSSISmall(counter,nn) = NaN;
                else
                    pksPDP = pdp_mag_small(ind,nn);
                    pksI = pdp_I_small(ind,nn);
                    pksQ = pdp_Q_small(ind,nn);
                    smallRSSwatts = sum(pksI.^2+pksQ.^2); %single element
                    smallRSSdBu = 10.0*log10(RSSwatts)+30;
                    smallRSSdBm = smallRSSdBu +offset;
                    RSSISmall(counter,nn) = smallRSSdBm;
                end

            end


        end
    end
    %savefilename = [timestamp,'_RSSIresults.mat'];
    %data = struct();
    outdata(q).time = timestamp;
    outdata(q).RSSI = RSSI(1:counter);
    outdata(q).small = RSSISmall(1:counter,:);

    fclose(datafile);
end
matlabpool close;
```

Appendix F

RSS Channel Visualization

```
% Plots the RSS vs. Distance and Plots in Google Earth
close all; clear all;
%timestamp = '2015.09.24.10.27.43';
matfile = 'sanityTest3.mat';
FILEPATH = 'D:\TTCI_Discone\';
kmlDir = 'sanity';
dPTT40 = [1:6,8:11];
dPTT20 = 12:17;
dPTT06 = 18:31;
dRTT06 = 32:39;
dRTT25 = 40:48;
dRTT32 = 49:58;
hPTT40 = 1:10;
hPTT20 = 11:16;
hPTT06 = 17:30;
hRTT06 = 31:39;
hRTT25 = 40:48;
hRTT32 = 49:58;
MIN = -110;
MAX = -40;
numbins=101;
mid = 51;
k = kml(kmlDir);
f = k.createFolder(kmlDir);
load(matfile);
start = 55;%dPTT40(1);
for i = [55,56]
    logfile = [FILEPATH,outdata(i).time,'_log.txt'];
    if exist(logfile,'file')==2
        [GPS, time] = NMEAGPSParser(logfile);
        [iGPS, iTime] = FRAGPSInterpolator(GPS,time);
        lat = iGPS(:,1);
        lon = iGPS(:,2);
        uplat = upsampler(lat,2);
        uplon = upsampler(lon,2);
        uplon = uplon+(double(i-start)*.001);
        rgb = RSSIcolorScale(outdata(i).RSSI,numbins,mid,MIN,MAX);
        rgb = cellstr(rgbtohexstringGE(rgb));
        [len, ~] = size(rgb);
        if(len>length(uplon))
            len = length(uplon);
        end
        f.scatter(uplon(1:len), uplat(1:len),
'name',outdata(i).time,'iconColor',rgb,'iconScale',.5);
    else
        logfile
    end
end
k.run
```

Appendix G

Path Loss Generator

```
%calculate path loss models
clear all; close all;
FILEPATH = 'D:\TTCI_Discone\';
MATFILE = 'RSSDiscone.mat';
set(0, 'DefaultAxesFontSize', 20)
set(0, 'DefaultAxesFontWeight','Bold')
%files = dir(d);
%First part of code compiles all the RSS data for a given scenario
Horn_PTT40 = 1:6;%[1:6,8:11];
Horn_PTT20 = 12:16;%12:17;
Horn_PTT6 = [17:25,27:30];%18:31;%
Horn_RTT6 = 34:39; %[32:34,36:39];%
Horn_RTT25 = 40:48;
Horn_RTT32 = 49:58;
Disc_PTT40 = [1:6,8:10];
Disc_PTT20 = [13:14,17];%12:17;
Disc_PTT6 = [19,21:31];%18:31;%
Disc_RTT6 = 36:39; %[32:34,36:39];%
Disc_RTT25 = 40:48;
Disc_RTT32 = [49:51,55:58];
load(MATFILE);
fixedPTTLat =38.436225*pi/180.0;%                %THESE VARIABLES NEED TO BE
EDITED
fixedPTTLon =-104.2821*pi/180.0;%
fixedRTTLat = 38.431433*pi/180.0;
fixedRTTLon = -104.294969*pi/180.0;
R = 6371000; %average radius of earth in meters
start = 1;
start2 = 1;
t = 'Discone RTT TX 32ft';
figFile = 'FinalizedPathLossPlots/DisconeApproachPathLoss/DisconeRTT32';
for i = Disc_RTT32
    %mark = [colors(mod(i-17,7)+1),markers(i-17)];
    timestamp = outdata(i).time;
    logfile = [FILEPATH,timestamp,'_log.txt'];
    if exist(logfile,'file')==2
        [GPS, time] = NMEAGPSParser(logfile);
        [iGPS, iTime] = FRAGPSInterpolator(GPS,time);
        lat = iGPS(:,1);
        lon = iGPS(:,2);
        uplat = upsampler(lat,2);
        uplon = upsampler(lon,2);
        distances =
DistancefromFixedGPS(uplon*pi/180.0,uplat*pi/180.0,R,fixedPTTLon,
fixedPTTLat);
        Thresh = find(outdata(i).RSSI>-95.0 & outdata(i).RSSI<0);
        RealRSS = outdata(i).RSSI(Thresh);
        RealDistances = distances(Thresh);
        split = find(RealDistances == min(RealDistances));
        len = length(RealRSS);
        if(len >length(RealDistances))
            len = length(RealDistances);
        end
```

```
        approachDistances(start:start+split-1) = RealDistances(1:split);
        approachRSSI(start:start+split-1)=RealRSS(1:split);
        departDistances(start2:start2+len-split-
1)=RealDistances(split+1:len);
        departRSSI(start2:start2+len-split-1)=RealRSS(split+1:len);
        start = start+split;
        start2 = start2+len-split;
    end
end
%semilogx(approachDistances,approachRSSI,'*')
%I = find(approachDistances>100);
%Generates the Path Loss Exponent and Sigma Value
Freq = 5.8*10^9; %carrier frequency
lambda = (3.0*10^8)/Freq; %wavelength
PtWatts = 3.1; %Transmit Power in Watts
PtdB = 10.0*log10(PtWatts)+30.0; %Transmit Power in dBm
HornGaindB = 20.0;
DisconeGaindB = 3.6;
PLd0 = 20.0*log10(((4*pi)/lambda));
Gt = DisconeGaindB;
Gr = DisconeGaindB;
distances = [1.0, approachDistances]; %reference distance = 1m
%PL(1) = PLd0;
PL = [PLd0,PtdB+Gt+Gr-approachRSSI];
[n, Sigma, fit_power]=findpathloss(distances,PL);
semilogx(distances(2:end),PL(2:end),'*');
hold on;
plot(1:10000,PLd0+n*10*log10(1:10000),'r')
title(t,'FontSize',20,'FontWeight','bold');
xlabel('Distance from Receiver (m)','FontSize',20,'FontWeight','bold');
ylabel('Path Loss (dB)','FontSize',20,'FontWeight','bold');
n
savefig(figFile);
```

Appendix H

Distance between GPS Points

```
function [indices] = DistanceBetweenGPS(Lon, Lat, R, n)
compPT = 1;
j = 1;
[~,numPts] = size(Lon);
for i = 2:numPts
    lat1 = Lat(compPT);
    lat2 = Lat(i);
    dLat = lat2-lat1;
    dLon = Lon(i)-Lon(compPT);
    a = sin(dLat/2)*sin(dLat/2)+cos(lat1)*cos(lat2)*sin(dLon/2)*sin(dLon/2);
    c = 2*atan2(sqrt(a),sqrt(1-a));
    d = R*c;
    if(d>=n)
        compPT = i;
        indices(j) = i-1;
        j = j+1;
    end
end
end
```

Appendix I

Get MSG count

```
function [msgCnt] = getMsgCnt(infile)
fid = fopen(infile);
data = fread(fid)';
fclose(fid);
tempdata = data;
[n,m] = size(tempdata);
pcapHeader = 6*4;
%do a byte swap to get the bits into linux hexdump format
for i=1:2:m
    if(i+1<=m)
        bytes = tempdata(i:i+1);
        data(i) = bytes(2);
        data(i+1) = bytes(1);
    else
        data(i) = 0;
        data(i+1) = tempdata(i);
    end
end
m = m-pcapHeader;
file_header = dec2hex(data(1:pcapHeader));
packetHeader = 16;
start = pcapHeader +1;
tempdata= data;
%need to correct the 32 bit Endians to get correct values, we care about
%some of this data
for i = start:4:start+packetHeader-1
    swap = data(i:i+3);
    data(i) = swap(3);
    data(i+1) = swap(4);
    data(i+2) = swap(1);
    data(i+3) = swap(2);
end
packet_header = data(start:start+packetHeader-1);
packetLen = bitshift(packet_header(packetHeader-
3),24)+bitshift(packet_header(packetHeader-
2),16)+bitshift(packet_header(packetHeader-
1),8)+bitshift(packet_header(packetHeader),0);
%size of all our packets for this pcap
start = start+packetHeader;
numPackets = m/(packetLen+packetHeader);
data = tempdata;                % the value we care about is only a byte

msgCnt = zeros([1,numPackets]);
j =1;
while(j<=numPackets)
    grab = 107;
    if(mod(start,2) == 0)
        tstart = start-1;
        for i = tstart:2:tstart+packetLen-1
            swap = data(i:i+1);
            data(i) = swap(2);
            data(i+1) = swap(1);
        end
```

```
        grab = 108;
    end
    packetBody = data(start:start+packetLen-1);
    msgCnt(j) = packetBody(grab);
    start = start+packetLen+packetHeader;
    j=j+1;
end
end
```

Appendix J

Get Msg Count for TX packets

```
function [msgCnt] = getMsgCntTX(infile)
fid = fopen(infile);
data = fread(fid)';
fclose(fid);
tempdata = data;
[n,m] = size(tempdata);
pcapHeader = 6*4;
%do a byte swap to get the bits into linux hexdump format
for i=1:2:m
    if(i+1<=m)
        bytes = tempdata(i:i+1);
        data(i) = bytes(2);
        data(i+1) = bytes(1);
    else
        data(i) = 0;
        data(i+1) = tempdata(i);
    end
end
m = m-pcapHeader;
file_header = dec2hex(data(1:pcapHeader)); %its not the completely correct
header but its good enough for now
packetHeader = 16;
start = pcapHeader +1;
tempdata= data;
%need to correct the 32 bit Endians to get correct values, we care about
%some of this data
for i = start:4:start+packetHeader-1
    swap = data(i:i+3);
    data(i) = swap(3);
    data(i+1) = swap(4);
    data(i+2) = swap(1);
    data(i+3) = swap(2);
end
packet_header = data(start:start+packetHeader-1);
packetLen = bitshift(packet_header(packetHeader-
3),24)+bitshift(packet_header(packetHeader-
2),16)+bitshift(packet_header(packetHeader-
1),8)+bitshift(packet_header(packetHeader),0);
%size of all our packets for this pcap
start = start+packetHeader;
numPackets = m/(packetLen+packetHeader);
data = tempdata;                % the value we care about is only a byte

msgCnt = zeros([1,numPackets]);
j =1;
while(j<=numPackets)
    grab = 99;
    if(mod(start,2) == 0)
        tstart = start-1;
        for i = tstart:2:tstart+packetLen-1
            swap = data(i:i+1);
            data(i) = swap(2);
            data(i+1) = swap(1);
```

```
        end
        grab = 100;
    end
    packetBody = data(start:start+packetLen-1);
    msgCnt(j) = packetBody(grab);
    start = start+packetLen+packetHeader;
    j=j+1;
end
end
```

Appendix K

Find packets in a given range of distance

```
function [numPacketsInRangeRX, numPacketsInRangeTX] =
findPacketsInRange(packets, bounds)
lowBound = 1;
upperBound = bounds(1);
[~,mR] = size(bounds);
numPacketsInRangeRX = zeros([1 mR-1]);
numPacketsInRangeTX = zeros([1 mR-1]);
[~,m1] = size(packets);
numPacketsInRangeTX(1) = upperBound-lowBound;
for i = 2:mR
    for j = 1:m1
        if((packets(j) >= lowBound)&&(packets(j)<=upperBound))
            numPacketsInRangeRX(i-1) = numPacketsInRangeRX(i-1)+1;
        elseif(packets(j)>upperBound)
                break;
        end
    end
    lowBound = upperBound+1;
    upperBound = bounds(i);
    numPacketsInRangeTX(i) = upperBound-lowBound+1;
end
```

Appendix L

NMEA GPS sentence Parser

```
function [GPS, time] = NMEAGPSParser(file)
if exist(file,'file')==2
fid = fopen(file);
i = 1;
while(~feof(fid))
    textscan(fid,'%s',1,'delimiter',':');
    gpsSentence=textscan(fid,'%s',1,'delimiter','\n'); %GPS Sentence
    parsedSentence = strsplit(char(gpsSentence{1}),',');
    GPS(i,:)=parsedSentence(3:6);
    textscan(fid,'%s',1,'delimiter',':');
    timestamp = textscan(fid,'%f-%f-%f %f:%f:%f',1,'delimiter','\n');
%timestamp

    time(i) = timestamp{4}*3600.0+timestamp{5}*60.0+timestamp{6}; %convert
time to seconds
    textscan(fid,'%s',3,'delimiter','\n');  %finish reading last line and
read next 2
    i=i+1;
end
end
end
```

Appendix M

GPS interpolator, to recover lost GPS samples

```
function [interpolatedGPS, interpolatedTime] = FRAGPSInterpolator(GPS, time)
%need to interpolate the data to upsample data for holes
[~,numel] = size(time);
prevTime = time(1);
interpolatedTime(1) = prevTime;
interpolatedGPS(1,:) = ConvertNMEA2DecDegrees(GPS(1,:));
j = 2; %this is to index through all the new points we interpolate
for i = 2:numel
    currTime = time(i);
    currGPS = ConvertNMEA2DecDegrees(GPS(i,:));
    diffTime = currTime-prevTime-1.0;
    if (diffTime>0.0)
        prevGPS = ConvertNMEA2DecDegrees(GPS(i-1,:));
        dlat = abs(currGPS(1)) - abs(prevGPS(1));
        dlon = abs(currGPS(2)) - abs(prevGPS(2));
        rlat = dlat/(diffTime+1.0);
        rlon = dlon/(diffTime+1.0);
        for k = 1:diffTime
            %this loop fills in the missing seconds maybe the GPS too?
            interpolatedTime(j) = prevTime+double(k);
            interpolatedGPS(j,:) = [prevGPS(1)+double(k)*rlat
prevGPS(2)+double(k)*rlon];
            j=j+1;
        end
    end
    interpolatedTime(j) = currTime;
    interpolatedGPS(j,:) = currGPS;
    j = j+1;
    prevTime=currTime;
end

end
```

Helper function Convert NMEA to a decimal number

```
function [DecDegreeGPS] = ConvertNMEA2DecDegrees(GPS)
numGPSLat = str2double(char(GPS{1}));
numGPSLon = str2double(char(GPS{3}));
lat = double(floor(numGPSLat/100.0))+rem(numGPSLat,100.0)/60.0;
if GPS{2} ~= 'N'
    lat = lat*-1.0;
end
lon = double(floor(numGPSLon/100.0))+rem(numGPSLon,100.0)/60.0;
if GPS{4} ~= 'E'
    lon = lon*-1.0;
end
DecDegreeGPS(1,:)=[lat, lon];
end
```

Appendix N

Calculate Distance between a fixed GPS point

```
function [d] = DistancefromFixedGPS(Lon, Lat, R, lon1, lat1)
[~,numPts] = size(Lon);
d = zeros([1 numPts]);
for i = 1:numPts
    lat2 = Lat(i);
    dLat = lat2-lat1;
    dLon = Lon(i)-lon1;
    a = sin(dLat/2)*sin(dLat/2)+cos(lat1)*cos(lat2)*sin(dLon/2)*sin(dLon/2);
    c = 2*atan2(sqrt(a),sqrt(1-a));
    d(i) = R*c;
end
end
```

Appendix O

Calculate Path Loss exponent and sigma. Provided by Dr. Christopher Anderson of USNA.

```
function [n, Sigma, fit_power]=findpathloss(distances,recv_powers_db)
%This function computes path loss exponent from a dataset of
%distances and received powers.
%
%The first point is assumed to be the reference power measurement.
%Received powers are input in dB units.
%Sigma is given in dB.
%Fit powers are given in dB units.
%n=findpathloss(distances,recv_powers_db)
%This is a least-squares estimator
%
%Haris I. Volos 2006
%Virginia Tech MPRG
%Modified Chris R. Anderson 2008
%USNA
r=recv_powers_db(2:end);
r0=recv_powers_db(1);
d0=distances(1);
d=distances(2:end);
N=length(d);

n=( r0*sum(10*log10(d0./d)) -
sum(10*log10(d0./d).*r))/sum((10*log10(d0./d)).^2);
% r=recv_powers_db;
% d0=1;
% d=distances;
% n=(-sum(10*log10(d0./d).*r))/sum((10*log10(d0./d)).^2)

fit_power(1)=r0;
fit_power(2:length(distances))=r0+10*n*log10(distances(2:end)./distances(1));

Sigma=sqrt(sum((fit_power - recv_powers_db).^2)/length(recv_powers_db));
%end
```

Appendix P

PER Plots for the RTT Test Site with the OBU Placed at 50m

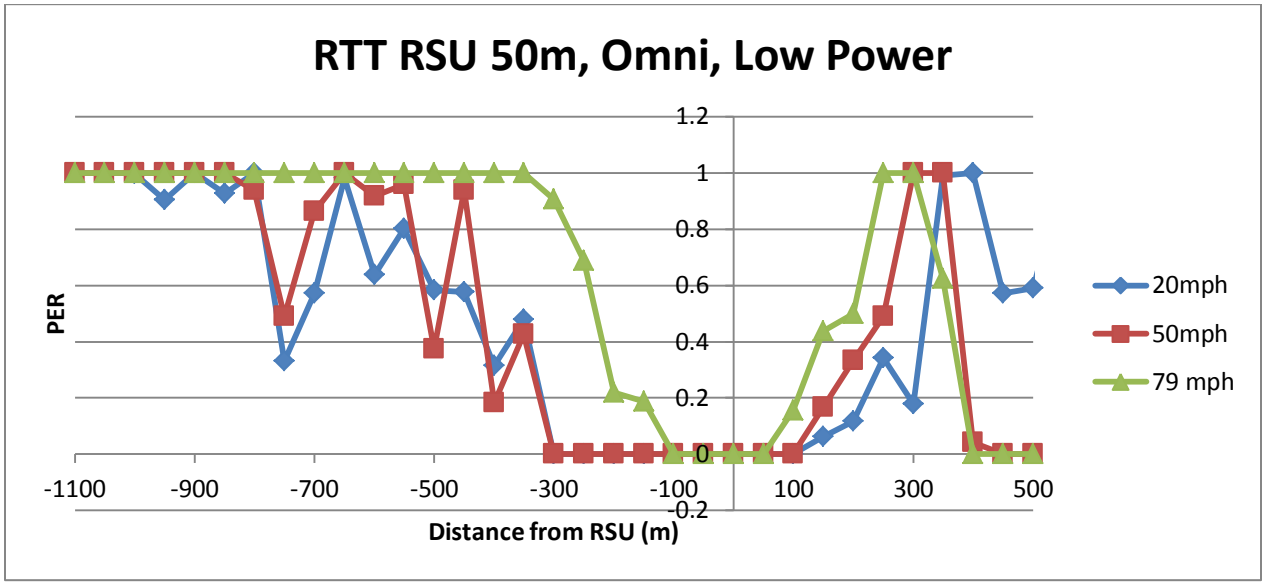

(a)

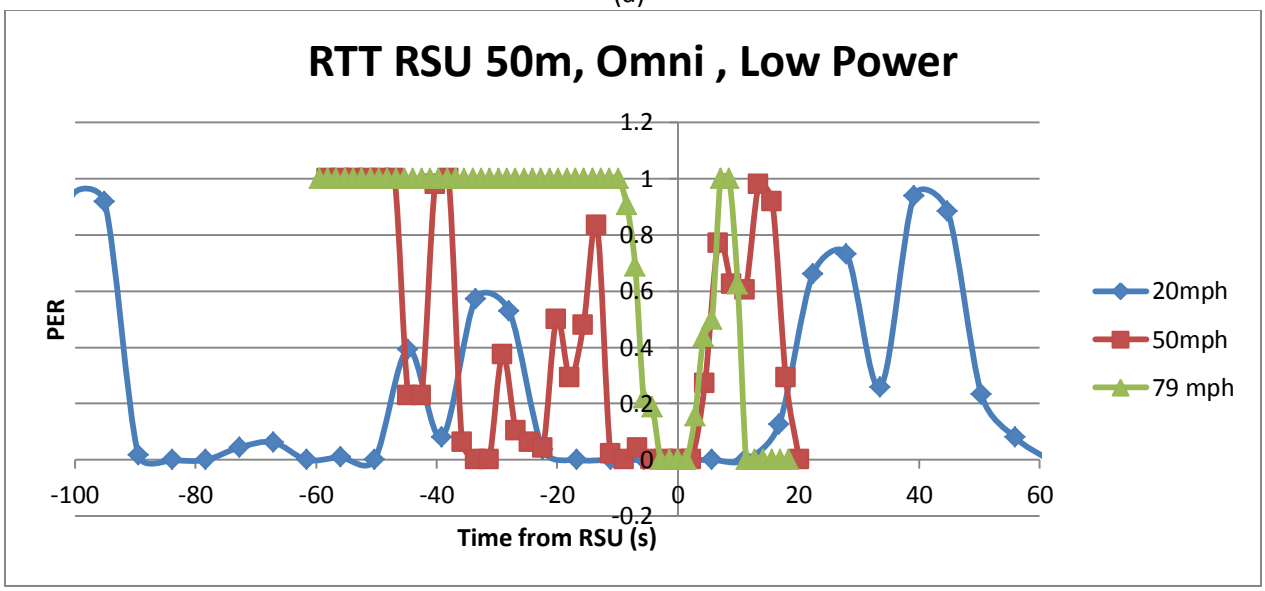

(b)

Figure P.1 PER at the RSU with an Omni Directional Antenna operating at Low Power, (a) gives PER vs. Distance Train is from RSU and (b) gives PER vs. Time between train and RSU.

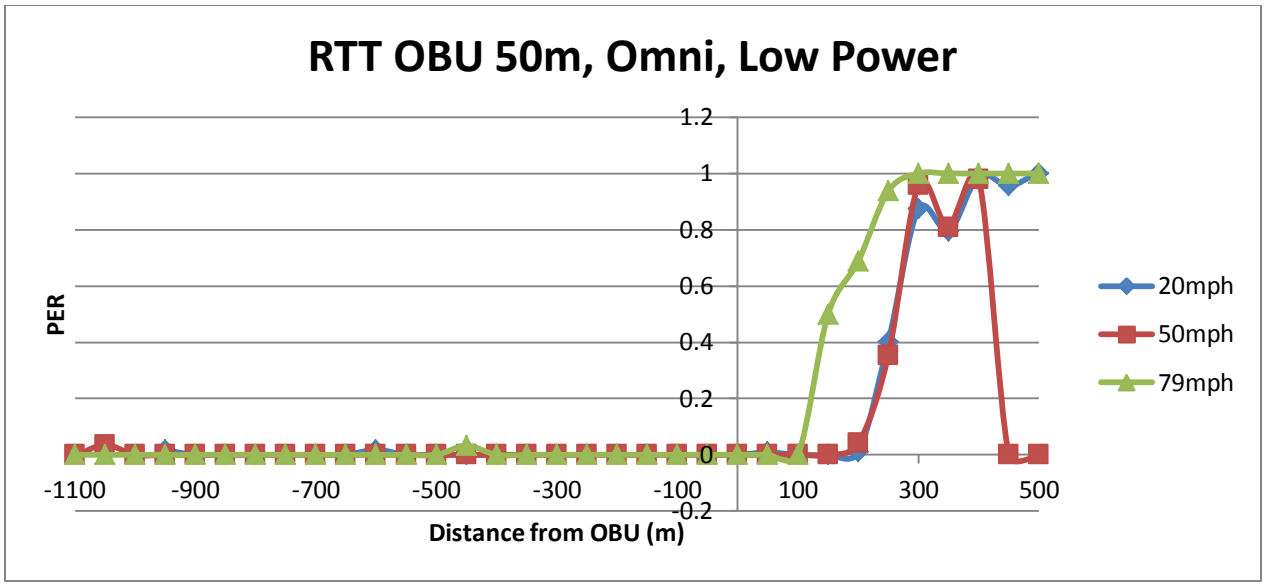

(a)

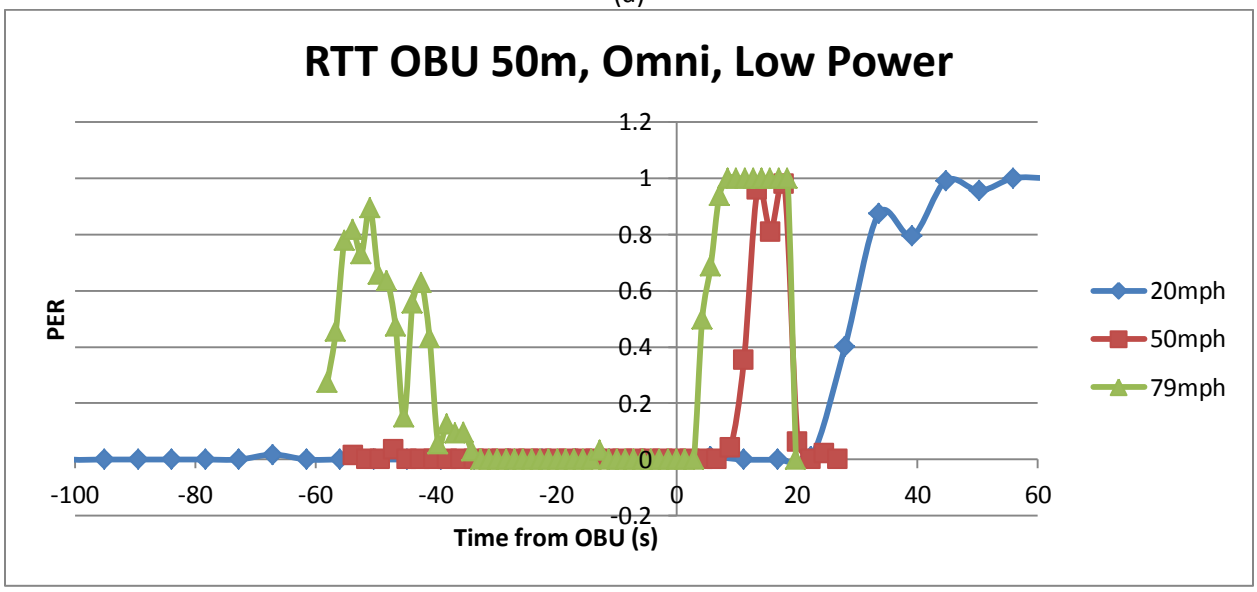

(b)

Figure P.2 PER at the OBU with an Omni Directional Antenna operating at Low Power, (a) gives PER vs. Distance Train is from OBU and (b) gives PER vs. Time between train and OBU.

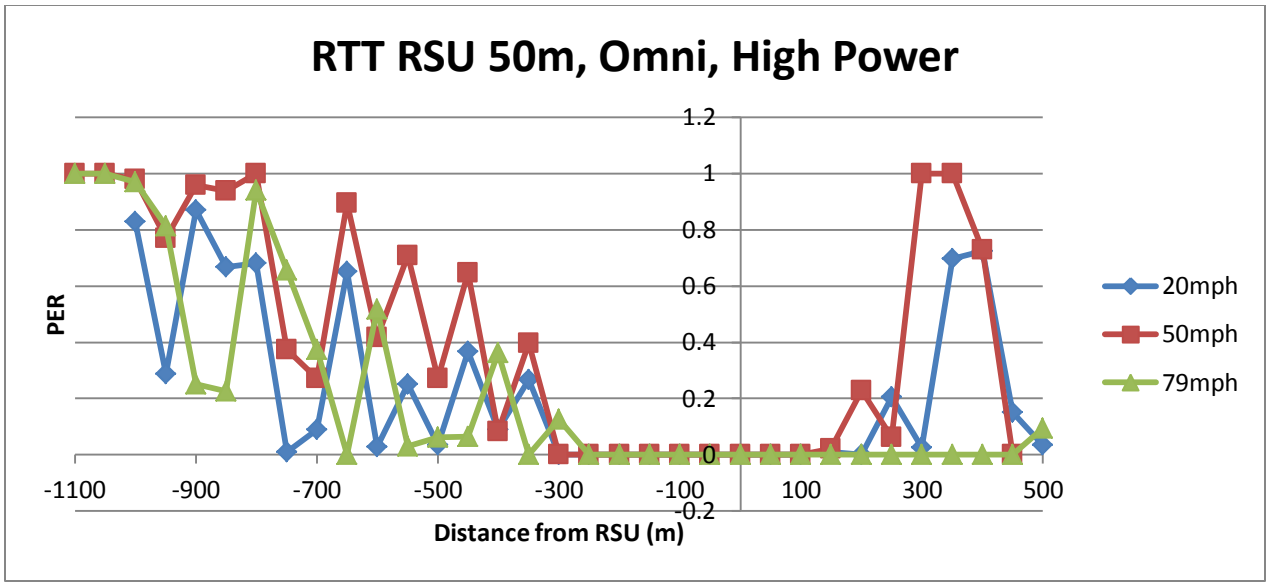

(a)

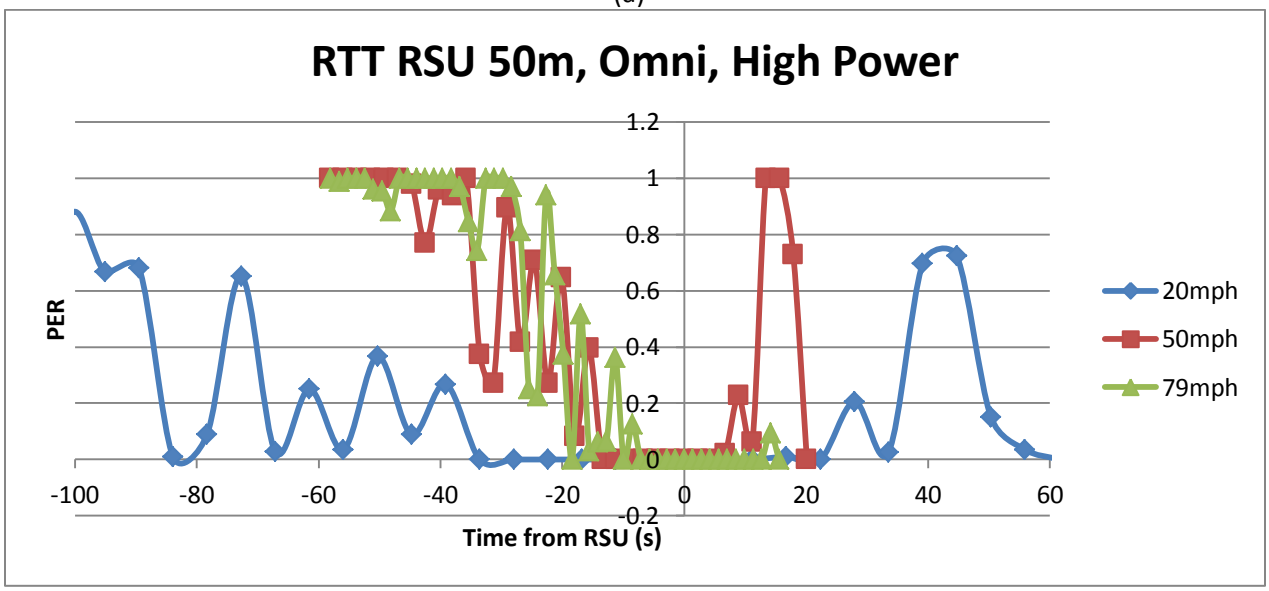

(b)

Figure P.3 PER at the RSU with an Omni Directional Antenna operating at High Power, (a) gives PER vs. Distance Train is from RSU and (b) gives PER vs. Time between train and RSU.

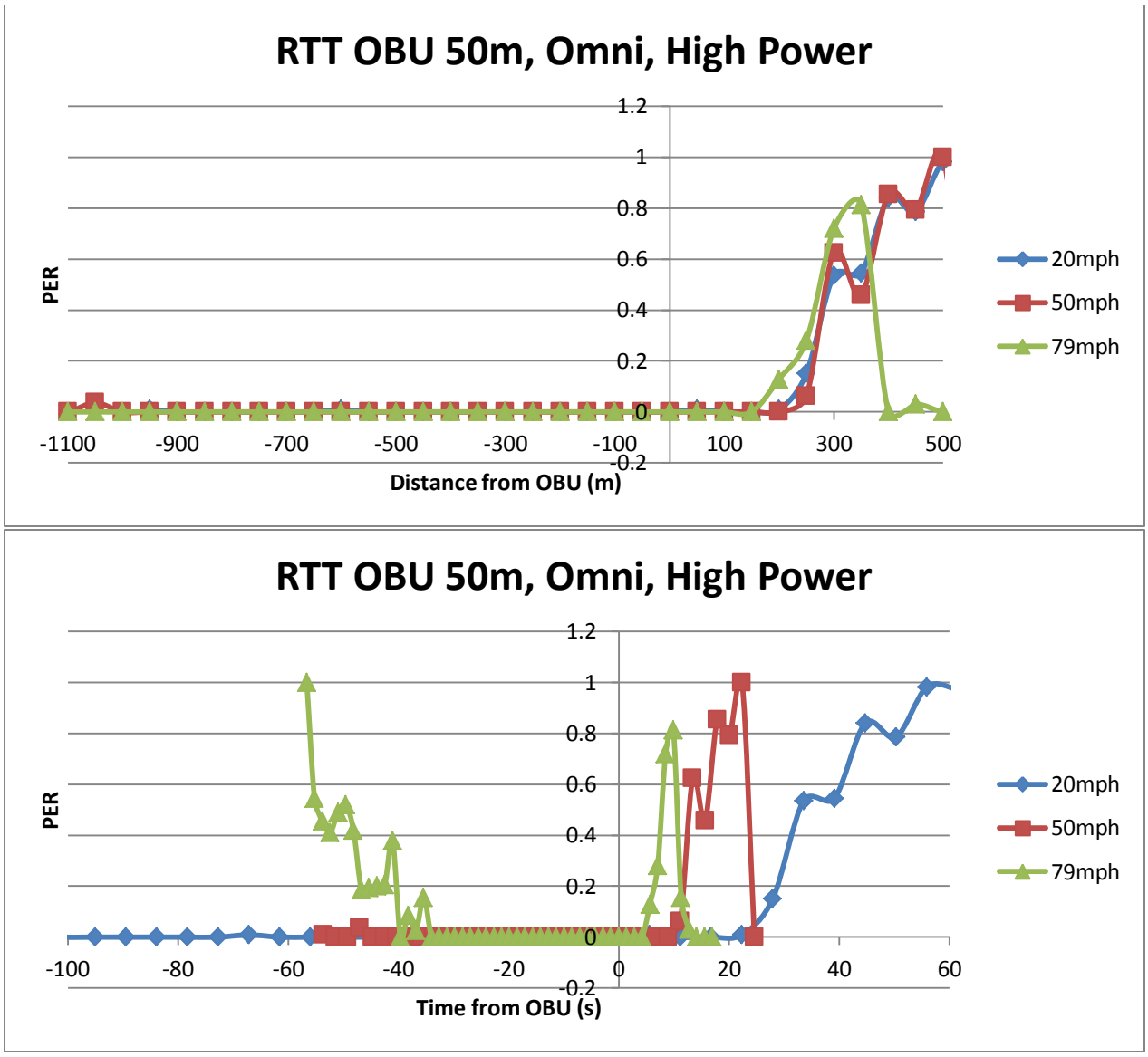

Figure P.4 PER at the OBU with an Omni Directional Antenna operating at High Power, (a) gives PER vs. Distance Train is from OBU and (b) gives PER vs. Time between train and OBU.

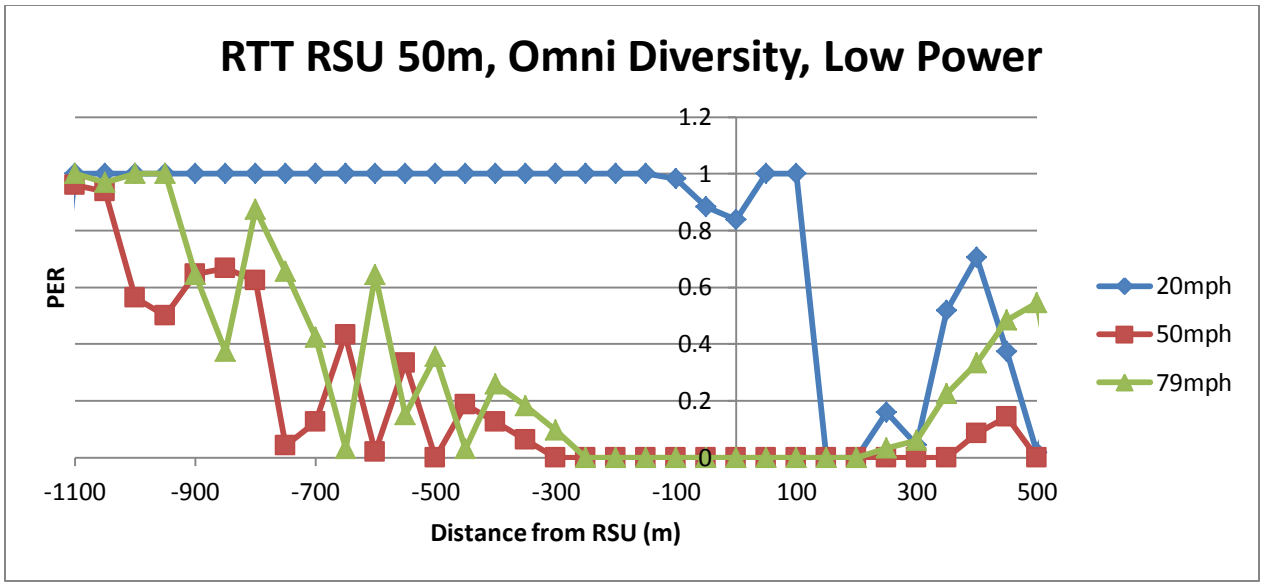

(a)

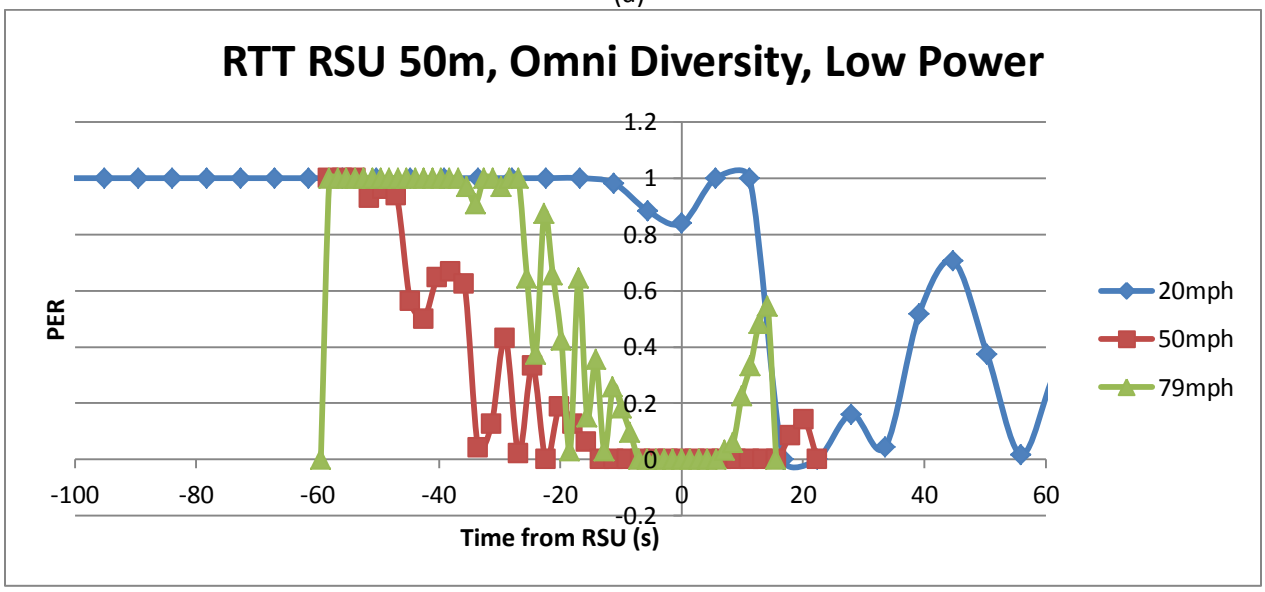

(b)

Figure P.5 PER at the RSU with an Omni Diversity Antenna operating at High Power, (a) gives PER vs. Distance Train is from RSU and (b) gives PER vs. Time between train and RSU.

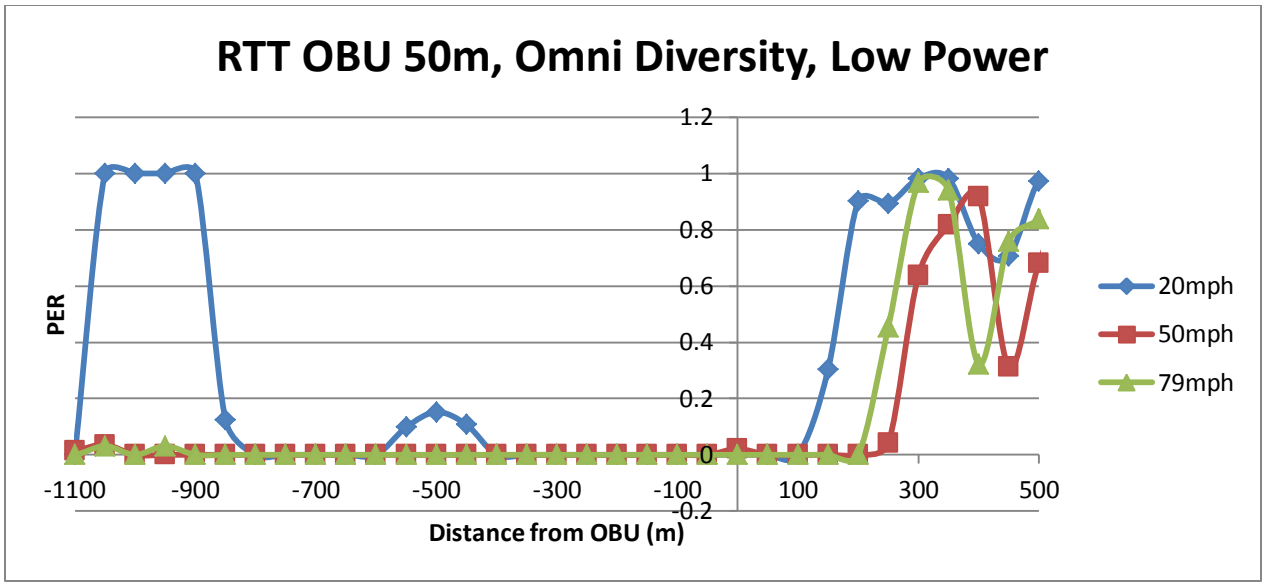

(a)

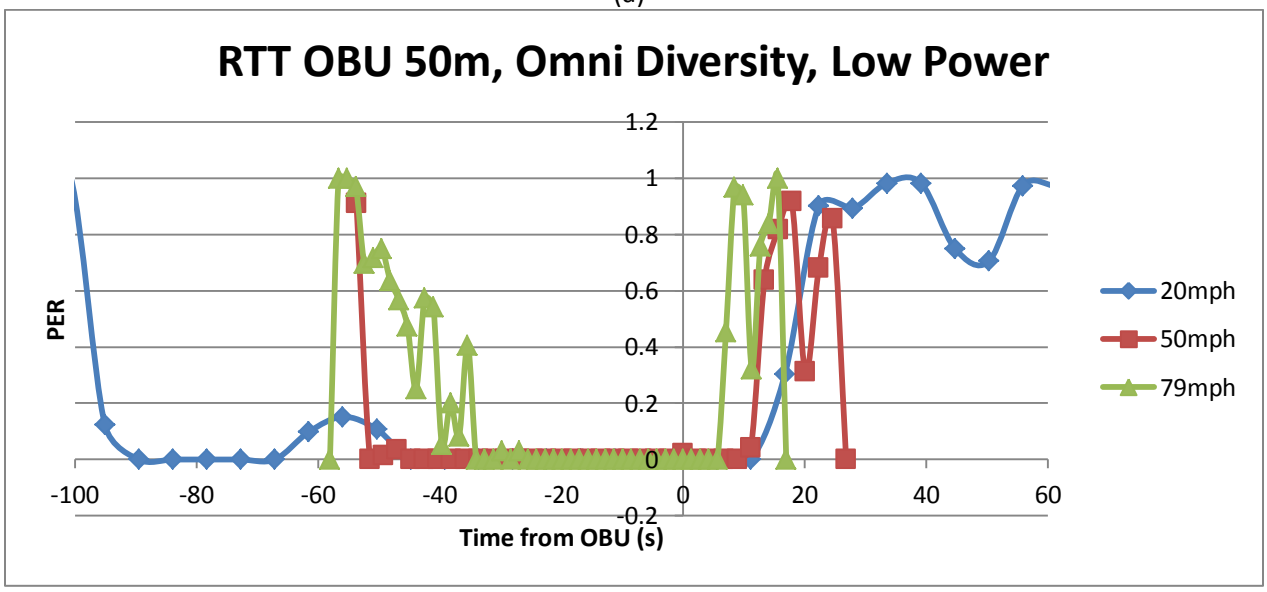

(b)

Figure P.6 PER at the OBU with an Omni Diversity Antenna operating at Low Power, (a) gives PER vs. Distance Train is from OBU and (b) gives PER vs. Time between train and OBU.

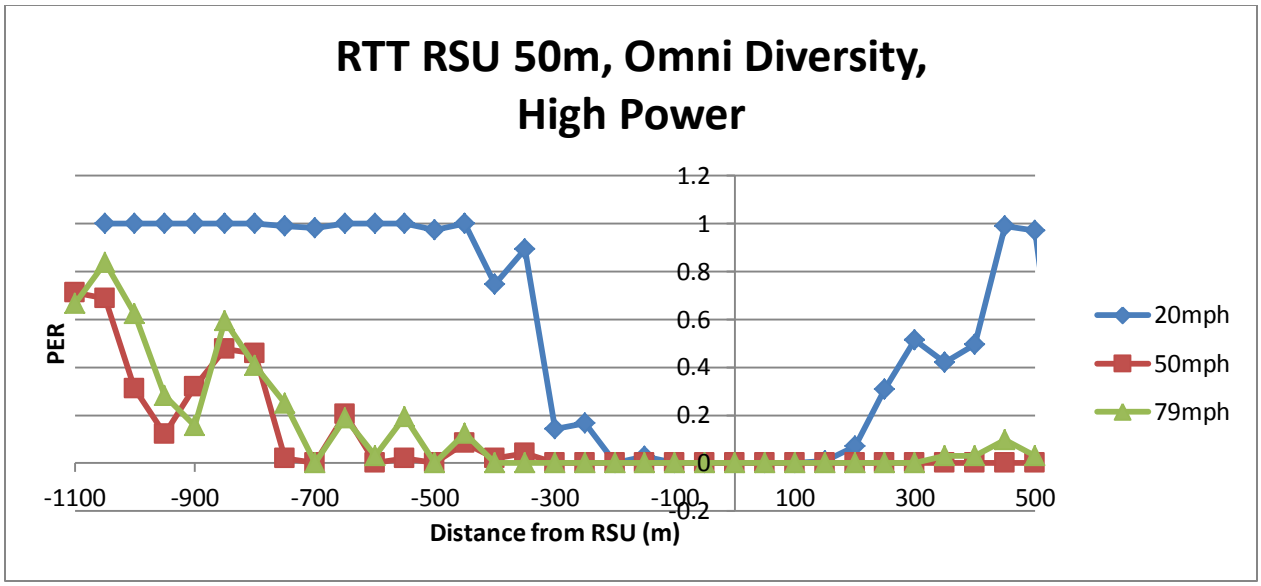

(a)

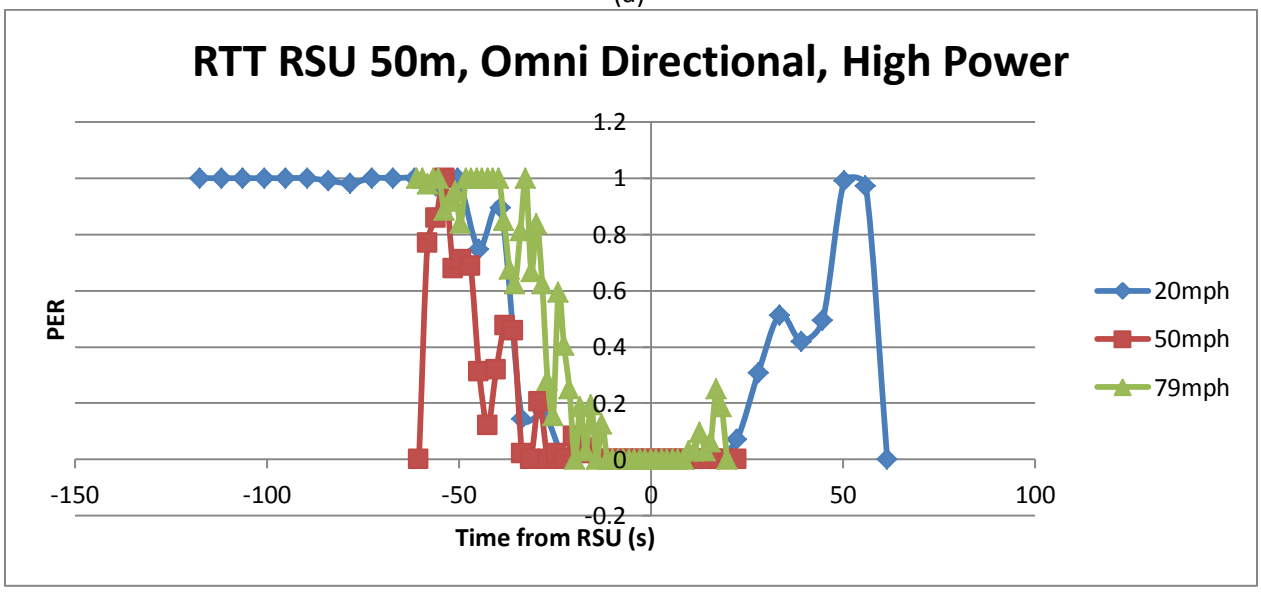

(b)

Figure P.7 PER at the RSU with an Omni Diversity Antenna operating at High Power, (a) gives PER vs. Distance Train is from RSU and (b) gives PER vs. Time between train and RSU.

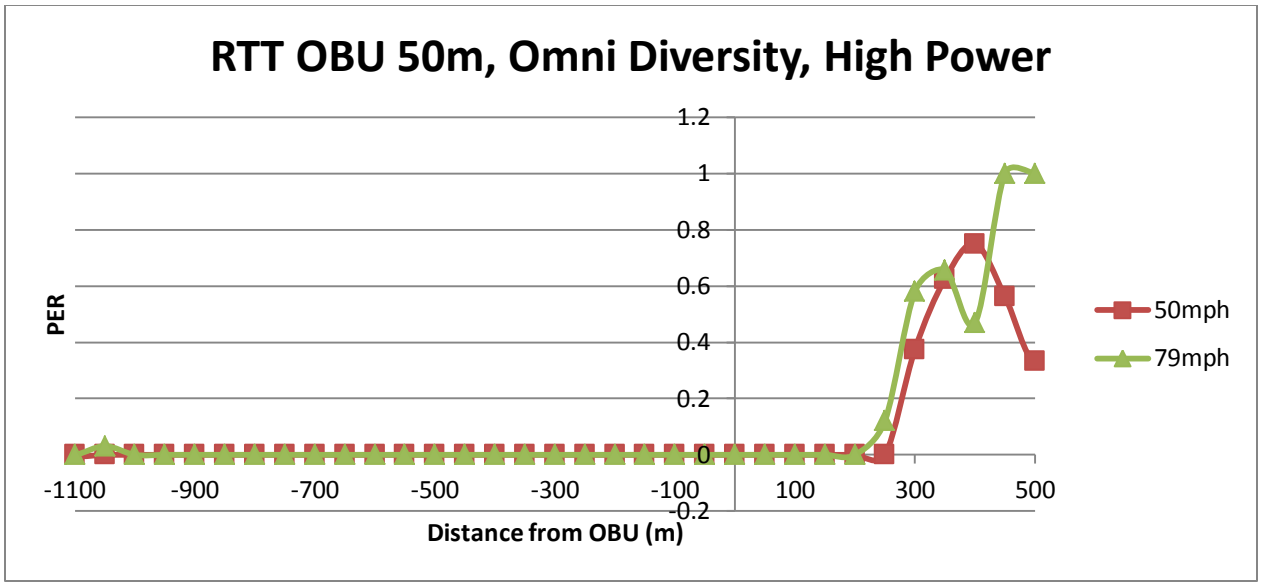

(a)

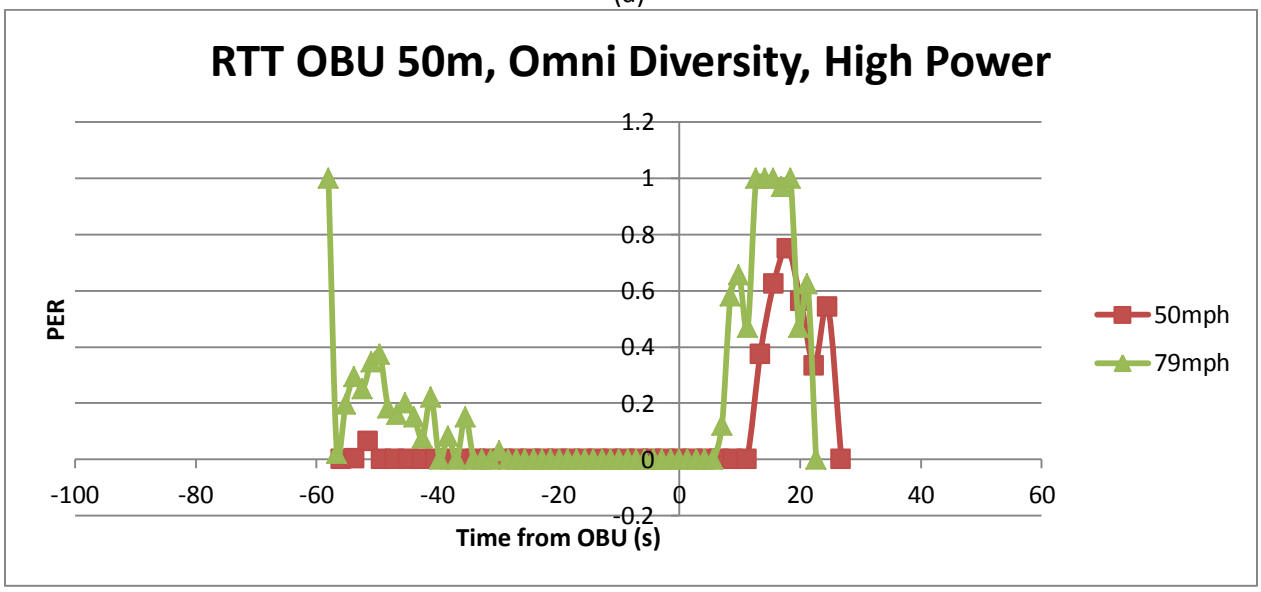

(b)

Figure P.8 PER at the OBU with an Omni Diversity Antenna operating at High Power, (a) gives PER vs. Distance Train is from OBU and (b) gives PER vs. Time between train and OBU.

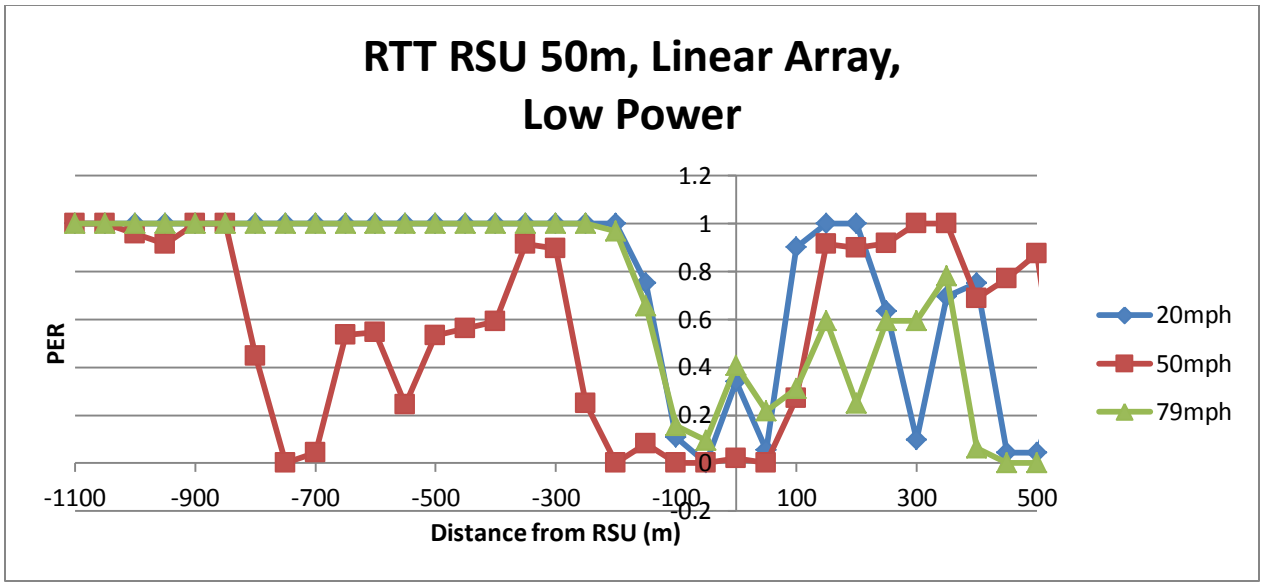

(a)

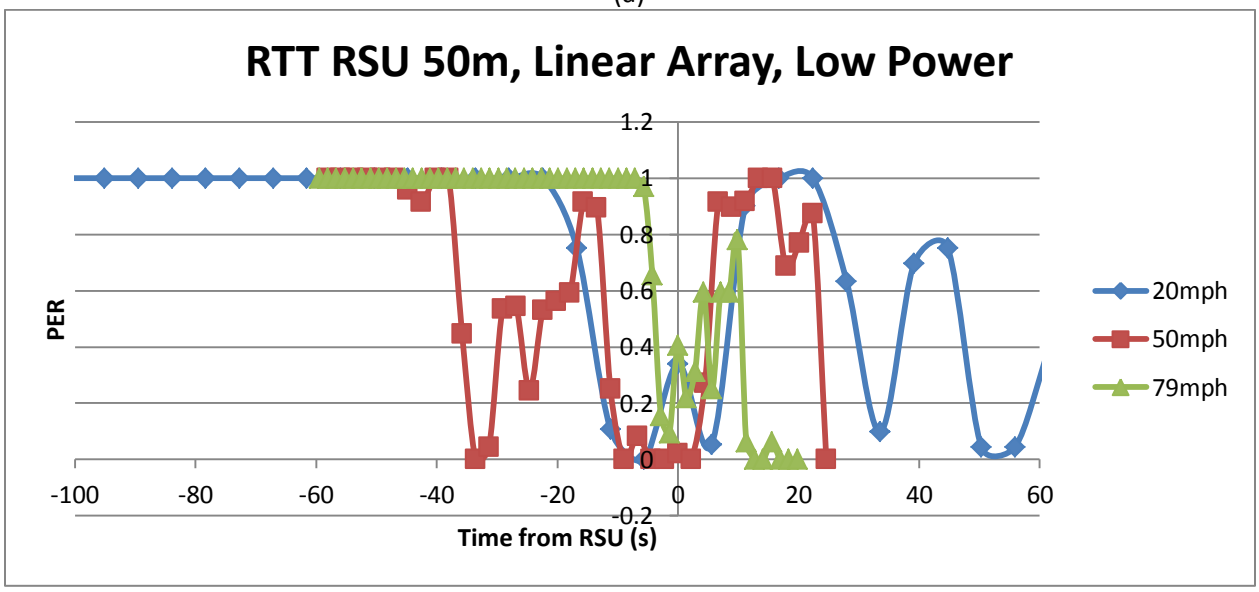

(b)

Figure P.9 PER at the RSU with a Linear Array Antenna operating at Low Power, (a) gives PER vs. Distance Train is from RSU and (b) gives PER vs. Time between train and RSU.

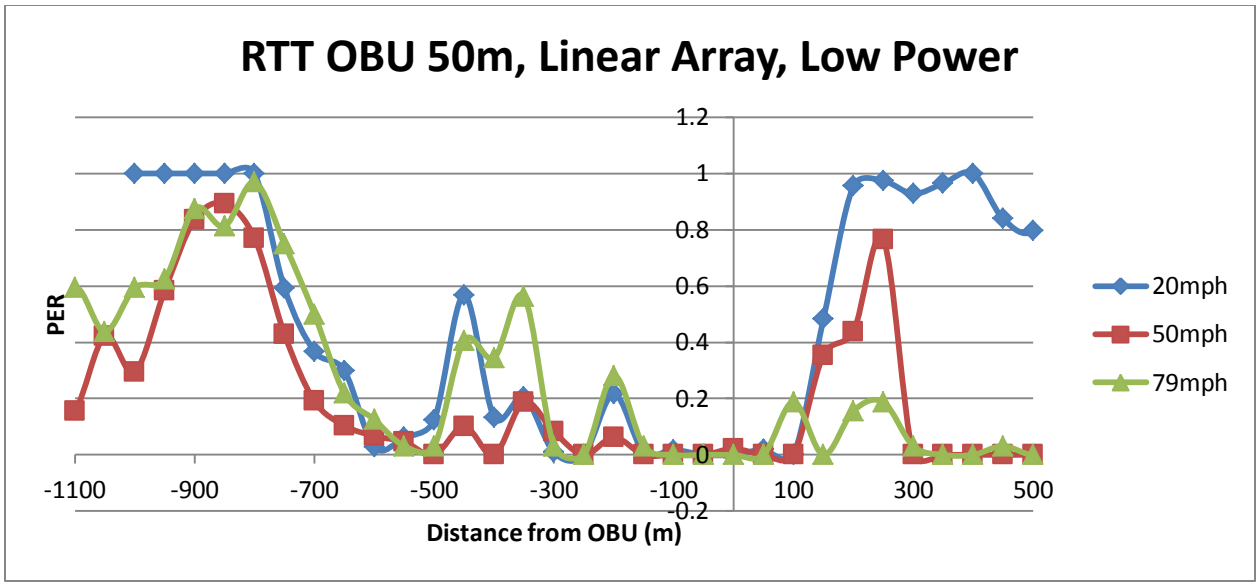

(a)

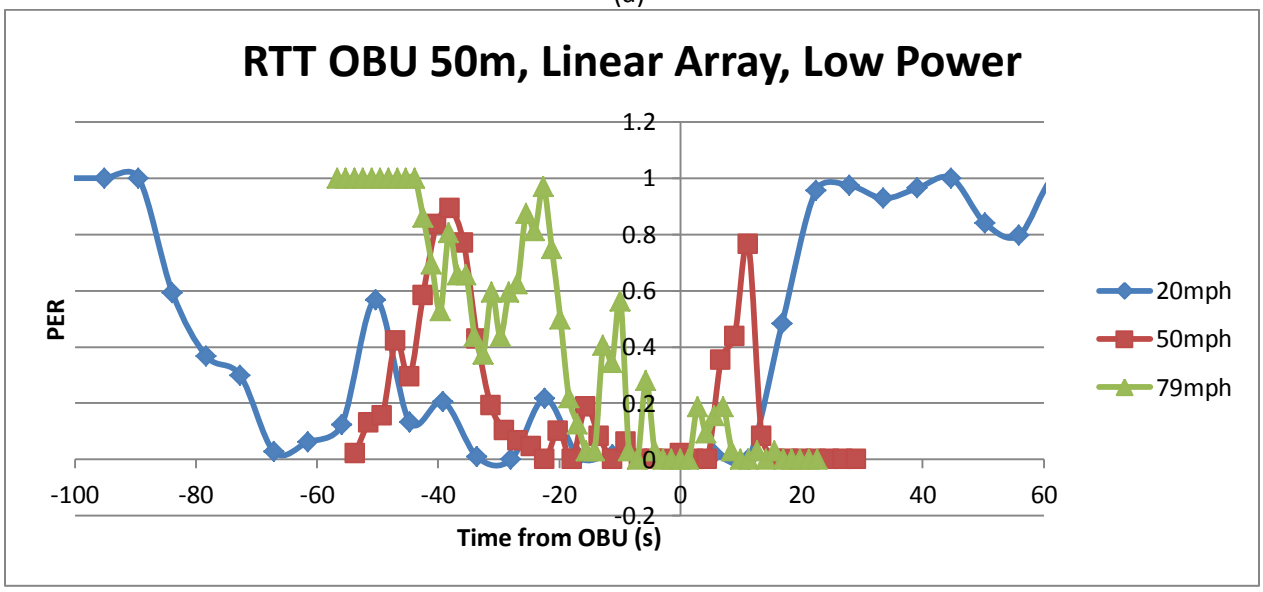

(b)

Figure P.10 PER at the OBU with a Linear Array Antenna operating at Low Power, (a) gives PER vs. Distance Train is from OBU and (b) gives PER vs. Time between train and OBU.

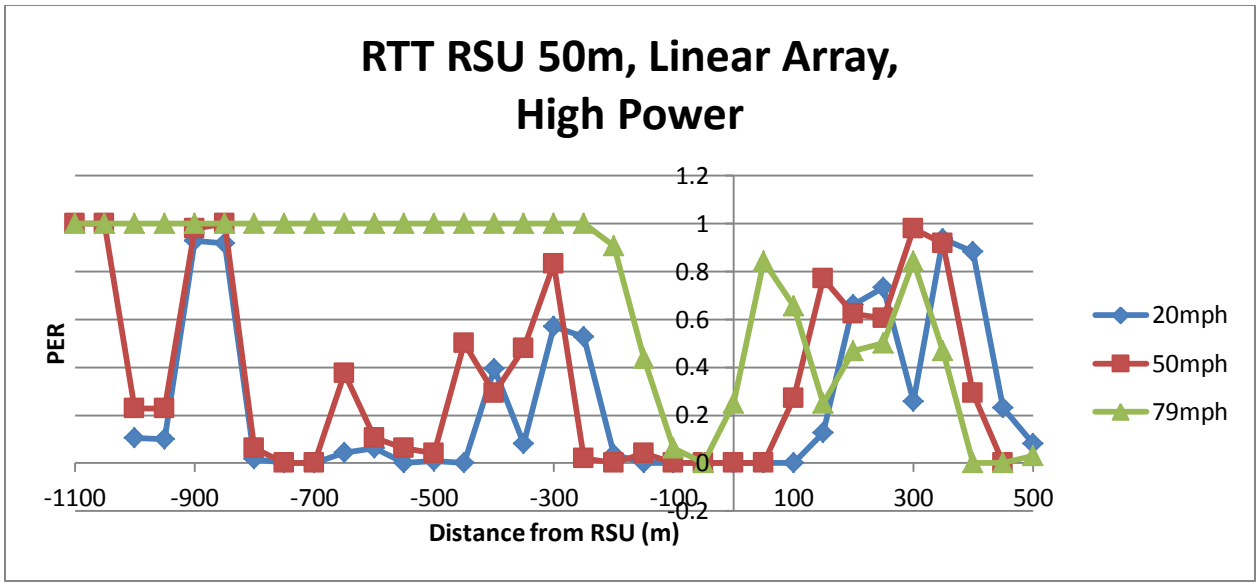

(a)

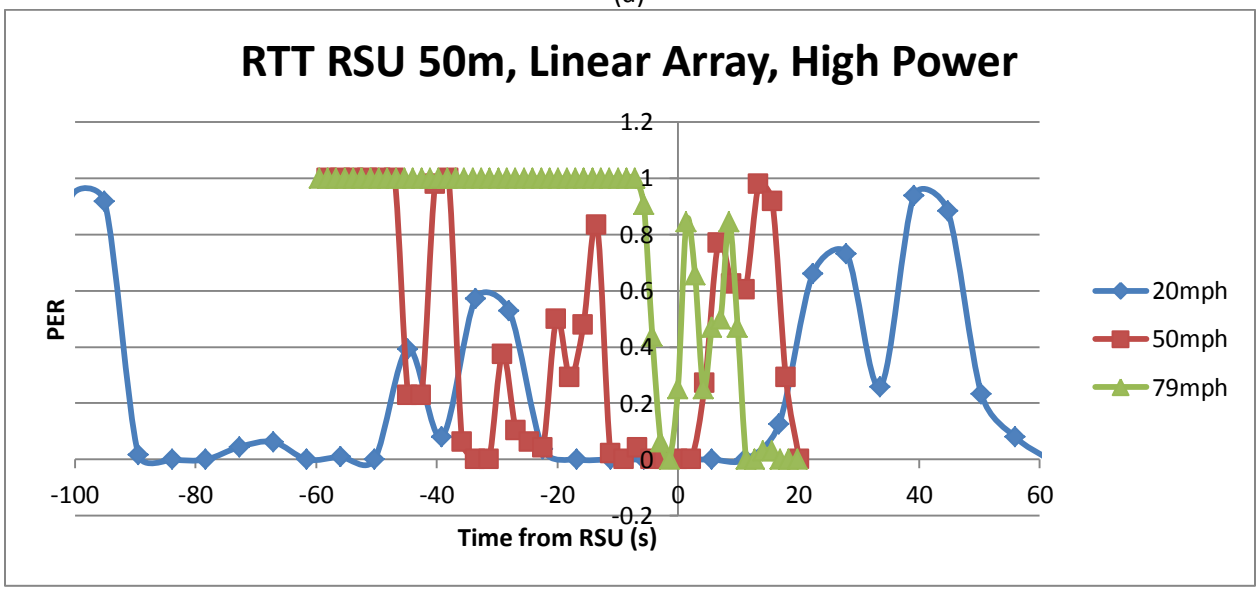

(b)

Figure P.11 PER at the RSU with a Linear Array Antenna operating at High Power, (a) gives PER vs. Distance Train is from RSU and (b) gives PER vs. Time between train and RSU.

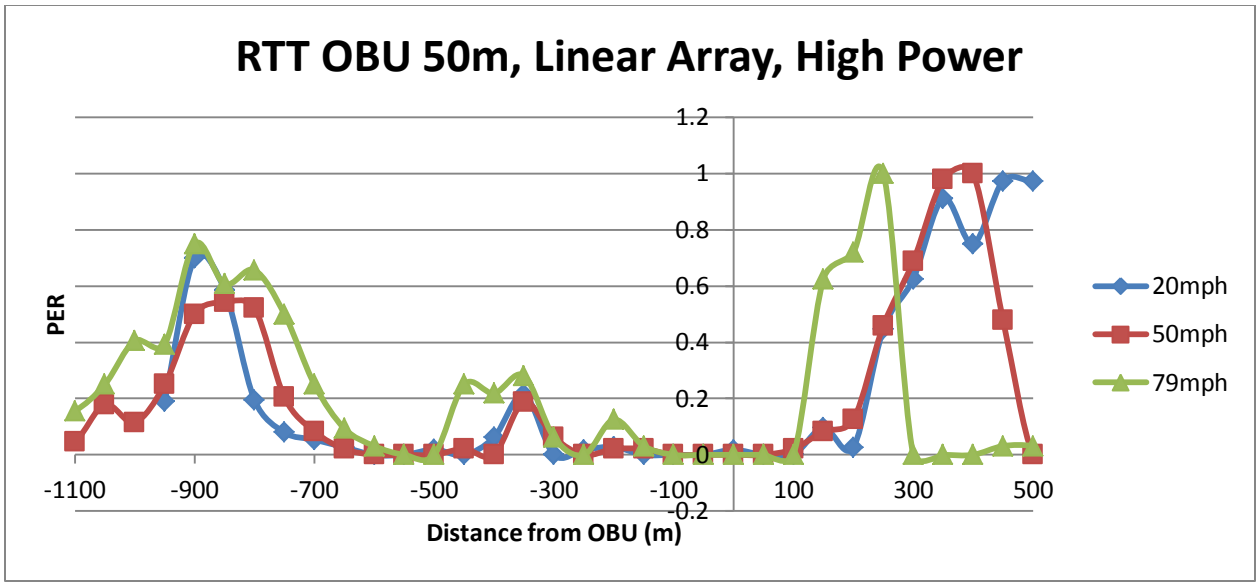

(a)

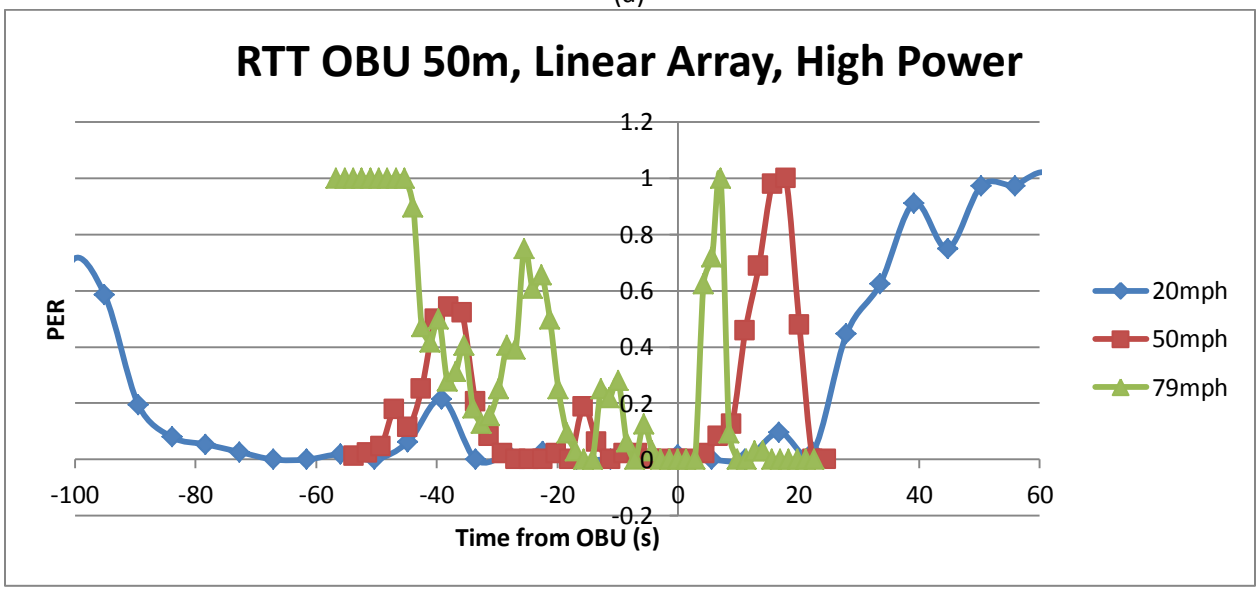

(b)

Figure P.12 PER at the OBU with a Linear Array Antenna operating at High Power, (a) gives PER vs. Distance Train is from OBU and (b) gives PER vs. Time between train and OBU.

PER Plots for the RTT Test Site with the OBU Placed at 200m

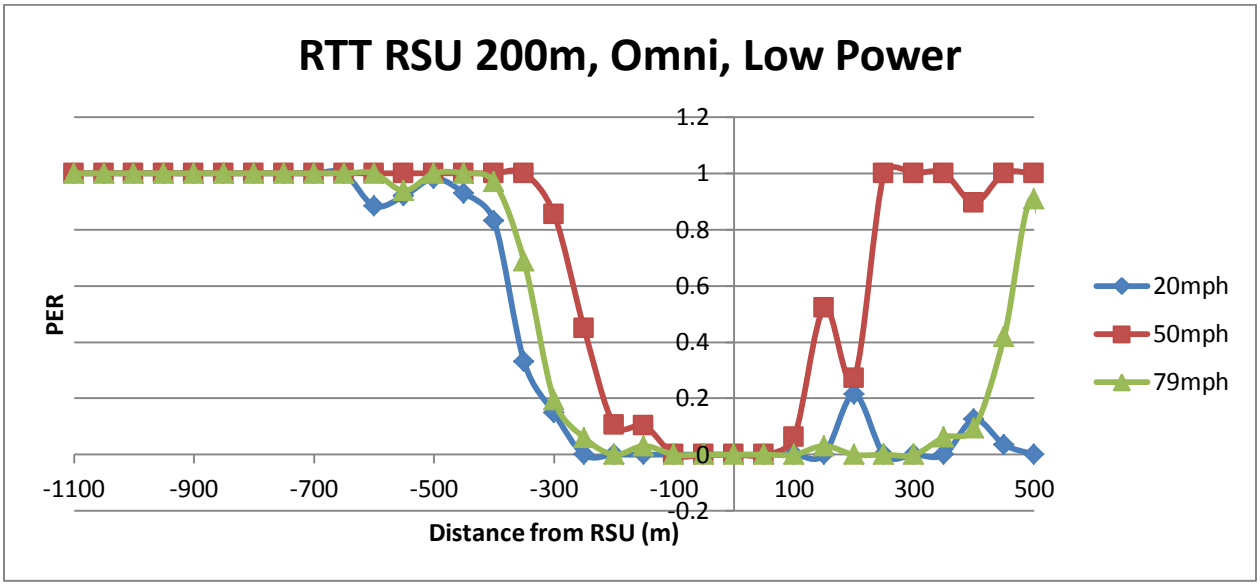

(a)

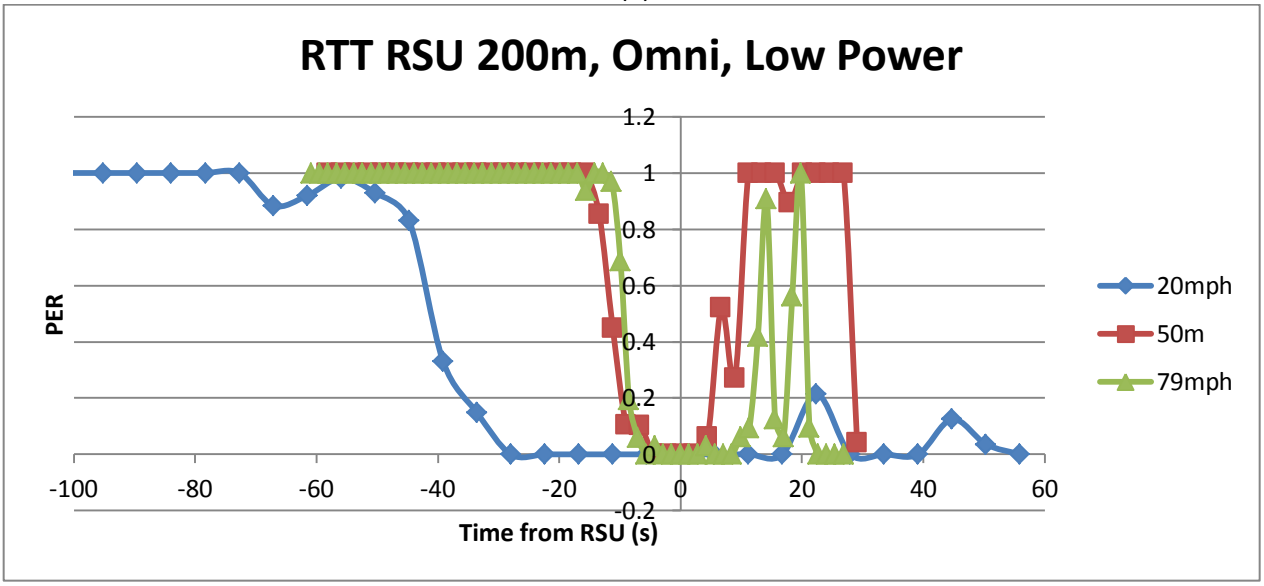

(b)

Figure P.13 PER at the RSU with an Omni Directional Antenna operating at Low Power, (a) gives PER vs. Distance Train is from RSU and (b) gives PER vs. Time between train and RSU.

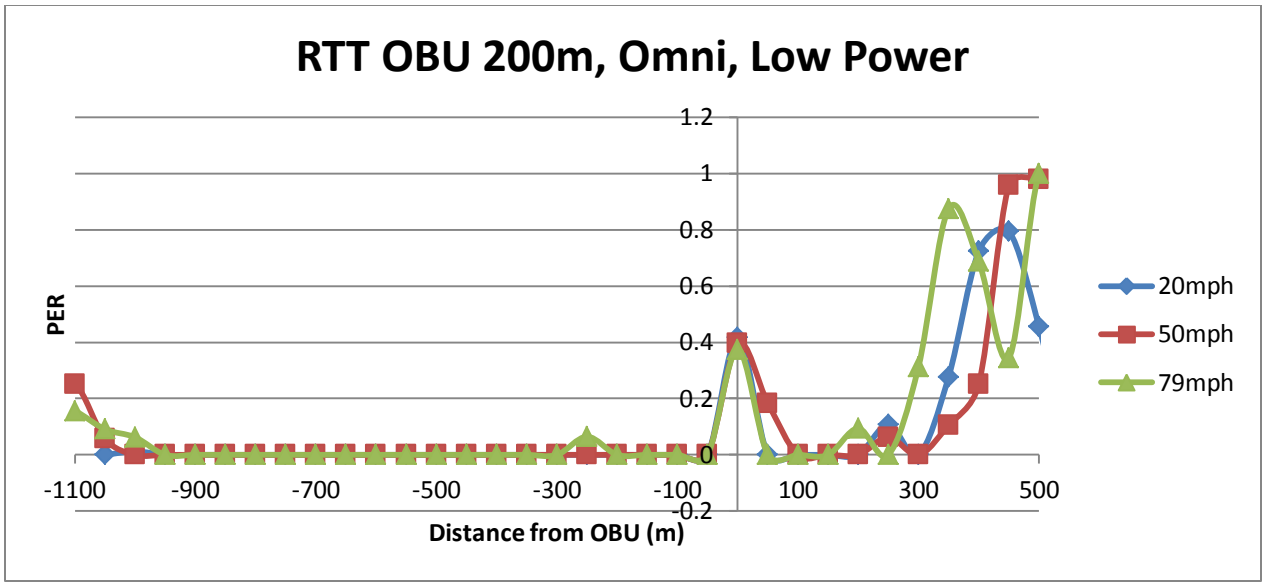

(a)

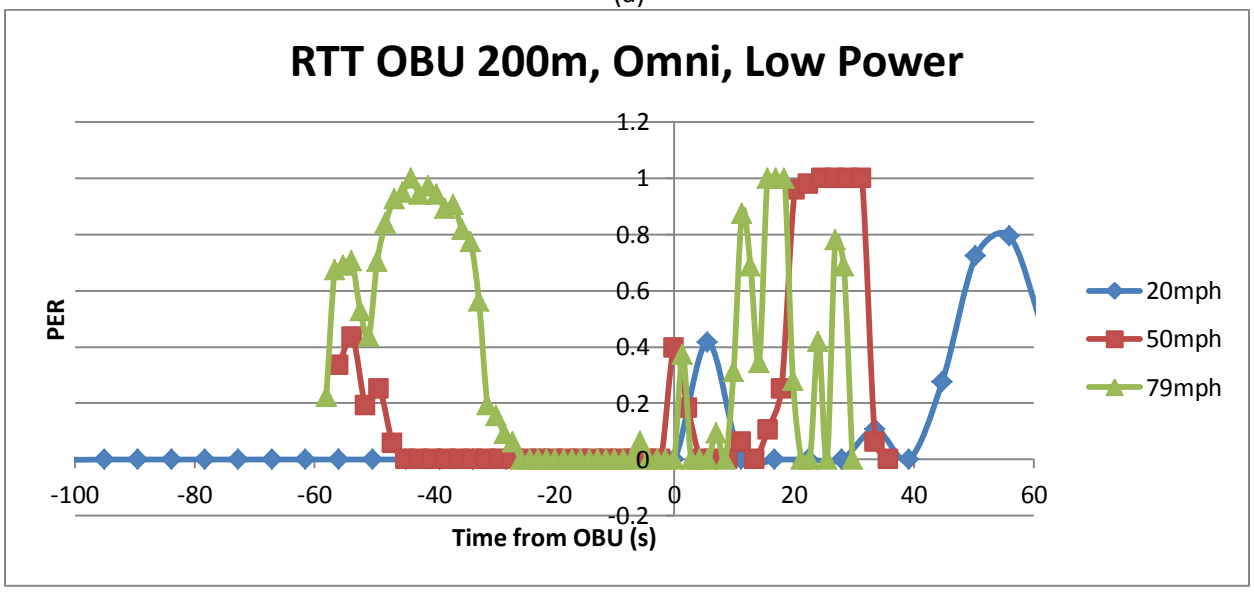

(b)

Figure P.14 PER at the OBU with an Omni Directional Antenna operating at Low Power, (a) gives PER vs. Distance Train is from OBU and (b) gives PER vs. Time between train and OBU.

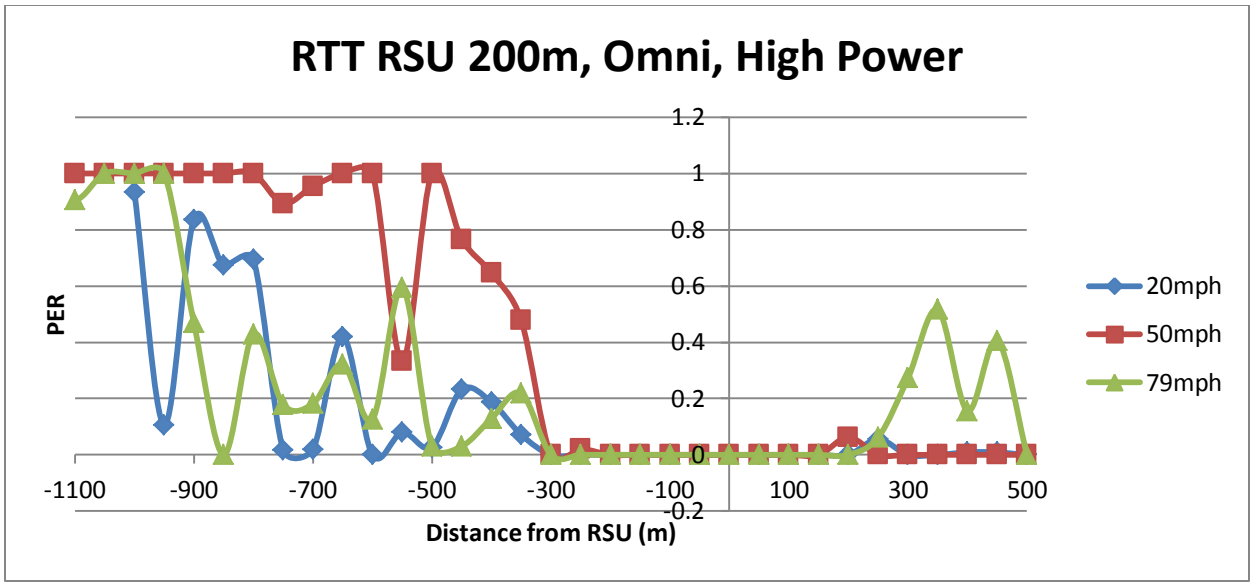

(a)

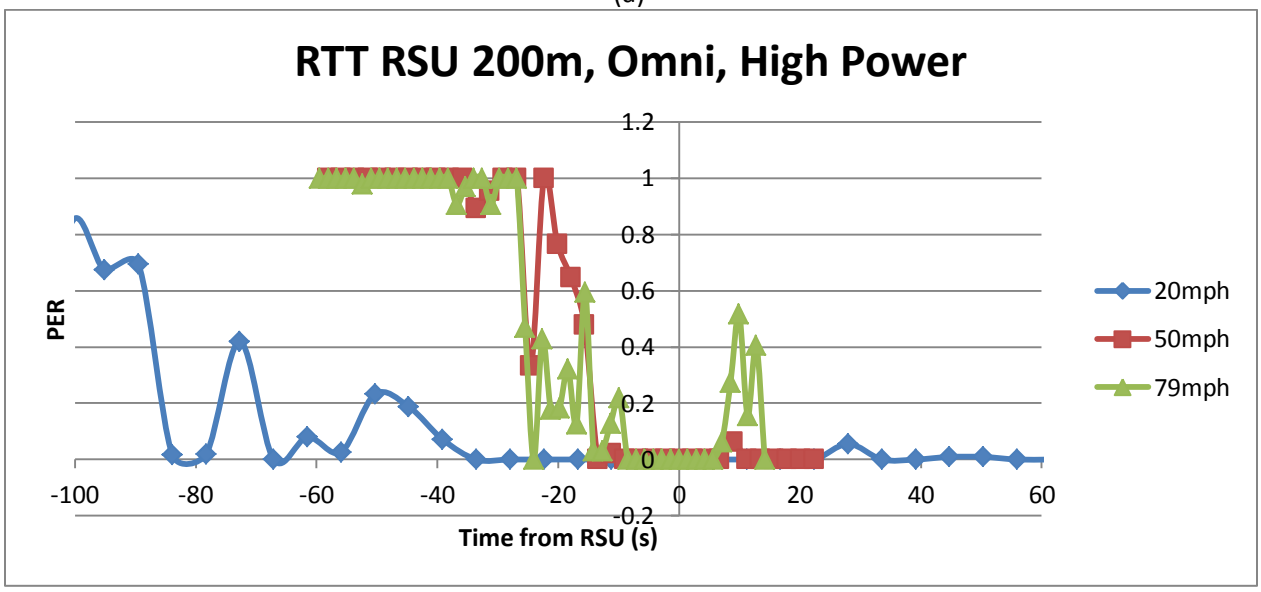

(b)

Figure P.15 PER at the RSU with an Omni Directional Antenna operating at High Power, (a) gives PER vs. Distance Train is from RSU and (b) gives PER vs. Time between train and RSU.

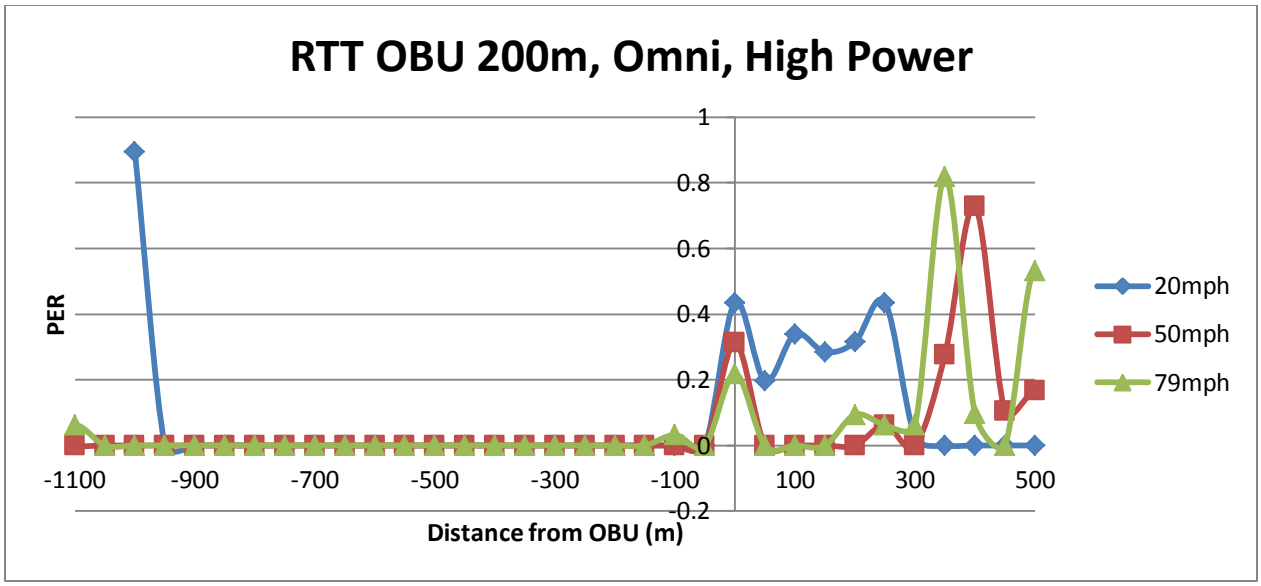

(a)

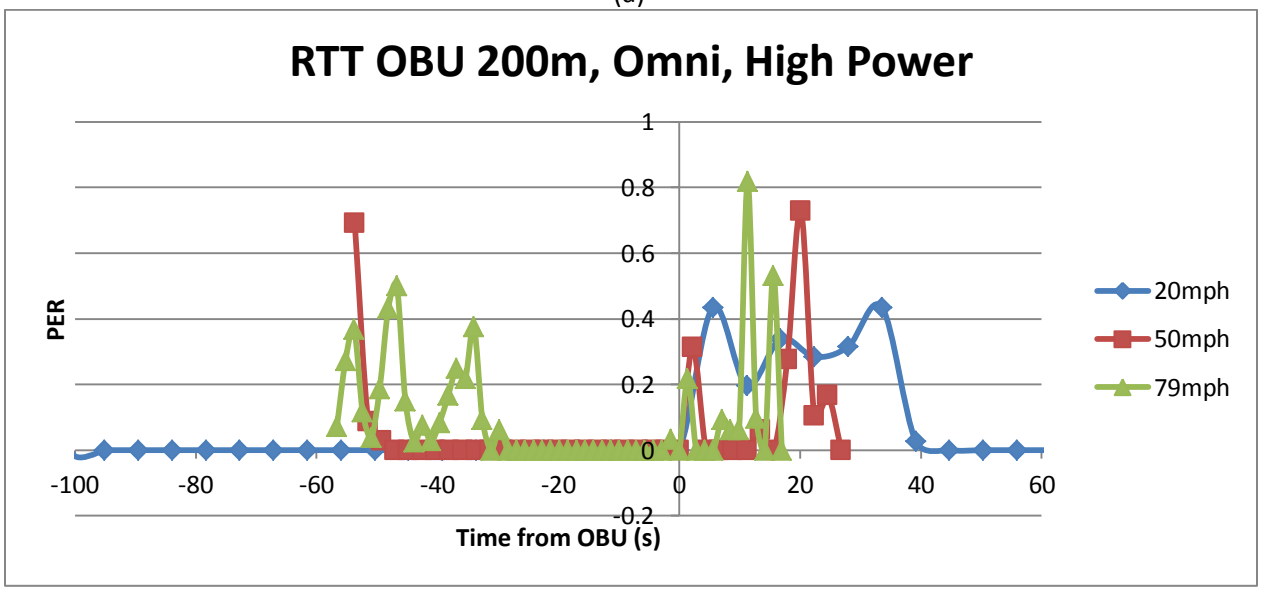

(b)

Figure P.16 PER at the OBU with an Omni Directional Antenna operating at High Power, (a) gives PER vs. Distance Train is from OBU and (b) gives PER vs. Time between train and OBU.

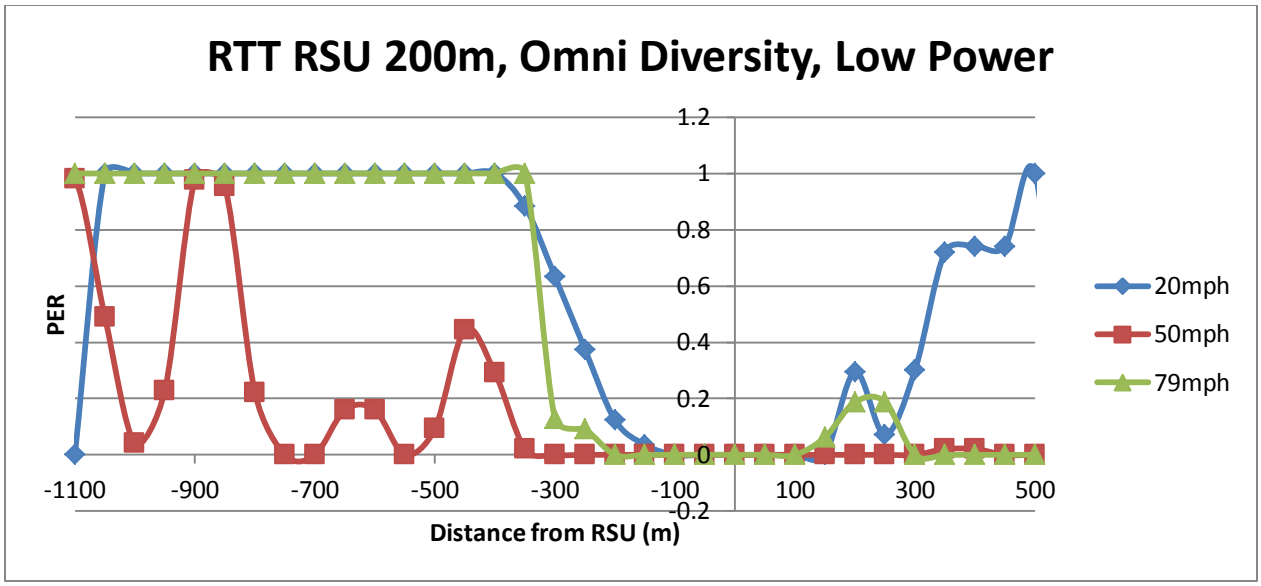

(a)

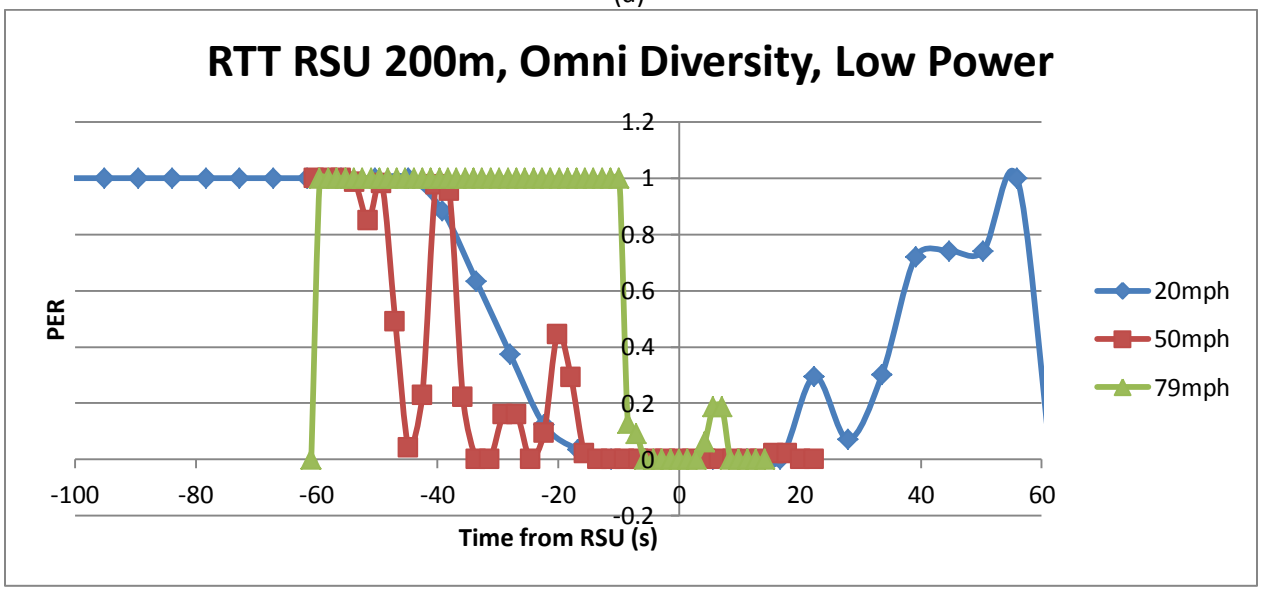

(b)

Figure P.17 PER at the RSU with an Omni Diversity Antenna operating at Low Power, (a) gives PER vs. Distance Train is from RSU and (b) gives PER vs. Time between train and RSU.

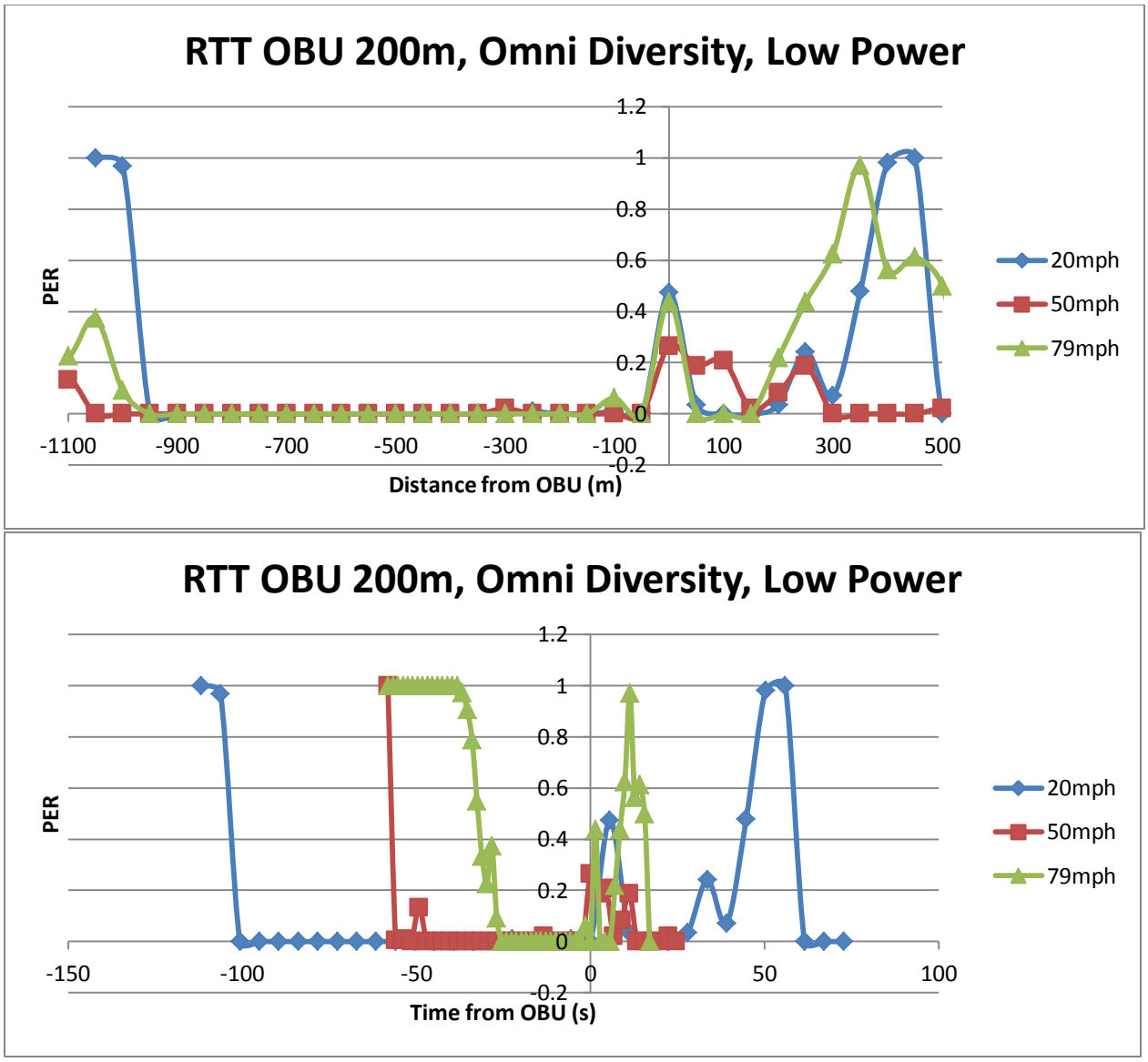

(b)

Figure P.18 PER at the OBU with an Omni Diversity Antenna operating at Low Power, (a) gives PER vs. Distance Train is from OBU and (b) gives PER vs. Time between train and OBU.

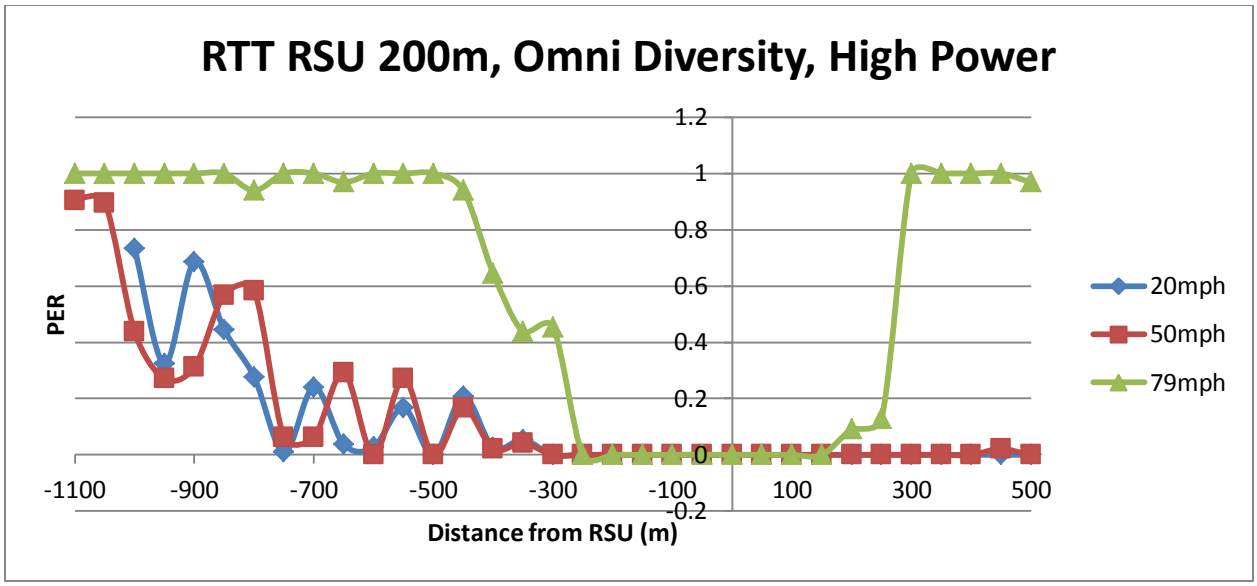

(a)

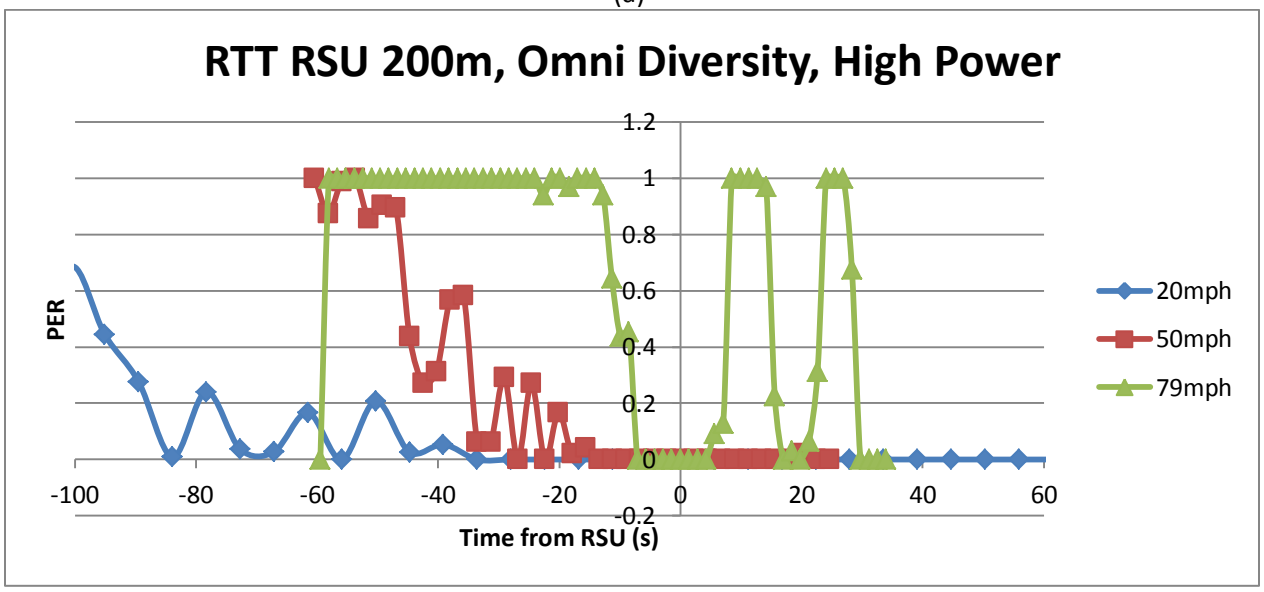

(b)

Figure P.19 PER at the RSU with an Omni Diversity Antenna operating at High Power, (a) gives PER vs. Distance Train is from RSU and (b) gives PER vs. Time between train and RSU.

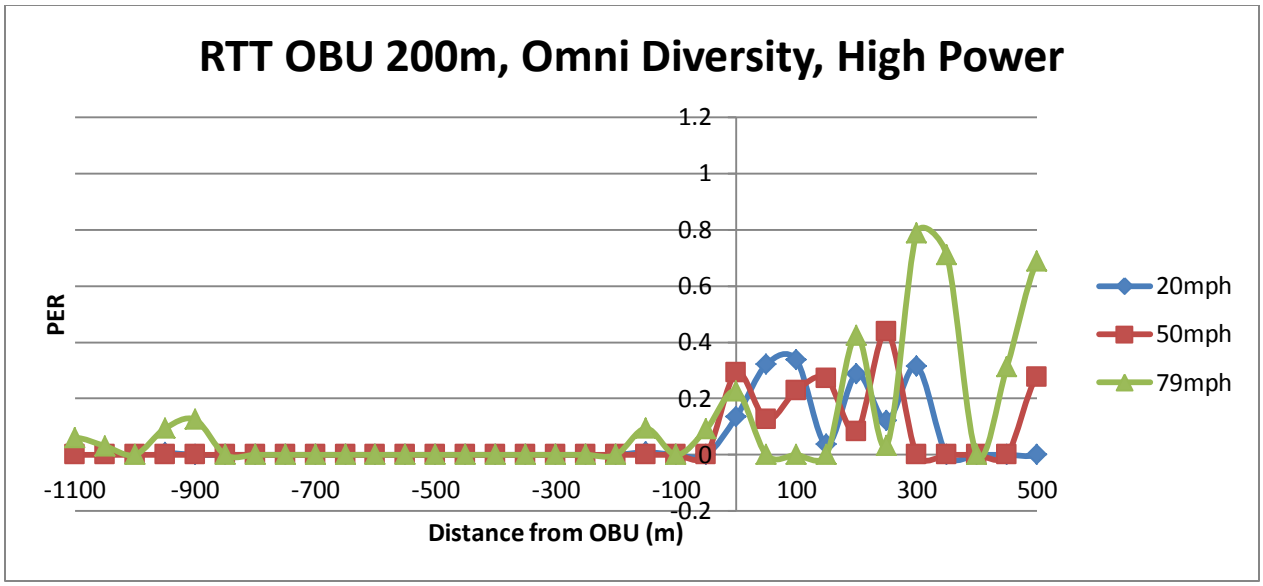

(a)

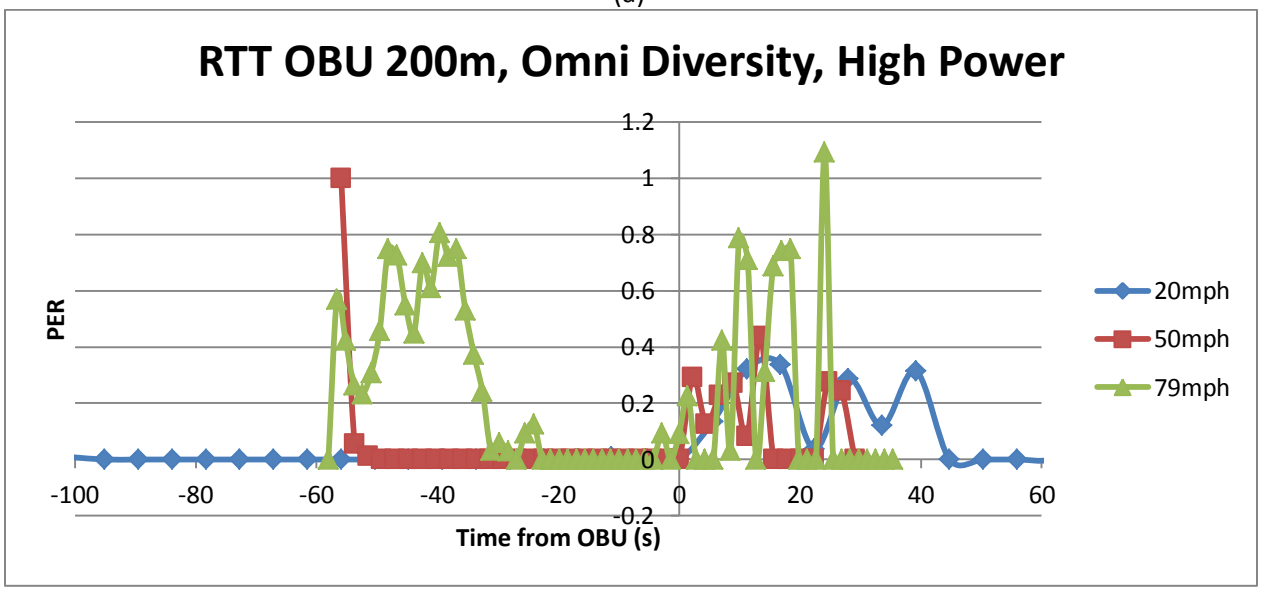

(b)

Figure P.20 PER at the OBU with an Omni Diversity Antenna operating at High Power, (a) gives PER vs. Distance Train is from OBU and (b) gives PER vs. Time between train and OBU.

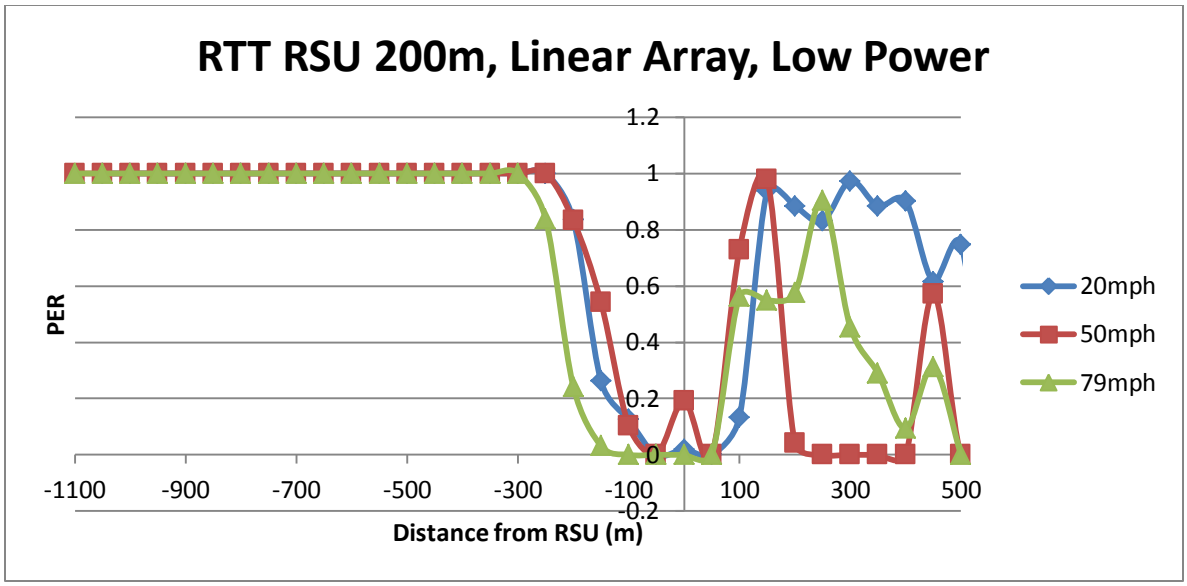

(a)

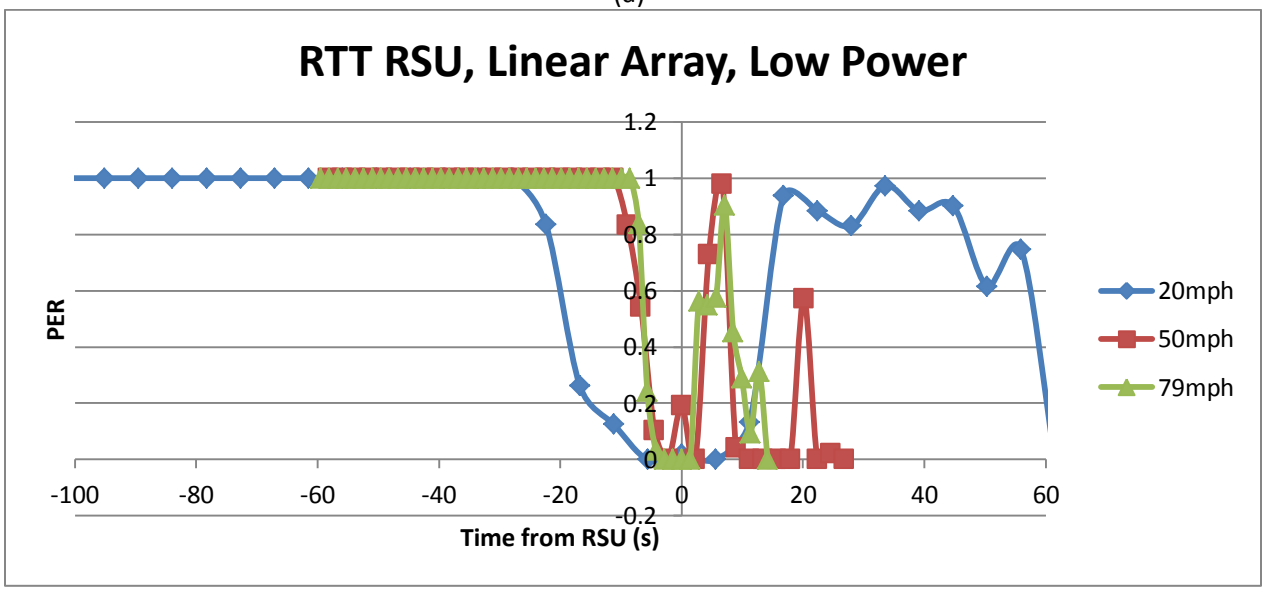

(b)

Figure P.21 PER at the RSU with a Linear Array Antenna operating at Low Power, (a) gives PER vs. Distance Train is from RSU and (b) gives PER vs. Time between train and RSU.

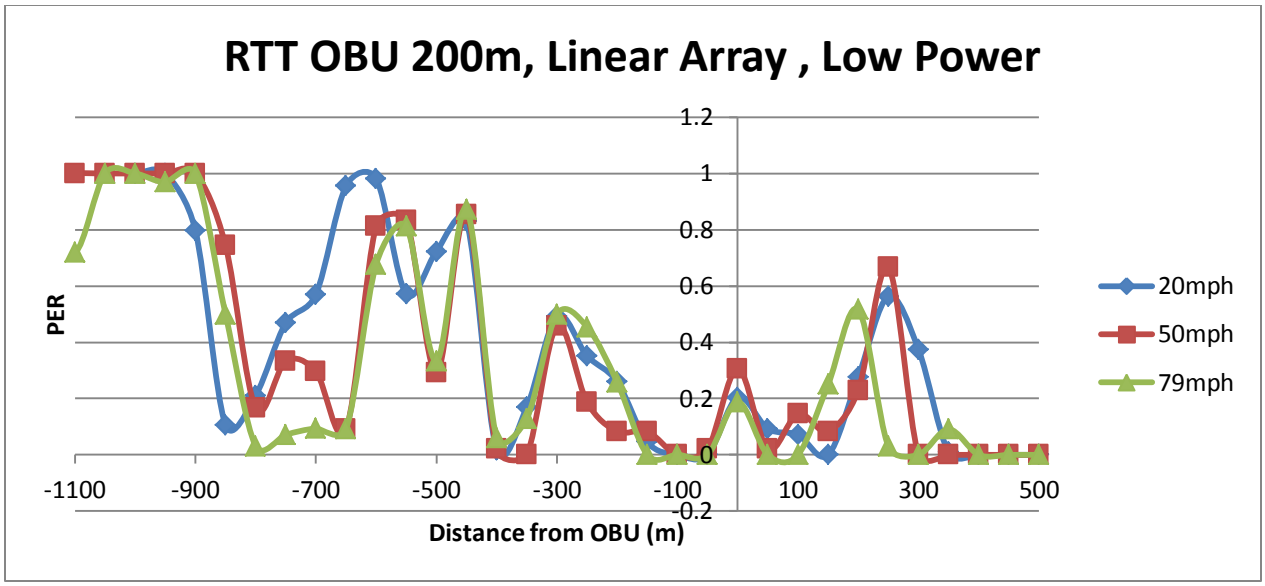

(a)

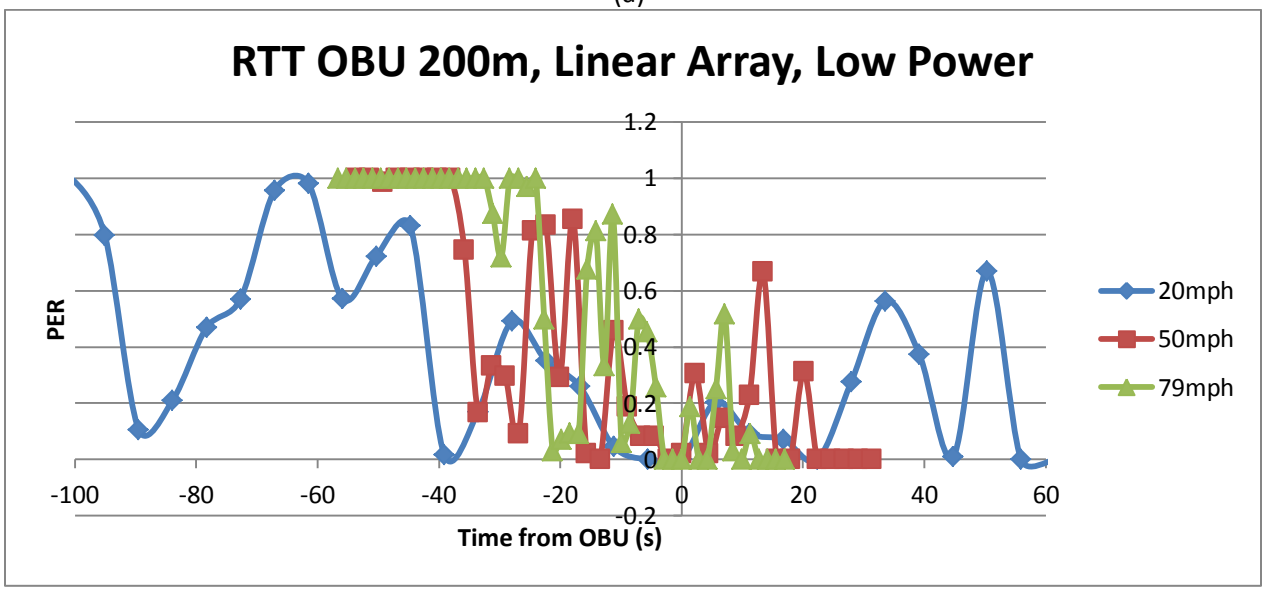

(b)

Figure P.22 PER at the OBU with a Linear Array Antenna operating at Low Power, (a) gives PER vs. Distance Train is from OBU and (b) gives PER vs. Time between train and OBU.

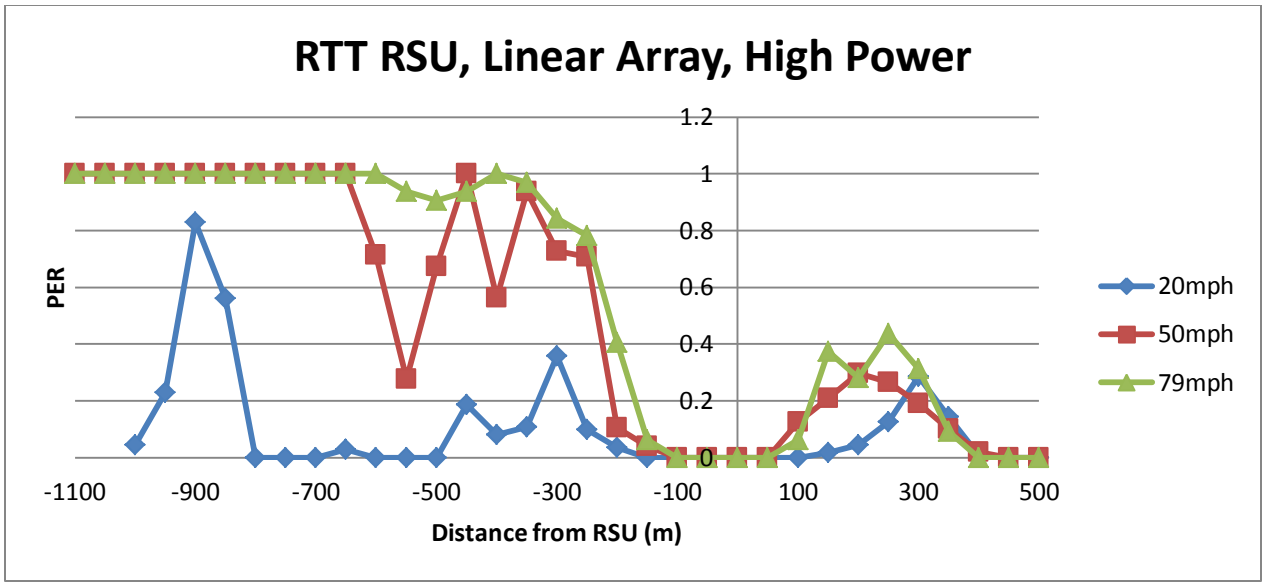

(a)

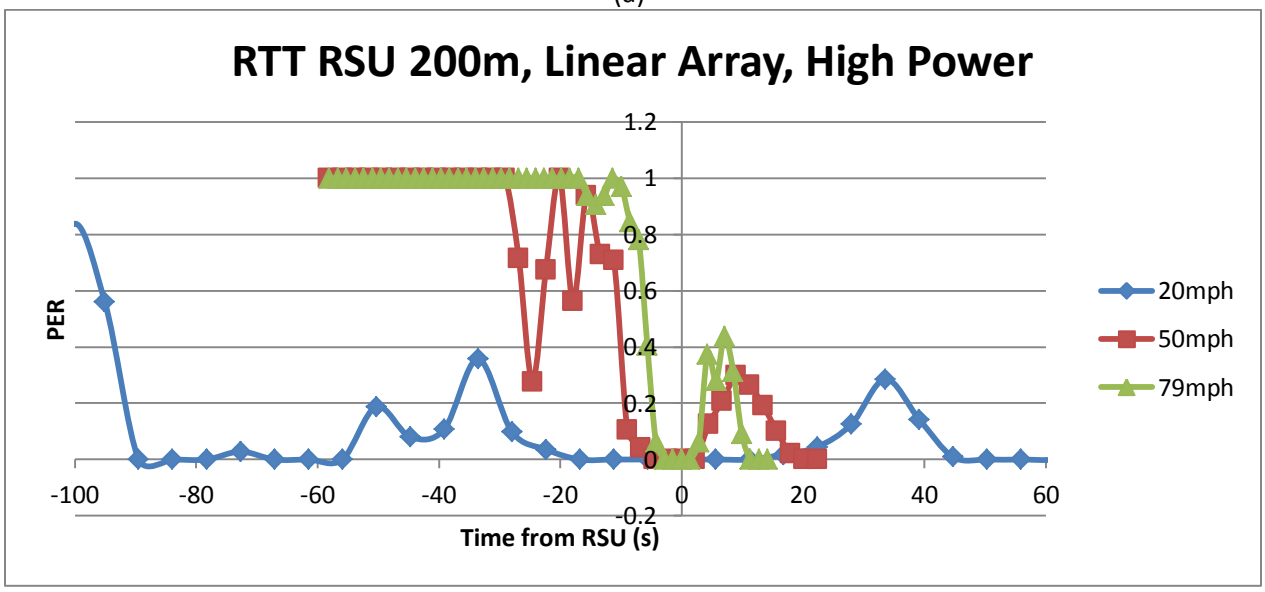

(b)

Figure P.23 PER at the RSU with a Linear Array Antenna operating at High Power, (a) gives PER vs. Distance Train is from RSU and (b) gives PER vs. Time between train and RSU.

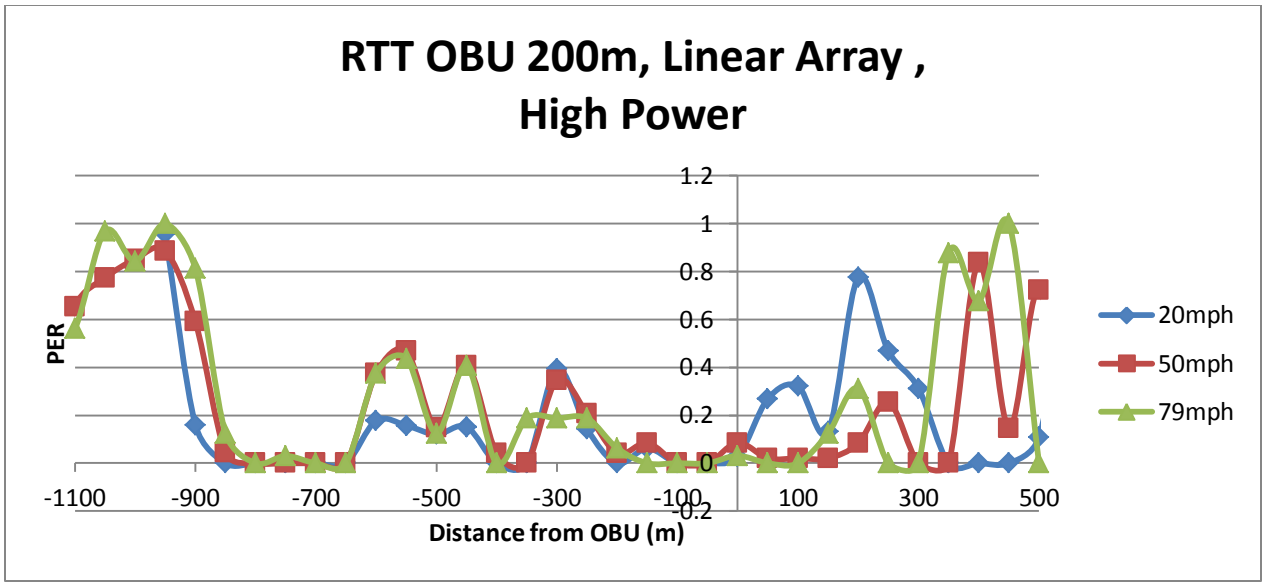

(a)

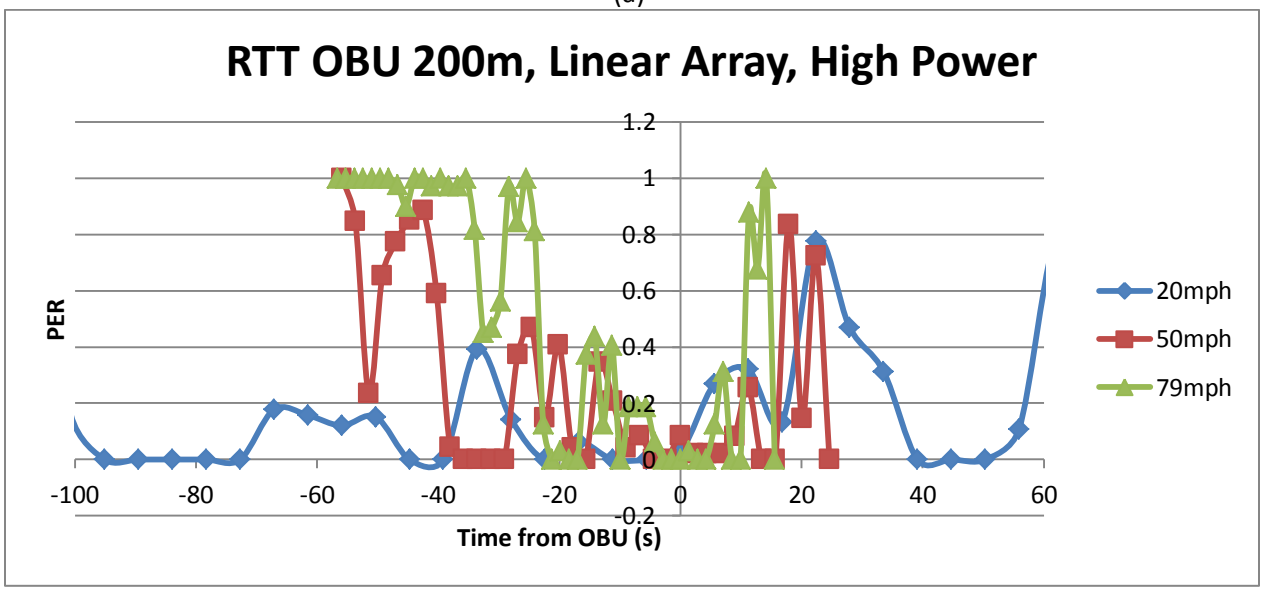

(b)

Figure P.24 PER at the OBU with a Linear Array Antenna operating at High Power, (a) gives PER vs. Distance Train is from OBU and (b) gives PER vs. Time between train and OBU.

PER Plots for the PTT Test Site

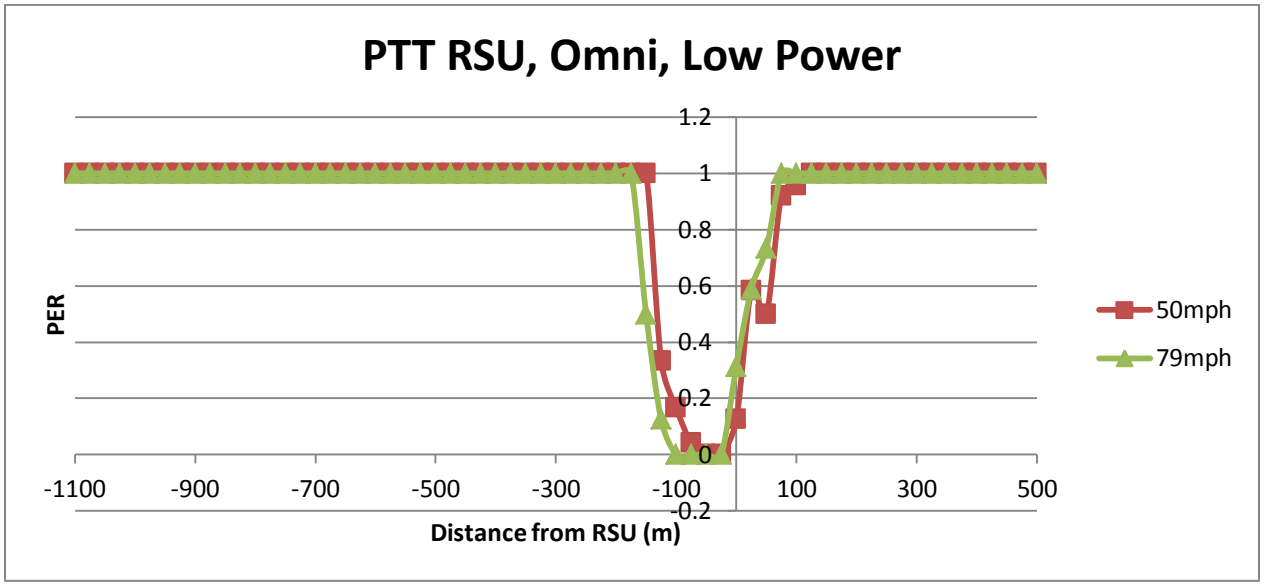

(a)

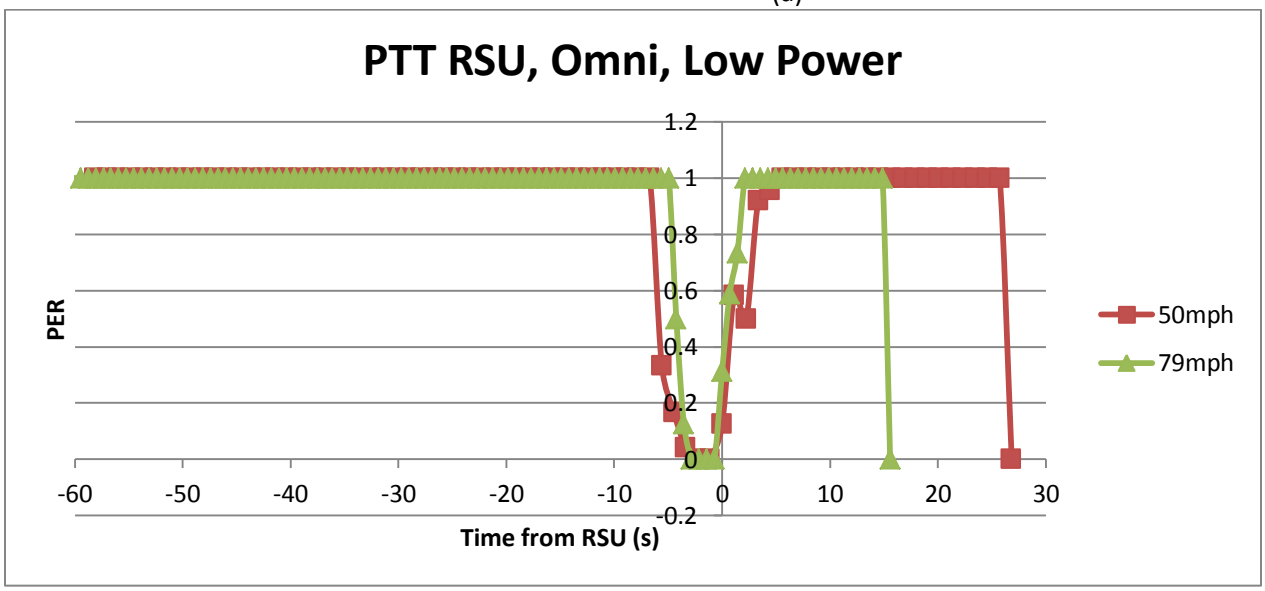

(b)

Figure P.25 PER at the RSU with an Omni Directional Antenna operating at Low Power, (a) gives PER vs. Distance Train is from RSU and (b) gives PER vs. Time between train and RSU.

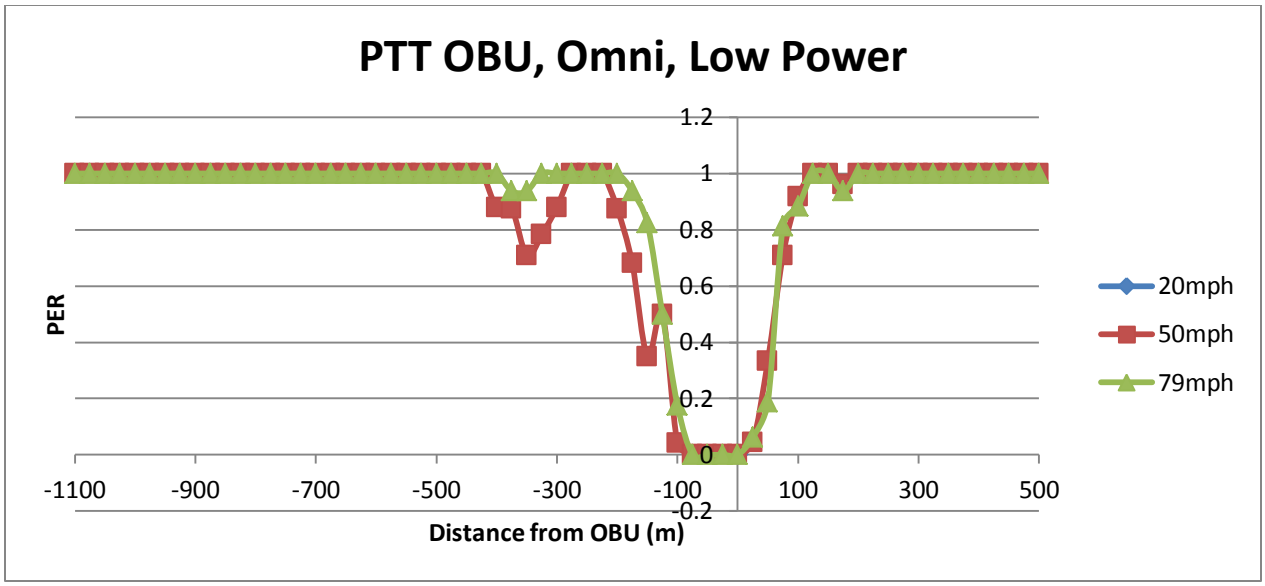

(a)

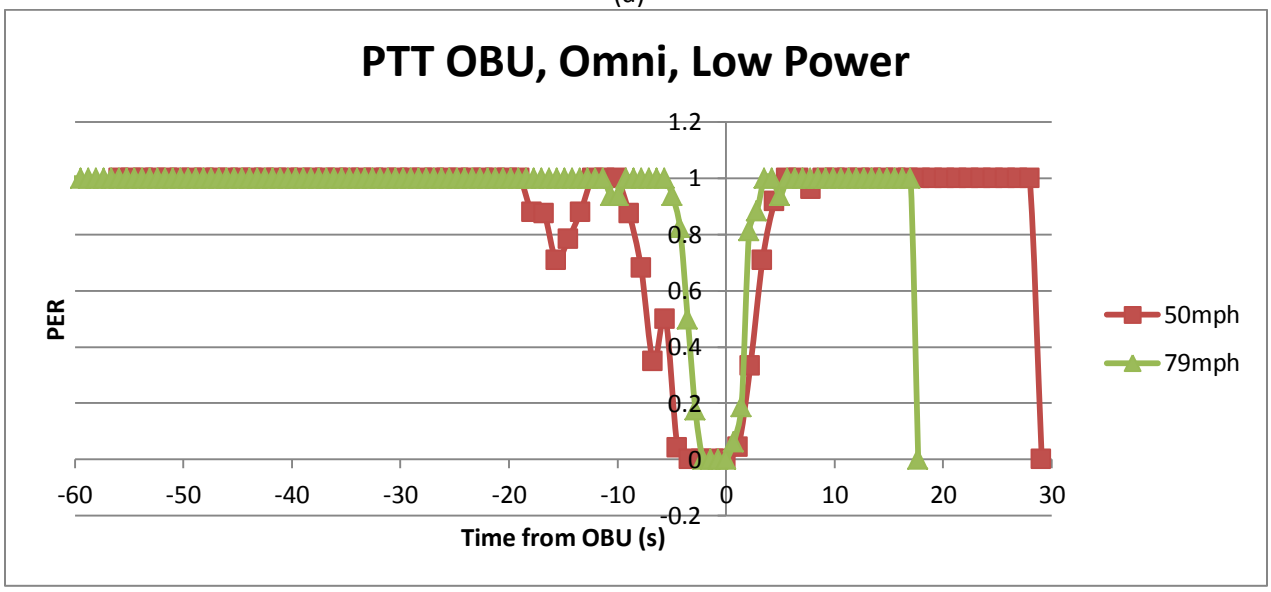

(b)

Figure P.26 PER at the OBU with an Omni Directional Antenna operating at Low Power, (a) gives PER vs. Distance Train is from OBU and (b) gives PER vs. Time between train and OBU.

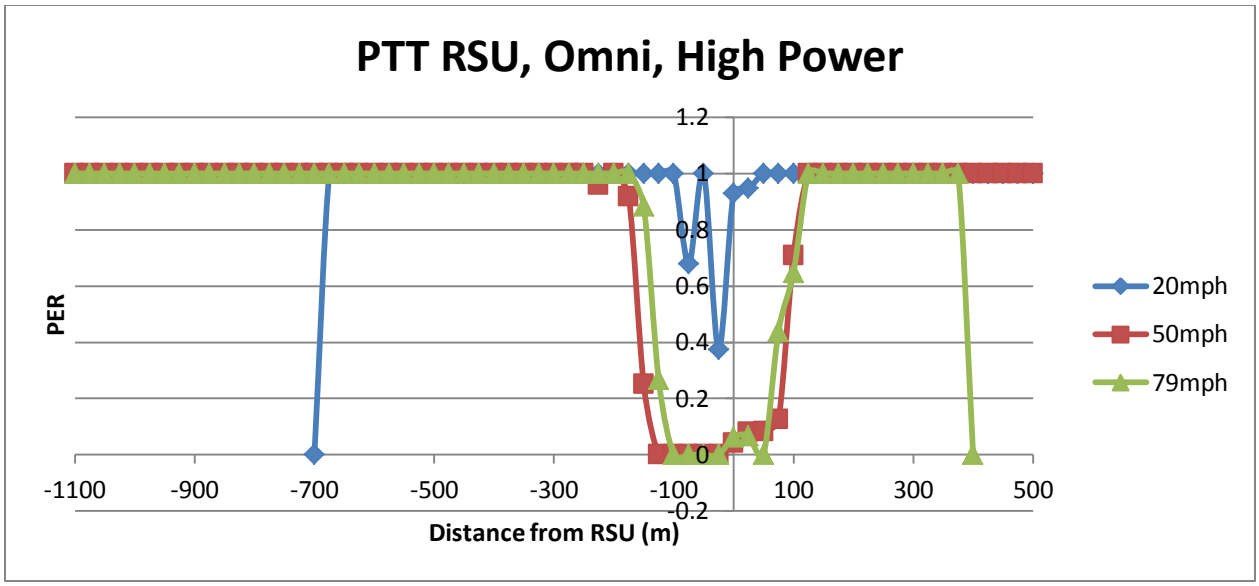

(a)

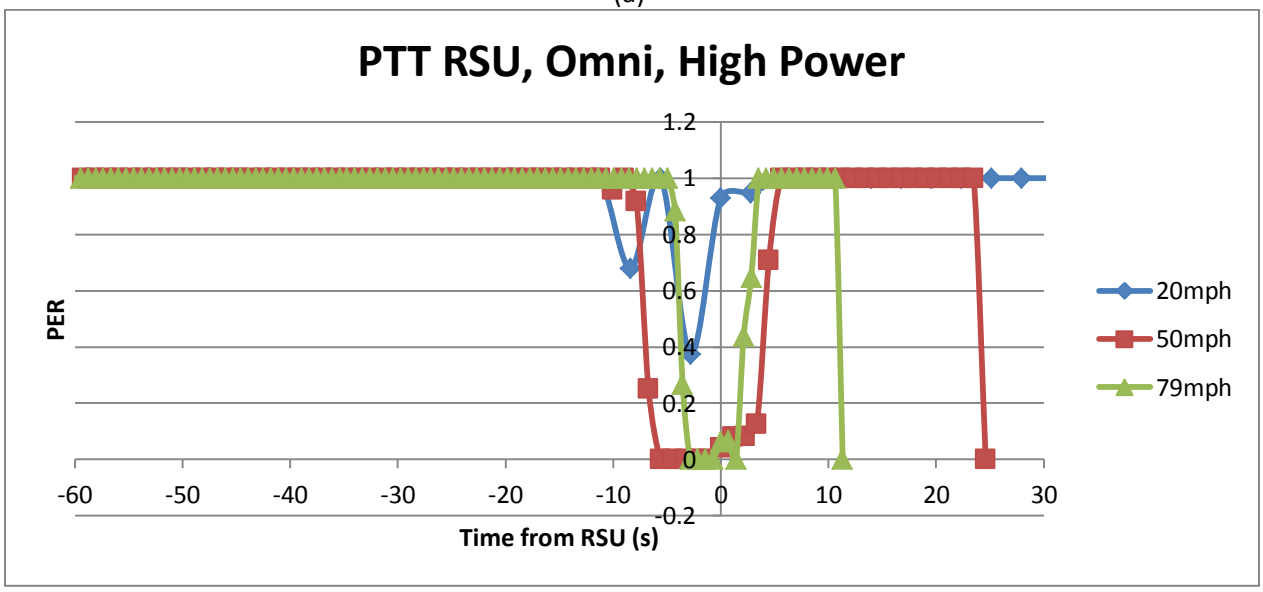

(b)

FigureP.27 PER at the RSU with an Omni Directional Antenna operating at High Power, (a) gives PER vs. Distance Train is from RSU and (b) gives PER vs. Time between train and RSU.

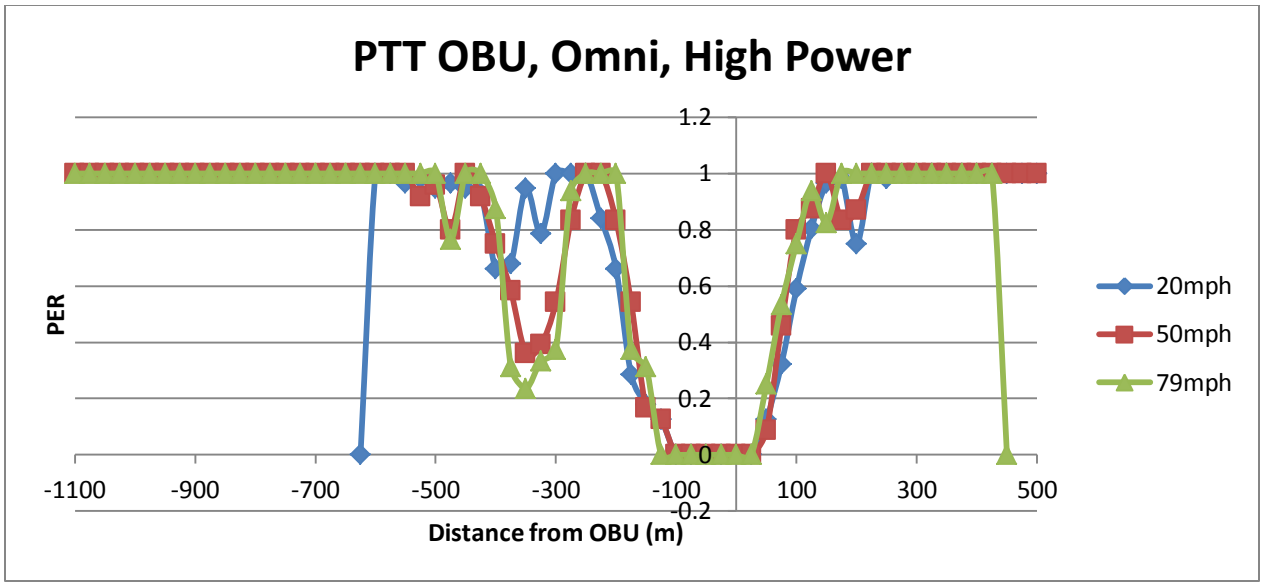

(a)

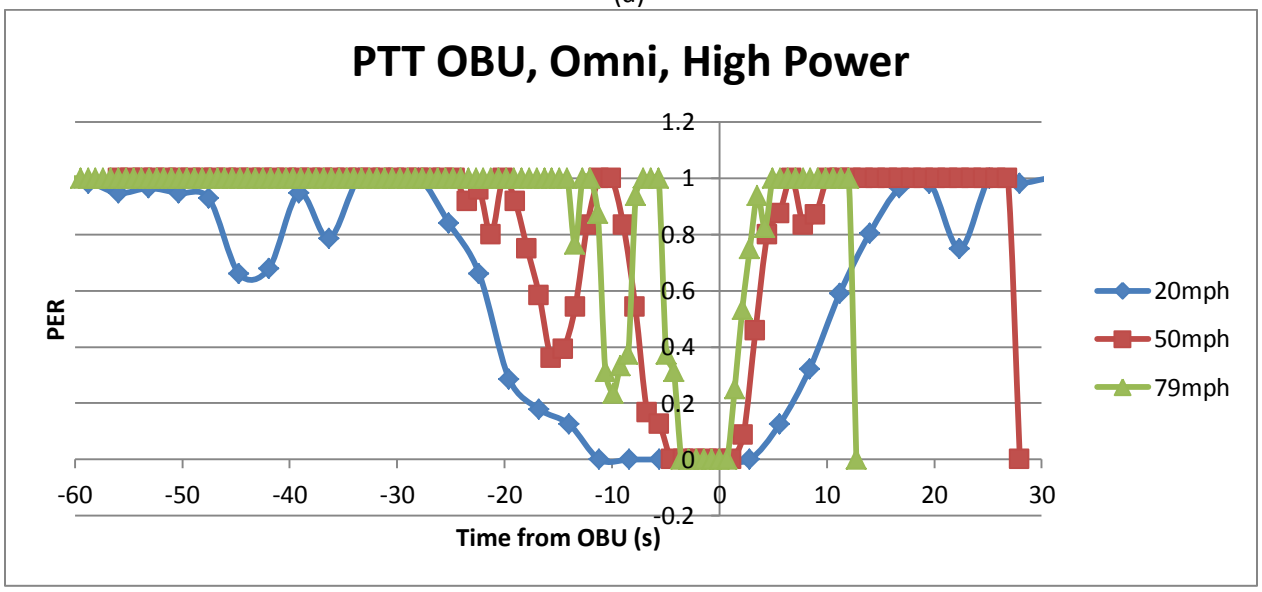

(b)

Figure P.28 PER at the OBU with an Omni Directional Antenna operating at High Power, (a) gives PER vs. Distance Train is from OBU and (b) gives PER vs. Time between train and OBU.

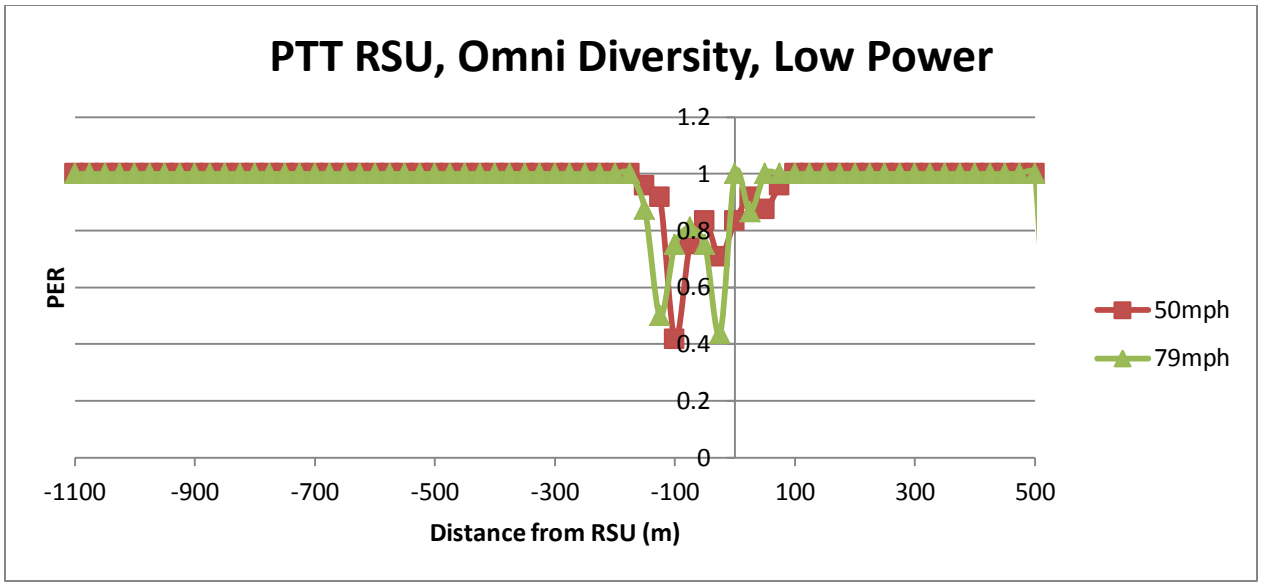

(a)

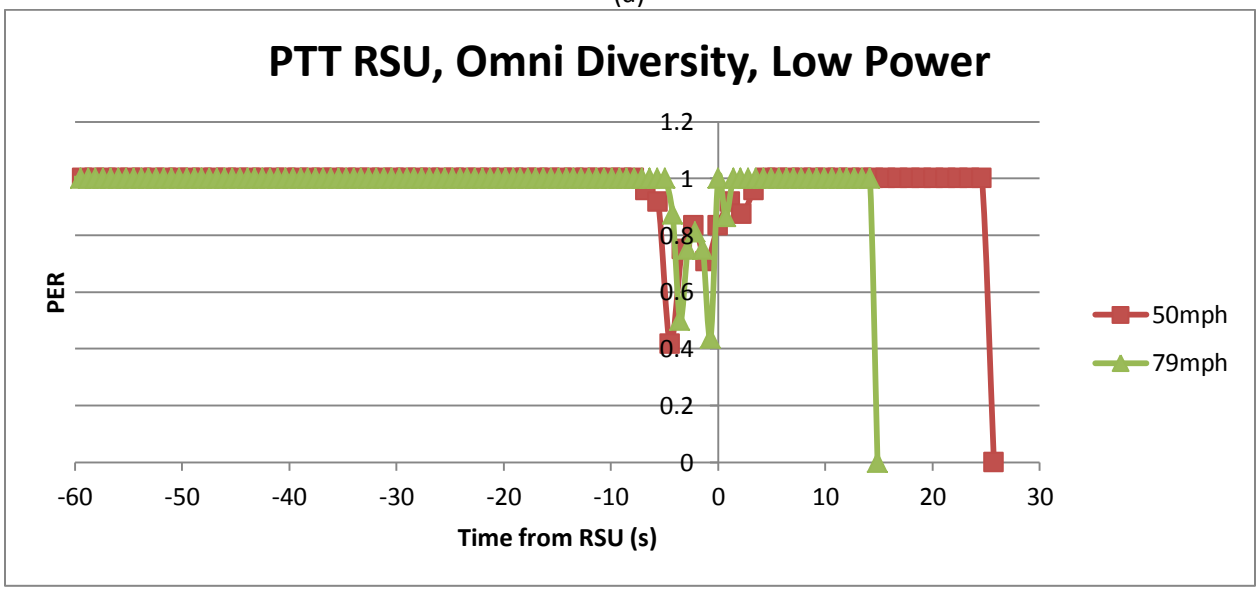

(b)

Figure P.29 PER at the RSU with an Omni Diversity Antenna operating at Low Power, (a) gives PER vs. Distance Train is from RSU and (b) gives PER vs. Time between train and RSU.

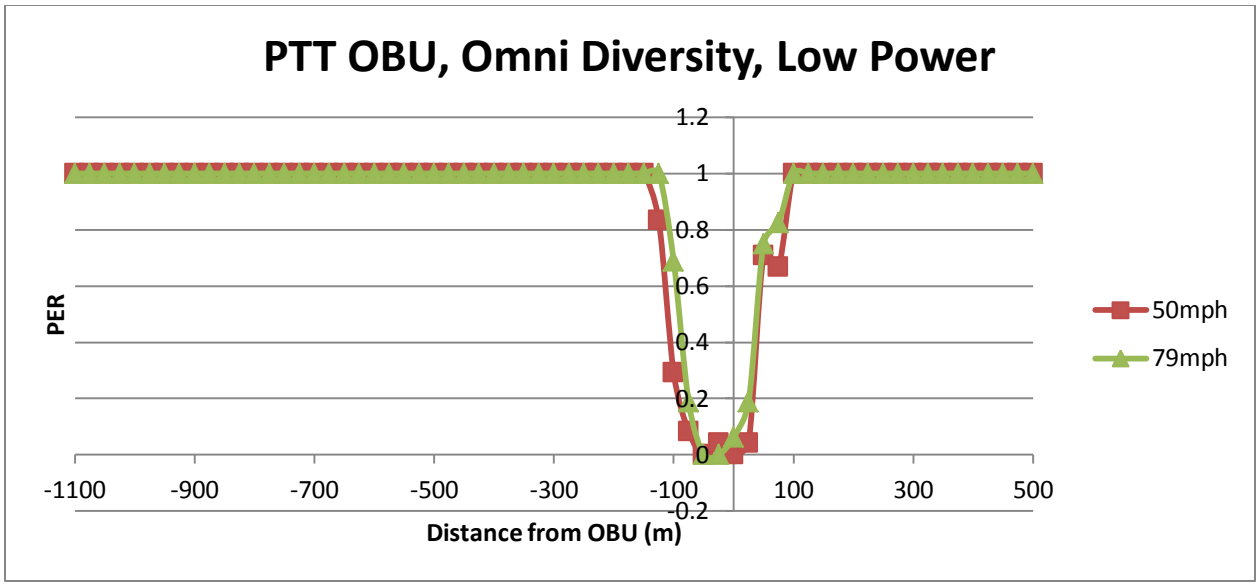

(a)

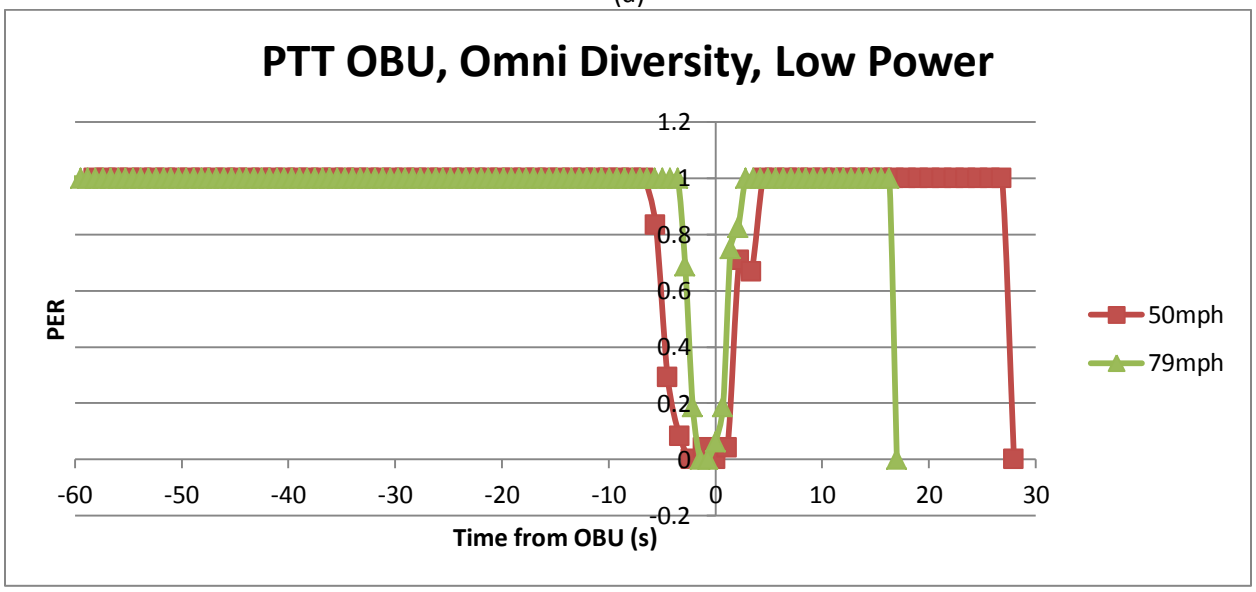

(b)

Figure P.30 PER at the OBU with an Omni Diversity Antenna operating at Low Power, (a) gives PER vs. Distance Train is from OBU and (b) gives PER vs. Time between train and OBU.

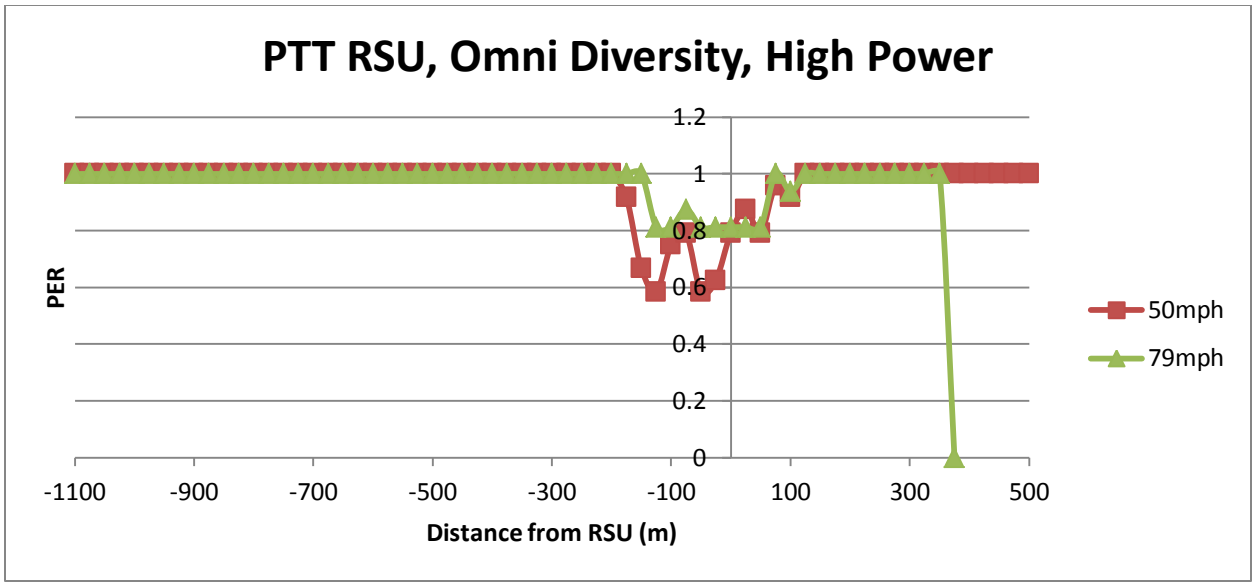

(a)

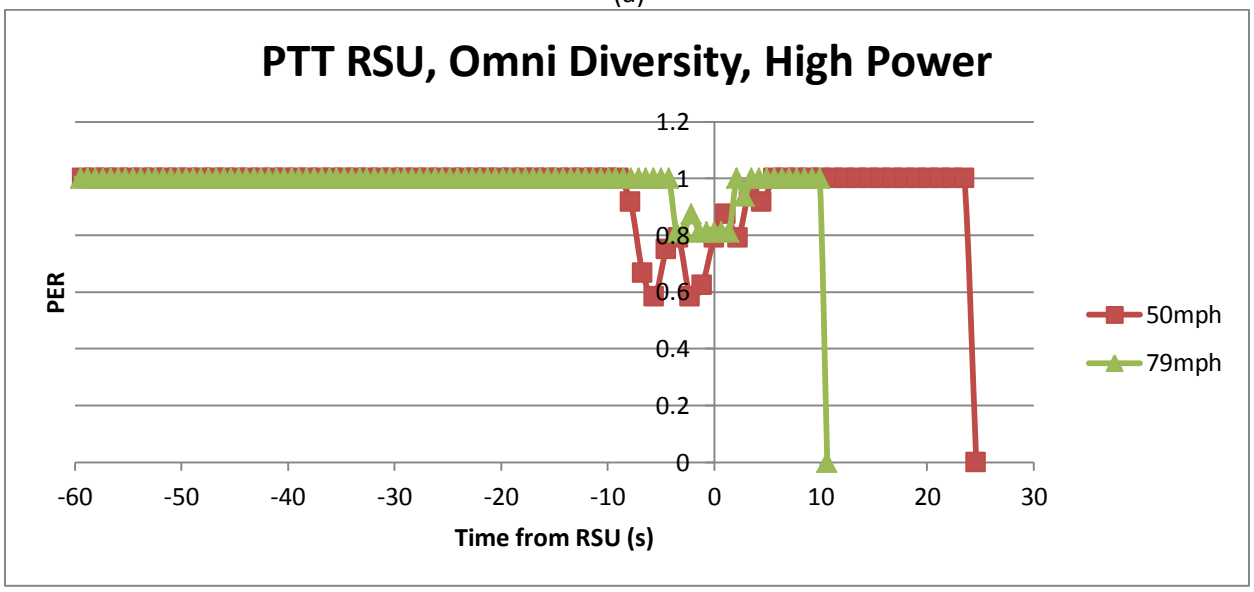

(b)

Figure P.31 PER at the RSU with an Omni Diversity Antenna operating at High Power, (a) gives PER vs. Distance Train is from RSU and (b) gives PER vs. Time between train and RSU.

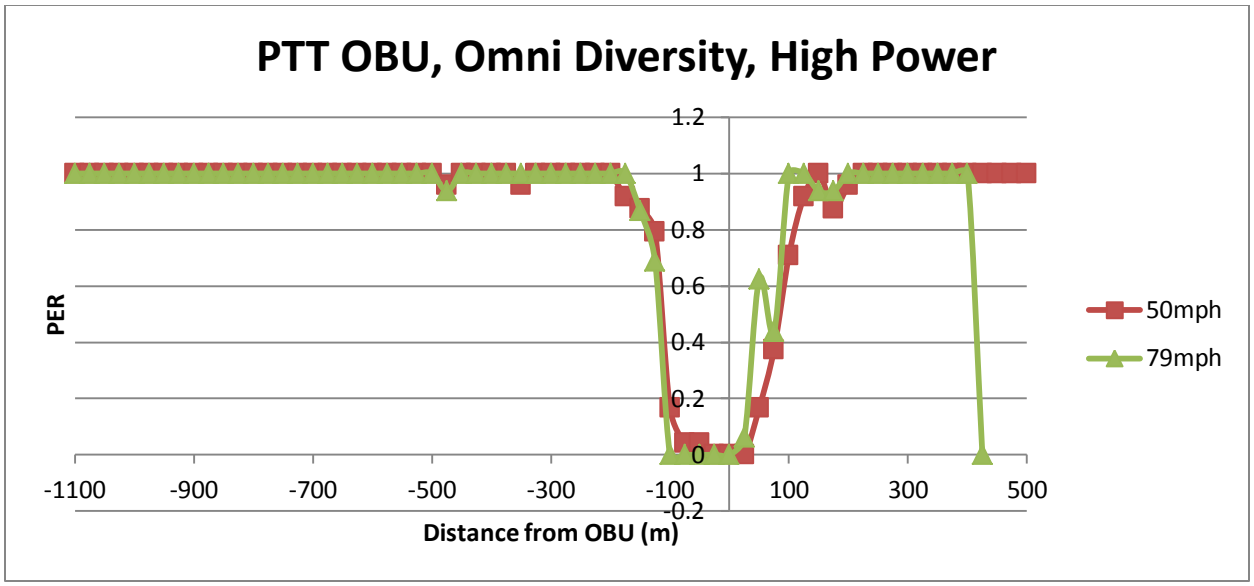

(a)

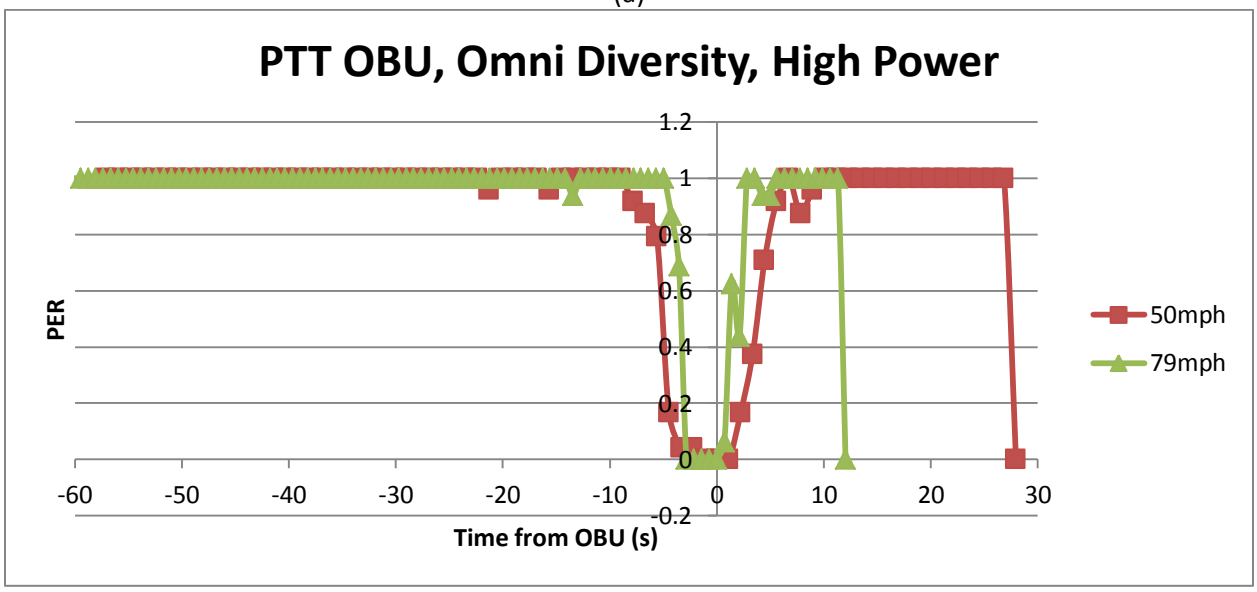

(b)

Figure P.32 PER at the OBU with an Omni Diversity Antenna operating at High Power, (a) gives PER vs. Distance Train is from OBU and (b) gives PER vs. Time between train and OBU.

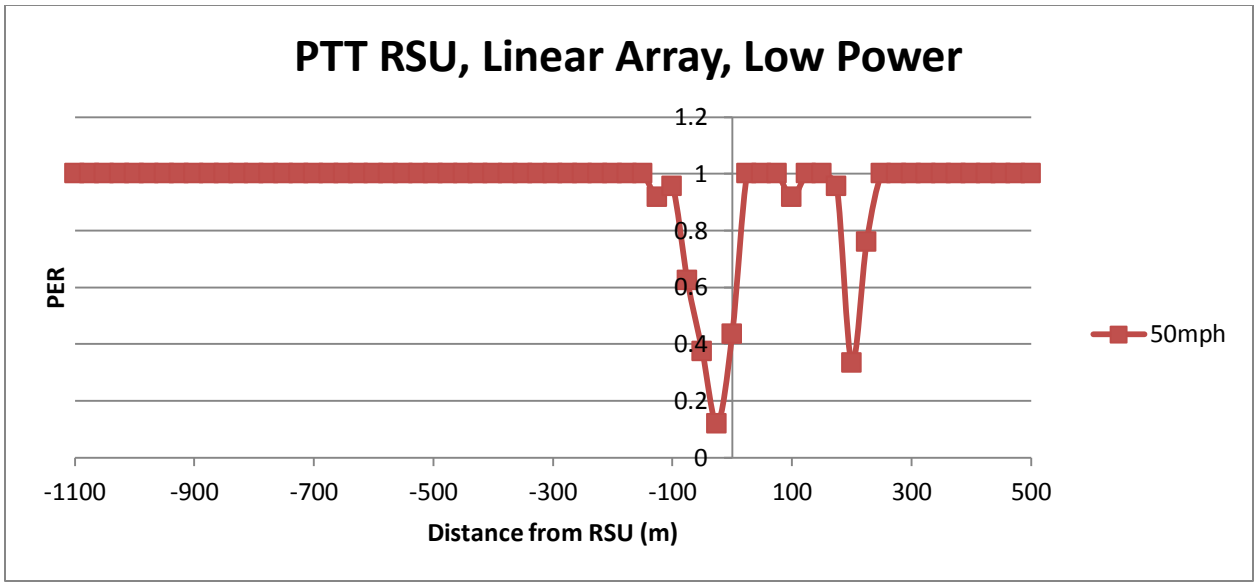

(a)

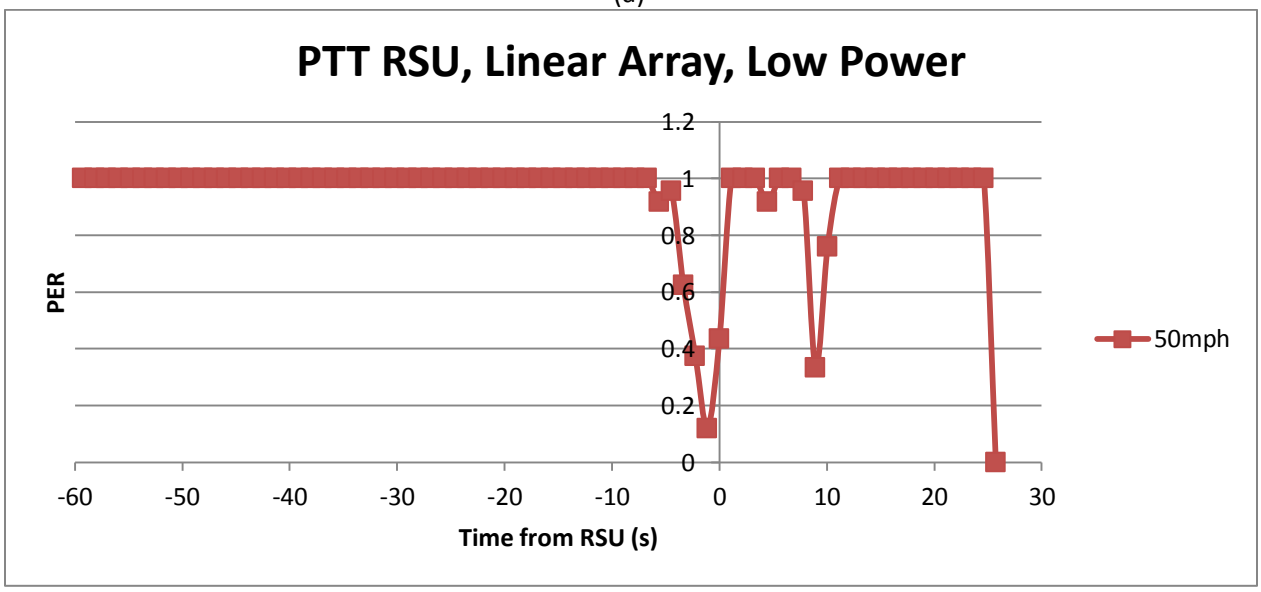

(b)

Figure P.33 PER at the RSU with a Linear Array Antenna operating at Low Power, (a) gives PER vs. Distance Train is from RSU and (b) gives PER vs. Time between train and RSU.

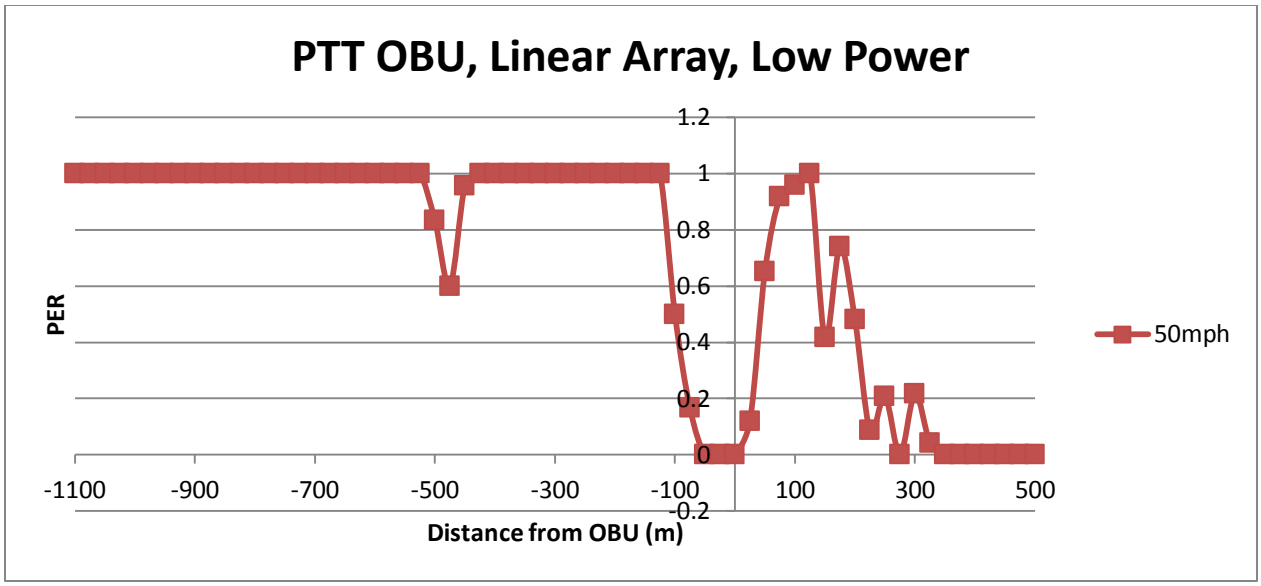

(a)

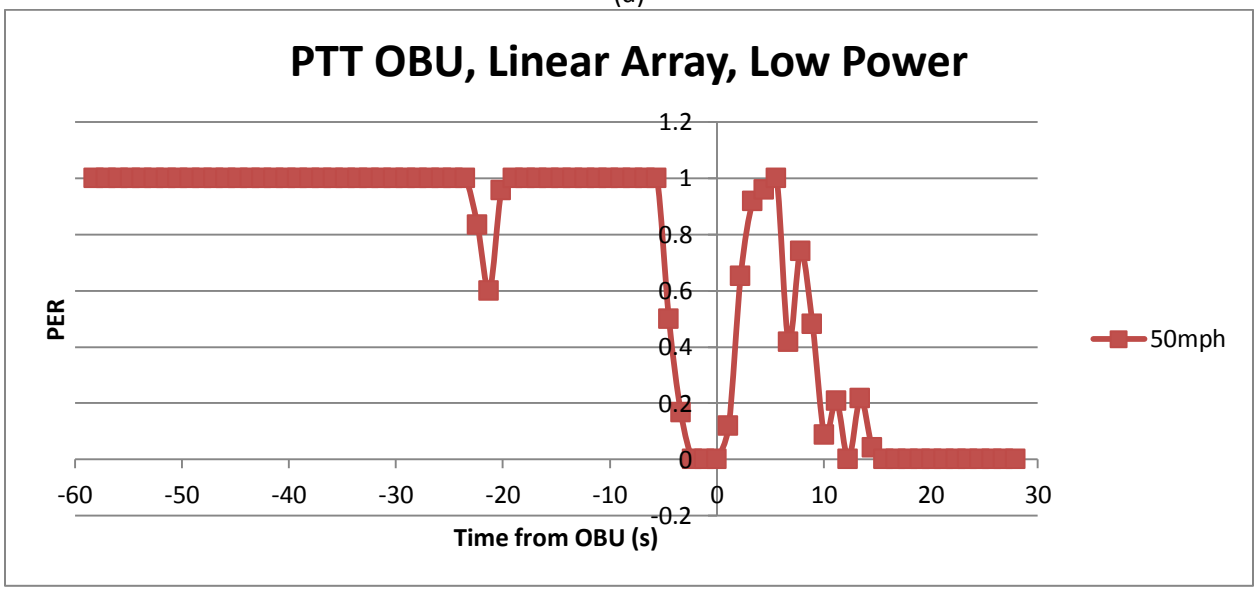

(b)

Figure P.34 PER at the OBU with a Linear Array Antenna operating at Low Power, (a) gives PER vs. Distance Train is from OBU and (b) gives PER vs. Time between train and OBU.

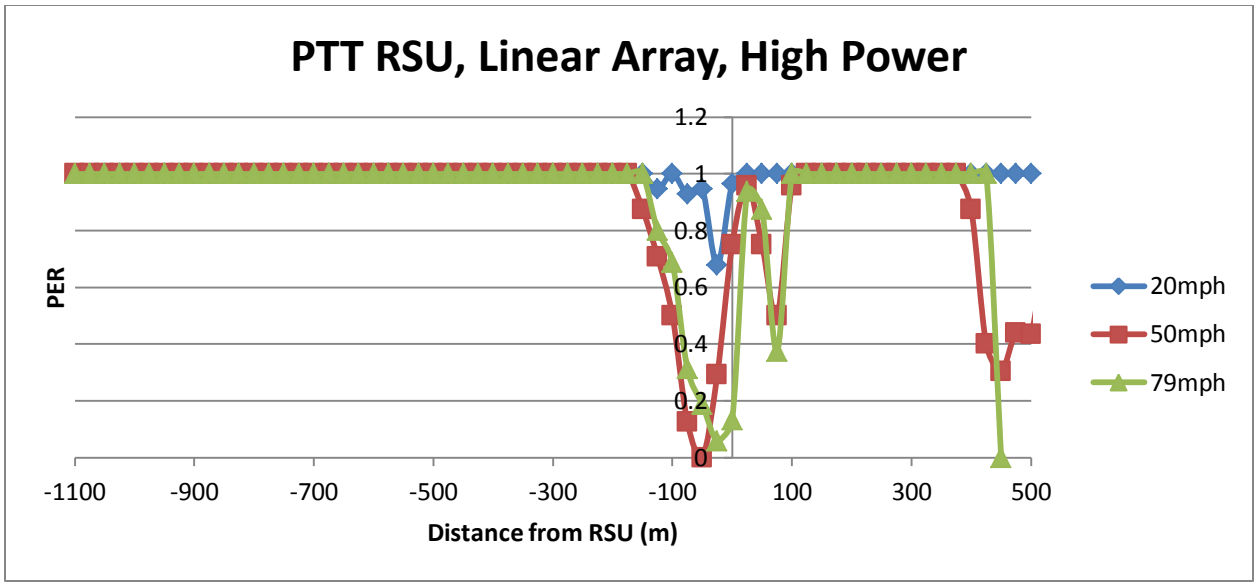

(a)

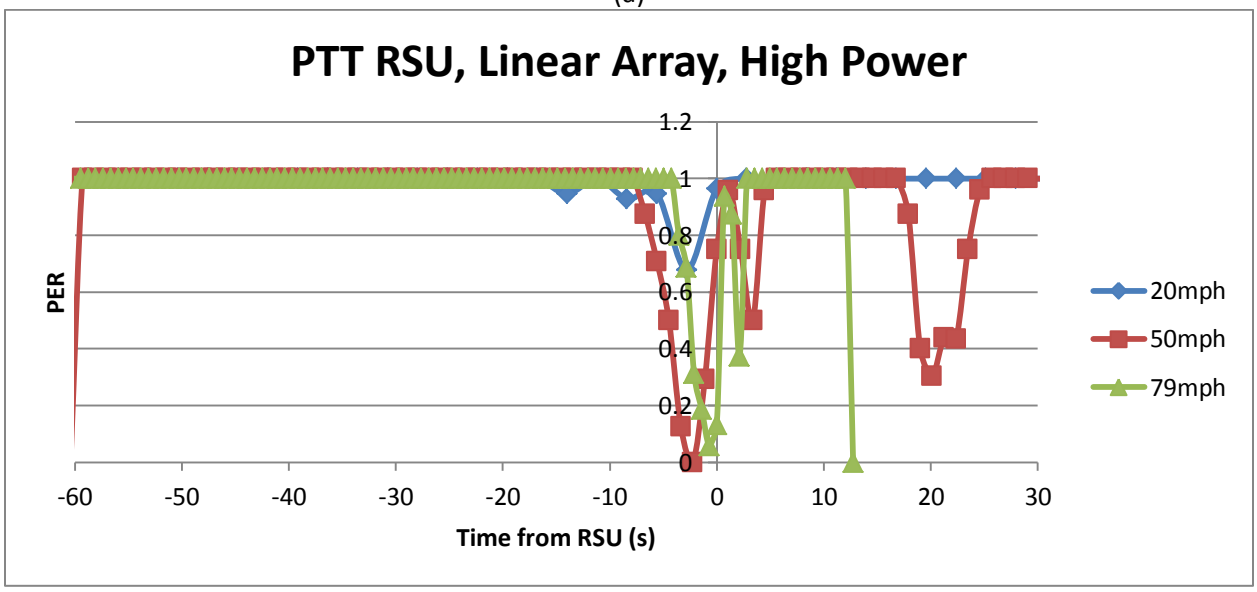

(b)

Figure P.35 PER at the RSU with a Linear Array Antenna operating at High Power, (a) gives PER vs. Distance Train is from RSU and (b) gives PER vs. Time between train and RSU.

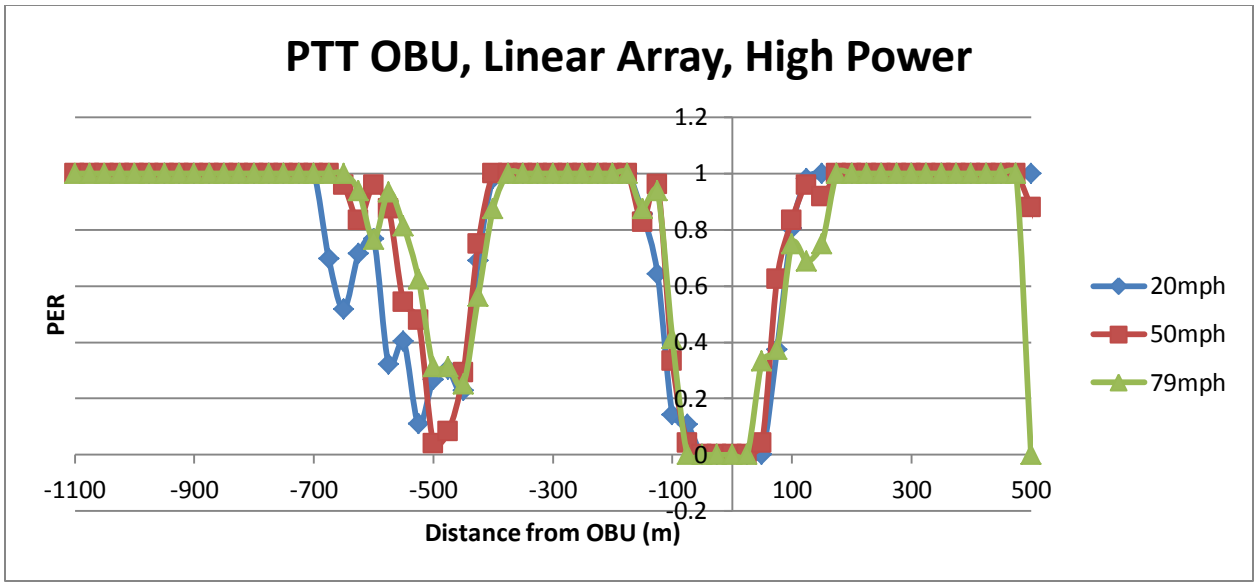

(a)

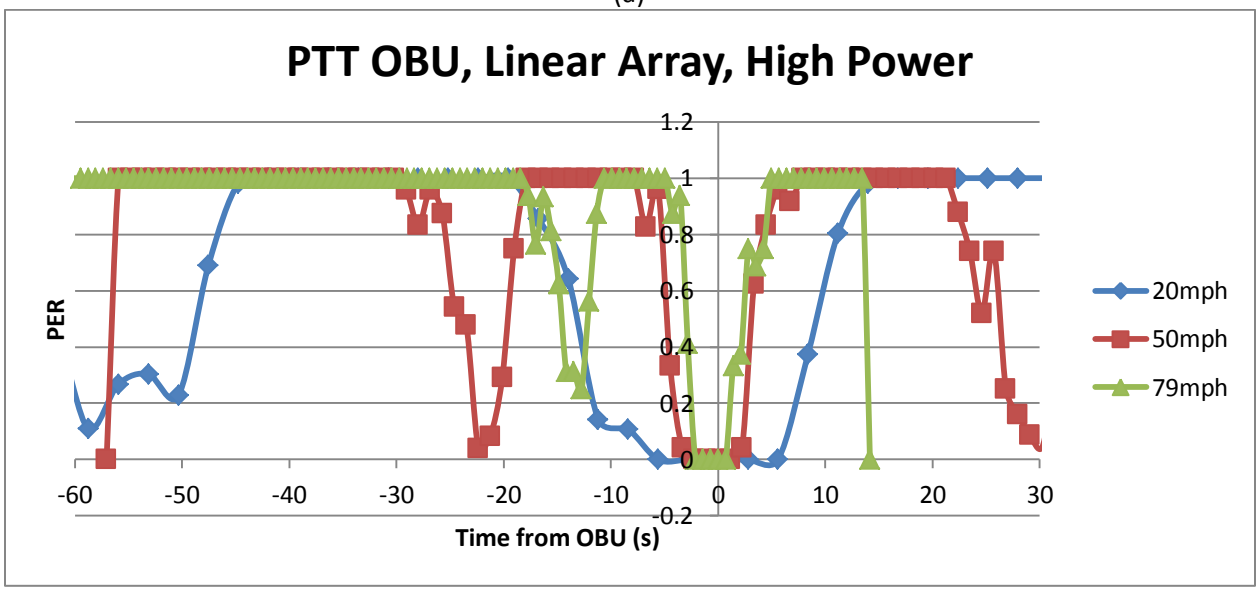

(b)

Figure P.36 PER at the OBU with a Linear Array Antenna operating at High Power, (a) gives PER vs. Distance Train is from OBU and (b) gives PER vs. Time between train and OBU.

Appendix Q

In the Google Earth plots given in the sections, white dots represent a packet that was not successfully received by either receiver, a blue dot represents a packet that was received by only the On Board Unit, a yellow dot represents a packet that was only received by the Road Side Unit, and a green dot represents a packet that was received by both units.

Google Earth Visualization Plots of Received Packets for RTT Test site with OBU at 50m

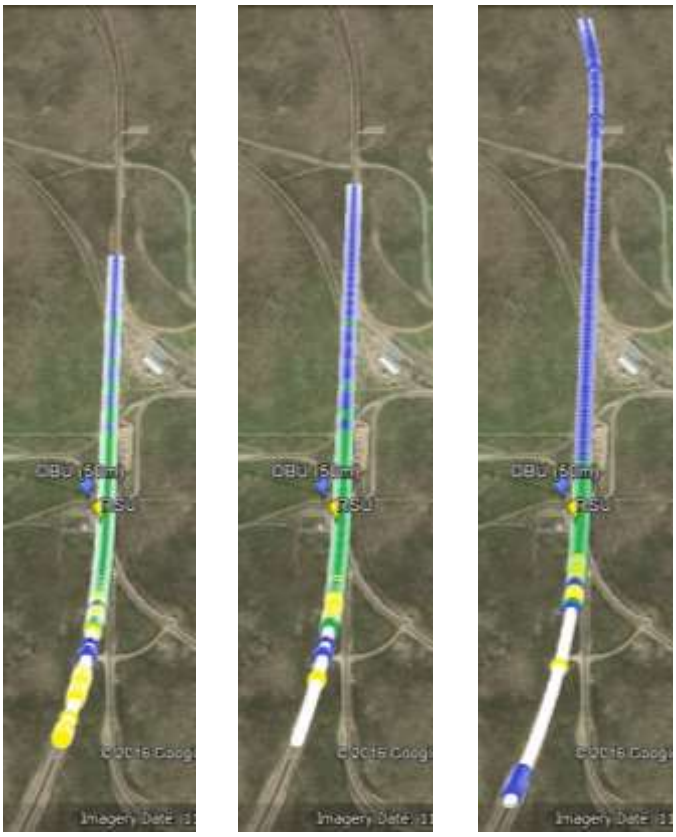

(a) (b) (c)

Figure Q.1 Geographic plots of which packets were received and which were dropped while the Omni antenna at Low Power was operated on a train moving at (a) 20mph, (b) 50 mph, (c) 79 mph.

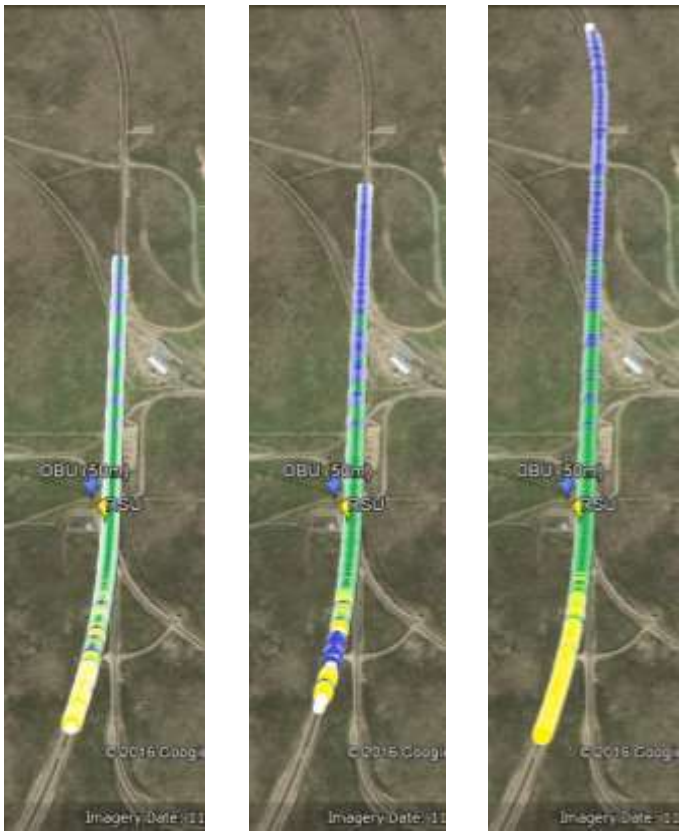

(a) (b) (c)

Figure Q.2 Geographic plots of which packets were received and which were dropped while the Omni antenna at High Power was operated on a train moving at (a) 20mph, (b) 50 mph, (c) 79 mph.

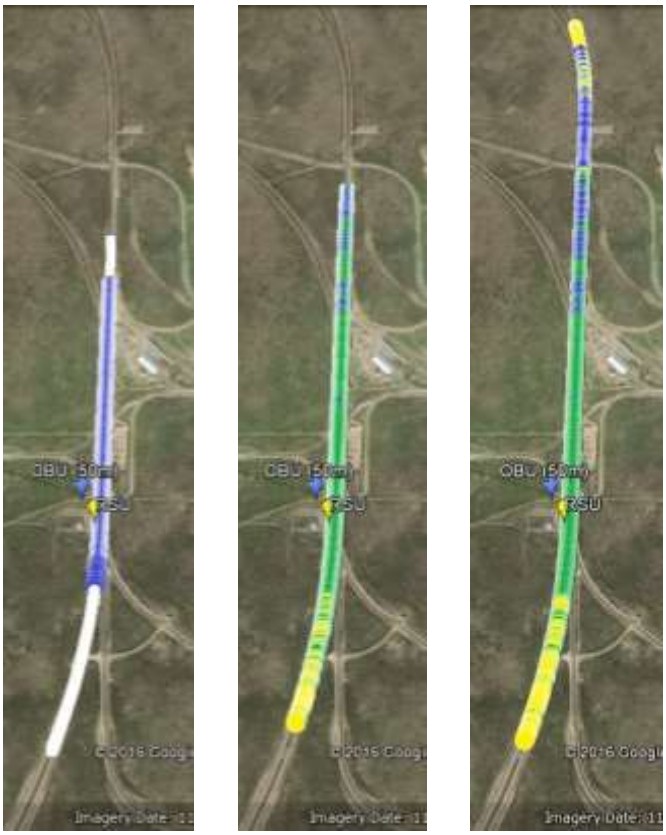

(a) (b) (c)

Figure Q.3 Geographic plots of which packets were received and which were dropped while the Omni Directional antenna at Low Power was operated on a train moving at (a) 20mph, (b) 50 mph, (c) 79 mph.

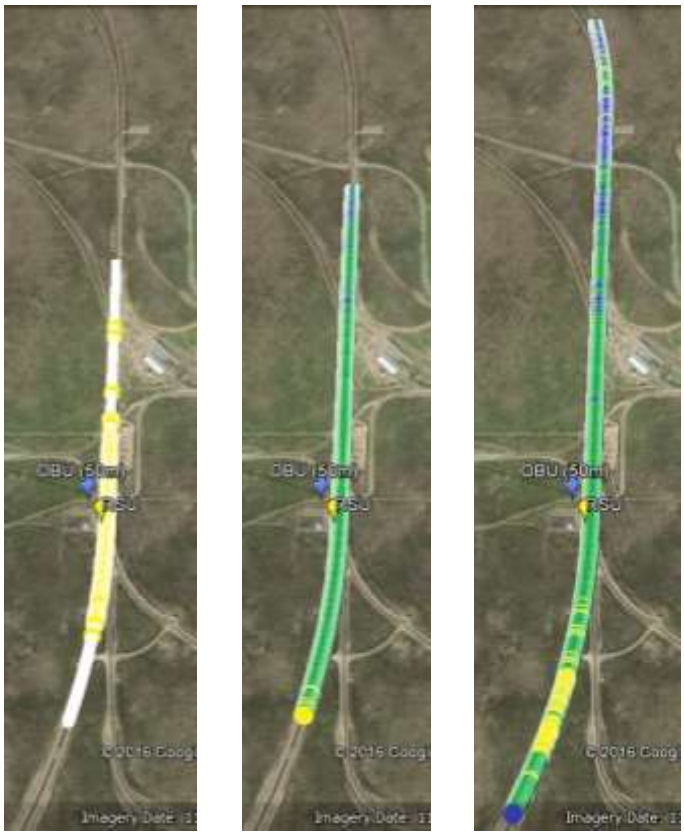

(a) (b) (c)

Figure Q.4 Geographic plots of which packets were received and which were dropped while the Omni Directional antenna at High Power was operated on a train moving at (a) 20mph, (b) 50 mph, (c) 79 mph

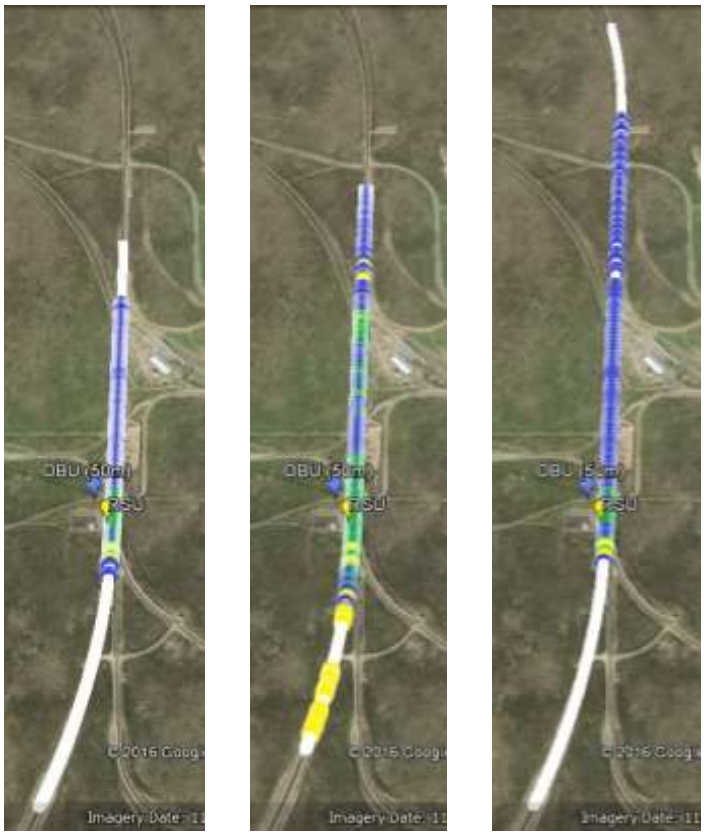

(a) (b) (c)

Figure Q.5 Geographic plots of which packets were received and which were dropped while the Linear Array antenna at Low Power was operated on a train moving at (a) 20mph, (b) 50 mph, (c) 79 mph.

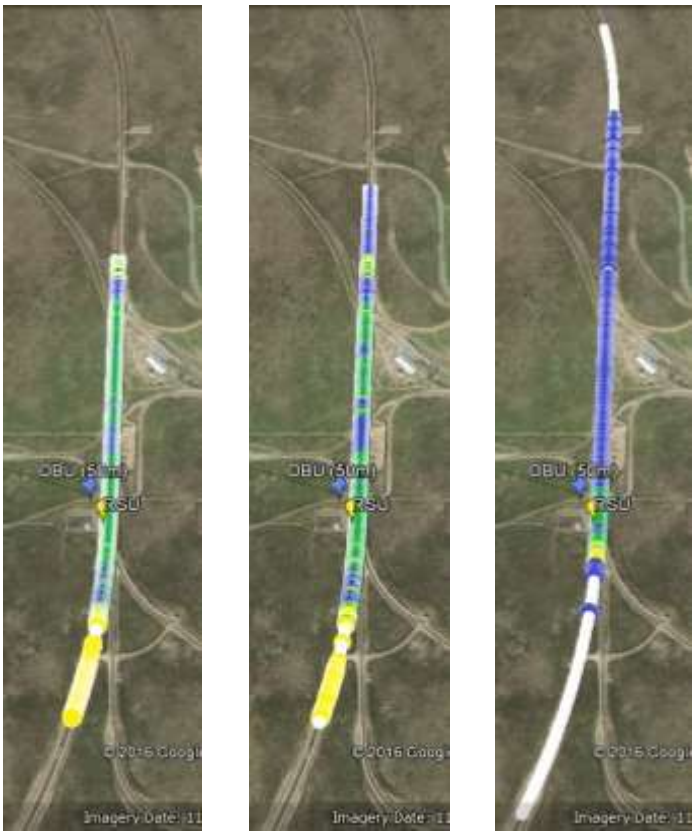

(a) (b) (c)

Figure Q.6 Geographic plots of which packets were received and which were dropped while the Linear Array antenna at High Power was operated on a train moving at (a) 20mph, (b) 50 mph, (c) 79 mph.

Google Earth Visualization Plots of Received Packets for RTT Test site with OBU at 200m

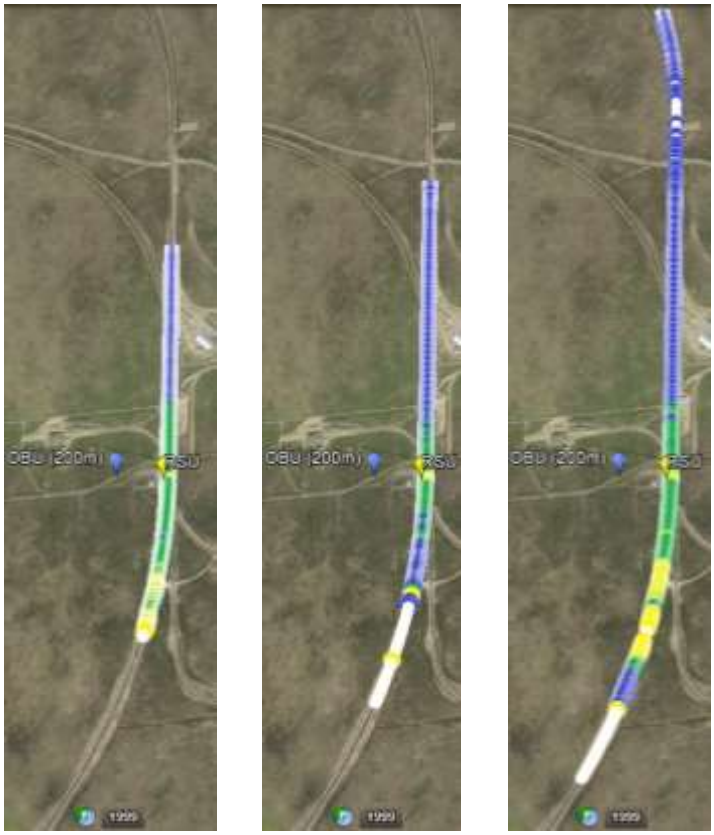

(a) (b) (c)

Figure Q.7 Geographic plots of which packets were received and which were dropped while the Omni Directional antenna at Low Power was operated on a train moving at (a) 20mph, (b) 50 mph, (c) 79 mph.

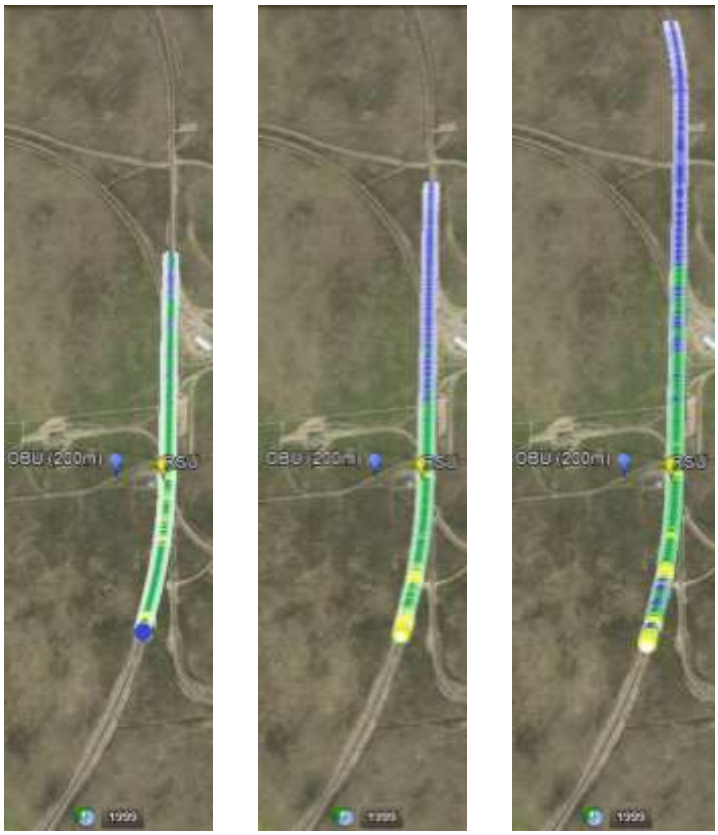

(a) (b) (c)

Figure Q.8 Geographic plots of which packets were received and which were dropped while the Omni Directional antenna at High Power was operated on a train moving at (a) 20mph, (b) 50 mph, (c) 79 mph.

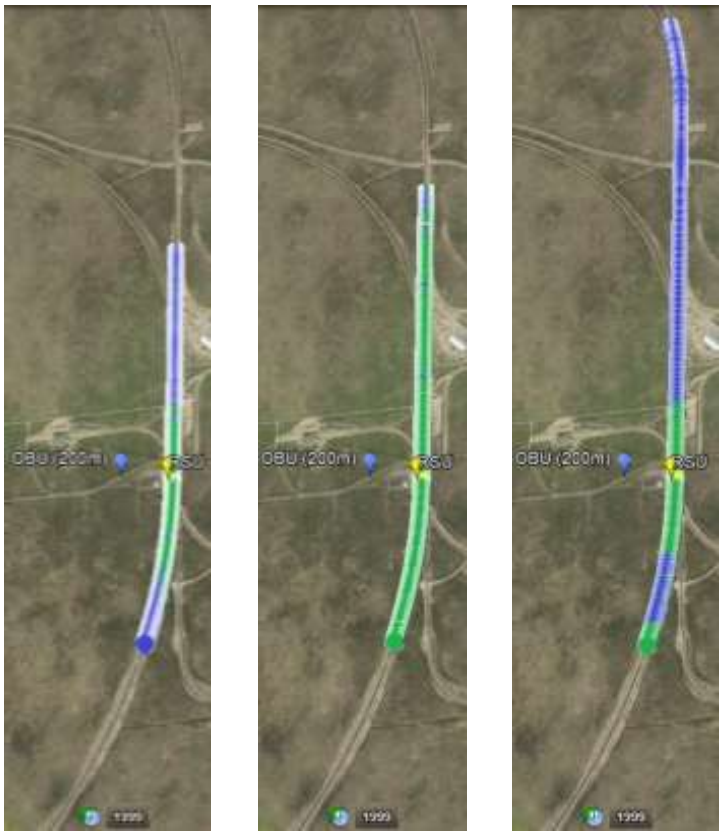

(a) (b) (c)

Figure Q.9 Geographic plots of which packets were received and which were dropped while the Omni Diversity antenna at Low Power was operated on a train moving at (a) 20mph, (b) 50 mph, (c) 79 mph.

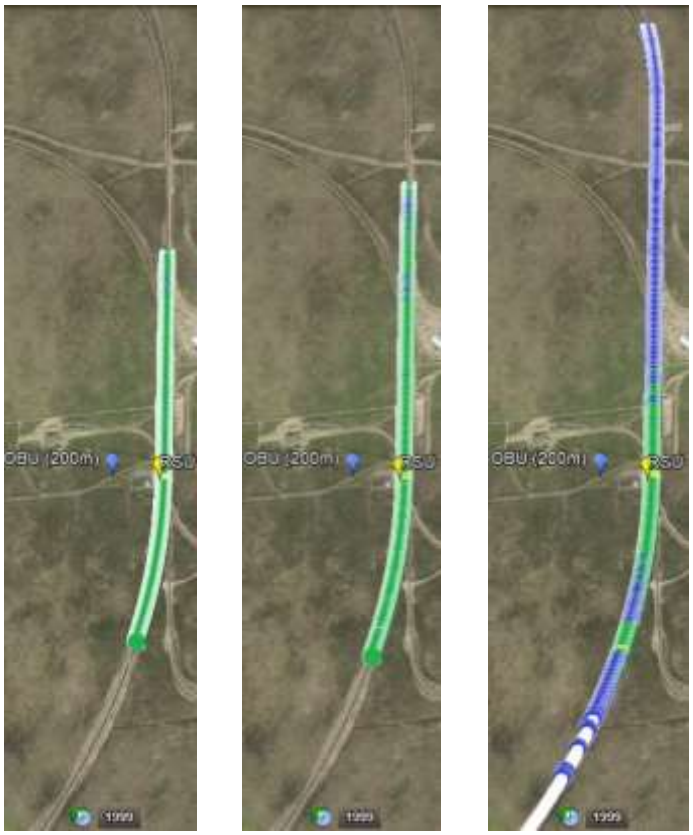

(a) (b) (c)

Figure Q.10 Geographic plots of which packets were received and which were dropped while the Omni Diversity antenna at High Power was operated on a train moving at (a) 20mph, (b) 50 mph, (c) 79 mph.

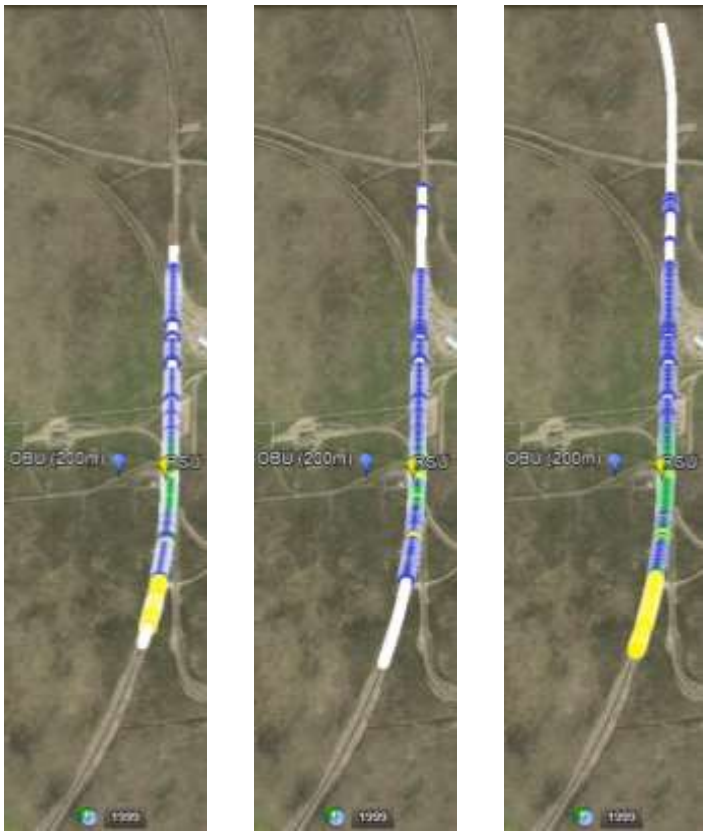

(a) (b) (c)

Figure Q.11 Geographic plots of which packets were received and which were dropped while the Linear Array antenna at Low Power was operated on a train moving at (a) 20mph, (b) 50 mph, (c) 79 mph.

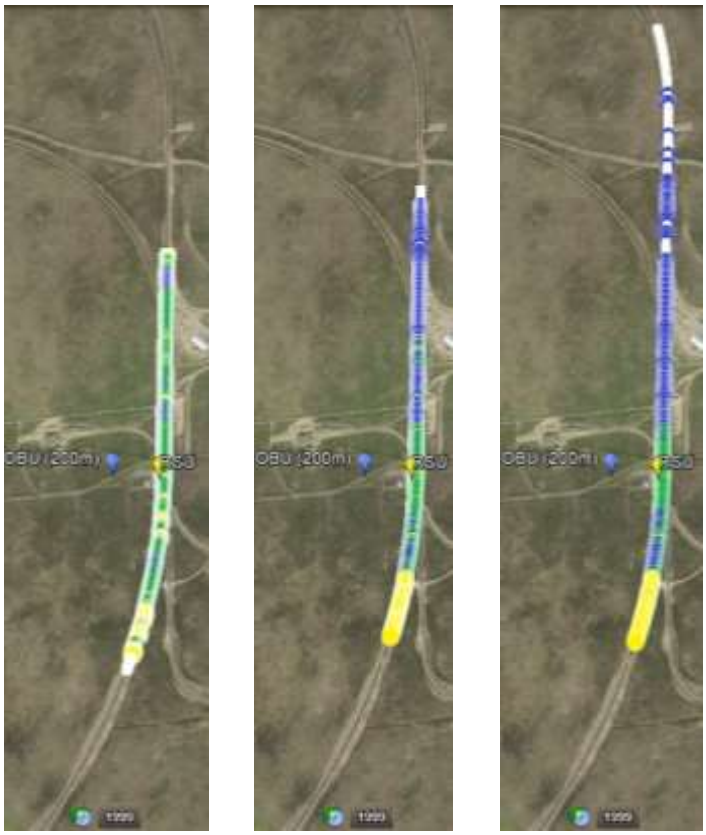

(a) (b) (c)

Figure Q.12 Geographic plots of which packets were received and which were dropped while the Linear Array antenna at High Power was operated on a train moving at (a) 20mph, (b) 50 mph, (c) 79 mph.

Google Earth Visualization Plots of Received Packets for PTT Test site

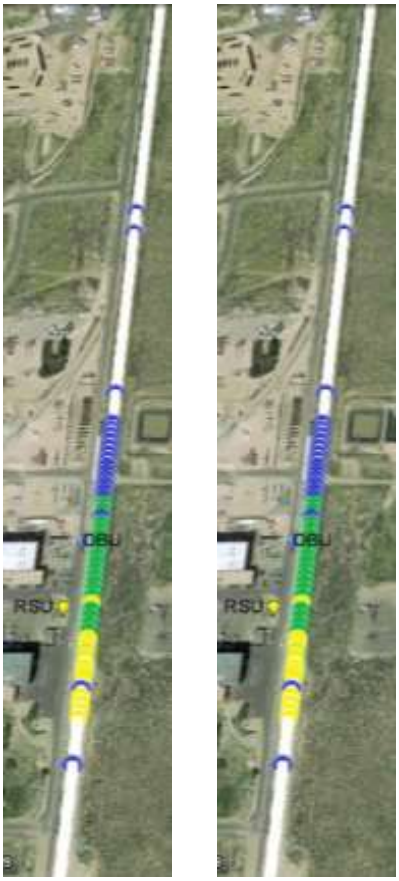

(a) (b)

Figure Q.13 Geographic plots of which packets were received and which were dropped while the Omni Directional antenna at Low Power was operated on a train moving at (a) 50 mph, (b) 79 mph.

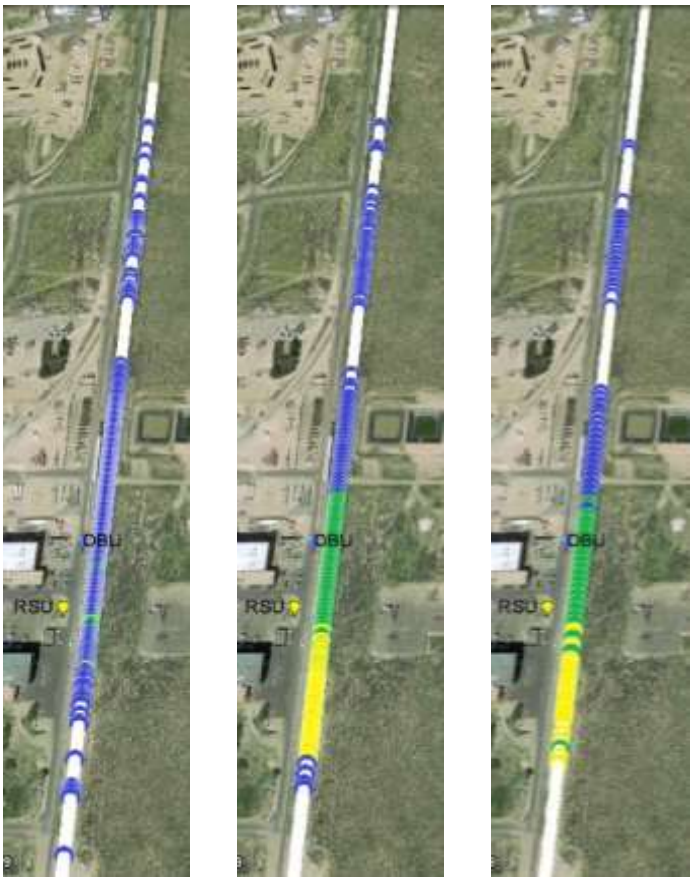

(a) (b) (c)

Figure Q.14 Geographic plots of which packets were received and which were dropped while the Omni Directional antenna at High Power was operated on a train moving at (a) 20mph, (b) 50 mph, (c) 79 mph.

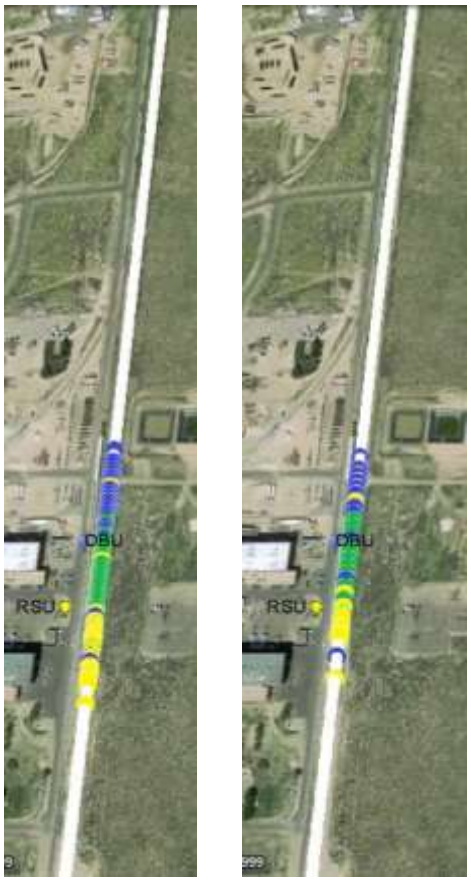

(a) (b)

Figure Q.15 Geographic plots of which packets were received and which were dropped while the Omni Diversity antenna at Low Power was operated on a train moving at (a) 50 mph, (b) 79 mph.

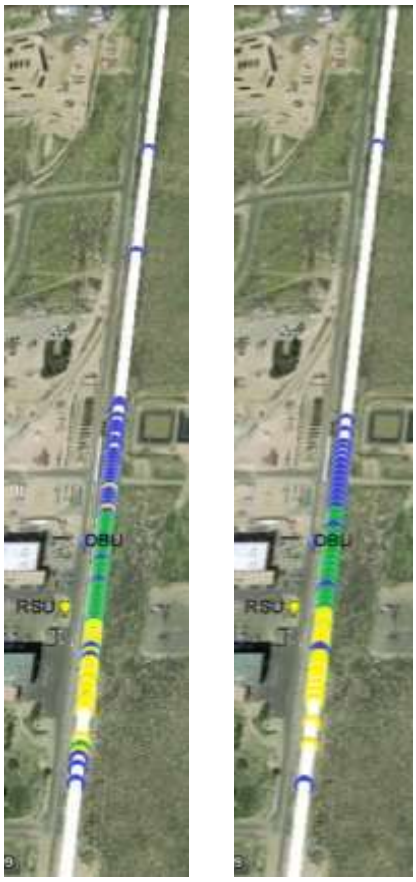

(a) (b)

Figure Q.16 Geographic plots of which packets were received and which were dropped while the Omni Directional antenna at High Power was operated on a train moving at (a) 50 mph, (b) 79 mph.

Figure Q.17 Geographic plots of which packets were received and which were dropped while the Linear Array antenna at Low Power was operated on a train moving at 50 mph.

(a) (b) (c)

Figure Q.18 Geographic plots of which packets were received and which were dropped while the Linear Array antenna at High Power was operated on a train moving at (a) 20mph, (b) 50 mph, (c) 79 mph.